

**Volcanological, geochemical and isotopic
studies of rocks from the Barren Island Volcano
and Andaman Subduction Zone, India**

A Thesis submitted to



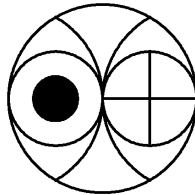
**The Maharaja Sayajirao University of Baroda,
Vadodara, India**

For the degree of

Doctor of Philosophy in Geology

By

ALOK KUMAR



**Geosciences Division
Physical Research Laboratory,
Navrangpura, Ahmedabad-380009, India
2011**

DECLARATION

I, **Mr. Alok Kumar**, S/o Mr. Ramnaresh Bhakt, resident of C-103, PRL Residences, Navrangpura, Ahmedabad - 380009, hereby declare that the research work incorporated in the present thesis entitled "*Volcanological, geochemical and isotopic studies of rocks from the Barren Island Volcano and Andaman subduction zone, India*" is my own work and is original. This work (in part or in full) has not been submitted to any University for the award of a Degree or a Diploma. I have properly acknowledged the material collected from secondary sources wherever required. I solely own the responsibility for the originality of the entire content.

Date:

(Alok Kumar)

Certified by:

Dr. J.S. Ray (Supervisor),
Associate Professor
Physical Research Laboratory

Countersigned by

Head of the Department
Department of Geology
Faculty of science

Dedicated

To

My Mamaji

Late Ashok kumar saini

and

My Parents,

Sri Ramnaresh Bhakt & Smt. Sushila Bhakt



Barren Island volcano, Andaman Sea, India



*Our team on Barren Island Volcano (From right to left): Dr. R. Bhutani, Dr. J.S. Ray (Thesis Supervisor), Dr. Hetu Sheth, **Author (Alok Kumar)**, Commandant S.K. Sahu and crew members of ICGS Bikhaiji Cama Coast Guard vessel*

Acknowledgements

There are many people without whom the work that has led to this thesis would have been impossible. I am grateful to all people that have supported me during my Ph.D. tenure. I want to mention a number of people in particular.

I would foremost like to thank my advisor, Dr. Jyotiranjana S. Ray, for giving me guidance, and the opportunity to work on this exciting research in Andaman and Barren Islands. He was involved in every step of this study. He introduced me to the field of geochemistry. His critical treatment of analytical results and of writing reports trained me to become a concise researcher. I appreciate the freedom he gave me to develop my ideas, and steering those ideas into the right direction when they become too playful at times. I especially want to thank him for the time he has put in giving advice and correcting the thesis, which are greatly improved its quality.

I am grateful to Mr. A.D. Shukla, Dr. Hetu sheth, IIT Bombay and Dr. Rajneesh Bhutani, Pondicherry University who have always been keen to help me many valuable discussions on the subduction zone study. I am proud of the members of the Andaman team (especially Barren and Narcondum Island's team), who were always highly motivated, hard working, and helpful in every way. Our field-work would not have been productive without their superb team work. I especially acknowledge Dr. Sheth, who infected me with his enthusiasm for studying volcanic features on Barren Island (Volcanology) and reconstructing the volcanic history of the Barren Island volcano.

I owe a debt of gratitude to Prof. S.K. Bhattacharya, Dr. S.K. Gupta and Dr. R.D. Deshpande for their guidance during initial period of my research life in PRL and a special appreciation to Dr. Navin Juyal, for his help and unfailingly positive encouragement throughout my research tenure. I thank Prof. L.S. Chamyal, for his interest in the thesis work and help in completing university registration procedures.

I would like to thank Prof. J. N. Goswami, the Director, Prof. Utpal Sarkar, Dean and A.K. Singhvi, former Dean, Physical Research Laboratory, for providing me support and facilities for my thesis work. I thank academic committee members for timely review of my work. Sincere thanks to Profs. R Ramesh, S.V.S. Murty, M.M. Sarin, Drs. Sunil Singh and D Banerjee for their informative lectures during course work. Prof. R. Ramesh deserves Special thanks for his encouragement and support during my thesis.

I extremely thankful to my juniors Mrs. Neeraj Awasthi, Gaurav and debasis for their help and support. Working with them has always been a pleasure. I would like to acknowledge R.S. Smitha, for her help and company in Andaman field work.

I am thankful to Prof. Harish Chandra, Drs. Ravi Bhushan, M.G. Yadava, R.P. Singh, Vinai K. Rai, Kuljeet Kaur, R. Rangarajan, Namit Mahajan, Dibyendu Chakravarty, Rajesh T.A., Som K. Sharma, and Bhushit Vaishnav for their reassurance towards my work. Thanks are also due to Dr. P. Sharma and Mrs. A.K. Sudheer, R.P. Singh, D. K. Rao, R.A Jani, D. Panda, R.R. Mahajan, Manan and Pranav Adhyaru for their kind support. I am grateful for the instrumentation facility in Planex and to Durga prasad and Jayesh for his help during measurements. Thank to Mr. J P Bhavsar for their kind help during experiments.

I am grateful to all the staff-members of Library, Computer Centre, Workshop, Administration, Transport, Dispensary, Maintenance section of PRL for their assistance and cooperation. Special thanks to Messrs. Ranganathan, R.S.Gupta, Senthilbabu, Pradeep, Jigar, Mishra ji, Sivadasan S.Yadav, Ubale, Viral, Sanjay, Shailesh, Bankim, Smt. Nistha, Parul, Preeti, Jayshree and Nandini for their concern.

I thank to the Director General, Indian Coast Guard, New Delhi for his permission and assistance to carry out field work on Barren Island. I thank H. N. Singh, Manager, and all staff of the ISRO Telemetry, Tracking and Command Network (ISTRAC) Centre, Port Blair, for their local support. Forest Department peoples of Andaman and Nicobar Islands are also appreciation the dedication of their logistic support that made our field work to mud volcanoes safe and productive.

I want to thank the persons that made my Ph.D. work an especially existing period in my life (in no particular order): I had great fun with my batch-mates Jitendra Bhatt, Gyana, Rahman, Naveen, Lokesh, Kirpa, Sumanto, Brajesh, Sumita, Ashish, Tyagi, Shuchita, Rajesh, Harinder, Manan, Ram, Sanjeev, CMS, Ayan, Timmy and Rohan. Gyana deserves special thanks for his help in numerical modelling and proof reading along with my junior Gaurav for reference checking.

I am lucky to have my seniors cum friend like Shreyas, A.S. Maurya, Ashutosh, Satya, Subimal, Sanat, Uma, Shilpey, Sasadhar, Santosh bhai, Neeraj, Antra, Vandana, Jayesh, Anirban, Morthekai, Nagar, Lokesh, Gowda, Madhav, Ritesh, Akhilesh, Santosh, Rohit, Salman, Zeen, Ruby, Sunil, Amitava and Kushwaha

who helped and supported at various stages. I thank to my juniors: Ashok, Arvind, Suratna, Rohit, Vineet, Satindar, Jayati, Rajput, Amzad, Srinivas, Chauhan, Rabiul, Ashish, Tapas, Sunil, Reddy, Moumita, Chinmay, Suman, Pravin, Bhaswar, Sandeep, Srikant, Soumya, Subrata, Vimal, Yogita, Pankaj, Dinesh, Sharad, Aslam, Damu, Arun, Fazlul, Midun, Shashi, Anirban, Shaweeta, Ikshu, Shraddha, Reddy, Diganta, Aditaya, Bala, Awadesh, Shinde and Rajpurohit for making my PRL's life enjoyable.

I owe a special word of thanks to my non-PRLite friends Amar, Bharti, Joshi, Prakash, Shekhar, Abhijeet Jitendra, Divesh, Rakesh, Manoj, Vishal, Abhishek, Gajendra, Shivesh, Raj, Bipin, Sakil, Zeya, Sanjeev, Chandan and Rajnish for their active encouragement.

I owe my sincere thanks to my brother 'Ashutosh' and my in laws (Kamlesh, Awadhesh, Vinay and Vikash) for extending every possible comfort and support to me during this work. I am deeply grateful to Reena, Archana and Anita for their affection, encouragement, care and support. Thanks are due to Santosh, Kunal, Kamlesh, Neeraj, Dhiraj, Amit, Rajeev, Rahul, Rohit, Anjali and Anamika for their faith and confidence on me. Love and affection to Abhinav, Anurag, Arpita and Abhiraaj for making my life cheerful.

I want to express my appreciation to my wife 'Vibha' for her patience, support and care especially during the last stage of my thesis. She must have thought we got married just for her to become 'thesis widow'. Your love and joy in life made the work so much easier to me.

Above all, I express my deepest gratitude to my parents for their encouragement, support and their continuing believe in me. It was their confidence that inspired me the most to complete this work, and therefore, I dedicate this thesis to them with my late Mamaji, who helped me become the person I am now.

Finally, my greatest regards to the Almighty for bestowing upon me the courage to face the complexities of life and complete this thesis successfully.

(ALOK KUMAR)

CONTENTS

		Page No.
List of figures		i
List of tables		v
Chapter 1	Introduction	
1.1	Modern Geodynamics	4
1.2	Subduction Zone	9
1.2.1	<i>The Structure of subduction zone</i>	12
1.2.2	<i>Accretionary Prism</i>	13
1.2.2.1	<i>Ophiolites</i>	13
1.2.2.2	<i>Sediments</i>	16
1.2.2.3	<i>Mud volcanoes and fluid activity</i>	16
1.2.3	<i>Island Arc</i>	17
1.3	Chemistry of subduction related ophiolites, slab and mantle wedge	
1.3.1	<i>Subduction related Ophiolite</i>	17
1.3.2	<i>Chemistry of Mantle wedge and slab</i>	19
1.4	Andaman Subduction Zone	20
1.5	Objectives of this study and their significance	27
Chapter 2	Geology and Earlier work	
2.1	Geology of Andaman and Nicobar Islands	34

Chapter 4	Materials and Methods	
4.1	Sampling Protocol	98
4.2	Analytical Methods	100
4.2.1	Petrography	109
4.2.2	Geochemical Characterization	
	<i>Major element content</i>	110
	<i>Loss on Ignition</i>	113
	<i>Trace element contents</i>	116
	<i>Radiogenic Isotopic ratio</i>	121
	<i>Stable oxygen and hydrogen isotopic ratios</i>	128
	<i>Total carbon(C) and nitrogen (N) contents in mud breccia</i>	129
Chapter 5	Results	
5.1	Petrological description	134
5.2	Geochemical Data	137
Chapter 6	Discussions	
6.1	Model descriptions	155
6.1.1	Mixing model	155
	<i>Two components mixing model</i>	155
	<i>Three components mixing model</i>	156
6.1.2	Rayleigh Fractionation	157
6.1.3	Water rock interaction model	158
6.1.4	Melting model	159
6.2	Field observations	160
6.2.1	Mud volcanoes of Andaman Islands	160

6.3	Rocks, Clasts, Breccias from Andaman Islands	160
6.3.1	Petrography of rocks and breccias	160
6.3.2	Geochemistry of rocks and breccias from Andaman Islands	162
6.3.2.1	Clues from Major oxides and trace elements <i>Rock clasts and breccias from Mud volcanoes Andaman Ophiolites</i>	162
6.3.2.2	The Radiogenic isotope studies of rocks of Andaman Islands	172
6.3.2.3	Stable isotopic studies of mud waters	175
6.4	Lavas and ash from Barren Island (BI) Volcano	178
6.4.1	Petrography of lava flows	178
6.4.2	Clues from Major oxides, trace elements and isotopic studies <i>Mantle source Characteristics</i>	180 186
Chapter 7	Summary and scope for future work	197
	<i>Scope for future work</i>	200
References		203-224
List of publications		225

LIST OF FIGURES

		Page No.
Fig. 1.1	Global tectonic map showing various plates And plate boundaries	5
Fig. 1.2	Plate boundaries observed on the Earth	6
Fig. 1.3	Isotopic ratios diagram showing chemical difference of magma at various tectonic setting with different oceanic island arc volcanics and sediments	8
Fig. 1.4	A schematic diagram showing various components of a subduction zone	14
Fig. 1.5	Model for formation of suprasubduction ophiolites	15
Fig. 1.6	Comparative isotopic plot for ophiolites, oceanic sediments and volcanic arc	18
Fig. 1.7	Mid-ocean-ridge-basalt (MORB)-normalized multi-elements diagram for ophiolites	20
Fig. 1.8	N-MORB normalized trace elements patterns for arc lavas and Ocean Island lavas	22
Fig. 1.9	Geologic and tectonic map of Southeast Asia and northeastern Indian Ocean	26
Fig. 1.10	A schematic diagram showing various components of an Andaman subduction zone	27
Fig. 2.1	A geological map of the Andaman Islands and a schematic section of the Ophiolite Group displaying its different members	38
Fig. 2.2	Field photographs of various members of the Ophiolite Group	40

Fig. 2.3	Location of mud volcanoes in Andaman Islands and major fault systems in the Andaman Sea	51
Fig. 2.4	Schematic diagrams of a cone shaped mud volcano with its various components	52
Fig. 2.5	Cross-sectional views of mud volcanoes of Middle and South Andaman Islands, based on author's identification and interpretation	55
Fig. 2.6	Field photographs of mud volcanoes from Andaman Islands	56
Fig. 3.1	Panoramic views (in 2008 and 2009) of Barren Island showing general morphological and geological features	63
Fig. 3.2	Recent lava flows (of 2008-09) on Barren Island volcano	65
Fig. 3.3	Geological map of Barren Island Volcano based on our observations	67
Fig. 3.4	Prehistoric, pre-caldera tuff breccias and lava flows exposed on the inner caldera wall	69
Fig. 3.5	Lithologs for the six locations examined on Barren Island in the present study	70
Fig. 3.6	Pyroclastic surge and fall deposits on the Barren Island	72
Fig. 3.7	Features observed on the beach section at Landing Site 2 on the western side of the island	74
Fig. 3.8	Uppermost prehistoric deposits representative of Caldera forming eruption at landing site 1	77
Fig. 3.9	Panoramic view of recent aa and toothpaste lava flows	80
Fig. 3.10	Recent ash blanket (2010-2011) on Barren Island volcano	88

Fig. 4.1	Geological map of the Barren Island Volcano with sampling location	99
Fig. 4.2	Geological map of Andaman Islands with sampling locations	101
Fig. 4.3	Calibration curves generated using XRF for major element oxides (wt%) and trace elements (ppm)	114
Fig. 4.4	Comparison of measured and reported concentration of various major element oxides in BHVO-2 and BCR-2 USGS rock standards	115
Fig. 4.5	Calibration curves for various trace elements generated on ICP-MS using USGS rock standard BHVO-2	120
Fig. 4.6	Temporal variation of measured $^{87}\text{Sr}/^{86}\text{Sr}$ in NBS-987, and $^{143}\text{Nd}/^{144}\text{Nd}$ in JNdi-1	126
Fig. 4.7	Temporal variation of $^{87}\text{Sr}/^{86}\text{Sr}$ and $^{143}\text{Nd}/^{144}\text{Nd}$ in USGS rock standard BHVO-2	127
Fig. 5.1	Photomicrograph of ophiolites of the Andaman rocks	135
Fig. 5.2	Photomicrograph of lavas of the Barren Island Volcano	136
Fig. 6.1	Diagram showing mixing of three components	157
Fig. 6.2	Chemical classification of Mud breccia and serpentine clasts of mud volcanoes of Andaman	162
Fig. 6.3	$\text{Al}_2\text{O}_3\text{-K}_2\text{O-Fe}_2\text{O}_3$ diagram for the Mud breccias and serpentine clasts of mud volcanoes	163
Fig. 6.4	TiO_2 vs. Al_2O_3 plot for the Mud breccias and clasts	164
Fig. 6.5	Variation diagram of mud breccias and clasts from Mud volcanoes	165
Fig. 6.6	Chondrite normalized REE patterns for mud breccia,	

	clasts compared with PAAS	168
Fig.6.7	Chondrite normalized REE patterns for mud breccia, Clasts and I MORB	169
Fig 6.8	MnO-TiO ₂ -P ₂ O ₅ diagram for Ophiolite group rocks of Andaman	171
Fig.6.9	ϵ_{Nd} versus $^{87}Sr/^{86}Sr$ plot for mud matix, HCl- residue Fraction of mud matrix and serpentinite clast samples from mud volcanoes of Andaman Islands	173
Fig. 6.10	ϵ_{Nd} versus SiO ₂ plot for Ophiolite Group of rocks of Andaman Islands	174
Fig.6.11	$\delta^{18}O$ and δD plots for water samples from mud volcanoes and fresh water sources of Andaman Islands	176
Fig. 6.12	Classification of rocks from Barren Island based on total alkali vs. Silica variation	181
Fig 6.13	MnO-TiO ₂ -P ₂ O ₅ discrimination diagram for Barren Island Lavas and ash beds	182
Fig. 6.14	Variation diagrams of selected major and trace elements vs. MgO in Barren Island lavas	183
Fig. 6.15	N MORB normalized (Sun and McDonough 1989) trace element patterns for Barren Island lavas	184
Fig. 6.16	Neodymium isotopic ratios and trace elements ratios for Barren Island lavas	187
Fig. 6.17	two and three components mixing plot for barren lavas	189
Fig. 6.18	Isotopic plots for Pb isotopes of Barren island lavas	191
Fig. 6.19	Melting model for Barren island lavas and Indonesian arc lavas	193

LIST OF TABLES

		Page No.
Table 2.1	Simplified stratigraphy of Andaman Island	36
Table 4.1	Descriptions of samples form lava flows and ash beds of the Barren Island Volcano	102
Table 4.2	Description of samples collected from the Ophiolite Group, Andaman Islands	104
Table 4.3	Description of mud breccia and rock clast samples collected from Mud Volcanoes of Andaman Islands	105
Table 4.4	Description of Water samples from Mud Volcanoes and other water bodies, Andaman Islands	107
Table 4.5	Description of Rock standards used during the generation of major element data	112
Table 4.6	Measured and reported values of major oxide concentrations in USGS rock standard BHVO -2 and BCR-2 to check of accuracy of the measurement	113
Table 4.7	Sample dissolution procedure for trace elements analysis	117
Table 4.8	Measured and reported concentrations for various trace elements in BHVO-2 to check accuracy of the measurement on ICP-MS	119
Table 4.9	Measured and reported concentrations for various trace elements in BCR-1 and BHVO-2 to check accuracy of the measurement for INAA	121
Table 4.10	Sample dissolution procedure for isotopic analyses	122
Table 4.11	Protocol for Sr and REE separation from sample solution	123

Table 4.12	Protocol for Nd separation from REE Cut	124
Table 5.1	Major oxide composition of mud breccia and rock clasts samples collected from mud volcanoes of Andaman Islands	139
Table 5.2	Major oxide composition of samples collected from the Ophiolites Group, Andaman Islands	140
Table 5.3	Major oxide composition of samples from lava flows and ash beds of the Barren Island Volcano	141
Table 5.4	Trace elements abundances of rock clasts samples collected from mud volcanoes of Andaman Islands	143
Table 5.5a	Trace elements abundances of samples from lava flows and ash beds of the Barren Island Volcano	144
Table 5.5b	Trace elements abundances of samples from lava flows and ash beds of the Barren Island Volcano	146
Table 5.6	Oxygen and hydrogen isotopic ratios of water samples from Mud Volcanoes and other water bodies, Andaman Islands	148
Table 5.7	Sr and Nd isotopic ratios of mud breccia and rock clasts samples collected from mud volcanoes of Andaman Islands	149
Table 5.8	Sr and Nd isotopic ratios of samples collected from the Ophiolites Group, Andaman Islands	150
Table 5.9	Sr and Nd isotopic ratios of samples from ash beds of The Barren Island Volcano	150
Table 5.10	Sr, Nd and Pb isotopic ratios of rock and ash samples from Barren Island Volcano	151

Chapter 1

Introduction

1.1 Modern Geodynamics

Based on the physical properties of Earth there are two important layers which govern most of the activities on and in the Earth; Lithosphere and Asthenosphere. The lithosphere is the top 100 km or so of the Earth's interior which is made up of the rocky crust and outermost rocky layer of the mantle that is also known as plate. The asthenosphere is that part of the upper mantle comprising the low velocity layer and more viscous mantle rocks beneath, down to about 700 km. Two types of lithospheric plates have been recognized: I) the oceanic lithosphere: that encompassed the oceanic crust and II) the continental lithosphere: that encompassed the continental crust.

The interior of Earth is hot, owing to the heat originally accumulated in the Earth during the time of formation and heat produced by ongoing radioactive decay. The present rate of radioactive heat production in the mantle is 2.5×10^{13} W for the two-layer model and 2.1×10^{13} W for the whole-mantle convection model (Spohn and Schubert, 1982). This internal energy causes instability in the Earth's interior and its surface plates leading to plate tectonics.

Earth is made up of seven major and several minor lithospheric plates, which are continuously moving with respect to each other (Fig. 1.1). The science and study of cause of, and relative motions of, the Earth's lithospheric plates form the study of plate tectonics. The motion of these plates is extremely slow due to the incredible amount of mass being moved, friction, and the high viscosity of the asthenosphere. The driving force behind these movements is mainly the mantle

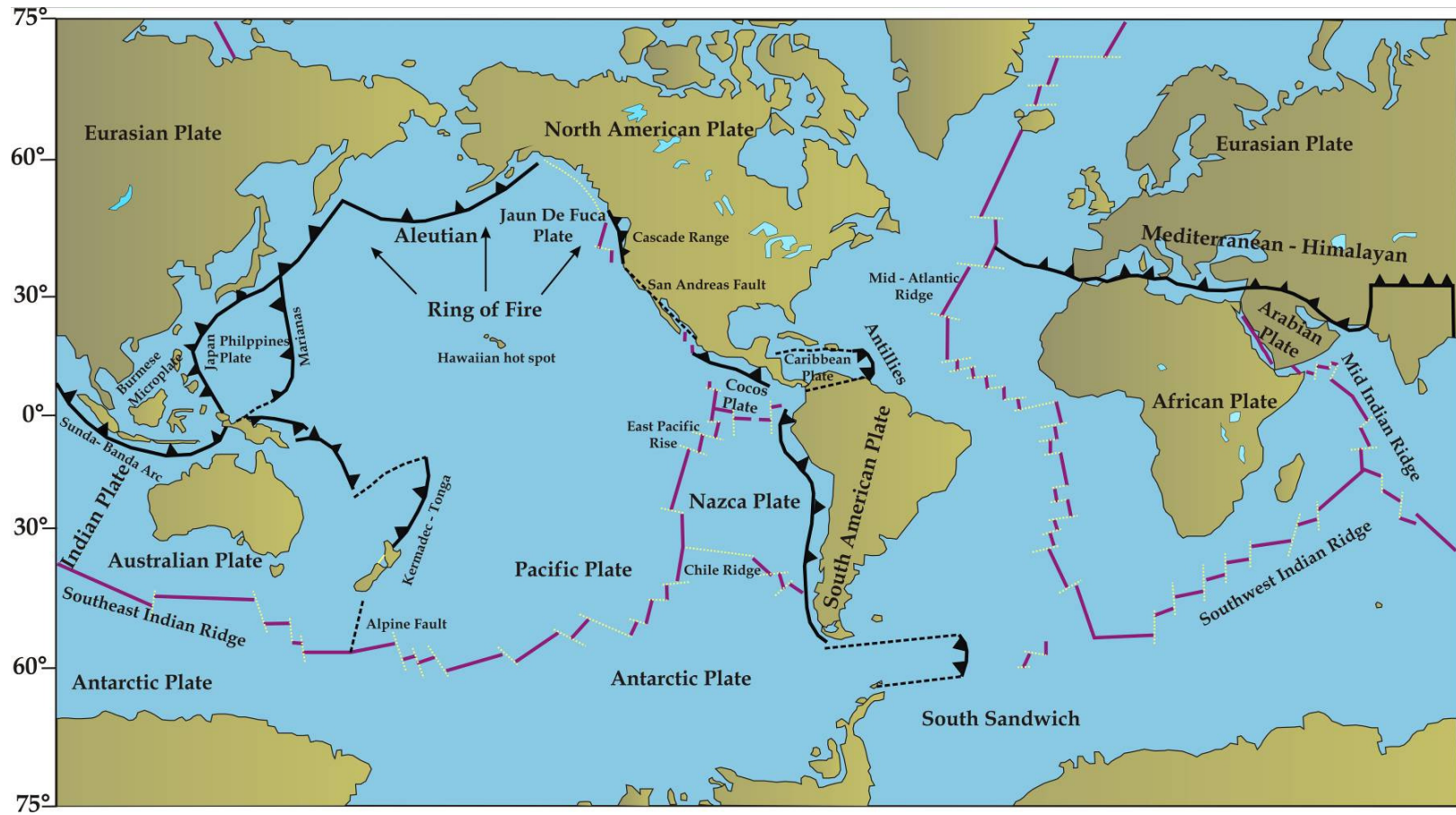


Fig. 1.1 Global tectonic map showing various plates, plate boundaries and different tectonic features (modified after Wilson 1989)

convection. Based on relative motion of these plates three types of plate boundaries are developed on the Earth crust; I) Transform II) Divergent and III) Convergent (Fig. 1.2).

At transform plate boundary the plates slide horizontally past one another without the production or destruction of lithosphere. The motion can be in the same direction or in opposite direction. If the motion is in the same direction but at different speeds earthquakes are created. In 1965 the Canadian Geologist, J. Tuzo Wilson was the first to observe the true nature of the transform fault. Wilson suggested that these large faults connect the global active belts in to continuous network that divides Earth's outer shell into several rigid plates (Tarbuck and Lutgens, 2006). Most transform faults are located within ocean basins, but a few cut through continental crust, e.g., the San Andreas Fault of California, western coast of North America.

At divergent plate boundary, two plates move apart resulting upwelling of mantle that melts to create new oceanic crust. These plate boundaries located along mid oceanic ridges (MOR) are known as constructive plate boundaries because new crust is forming continuously at divergent plate boundaries. The interconnected oceanic ridge system is the longest topographic feature on the Earth's surface, exceeding 70,000 km in length, which represent 20 % of Earth's surface (Fig. 1.1).

Farther away from MOR, driven away by the mantle convection current when an older and denser lithospheric plate collide with another lithospheric plate, relatively younger and lighter, it becomes negatively buoyant and sinks into the mantle. This place represents the zone of convergent plate boundaries and also known as subduction zones, which are tectonically most active regions on our planet. Subduction of an older

plate beneath a younger plate results in the formation of several tectonomorphic features such as trench, accretionary prism, volcanic arc and back arc spreading ridge. New continental crust also gets generated along these zones as a result of magmatism on the leading margin of the overriding plate (Hawkesworth et al., 1993).

Both volcanic and earthquake activities are indications of, and a consequences of, the movements of the lithospheric plate. The world distribution of earthquakes and volcanoes are observed along zones of higher than average heat flow from the Earth's interior. This information has been used to define the tectonic active areas of the world and therefore the margins of the lithospheric plate. Minor earthquakes can occur almost anywhere in the world; they may be the result of movement along old faults and may be due to change in the lava level in the magma chamber beneath a volcano (Neuberg et al., 2006). Spreading oceanic ridges and transform faults are characterized by shallow earthquakes limited to axial rift zones. These earthquakes are generally small in magnitude, commonly occur in swarms and appear to be associated with intrusion and extrusion of the basaltic magmas. The most destructive earthquakes found along subduction and collision zones. The subduction zones are defined by earthquake hypocentres that lie in an approximate plane and dip beneath arc systems. This plane, known as the seismic zone or Benioff zone, dips at moderate to steep angles and extends in some instances to the 660 km seismic discontinuity (Condie, 1997). The seismic zone is interpreted as a brittle region in the upper 10-20 km of descending lithospheric slabs. Although collision zone are seismically very active, earthquake foci tend to be shallow, probably because there is no longer a subducting plate beneath the mountains.

Volcanism is found along subducting zones, spreading ridges, continental rift valleys and at isolated locations inside the plate boundaries, where 'hot spots' are created by rising plumes of the materials within the mantle. The source of magma and type are different in different tectonic environment; The magma involved in spreading, rift valley and hot spot volcanoes is a result of decompression melting of the mantle and is basaltic in nature which reflect chemistry of the mantle; whereas the

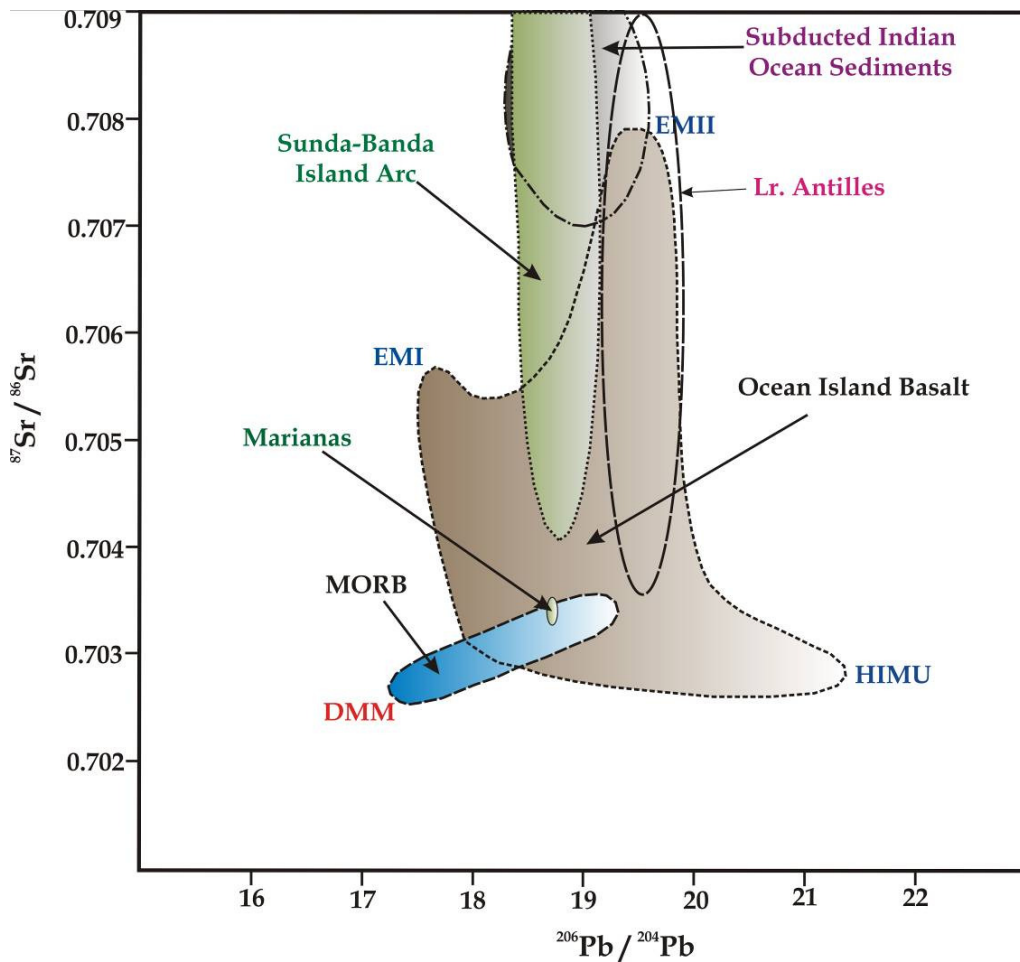


Fig.1.2 Sr and Pb Isotopic ratios diagram showing chemical difference of magma at various tectonic setting with different oceanic island arc volcanics and sediments (modified after Tatsumi, ----) MORB – Mid-ocean-ridge basalt; DMM – Depleted MORB mantle; EMI – Enriches mantle I, EMII – Enriches mantle II, HIMU- High μ .

magma found in subduction zones whether in island arc or in orogenic belt, has its origin in the partial melting of heavily metamorphosed mantle wedge in presence of fluids derived from subducting oceanic crusts. The compositions of these lavas are complex, but are mainly andesitic.

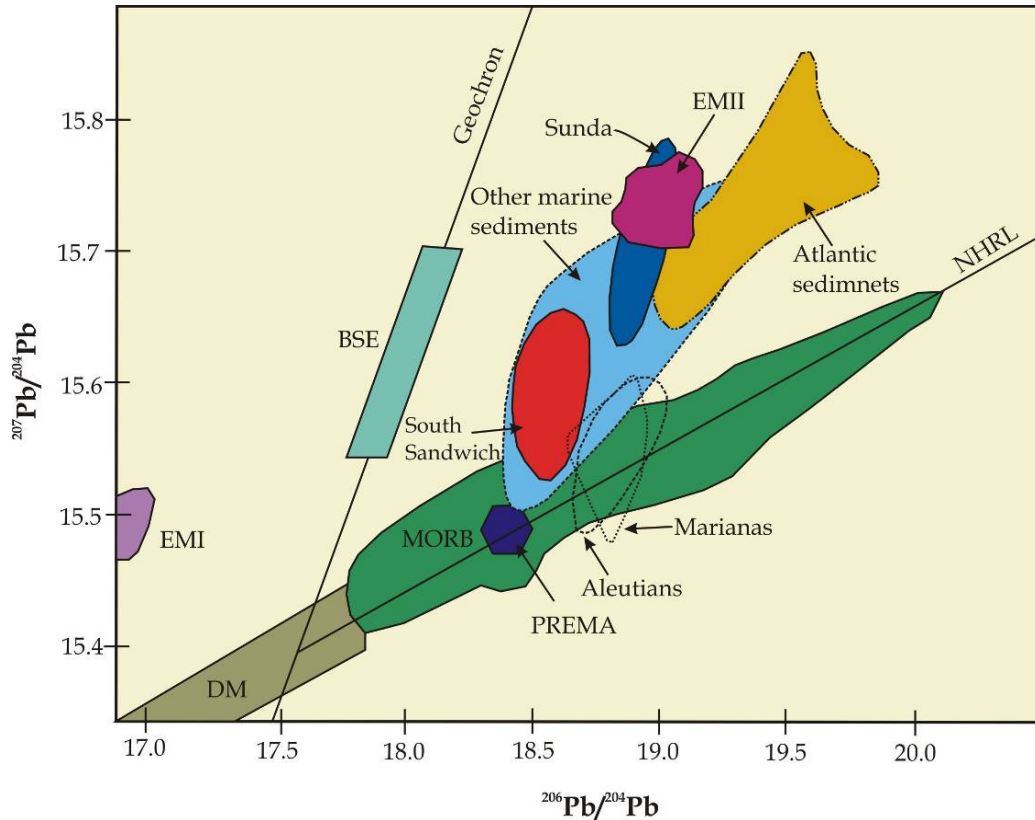


Fig.1.3 Pb Isotopic ratios diagram showing chemical difference of magma at various tectonic setting with different oceanic island arc volcanics and sediments (modified after Wilson 1989) MORB – Mid-ocean-ridge basalt; NHRL – Northern Hemisphere reference line; DM – Depleted mantle; EM – Enriches mantle, PREMA- Primitive mantle, BSE- Bulk Silicate Earth

Based on isotopic compositions (Fig. 1.2 and 1.3), geochemists have found different mantle source compositions at different places (EMI, EMII, PREMA, MORB, DMM). It is believed that the changes of mantle source compositions are primarily due to subducted materials; as for example the

evolution of EMI and EMII type of mantle sources is due to addition of mafic lower crustal materials and oceanic sediments in the pristine mantle source respectively, which have high $^{87}\text{Sr}/^{86}\text{Sr}$ and relatively low $^{143}\text{Nd}/^{144}\text{Nd}$. The HIMU, or high- μ ($\mu = ^{238}\text{U}/^{204}\text{Pb}$), source is characterized by higher $^{206}\text{Pb}/^{204}\text{Pb}$, but depleted MORB-like $^{87}\text{Sr}/^{86}\text{Sr}$ and $^{143}\text{Nd}/^{144}\text{Nd}$ compared to other end member components (EMI, EMII etc.), the composition of HIMU mantle source is the product of the mixing of subducted oceanic crust and pristine mantle source, because the subducted oceanic crust contains high concentration of U and Th. PREMA (primitive mantle) is defined as the composition of mantle after separation of core but before separation of the crust.

1.2 Subduction Zone

Subduction zones are extremely dynamic regions of the Earth's surface. They are the collision sites between Earth's tectonic plates, where a subducting plate is carried deep into the Earth's mantle beneath an overriding plate. These zones are also known as our planet's largest recycling system, where oceanic lithosphere, sediments (pelagic and terrigenous) and sea water return to and reequilibrate with Earth's mantle. Arc magmas are produced along the zones that solidify to generate young continental crusts.

There are two types of subduction zones which are defined based on the nature of convergent of two lithospheric plates: I) ocean-ocean plates subduction and II) ocean-continental plates subduction. When an oceanic plate subducts beneath oceanic plate a deep trench, such as the Marianas, is created at boundary between the two. The volcanic products of this type of setting are usually basalt and basaltic andesitic. In the second case when an oceanic plate subducts beneath a continental plate, a

shallow trench, Chilean type is created. The volcanic products of this type of setting are mainly calc-alkaline andesite.

Subduction of lithospheric plates plays an important role in plate tectonics mechanism because it is considered that the gravitational pull of subducted slabs drives the motions of Earth's tectonic plates, but the coupling between slabs and plates is not well established (Conrad and Bertelloni, 2002). It is also believed that mantle convection which is responsible for the plate motions, may be driven primarily by the descent of dense slabs of the subducted oceanic lithosphere (Hager, 1984). The initiation of subduction is always debated. How a subduction zone begins remains still poorly understood (Niu et al., 2003) but a recent study by Michael et al. (2004) has proposed two principal views on the physical mechanism leading to the initiation of subduction. The first and most common is that as the oceanic lithosphere ages and cools, its density increases so that an instability arises and the plate sinks spontaneously in the mantle under its own weight and the second view proposes that the externally applied compressive stresses and moderate convergence are necessary to form a new subduction zone. The most likely mechanism would be through a transfer of stress induced by a collision, leading to 'forced' subduction initiation elsewhere. Silver and Behn, (2008) proposed that the subduction has operated continuously on Earth without interruption, subduction zones are routinely terminated by ocean closure and supercontinent assembly. He has also agreed with Niu et al. (2003) that subduction initiation is probably the least well-understood aspect of plate tectonic theory. Hansen (2007) presented a hypothesis that mantle upwelling and similar thermal processes, combined with an impact from an extraterrestrial source, would give the early Earth the discontinuities in the crust for the subduction of the denser material underneath lighter material. In a recent work, Lowman (2011) proposed that the difference of

densities between two adjacent lithospheric slabs is sufficient to lead to the initiation of subduction.

1.2.1 Structure of a subduction zone

The structure of a typical ocean - ocean subduction zone with its various components is presented in Fig. 1.4. When a lithospheric plate begins to descend beneath another plate along a subduction zone, the point of contact where the bending of the subducting slab from a horizontal to a dipping position occurs is known as a trench (Fig. 1.4). During the process of subduction, the surface of the downgoing plate shears against the edge of the overriding plate. The shearing leads to scrapping off materials from the downgoing slab onto the overriding plate producing an accretionary prism or wedge. The angle of subduction varies significantly, as inferred from seismic data on Benioff zone earthquakes (Hamilton, 1998).

The Benioff Zone is a planar trend of earthquakes along the upper boundary of subducted slab, which can extend up to 700 km into the mantle. The wedge shaped mantle that lies in - between the slab and the overriding plate is called the mantle wedge (Fig.1.4). When the cold subducting slab comes in contact with hot mantle wedge dehydration takes place and fluids are released into the wedge leading to melting - which generates the volcanic arcs or Island arcs (Fig. 1.4).

An island arc set up begins on the overriding plate with the forearc (the portion of the arc between the volcanic front and the trench is called the 'forearc'), which contains both volcanic rocks and sedimentary rocks derived by weathering of the arc. Behind the forearc is the main volcanic arc, which runs parallel to the trench at a distance that correlates with the dip angle of the subducting slab (Pluijm and Marshak, 2004). The basin

behind the volcanic arc is called a backarc basin, which is underlain by basaltic oceanic crust and may contain a spreading ridge (Fig.1.4). Extensional tectonic features are common in backarc environments. The trench and forearc realms are characterized by low heat flow because the downgoing slab of cold oceanic lithosphere acts as a heat sink (Pluijm and Marshak, 2004). The volcanic arc and the adjacent back arc basin are areas of unusually high heat flow, partly because of localized magmatic activity, but principally because of mantle convection (Hamilton, 1998).

1.2.2 Accretionary Prism

The accretionary prism or wedge consists of ophiolites, deformed pelagic sediments, and of the deformed trench deposited turbidities. It also contains a special type of sedimentary feature, known as Mud volcanoes. The details of all the components of a typical accretionary prism are described in the following paragraphs.

Ophiolites

Ophiolites represent masses of oceanic crust and upper mantle that have obducted on the edge of the oceanic crust, (Dewey and Bird, 1971; Coleman, 1977; Nicolas, 1989) that were incorporated into continental margins during continent-continent and arc-continent collisions (Dilek and Flower, 2003), ridge-trench interactions (Cloos, 1993; Lagabrielle et al., 2000), and/or subduction-accretion events (Cawood et al., 2009). However, in recent times it has been realized that a great majority of ophiolites form at the subduction zones. Dilek and Furnes (2011), categorized ophiolites into two types; subduction-related and subduction-unrelated types. Subduction-related ophiolites include suprasubduction zone (SSZ) varieties whose geochemistry is similar to island arc magma. They further divided subduction-unrelated ophiolites into three types; continental-margin, mid-ocean ridge, and plume-type, whose composition usually

similar to MORB. Pearce et al. (1984), suggested that the SSZ ophiolites develop during the initial stages of subduction prior to the development of any volcanic arc and that the more common mechanism for formation of SSZ ophiolites have been pre-arc rather than back-arc spreading, whereas subduction-unrelated types evolve during rift-drift and seafloor spreading. Fig. 1.4 depicts a generalized model for the generation of SSZ ophiolites.

Sediments

Sediments are an important constituent in subduction environment. It is the water holding capacity of the sediments that makes them crucial for magmatic activity in a subduction zone. The dewatering process of sediments along the interface of slab and mantle wedge contributes significantly to the melting processes in the wedge leading to volcanism on the overriding plate. Jarrard (2003) suggested that addition of less than 1 % of water can lower the melting point by several hundred degrees of mantle wedge. Apart from this the sediments are the ultimate sources of many of the unusual enrichments and chemical signatures found in arc lavas (Stern, 2002).

Mud volcanoes and fluid activity

Mud volcanoes are common features in forearc region. Apart from the main fault of the subduction zone, i.e. the decollement fault along which the two plates come into contact, there exist numerous faults along the convergent margin that are loci of earthquakes. Some of these faults play an important role in the formation of mud volcanoes. These faults help to release high pressurized fluids and solid materials from the subduction zone through deep conduits and serve as a window of subducting slab.

Moore and Vrolijk (1992) proposed; in accretionary prisms, fluid rock interactions occur in most dynamic structural environment on Earth. The prism materials loose fluids both through tectonically induced consolidation and thermally induced dehydration processes. Peacock (1990) argued the expulsion of large volume of pore waters and CH_4 - H_2O fluids produced by diagenetic and low grade metamorphic reactions at shallow depth affect the thermal and rheological evolution of the accretionary prism and at greater depth it alter the bulk composition of mantle wedge after released CO_2 and H_2O by metamorphic reactions in the subducting altered crust and trigger partial melting reactions which are responsible for magma generation.

1.2.3 Island Arc

In a convergent margin where two oceanic lithospheres are involved the descending oceanic lithosphere contributes to melting process in the mantle wedge. These melts rise from the point of melting through the overriding plate to form volcanoes just behind the leading plate edge. The resulted volcanoes on the overriding plate occur in a series of volcanoes and make a chain of volcanic islands forming an arc shaped chain, popularly known as "Island Arc". In the globe there many such boundaries have been recognized: e.g., the islands of Japan, Aleutian, Mariana, and Lesser Antilles. Island arcs are generally 200 to 300 km wide and can be several thousand kilometers long.

1.3 Chemistry of subduction related ophiolites, slab and mantle wedge

1.3.1 Suprasubduction Ophiolite

Subduction related ophiolites are known as supra-subduction zone (SSZ) ophiolites. Its geochemical characteristics are akin to island arc lavas but

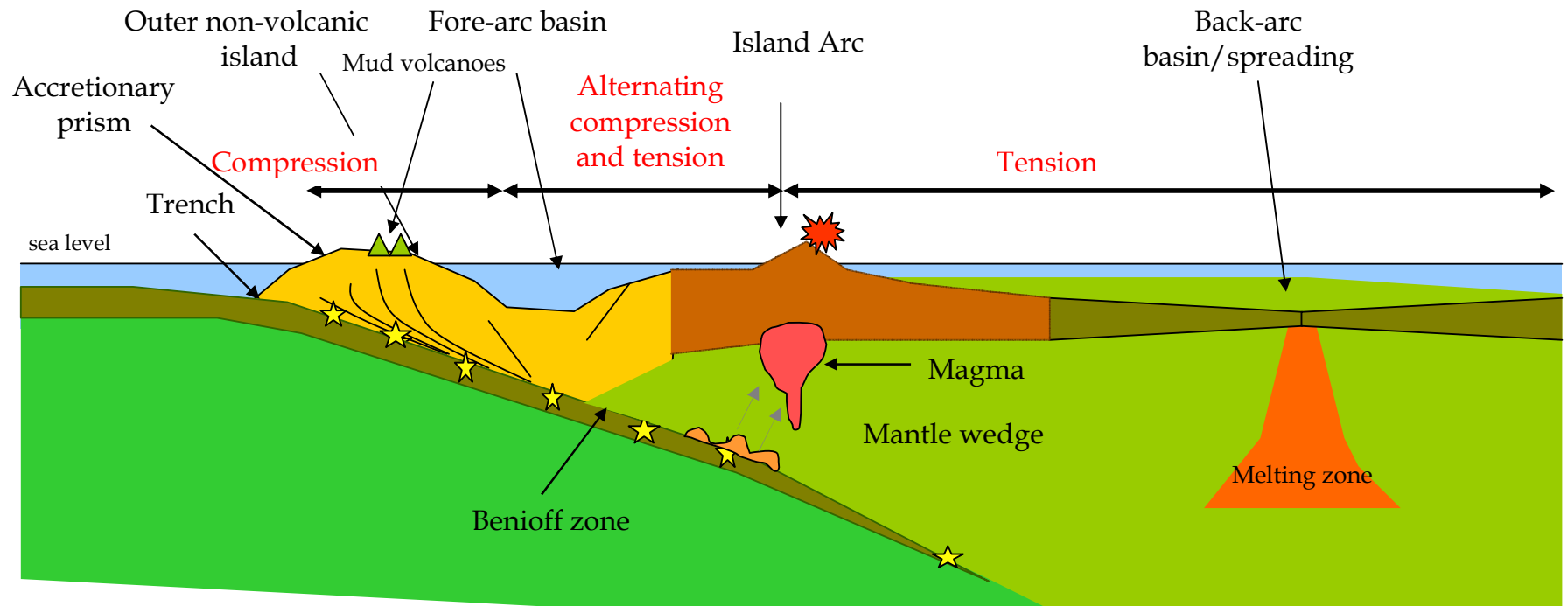


Fig.1.4 A schematic diagram showing various components of a subduction zone, stars indicate hypocentres of earthquakes, solid curve lines in accretionary prism indicate the direction of off scraped materials which resist to go inside with lithospheric plate and the straight solid line indicate fault lines.

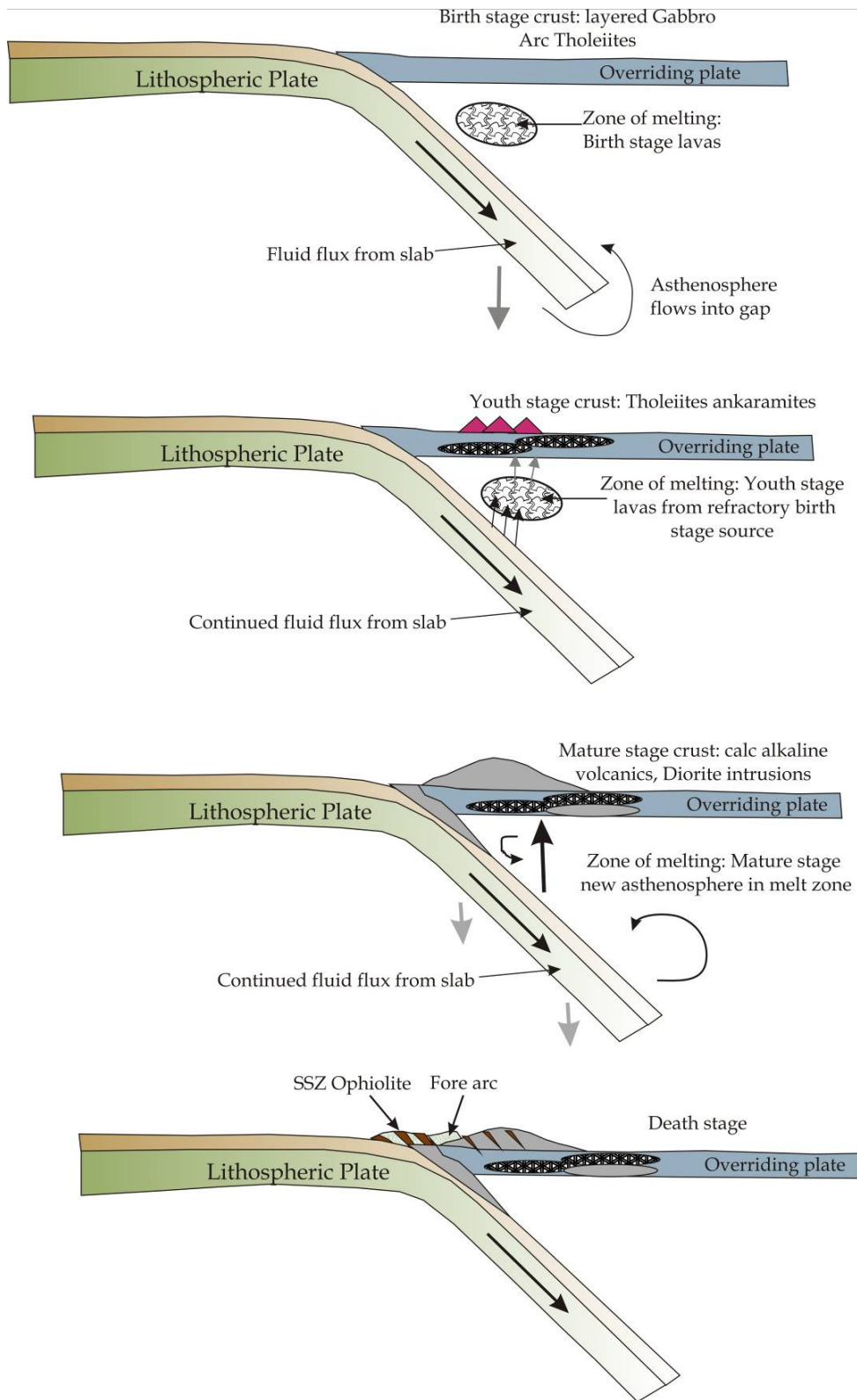


Fig. 1.5 Model for formation of suprasubduction zone (SSZ) ophiolites (modified after Shervais et al., 2004)

they are thought to have formed by sea-floor spreading directly above subducted oceanic lithosphere (Pearce et al., 1984). They differ from 'MORB' ophiolites not only in their geochemistry but also in the more depleted nature of their mantle sequences. These types of ophiolites are mostly best-preserved in orogenic belts (Pearce et al., 1984).

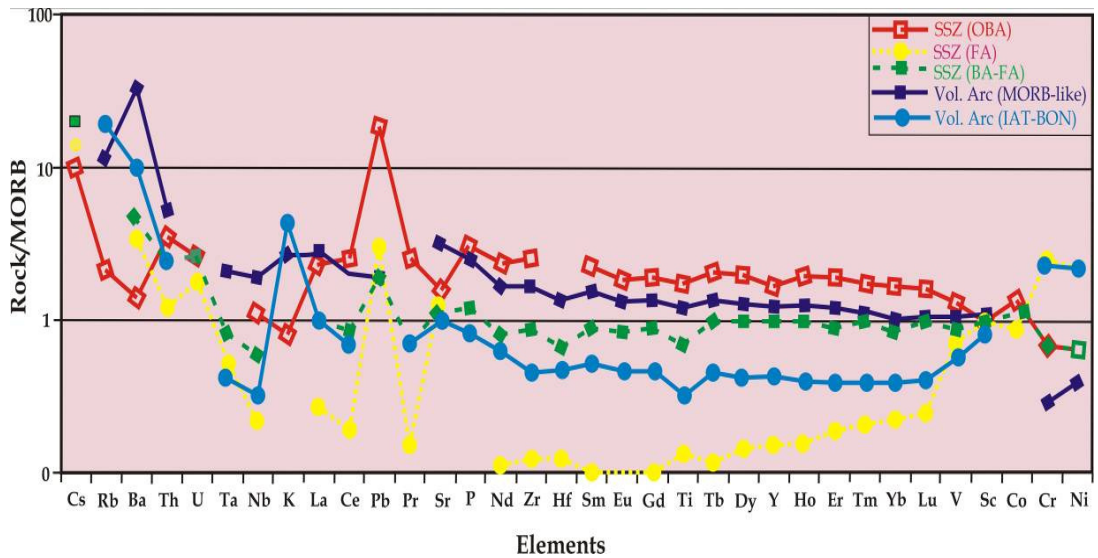


Fig. 1.6 Mid-ocean-ridge-basalt (MORB)-normalized multi-elements diagram, showing average compositions of subduction-related ophiolites and Island arc type ophiolites. IAT – island - arc tholeiite; Bon – boninite. Suprasubduction - zone (SSZ), backarc to forearc (BA-FA), forearc (FA) and oceanic backarc (OBA). (Data sources and normalizing values: Dilek and Furnes, 2011)

Pearce et al. (1984) also argued that these ophiolites are the first magma to form in response to intra-oceanic subduction and are boninitic in composition, derived by partial melting of hydrated oceanic lithosphere in the 'mantle wedge'. As subduction proceeds, the magma composition changes to island-arc tholeiite, probably because the hydrated asthenosphere of the 'mantle wedge' eventually becomes the dominant mantle source. Other SSZ ophiolites formed in the early stages of back-arc spreading following splitting of a pre-existing arc. The characteristic of suprasubduction zone basaltic magma compositions is elevated

concentrations of large ion lithophile elements (LILE: CS, Rb, Ba, Th, K, Sr and Pb) relative to high field strength elements (HFSE: Nb, Ta, Hf, Zr and Ti) (Fig. 1.6). Isotopic compositions of these ophiolites overlap with those of MORB and Island Arc lavas (Fig. 1.7).

1.3.2 Chemistry of Mantle wedge and Slab

The asthenospheric mantle that lies between the slab and the overriding plate is called the mantle wedge. It is called so because of its shape. The prime importance of the mantle wedge lies in its role in the generation of new continental crust at the volcanic / magmatic arc region. The chemistry of mantle wedge, although is similar to a depleted MORB mantle at the initiation of subduction, gets continuously modified through metasomatism by material derived from the slab.

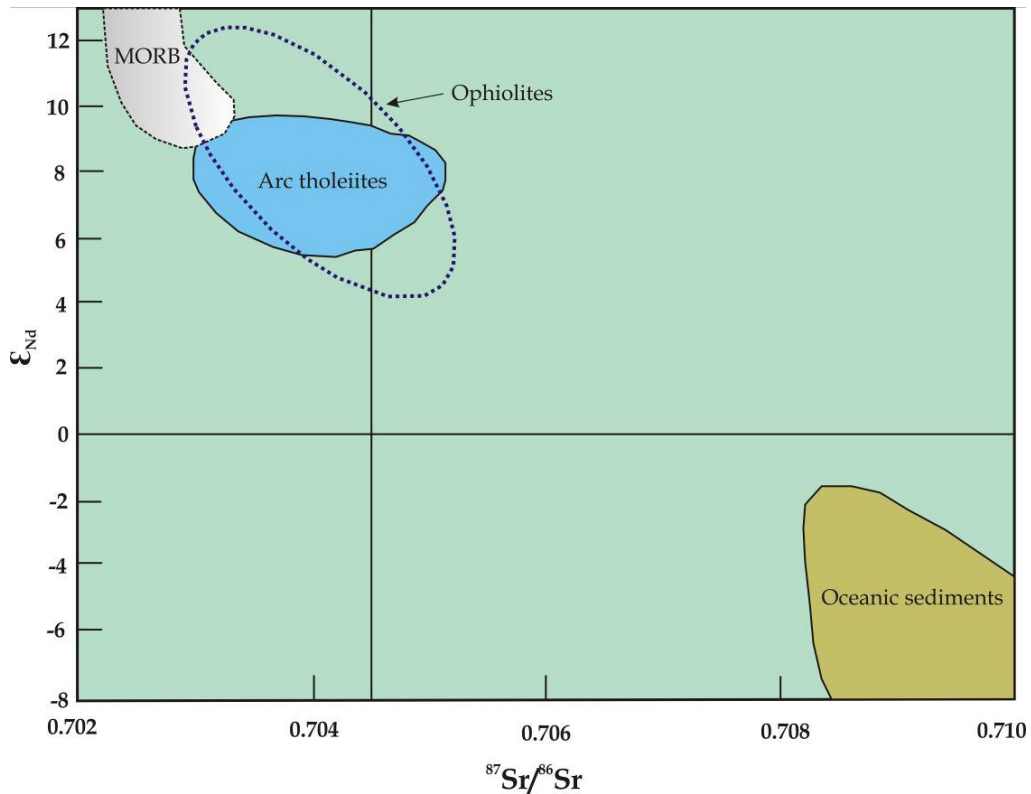


Fig. 1.7 Comparative ϵ_{Nd} vs $^{87}Sr/^{86}Sr$ plot for MORB, SSZ ophiolites, island arc tholeiites and oceanic sediments (modified after Wakabayashi et al., 2010)

The slab introduces chemically different materials to the mantle. It contains older oceanic lithospheric mantle altered oceanic crust, pelagic and terrigenous sediments. It is believed that slab which gets chemically modified by subduction processes, such as for dehydration and melting, creates delaminated mafic lower arc crust. This mafic arc crust found in deeper part of mantle plays a significant role in the evolution of mantle (Tatsumi, 2005). Therefore, it is necessary to understand the chemistry of the mantle wedge through the island arc lavas that are little contaminated by the oceanic crust. Composition of arc magmas are mainly controlled by three sources: subducted oceanic lithosphere, subducted sediments and the mantle wedge overlying the slab. In general, arc magmas are fractionated, porphyritic and wet compared to mid-ocean ridge or hot spot magmas (Tatsumi and Eggins, 1995). Their petrology also depends on crustal thickness through which they pass through.

In general, the chemistry of island arc lavas has the following major characteristics that reflect the nature of the mantle wedge from which they are derived.

- I) Enrichments in fluid soluble trace elements (K, Rb, Cs, Ba, Pb, Sr, LREE) as compared with MORB.
- II) Be and Th are relatively enriched in arc basalts, but believed to be relatively insoluble in H₂O-rich fluids that suggest sediment melting.
- III) Depleted in high field strength elements (Ta, Nb, Zr, Ti)
- IV) Mostly basaltic to basaltic andesite in composition.

- V) Sr and Nd isotopic ratios are highly variable ranging from MORB to highly enriched compositions (Fig. 1.9)

The slab chemistry plays an important role in the evolution of arc magmas and the mantle as a whole. Age of the slab is a crucial factor that controls its chemistry older slabs carries lots of fluids and sediments and subducts to greater depths affecting the depth and degree of partial melting in the mantle wedge. Initially, when a cold subducting slab comes in contact with hot mantle wedge, dehydration takes place and fluids from slab migrate to the mantle. In second stage, sediments also move with fluids to mantle wedge and lastly when the slab reaches greater depths it melts. On the basis of fluid transport, Johnson et al. (1994) proposed that the arc magmas contain up to 6% water compared to MORB and hot spot tholeiites which contain 0.4 % and 1% of water respectively.

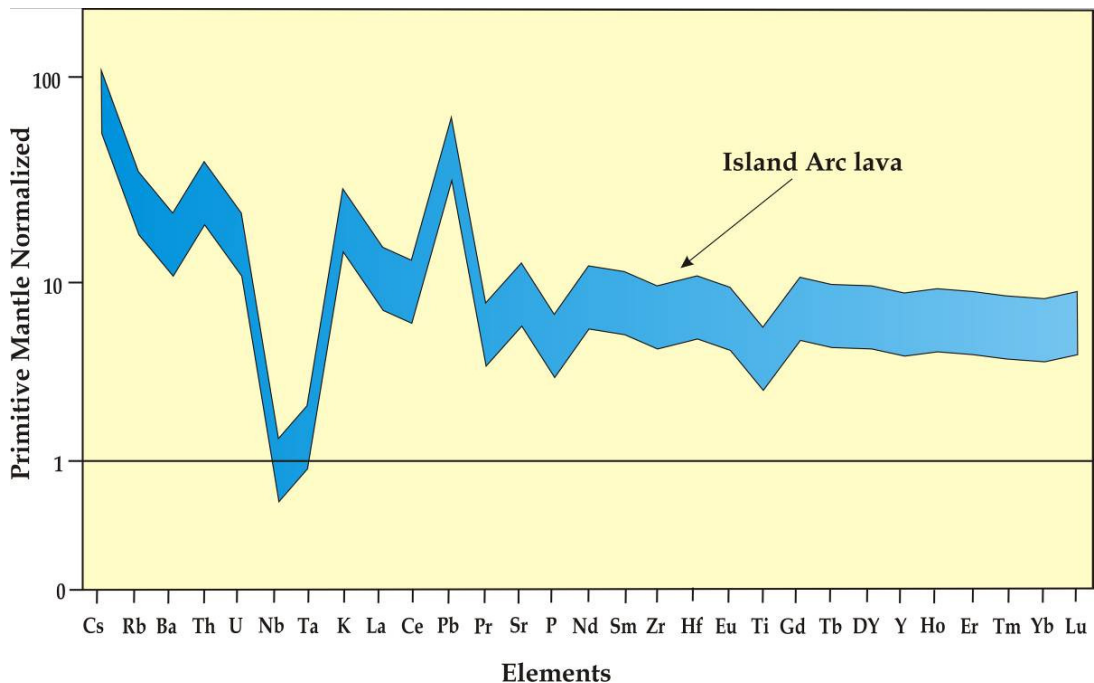


Fig. 1.8 Primitive mantle normalized trace elements patterns for arc lavas

As stated earlier, the lithospheric slab is the central for modification for the chemical changes in the mantle. But still the chemical characterization of slab materials (sediments and rocks) is not fully understood. Interestingly the mud volcanoes that occur in forearc area appear to serve as a window to the subducting slab, because it carries high pressurized fluids and solid materials from the subducting slab at depth. Therefore chemical characterization of these material emitted by these unique vents can help answer some of questions pertaining to the chemistry of the slab.

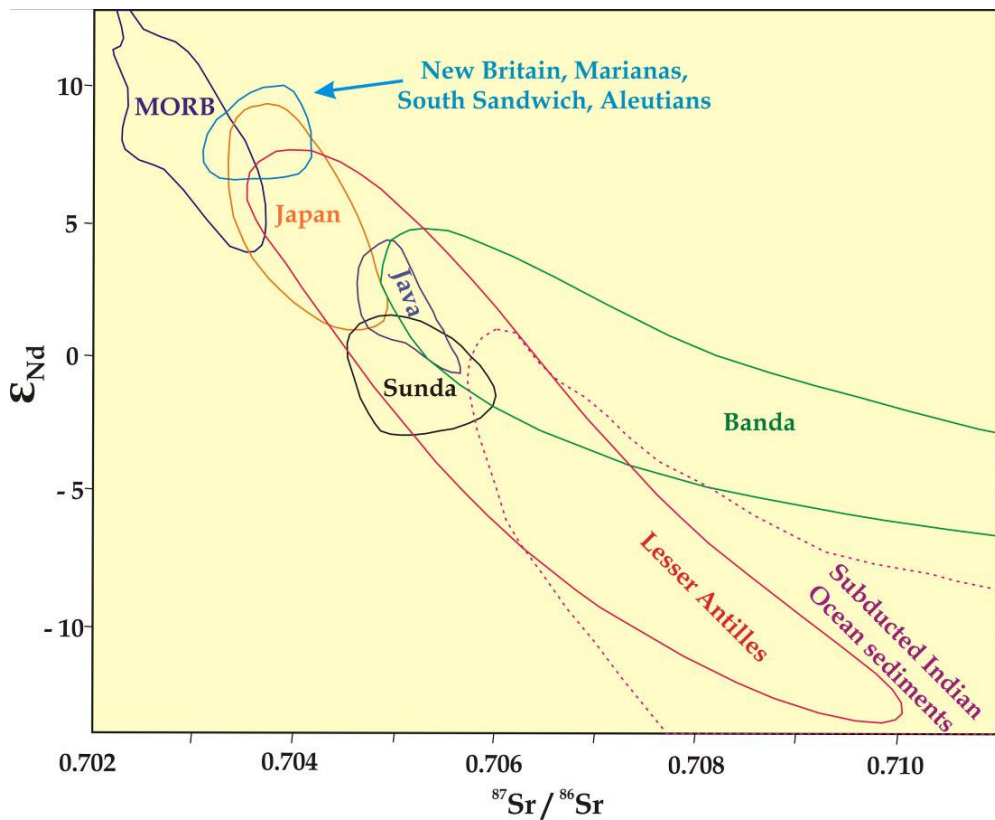


Fig. 1.9 Sr and Nd isotopic variations plot for various arc magmatism and Indian Ocean subducted sediments (modified after Wilson 1989)

In spite of numerous studies on subduction zone processes several important questions pertaining to the chemistry of various components of

these zones remain unanswered. Some of these, as listed below, form the basis of this thesis work.

- I) What is the chemistry of subducting materials and how does it influence the arc volcanism?
- II) Where is the exact location of the source of the magma for the arc lavas and how much of melting required generated these?

1.4 The Andaman Subduction Zone

The Andaman subduction zone (Fig. 1.10) is one of the most seismically active and young subduction zones of the globe. The Andaman arc trench system in north-east Indian Ocean extends from Myanmar in the north to Indonesia in the south. It is the result of subduction of NE-moving Indian Plate beneath the Burmese Plate. This subduction process gave rise to the Indonesian Arc system that also includes the Andaman and Nicobar Islands and contains more than 100 volcanoes. The Barren Island volcano (12.29°N; 93.85°E) located in the Andaman Sea in the northernmost active center of this arc system and is the only active volcano of India.

The timing of initiation of the Andaman subduction zone has been always in debate. About the timing of initiation two schools of thoughts exist. The first school (Acharyya et al., 1990; Sengupta et al., 1990) argues that the present subduction, all around the western Sunda arc, began during Miocene times and onland emplacement of ophiolites took place during terminal collision in Oligocene. In their model, a second trench further east of the present trench with a protocontinent was assumed. Also, Cretaceous ophiolites and Eocene sediments were considered as a part of

this accretionary prism related to second subduction margin and believed to have subsequently emplaced as east to west propagating allochthonous nappe sheets on present subduction margin. The second school of thought is based on the presence of melange and the highly deformed sediments. These authors suggest that the onset of subduction took place during Late Cretaceous times, after the early Cretaceous break-up of the Gondwanaland (Curry and Moore, 1974; Karig et al., 1979) or from Late Palaeozoic (Hamilton, 1979; McCourt et al., 1996).

Srivastava et al. (2004) suggested that the Andaman ophiolites are geochemically similar to N-MORB. Pal et al. (2003) and Pal (2011) gave models for the geodynamic evolution of the Andaman Islands and for the petrogenesis of the Andaman ophiolites. Apart from these there have several other important studies on these rocks (Shastri et al., 2001, Searle & Pederson, 2001, Ray, 1987, Acharyya, 2007, Pal and Bhattacharya, 2010 etc. references), however, no isotopic study has been carried out so far.

Unlike the ophiolites the mineralogical, petrological, geochronological and geochemical aspects of the arc lavas of the Andaman subduction zone have been studied by several workers [Alam et al., (2004), Luhr and Halder (2004), Chandrashekaram et al., (2009), Sheth et al., (2009, 2010 and 2011), Pal et al., (2010), Banerjee (2010), Streck et al., (2010) Awasthi et al., (2010), Ray et al., (2011)]. However, these studies with their limited datasets (very little isotopic data) have not been to answer many of the most important questions pertaining to the evolution of these lavas (Barren Island and Narcondam). In particular, they fail to address the role of the Andaman slab in the generation of arc magmas (type and amount of contribution?), depth and degree of melting of the mantle wedge and geochemical and isotopic evolution of the magma through time.

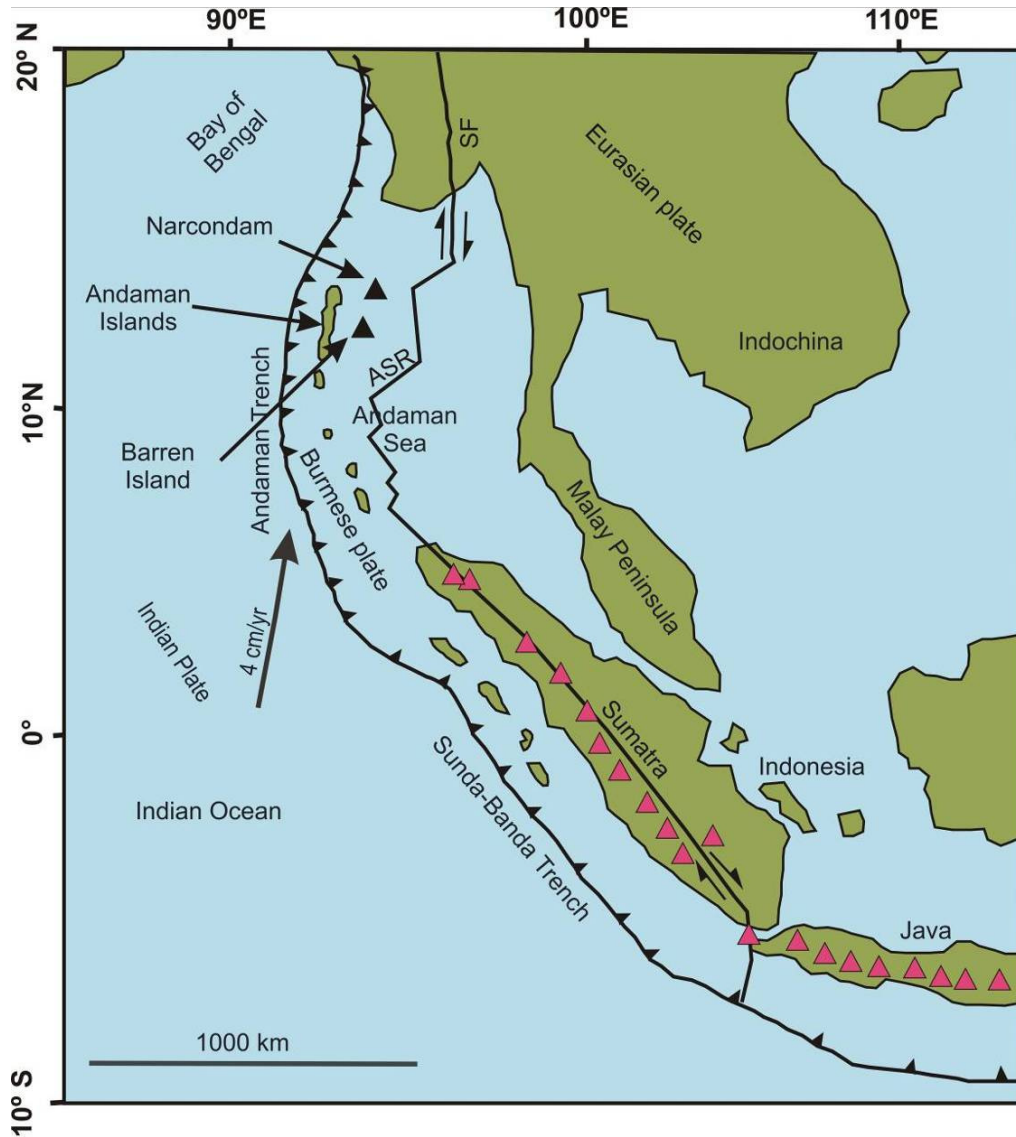


Fig. 1.10 Map of Southeast Asia and northeastern Indian Ocean showing major geological and tectonic features. ASR: Andaman Sea ridge; SF: Saigang Fault.

1.5 Objectives and significance

The Andaman subduction zone is one of the few accretionary convergent margins where all the important components of a convergent margin are exposed and are available for scientific scrutiny. These include a trench, a outer arc accretionary prism, a forearc, a volcanic arc, a back arc basin etc. (Fig 1.11).

In an effort to understand the subduction zone processes, crust – mantle interaction and origin and evolution of arc magmas a comprehensive geochemical study was undertaken in this thesis. The specific objectives of this study are:

- I) to understand the origin and evolution of subducting fluids through their chemistry.
- II) to characterized subducting solid materials and understand their impact on the chemical evolution of the mantle wedge
- III) to characterize the chemistry and nature of subduction of ophiolites and understand their evolution
- IV) to characterize the type and history of arc volcanism (on Barren Island)
- V) to decipher the the nature and composition of lava flows and magmatic differentiation processes (for the Barren island lavas)
- VI) to determine the degree of partial melting and the depth of magma generation
- VII) to understand the chemical evolution of the mantle source for Barren Island magmas

To answer the questions pertaining to the slab chemistry efficiently focus has been given in this work on the study of the fluids and solid materials emitted from the mud volcanoes located on the accretionary prism. To understand the evolution of the arc mantle melting in the

mantle wedge we focussed our study on the Barren Island volcano. This volcano is young, mafic and is believed to lie on a young lithosphere, and therefore the lavas from this volcano can be considered to represent a source in the Andaman mantle wedge that is at very initial stages of chemical modifications resulting from mixing with crustal material derived from the slab. Hence geochemical and isotopic studies of these lavas

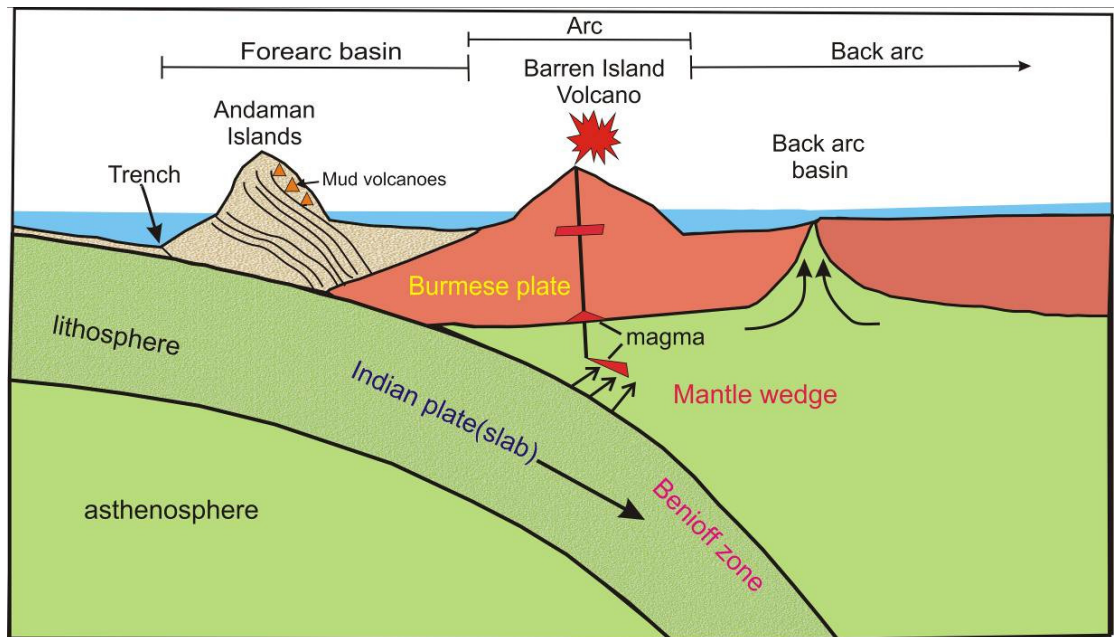


Fig. 1.11 A schematic diagram showing various components of the Andaman subduction zone (Based on author's interpretation)

can reveal a great deal about the nature of interactions of the mantle wedge and slab derived materials. This work is one of the few studies where the chemical evolution of the mantle is studied at the subduction zone with a focus on the chemical characterization of subducting material at depth. This is also the first study on the Barren Island volcano where an extensive sampling has been done to understand the evolution of the volcano since its emergence for the sea surface.

Chapter 2

Geology and Earlier work

Andaman and Nicobar Islands of India are located between 6° N and 14° N latitudes in the northeast Indian Ocean. This archipelago consists of 319 islands (Bhoothalingam, 1972) in which the Andaman group of islands comprises 258 and the Nicobar group comprises 61 islands. A channel at 10° N latitude, which is popularly known as the “Ten Degree Channel”, separates these islands. The archipelago forms a dividing line between the Bay of Bengal in the west and the Andaman Sea in the east. These islands are part of an accretionary prism or wedge which forms the outer arc ridge of the Andaman subduction zone (northernmost section of the Sunda-Banda subduction zone) (Fig. 1.10). This accretionary wedge is a result of the northward but oblique subduction of Indian plate below the Burmese microplate at a rate of 4-6 cm/year along the Andaman-Java Trench (Curry, 2005). This chain of islands, more than 4000 km long, extends from the Myanmar Arakan-Yoma coast in the north down to Sumatra and Java in the south. Sewell (1925) suggested that the Andaman-Nicobar Ridge had drifted toward the west away from the South-East Asian mainland, and had thus formed a pronounced curve with its apex in the region of ‘Little Andaman’ Island.

The first accounts on the geology and origin of the Andaman - Nicobar Ridge was given in mid nineteenth century. However these were localized restricted to an island or a part of it and was in the form of preliminary reports on lithology. Helfer (1840) was the first worker to carry out geological field work on these islands, in 1840. Rink (1847) suggested that this ridge had been formed of sediments uplifted from the deep ocean floor, and consisted ‘partly of those stratified deposits which occupied the level bottom of the sea’, an early statement of the modern

hypothesis of uplift and incorporation of sea floor deposits into an accretionary prism. He also divided the rocks of Nicobar Islands into three groups, viz., Brown Coal Formation, Plutonic Rocks and Older Alluvium, in ascending order of age. During the years 1850 to 1864, several geologists presented preliminary reports on lithology and petrography of some islands (Oldham 1885). Hochstetter (1869), a geologist from Austria pointed out that the same ridge extended southward as the outer arc ridge off Sumatra and Java after reorganization of two sedimentary units in Java. Ball (1870) was the first to describe the geology of the area around Port-Blair.

2.1 Geology of Andaman and Nicobar Islands

The tectonic evolution of Andaman and Nicobar Islands has been modelled based on three components these are i) tectonic features recorded from the Sea (Curry and Moore, et al., 1982). ii) seismic records (Dasgupta and Mukhopadhyay, 1993) and iii) regional correlation of tectonic elements of the eastern part of the Himalaya (Sengupta et al., 1990). The temporal history of subduction in this part (central part of Sunda arc) has been a matter of debate. There exist two schools of thoughts. The first school (Acharyya et al., 1990; Sengupta et al., 1990) argues that the present subduction, all around the western Sunda arc, began during Miocene times and onland emplacement of ophiolites took place during terminal collision in Oligocene. In their model, a second trench further east of the present trench with a protocontinent was assumed. Also, Cretaceous ophiolites and Eocene sediments were considered as a part of this accretionary prism related to second subduction margin and believed to have subsequently emplaced as east to west propagating allochthonous nappe sheets on present subduction margin. The second school of thought is based on the presence of melange and the highly deformed sediments. These authors suggest that the onset

of subduction took place during Late Cretaceous times, after the early Cretaceous break-up of the Gondwanaland (Curry and Moore, 1974; Karig et al., 1979) or from Late Palaeozoic (Hamilton, 1979; McCourt et al., 1996).

The currently accepted stratigraphy of the Andaman Islands (Table 2.1) is partly based on the earliest lithological mapping done by Oldham (1885). Who first divided the rocks of Andaman into two parts; older Port Blair series and younger Archipelago series, separated by volcanic rocks and serpentines, later recognized as an ophiolites sequence. In 1960s paleontological constraints were used to identify the Paleocene-Neogene lithostratigraphic units and subsequently in last five decades the stratigraphy has been modified and formation names have been changed. Allen et al. (2007) divided the Andaman Island stratigraphy into four groups (Table 2.1). In this thesis I have modified this by introducing a new group at top, the Island Arc Group (Table 2.1). Accordingly, the present stratigraphy now comprises five units, which, in ascending order, are the ophiolites Group, the Mithakhari Group, the Andaman Flysch Group, The Archipelago Group and the Island Arc Group (Table 2.1).

2.1.1 The Ophiolite Group

The Ophiolite Group forms the basement of the Andaman Islands, a part of the Indo-Burma accretionary complex. It contains numerous north-south trending slices of Cretaceous-Palaeocene ophiolites. The group is made up of a plutonic complex, a volcanic sequence and pelagic sedimentary rocks (Fig. 2.1). Due to thick vegetation and soil, continuous ophiolite sections are rare. Pal and Bhattacharya (2010) developed regional ophiolites stratigraphy on the basis of local contact relationships. They reported that the lower part of the group (80% of the total outcrop) comprises foliated and highly serpentinitized peridotite. The upper part

Table 2.1 Simplified stratigraphy of Andaman Island (modified after Allen et al., 2007)

Approximate Age	Group	Formation	Lithology
Pliocene to Quaternary	Island Arc Group		Subaerial lava flows and volcanoclastics of Narcondam Island and Barren Island Volcanoes
Miocene to Pliocene	Archipelago Group		Cross-stratified and graded sandstones, silty mudstone and limestone marls, and chalky limestones
Oligocene-Late Eocene (?)	Andaman Flysch Group (formerly Port Blair Group)		Bouma sequences, sandstone-shale and mudstones
		Namunagarh Grit	Pebbly and coarse to fine grained volcanoclastic sandstones and grits
Early to Middle Eocene (?)	Mithakhari Group (formerly Baratang and Port Meadow groups)	Hope Town Conglomerate	Interstratified massive and graded polymict conglomerates, massive cross-stratified and graded sandstone, shales and thin coals
		Lipa Black Shale	Pyritiferous black Shale
Late Cretaceous to Paleocene (?)	Ophiolite Group		Pillow lava, basalt, gabbro, pyroxinite, hornblende, serpentinite, andesite, diorite, plagiogranite, rhyolite, serpentinitized hornblende, pyroxinite, and pelagic sediments, radiolarian chert and hematitic mudstones

comprises a layered sequence of ultramafic–mafic rocks, an intrusive section of homogeneous gabbro–plagiogranite–diorite–dolerite and an extrusive section of boninite and tholeiitic basalt lavas (Fig. 2.1). Although ophiolite occurrences are reported from almost all the major Andaman Islands, the greatest numbers of ophiolites slices are present in South Andaman island, where the largest slices range in thickness from 300 to 750 m, but the largest volume of mantle sequences are exposed in Middle and North Andaman Islands (Pal et al., 2003). On the basis of lithology Pal (2011) divided the Ophiolite Group into five parts. In present study we would be following his classification. Fig 2.1 presents the geological map of the Andaman Island and a litholog of the Ophiolites Group. In the following subsections I discuss various units of the Ophiolite Group in details.

Mantle tectonite

This section contains foliated peridotites (maximum thickness ~ 750 m, in North Andaman) which are serpentinized lherzolites and harzburgites assemblage (Fig. 2.2a). It locally contains subconcordant lenses and pods (2 cm to 4 m long) of serpentinized dunite. The foliated peridotites, typical of many ophiolites, are also described here as tectonite (e.g., Gass, 1990). Lherzolite usually occurs in the lower part of this unit and is less abundant than harzburgite. Chromitite pods are restricted to the upper part of the tectonite near the contact with the layered sequence. Most of the chromitites form elliptical pods (up to 11 m by 3.5 m), and enveloped by a thin dunite rim within the host harzburgites. These peridotites as well as the dunite and chromitite pods represent the mantle rocks of the Andaman ophiolites (Pal, 2011).

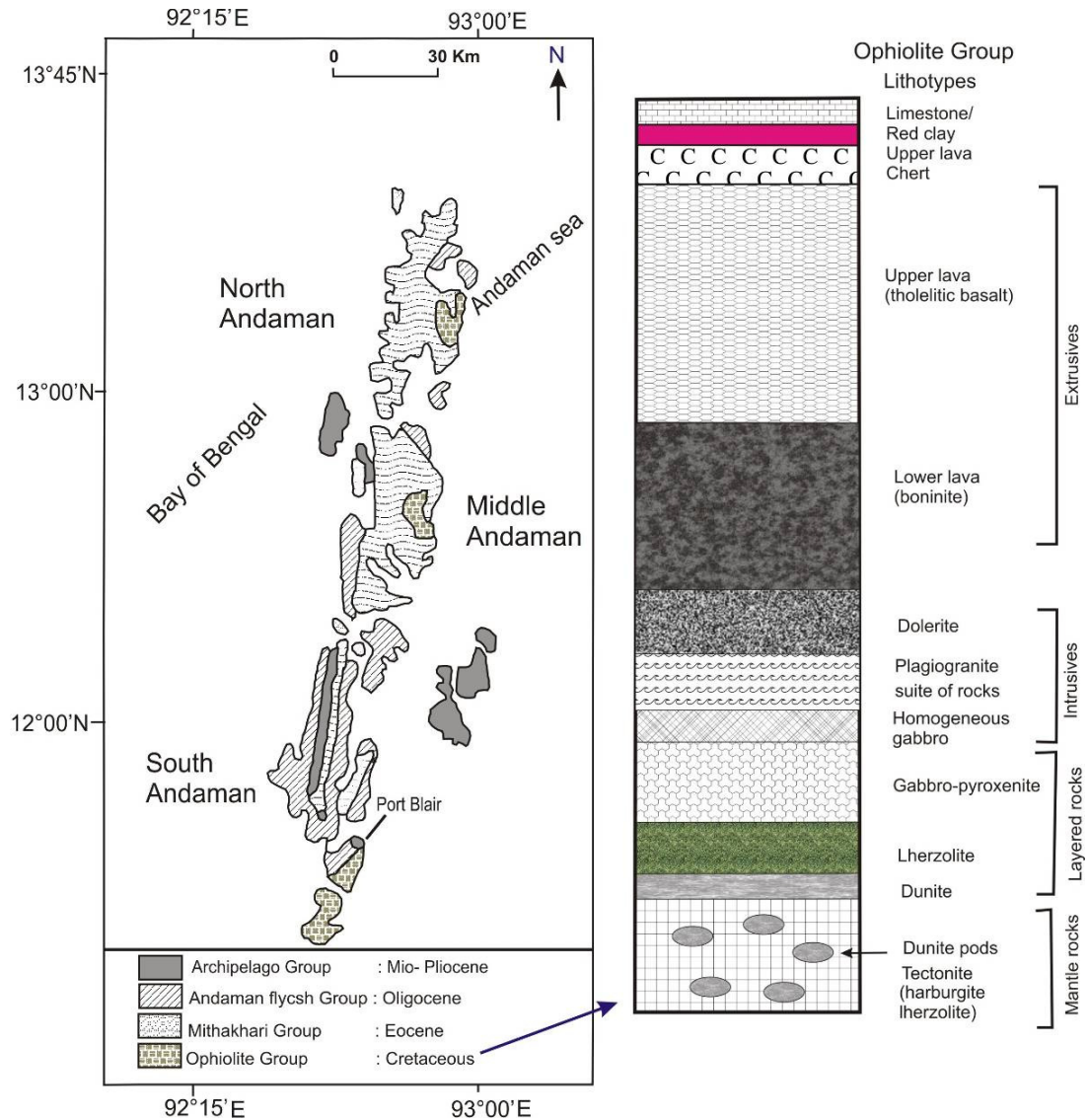


Fig.2.1 A geological map of the Andaman Islands and a schematic section of the Ophiolite Group displaying its different members (modified after Pal 2011)

Layered ultramafic-mafic sequence

The layered ultramafic-mafic sections (maximum thickness ~ 80 m, on South Andaman) are made up of mantle and crustal plutonic rocks. The mantle sequence consists of layered serpentinized dunite and lherzolites, whereas the crustal section constitutes plutonic rocks and extrusives such as layered gabbros and pyroxinites (Fig. 2.1; Fig. 2.2 b, c).

In the Kodiaghat section (South Andaman), mantle tectonite is overlain by layered gabbro–pyroxenite. The gabbro–pyroxenite unit here shows repetitive and undeformed parallel layers of alternating olivine gabbro or norite and pyroxenite that vary in thickness from 2 to 40 cm (Pal, 2011).

Intrusive units

These intrusive units of the Ophiolites Group are composed by a suite of homogeneous gabbro, plagiogranite, diorite and dolerite assemblage (Fig. 2.1 and 2.2). These intrusive rocks (maximum thickness ~ 60 m, in South Andaman) are intermingled with, and locally intrude, the layered ultramafic–mafic rocks. Unlike normal oceanic crust ophiolites the ophiolites of Andamans do not contain sheeted dykes in the sequence. However, a few thin dykes of basalt and dolerite are found intruding into the plagiogranite-diorite unit in South Andaman (Fig. 2.3d).

Extrusive lavas

The uppermost part of the ophiolite is a thick sequence of lavas (maximum thickness ~ 500 m, in South Andaman) that occur as two tectonic slices. One slice, more frequent, consists of dark-colored pillow lavas of basaltic composition (Fig. 2.2e and f) and consistently occurs along the eastern coast of the island and is called East coast volcanics (Ray, 1987).

Lava flows compositionally are of two types, dacitic to andesitic basalts and tholeiitic basalts (Ray et al., 1988; Vohra et al., 1989). These rocks are plagioclase phyric and plagioclase-pyroxene phyric with minor quartz set in a ground mass of epidote-chlorite-glass (Pal et al., 2003; Acharyya, 2007). Tholeiitic pillow basalts occupy a major part of the Ophiolite Group in south Andaman Islands. The first slice is more abundant than the second.



Fig. 2.2 Field photographs of various members of the ophiolite group a) harzburgite, South Andaman b) pyroxinite and serpentine out crop, Bachrapahar, South Andaman c) gabbro with tachylite vein, Kodyaghat, South Andaman d) dolerite dike along with plagiogranite outcrop, Mundapahar, South Andaman e) outcrop of pillow lavas, Carbon cove, South Andaman f) pillow lava, Carbon cove, south Andaman

Sedimentary cover

The topmost portion of the ophiolite sequence is composed of sediments of heterogeneous origin, both compact and non-lithified, with remains of radiolarians and other planktons. It can be tectono-stratigraphically divided into oceano-pelagic sediments, ophiolite derived

clastics, rhythmites and olistostromal argillaceous sediments (Roy et al., 1988). The intercalated tuffaceous sediments are thought to be derived from sub oceanic transport by turbidite currents. The oceano-pelagic sediments consist of argillites, cherty limestone, clay stone and fossiliferous limestone. These sediments are directly associated with the pillow volcanics, and are richly enriched with foraminiferal assemblage of cretaceous to Eocene age, the earlier one being the predominant (Roy et al., 1988).

Sediments and basic rocks of Andaman have been subjected to metamorphic changes, in conditions of intense thrusting and deformation, to green schist to amphibolite facies. These are widely distributed along the thrust contact between ophiolites and trench slope sediments (Pal et al., 2003) as discontinuous patches. Metasediments are represented by quartzites, phyllites and quartz-mica schists while metabasics are represented by amphibolite bearing chlorite-epidote-carbonate schists.

There are a few studies which deal the geochemistry of Andaman ophiolites. Shastry et al. (2001) and Srivastava et al. (2004) studied mafic rocks of south Andaman ophiolite suite and suggested that the rocks are enriched in Fe- Ti. However based on Ti oxide Srivastava et al. (2004) suggested that the Andaman ophiolites are geochemically similar to N-MORB. This interpretation is supported by Pedersen et al. (2010) based on trace elements studies of pillow lavas from carbyn's cove and basaltic dyke from Chiriya Tapu of south Andaman.

The age of Andaman ophiolites and the timing of their obduction remain controversial. In a couple of studies recently, two independent groups of researchers, dated zircon from plagiogranites of the Ophiolite Group from south Andaman by U-Pb dating method, and suggested that

the formation age of these could not have been younger than ~ 95 Ma (Srinivasa Sarma et al., 2010, Pedersen et al., 2010). These workers also suggested that the new age of Andaman ophiolites is similar to that of the Oman and Troodos, Cyprus ophiolites and that it extends the range of Late Cretaceous ophiolite formation along the Tethyan suture zones from the Mediterranean to the Andaman Sea. The similarity in age between the Troodos, the Oman and now the Andaman ophiolite seems best explained by a suprasubduction zone origin (Pal, 2011).

2.1.2 The Mithakhari Group

Karunakaran (1968) was the first geologist who introduced the term Mithakhari Group. The thickness of this thick sedimentary unit is ~ 1.4 km, and is divided into three formations by Ray (1982): i) the Lipa Black Shale ii) the Hope town conglomerate iii) the Namunagarh Grit (Table 2.1). The Lipa Black Shale is a minor unit with very limited exposures. The rocks in this group consist of immature gravels, coarse to fine sandstone and pyroclastic sandstones, polymictic conglomerate and thin beds shale, mudstone and coal. Pal et al. (2003) recognized eight different lithofacies in these formations on the basis of the bed geometry and recorded sedimentary structures. These lithofacies include disorganized and graded matrix supported conglomerate, graded pebbly sandstone, massive and thick bedded sandstone, plane laminated and cross-stratified sandstones, interbedded sandstone and mudstone, massive to faintly laminated shale and interbedded shale and coal. The conglomerates contain clasts of vein quartz, lithic shale fragments, limestone, sandstone, chert, ultramafic rocks, porcellinite and basalt. Sandstone units are massive, thickly bedded with some plane-laminated and cross-stratified facies. The shale facies consist of massive to laminated pyritiferous shale interbedded with silt/fine sandstone. Apart from above a number of mud volcanoes are also

reported in the Middle and North Andaman Islands in shale dominated facies of the Mithakhari Group.

2.1.3 The Andaman Flysch Group

The rocks of Andaman Flysch along with the Archipelago Group are deposited in a forearc environment. The Andaman Flysch Group overlies the Mithakhari and underlies the Archipelago Groups (Fig. 2.1). The Andaman Flysch is a siliciclastic turbidite sequence deposited on a submarine fan. The best and most completely documented exposures are found on South Andaman, at Corbyn's Cove, where outcrops of steep, westerly dipping beds are seen adjacent to the pillow basalt of the Ophiolite Group, although the nature of the contact is uncertain. The overall thickness is not well defined, with estimates varying from 750 m (Roy, 1983) to 3000 m (Pal et al., 2003). Individual sandstone beds can be traced along strike for distances of several kilometers, but the total thickness is only 250–300 m. Several sedimentary structures have been identified in sandstone beds including flute casts, groove casts, and current bedding. On the basis of the orientation of flute casts at the base of overturned sandstone beds near Corbyn's Cove southward-directed paleocurrents are suggested (Pal et al., 2003). The relationship between the turbidites and underlying lithostratigraphic units is unclear. Onlap of the Andaman Flysch with the Mithakhari Group has been reported (Chakraborty and Pal, 2001), but no supporting evidence was found in this study. However, there is a marked change in lithology and provenance with up to 50% quartz in the Andaman Flysch in contrast to the relatively quartz-free Mithakhari Group (Pal et al., 2003). Lithic fragments in the Andaman Flysch range from micaceous metamorphic clasts diagnostic of continental sources to cherts, basalts, and weathered volcanic glass consistent with derivation from volcanic arc and ophiolite sources.

2.1.4 The Archipelago Group

The Archipelago Group represents the topmost stratigraphic unit of the Andaman accretionary prism. The deposition of this unit was believed to have taken place mostly in a slope environment (Roy, 1983). The lower members of this group comprise basal conglomerates and sandstones, overlain by calcareous arenites of the Strait Formation. This is followed by chalk and limestone with some argillaceous limestones and shale, described as the Melville Limestone (Shell Limestone) Formation (Pal et al., 2005). These sedimentary rocks most likely covered most of the Andamans, but recent uplift and erosion means that today only small patches can be found on the main islands, with most exposures confined to Havelock Island and associated smaller islands to the east of South Andaman in Richie's Archipelago. On the basis of Radiolarian and planktonic foraminiferas and calcareous nano fossils from Jhon Lawrence Island, Singh et al. (2000) reported depositional ages for this group in the range of 18.3-15.6 Ma, but Pal et al. (2005) has argued for a younger range.

2.1.5 Island Arc Group

The Island Arc Group, classified for the first time through this work, represents the topmost stratigraphic unit of Andaman Islands. The group consists of subaerial lava flows and volcanoclastic materials of extinct Narcondam Island and active Barren Island volcanoes. These volcanoes lie in the chain of inner arc volcanoes extending from Burma to Indonesia (Fig. 1.10). Well constrained radiometric ages are not available for the rocks of these islands; however a couple of recent studies by Awasthi et al. (2010) and Streck et al. (2011) provided rough estimates. On the basis of C-14 ages of inorganic carbon in ash layers sampled in a marine sediment core, Awasthi et al. (2010) suggest the prehistoric activities of the Barren Island volcano goes back to at least 72 ka, that its caldera may have formed earlier to 10 ka. Based on ^{40}Ar - ^{39}Ar dating Streck et al. (2011)

reported two dates of 33 ± 70 ka and 32 ± 88 ka (2σ) for two lava samples from Barren Island, however very high analytical uncertainties make this unusable. The eruptions on Narcondam Island are found to be much older with two samples plateau ages of 548 ± 22 ka and 707 ± 170 ka (Streck et al., 2011). Based on these data the authors suggest that the cone building activity on the volcano is younger than 700 ka.

Narcondam Volcano

The Narcondam Volcano forms a small island, ~ 3.5 km across and 710 m high. On the basis of depth contours of the office of Naval Research (2002) the submarine and subaerial volumes of the island are 95 km^3 and 4 km^3 respectively. The latest eruption of the volcano is believed to have occurred in Holocene but one of the subaerial lava flows has been dated to as old as 550 ka (Streck et al., 2011). The Narcondam volcanics are represented by i) porphyritic dacite, ii) amphibole-andesite and iii) andesite. Dacite contains plagioclase, hornblende, biotite and quartz with minor apatite as phenocrysts set in a groundmass comprising plagioclase, hornblende, opaque minerals (magnetite, ilmenite) and glass (Pal et al., 2007). These workers report presence of amphibole, plagioclase and cummingtonite as phenocrysts as well as groundmass phases along with minor quartz and apatite in amphibole-andesites. In contrast, in andesite, calcic plagioclase, olivine, orthopyroxene (hypersthene, bronzite) and clinopyroxene (augite, diopside) represent both phenocrysts and groundmass phases.

Pal et al. (2007) reported the lavas of Narcondam Island are andesite to dacite that display the evidence for interplay of two types of magmas. They suggested the lavas are mixing product of rhyolitic and basaltic magmas. Streck et al. (2011) suggested based on primitive mantle normalized trace element contents the Narcondam lavas are subduction

origin magmas which show typical signature depletions of Nb, Ta and Ti and enrichments in K and Pb, with lesser enrichment of Sr. They also stated the higher Sr and Pb isotopic values of Narcondam lavas are due to crustal contamination.

Barren Island Volcano

The first recorded observation of Barren Island was by Van Lineshooter in 1595 that hasn't mentioned the volcanic character of this island and reported it as one of many emergent islands within the Andaman Sea. First volcanic behaviour of this island was reported by Lieutenant Colebrook in 1787 after he noticed column of smoke ascending from the summit (Shanker et al., 2001). The geologists who had established the basic stratigraphic framework by early survey of this island were Mallet (1895) and Ball (1888) from Geological Survey of India (GSI). They reviewed the history of observations of eruption of Barren Island and reported that, the first known landing on the island by a westerner was by Captain Archibald Blair in 1789, after which Port Blair on South Andaman Island has been named (Curry, 2005). The first short petrography studies were published in 1924 by Washington, who collected five samples from GSI. He identified those samples as basalt and augite bearing andesite (Shanker et al., 2001). Halder (1989, 1991) and Halder et al (1992a, b, c, 1994, 1999) described petrology, chemistry of the recent volcanics and eruptive history of the volcano.

Apart from geological studies, geophysical studies were also done in and around Barren Island. Dasgupta and Mukhopadhyay (1993) mapped this island using seismic methods and described the tectonic framework of the island and its delineation by a set of faults, such as the west Andaman fault connecting to the semangko faults in Sumatra. Banarjee et al. (1998) carried out magnetic measurements and ocean-

bottom magnetometer surveys around Barren Island after a volcanic eruption in 1991. From the spectral analysis of magnetic data, the depth obtained to the Curie isotherm is about 3-5 km on the eastern side of Barren Island, whereas on the western side it falls sharply to 12 km. suggesting a high heat flow on the eastern side of Barren Island associated with volcanism. They believed that such a sharp difference in the heat flow could be related to a structural barrier aligned in the north-south direction that prevented volcanic material flowing towards the west. The worker also suggested that there existed a partial melting zone at a depth of 17-27 km.

Since ground monitoring is difficult on the Barren Island Volcano because of its rough terrain, geophysicists used Remote Sensing Temporal Monitoring (RSTM) tool for monitoring the volcanism. First remote sensing on the island was done by Bhattacharya et al (1993), who reported the changing size and position of erupting vents, identified westward flow of lava on digitally enhanced TM images, delineated and mapped lava flows of different eruptive phases of 1991 eruptions. He also reported that the 1991 volcanic activity started around March 25, 1991 and appeared to end by late December 1991. On the basis of nearly 20 TM imagery acquired in between 1986-1993, Reddy and Bhattacharya (1997) carried out comparative studies of pre- and post-eruptions landforms on Barren Island. He reported four significant aspects of the volcano which were brought out by TM images viz. : i) geomorphic changes in the form of a newly formed crater, which is 500 m across, ii) seaward extension of the land due to the deposition of the recent lava flows, iii) regrowth of vegetation burnt due to the eruption seen clearly (in bluish tint) on the southern flanks of volcano, and iv) delineation of recent lava flows (erupted in 1991) based on their sharp tonal contrast with the older flows. The 1991 lava flows have lighter tones on the FCC image (RGB=7, 5, 4)

whereas the older flows erupted during 1789-1803 (second episode) have distinct darker tones on all the pre-eruption images. Based on these observations and in conjunction with the geochemical analyses on lava samples Halder et al. (1992) it can be inferred that the recent flows are mostly basaltic andesites, whereas the older flows are high alumina olivine tholeiites.

As a part of the present study we have carried out field observations on Barren Island and reported several new features including new lava flows. We also have prepared a new geological map of the island, which is more accurate than the existing ones. Detailed descriptions of these studies are given in a separate chapter called the “volcanological studies of Barren Island” (Chapter 3).

2.2 Structure of the Andaman and Nicobar Islands

The Andaman and Nicobar ridge is the main feature of the Andaman forearc, which is the result of oblique subduction of Indian plate beneath the Burmese plate. The main elements of the forearc are the accretionary prism and outer arc ridge, a series of forearc basins and major N-S faults. The accretionary prism is an imbricate stack of fault slices and folds consisting of ophiolites and sediments (Roy, 1983). The western, outer slope of the accretionary prism is very steep, rising from depths of 1500–2000 m within a distance of 30 km. There is a difference in the short wavelength morphology between the western and eastern portions of the accretionary prism. The outer portion consists of a series of faulted anticlines and synclines with amplitudes of a few 100 to ~ 1000 m and widths of 5–15 km resulting from ongoing deformation of the sediments (Curry, 2005). The inner portion is smoother with lower slopes and forms a strong backstop. The width of the deforming portion of the accretionary prism narrows from 80 to 100 km in the south to about 40 km between 10°

N and 11°30' N. It remains at about 40 km to ~ 14°40' N. North of there, the inner trench wall becomes a single steep slope up to the Myanmar shelf (Billham, 2005). The eastern edge of the outer arc ridge is fault bounded and north of the Nicobar Islands, a forearc basin is located immediately to the east. A deep gravity low with very steep gradients lies directly over the forearc basin (Cochran, 2010). The West Andaman Fault (WAF) and/or the Seulimeum strand of the Sumatra Fault System form the boundary between the Burma and Sunda plates south of the Andaman spreading centre. The WAF is the most prominent morphologic feature of the Andaman Sea and divides the sea into a shallow forearc and a deeper backarc region (Curry et al., 1979). The Diligent Fault runs through the forearc basin east of Little Andaman Island (Fig 2.3). Although it has the general appearance of a normal fault, multichannel seismic data show that it is a compressional feature that probably resulted from deformation of the hanging wall of the Eastern Margin Fault (Kamesh Raju et al., 2004). This could occur if the forearc basins were formed by subduction erosion of the underlying crust rather than by east-west extension (Cochran, 2010). Andaman forearc is a zone of high compressional stress and high seismicity and the mud volcanoes of the forearc are a result of such activities. In the present study we have studied these features to understand their origin and relationship to the fluid activity in the forearc region.

2.3 Mud Volcanoes of the Andaman Islands

Mud volcanoes are very small volcano like geological features that ooze out mud, water and hydrocarbon gases at a much lower temperature (30-40°C) than the real volcanoes. The diameter of mud volcanoes ranges from a few centimeters to several meters.

Although mud volcanoes are observed all over the globe, they are predominantly found in areas of tectonic compression like the subduction zones, and are usually associated with hydrocarbon deposits (Kopf, 2002).

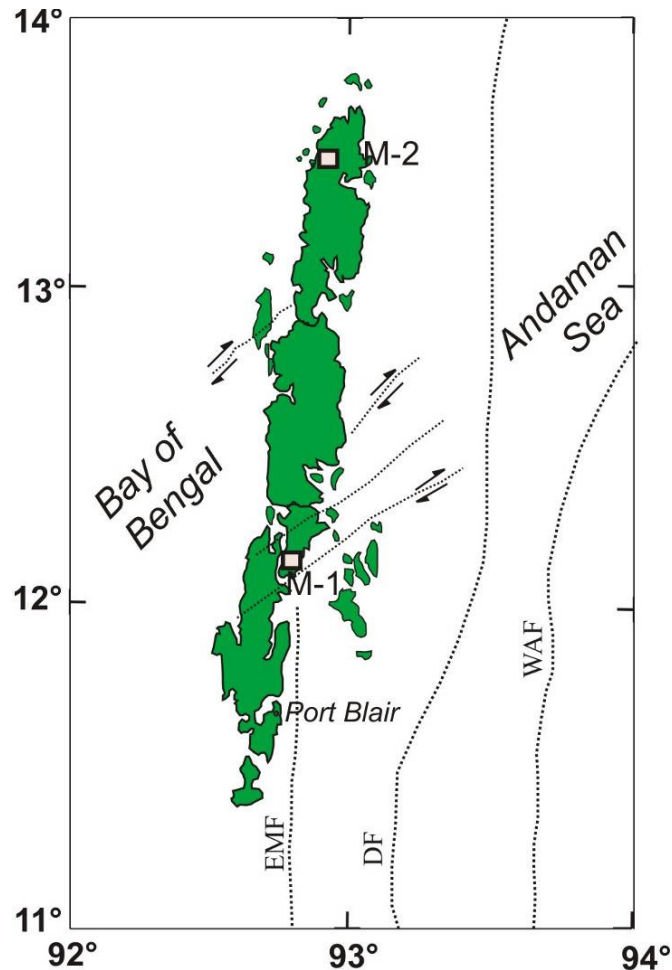


Fig. 2.3 Location of mud volcanoes in Andaman Islands and major fault systems in the Andaman Sea (M-1: Middle Andaman and M-2 North Andaman; EMF: East Margin Fault, DF: Dilligent Fault, WAF: West Andaman Fault).

Mud volcanoes of accretionary prisms that tap fluids and clay rich sediments of the slab at shallow levels (2-4 km) can reveal a lot about the subducting material prior to its journey into the mantle. The detailed structure of the mud volcano is largely unknown; however, Kopf (2002) made attempts to describe various features associated with these. The

main structure of a mud volcano consists of the fluid source with a feeder channel above and a complex system of fractures and dykes filled with mud through which fluid-sediment-rock clast mixture erupts out to Earth's surface to form the mud volcano (Fig 2.4).

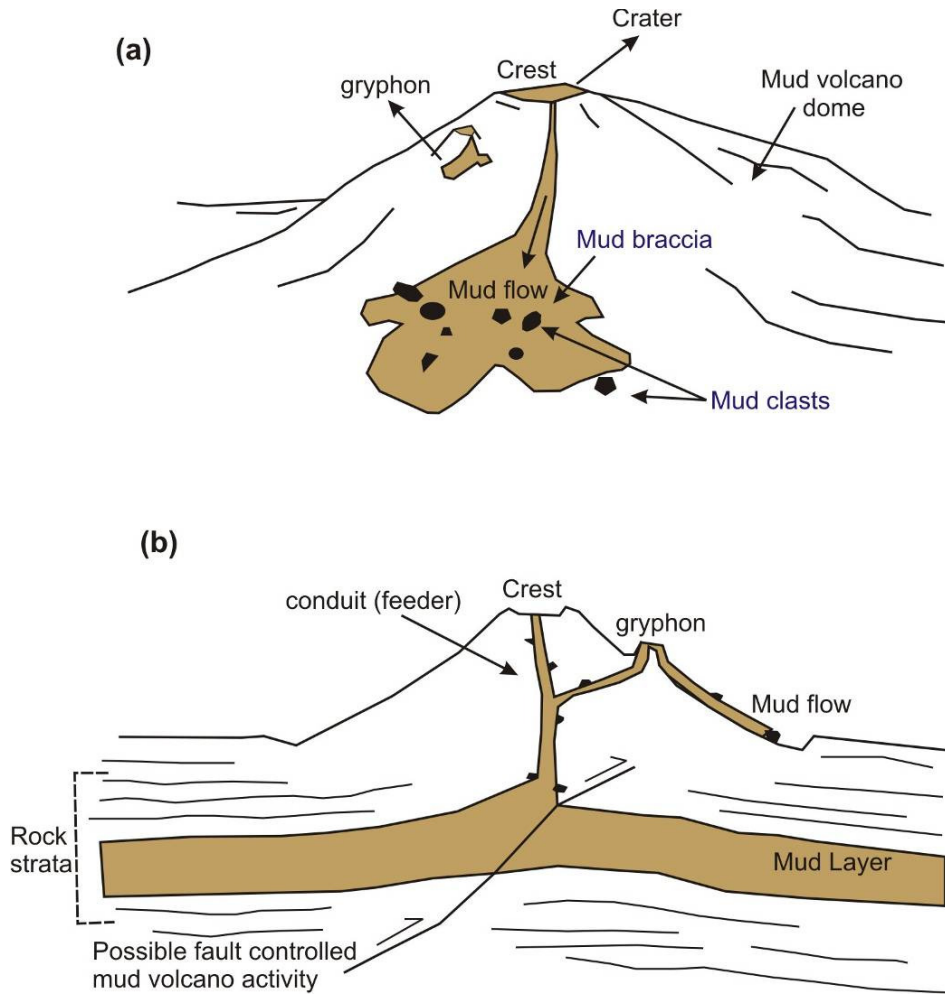


Fig. 2.4 Schematic diagrams of a cone shaped mud volcano with its various components (after Koef, 2002) a) a general surficial view; b) a cross sectional view

The solid material that gets expelled through mud volcanoes along with fluids is known as 'mud breccia, which is made up of rock fragments embedded in mud matrix. These clasts are a very complex mixture of

material from the rock sequences through which mud volcanoes have erupted.

Several active mud volcanoes have been reported in the Andaman and Nicobar Islands (Dimitrov 2002) and these represent mud expulsion in a compressional regime. A majority of these are reported from the Baratang Island of the Middle Andaman, and from Diglipur Island in the North Andaman (Fig. 2.3). These mud volcanoes are located along fault zones trending mainly in N-S direction. The N-S aligned faults are part of the imbricated thrust sheets that dip eastward, parallel to trench of the subduction zone. The diapiric ascent of fine sediments through these faults is believed to be due to post-Eocene compressional forces resulting from overthrusting (Badve et al., 1984; Ling et al., 1995). These thrust faults provide the pathways for the material in the accretionary wedge to come up through the mud volcanoes. These faults are probably the continuation of East Margin Fault (Curry, 2005) further north or the Jarawa Thrust Fault (Fig 2.3). On the basis of our observations we have prepared two mud volcano regions (Fig. 2.5a, c) and a blow up of the Middle Andaman mud volcano zone (Fig. 2.5b)

Very Limited work exists on the mud volcanoes and a majority of these are mainly on microfossils which are present in mud breccia. The prime objectives of these studies were to explore hydrocarbon reservoir in this area as mud volcanoes are believed to be indicators of potential reservoir of hydrocarbon.

Various workers (Badve et al., 1984; Rajshekhar, 1985, 1989, 1992; Jafar, 1985 Jafar, et al., 1989a; Ling et al., 1995) have reported foraminiferas, coccoliths and radiolarian, of age ranging between Late Cretaceous to Miocene, from these mud volcanoes. Apart from these studies one

interesting work has been done by Achyuthan and Eastoe (1999) in Jarawa creek mud volcanoes, Baratang Island where they report volcanic glass and sulphide nodules in the mud breccia and on the basis of sulphur isotope composition of the mud, brines, and nodules they suggest that there have been a large influx of groundwater into the system prior to its eruption.

Andaman mud volcanoes eject sediments and rocks of various shapes, compositions and ages that may have come from greater depths. We examined the rock clasts and sediment that are ejected from these mud volcanoes and found that along with pillow lava and sediments from the underlying sedimentary formations it also brought out plenty of organic matters- possibly related to deep petroleum systems. In the breccia we observed at least seven types of lithoclasts viz.: i) serpentinites - derived from Ophiolite Group, ii) limestones, iii) shales iv) siltstones, v) sandstones; vi) pillow basalts, and vii) quartz bearing rocks. These rock clasts provide important information about the type and composition of rocks in deep-seated formations through which eruption of the mud volcanoes have occurred. As we know the water plays an important role in subduction zone magmatism (Jarrard 2003), therefore study the mud water throw some light on the role of dewatering processes of Andaman forearc region and their influence on overall fluid of Andaman subduction zone. To characterize these fluids we took up a geochemical investigation of the gases and water erupting out of these mud volcanoes. Fig. 2.6 shows various field observations on these mud volcanoes.

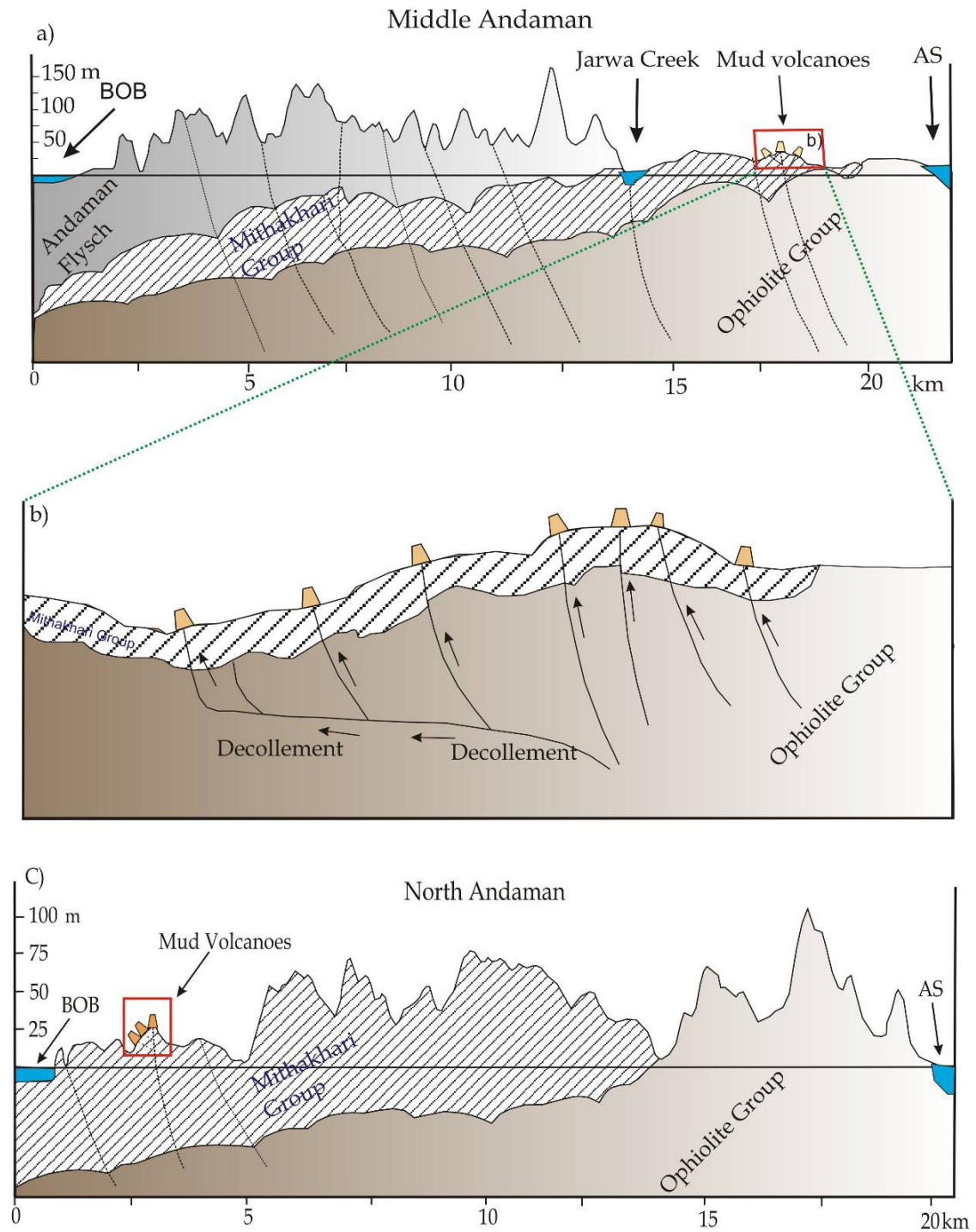


Fig. 2.5 Cross-sectional views of mud volcanoes of Middle and South Andaman Islands, based on author's identification and interpretation. a) Middle Andaman, b) Blow up of rectangular area in (a). c) North Andaman. BOB: Bay of Bengal, AS : Andaman Sea.



Fig 2.6 Field photographs of mud volcanoes from Andaman Islands a) active mud volcano cone at Jal Tekari, Shyamnagar, Diglipur, North Andaman b) active mud volcano oozing out mud water and hydrocarbon, gases Baratang Island, Middle Andaman c) mud breccia containing fine mud and rock clasts d) the rock clast contains pillow basalts oozing during explosive eruption e) showing gas bubble coming out continuously f) Field of active mud volcanoes destroyed all the plants, Baratang Island Middle Andaman

This page left blank intentionally

Chapter 3

Volcanological Studies of Barren Island

In the volcanological studies, we study the formation of volcanoes, and their historic and current eruptions on the basis of eruptive products including tephra (such as ash or pumice), lava and rock samples. In this work, I report the results of our detailed geological and volcanological observations and interpretations of volcanic sequences on Barren Island, based on three field trips to the volcano in January 2007, April 2008 and March 2009. During the field investigations we have identified different flows and structures on the island, mapped the island, and made an attempt to understand the origin and evolution of the volcano. These results have already been published (Sheth et al., 2009, 2010 and 2011).

3.1 Introduction

The Barren Island active volcano lies in the Andaman Sea, northeastern Indian Ocean. It is situated ~70 km east of India's Andaman and Nicobar Islands chain, where sequences of oceanic volcanic and metavolcanic rocks (pillow basalts, ultramafics, serpentinites, greenstones) as well as flysch sediments are exposed (e.g., Allen et al., 2007). The Andaman Trench, along which the NE-moving Indian Plate currently subducts beneath the Burmese Plate, is ~ 250 km west of the volcano (Fig. 1.10). The tectonic scenario is complicated by the presence of active back-arc spreading in the Andaman Sea ESE of Barren Island (Curry et al., 1979; Kamesh Raju et al., 2004; Khan and Chakraborty 2005, Subba Rao, 2008).

Barren Island is the only active volcano in Indian territory, and the northernmost active volcano of the great Indonesian arc. To the north of Barren Island is one more important dormant volcano in Indian

subcontinent named as Narcondam (Fig. 1.10), which is situated ~140 km NNE of Barren Island, may have erupted in the Holocene (Simkin and Siebert 1994, Siebert and Simkin, 2002).

Barren Island is only ~3 km across. It is not all barren and has a lush jungle on its southern and eastern sides, with some freshwater springs (Chandrasekharam et al., 2003). But it is uninhabited by man, which may explain its name. Wildlife on the island includes feral goats, fruit bats, rats, and parrots.

Barren Island has restricted public access and can be reached by Indian Navy or Indian Coast Guard vessels from Port Blair (135 km), the capital of the Andaman and Nicobar Islands. A few scientists from the Geological Survey of India (GSI) have been studying the volcano for nearly two decades; however, with rare exceptions their studies have been published as the GSI's internal reports and as conference abstracts, not easily accessible (e.g., Haldar, 1989; Haldar et al., 1992a, 1994, and several others). The volcano has therefore had quite low visibility internationally. There is also no continuous monitoring of the volcano. A GSI photographic atlas dedicated to the volcano (Shanker et al., 2001) gives some valuable first-hand information on the recent eruptive activity in the form of eyewitness accounts; however, the atlas is targeted in part at the layman, and our identifications and interpretations of several volcanic features on the volcano differ significantly from those offered in the atlas. When we started working on the Island in 2007 only a few studies existed in peer-reviewed Indian and international literature (Haldar et al., 1992b; Haldar and Luhr, 2003; Alam et al., 2004; Luhr and Haldar, 2006; Pal et al., 2007) which addressed aspects of magma evolution at the volcano and provided accounts of its recent post 1991 eruptions. Since 2007 several publications including ours, have come into public domain (e.g., Sheth et

al., 2009, 2010 and 2011; Chandrasekharam et al., 2009; Banerjee, 2010; Pal et al., 2010; Streck et al., 2010; Awasthi et al., 2010, Ray et al., 2011). In following paragraphs I discuss our finding of the volcanological studies on the Island.

3.2 Geology

Barren Island (Figs. 3.1, 3.2) is roughly circular with a diameter of ~3 km and represents the topmost part of a submarine volcano rising more than 2 km above the sea floor. In the absence of proper geophysical survey, drilling or dredging no information is available about the rocks that make up its submarine mass. Luhr and Haldar (2006) estimate its submarine volume to be ~390 km³ based on the bathymetry and the subaerial volume to be only 1.3 km³. The volcano has a nearly circular caldera of ~2 km diameter, with a breach in the caldera wall on the northwestern side, which has existed since at least 1787 as the earliest sketches of the volcano (by Colebrooke and Captain Blair, reproduced in Shanker et al., 2001) show.

A cinder or scoria cone rising to about 500 m above sea level exists roughly at the caldera centre. The caldera wall exposes prehistoric volcanoclastic deposits and lava flows, which are interbedded with radial outward dips (Fig. 3.1a, b and 3.2b). By “prehistoric” is meant that these deposits formed at some (unknown) time before the first “historic” eruptions which began in 1787 and continued till 1832 (Shanker et al., 2001; Luhr and Haldar, 2006). Alam et al. 2004 reported for a 5-m-wide, NNE-SSW-trending basaltic dyke cutting the prehistoric lava flows on the southeastern inner caldera wall, no intrusions are known on the volcano.

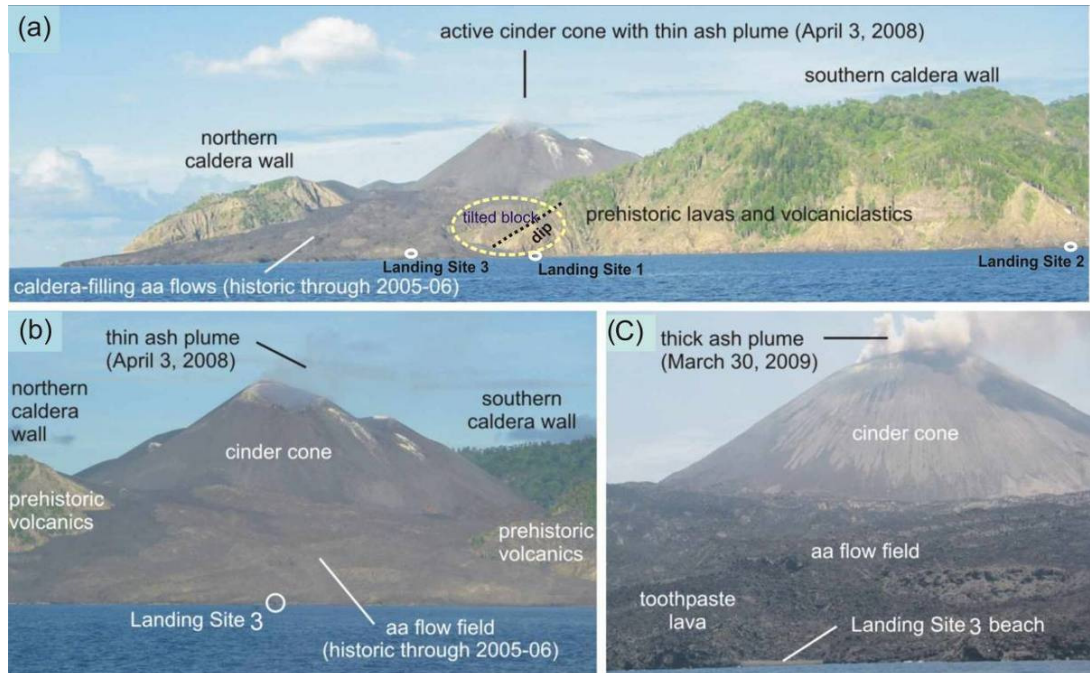


Fig. 3.1 **a-c** Panoramic views (in April 2008 and March 2009) of Barren island taken aboard Indian coast guard vessels, showing general morphological and geological features. The cinder cone is ~ 500 m high above the sea and the south caldera wall 334m. Yellowish white patches on the cinder cone in (a) and (b) are fumarolic deposits. In (c) ~20m wide beach at landing site 3 and the lava flows and first time reported tooth paste lava flows also marked.

Barren Island has had four recent eruptions in 1991, 1994–95, 2005–06 and 2008–09 (Fig 3.2) during which it has erupted aa lava flows of basalt and basaltic andesite and pyroclastic materials. Previous workers have used variable terminology for the various eruptions. Shanker et al. (2001) call the 1991 and 1994–95 eruptions, which they describe, as “recent”, or the “third cycle”, their second and first cycles referring to the historic (1787–1832) and the prehistoric eruptions respectively. Luhr and Haldar (2006) include the 1991 and 1994– 95 eruptions among “historic” volcanism. Here we use the terms (recent, historic, prehistoric) following Shanker et al. (2001), and also introduce two new useful terms. Because the prehistoric deposits exposed on the caldera wall must predate the formation of the caldera itself, we call them the “pre-caldera” volcanic

deposits. The historic (1787–1832) as well as the recent eruptions have occurred from the central cinder cone, well within the caldera. We therefore address both the historic and recent eruptive products as “caldera-filling” volcanic deposits.

Regarding caldera forming event, Shanker et al. (2001) speculated that the caldera may have formed in late Pleistocene time, by an original, 1,100-m-high cone blowing its roof off in a giant eruption. However, our observations suggest that the formation of caldera on the Barren Island volcano is not associated with eruptions because we didn’t get evidence for a high proto-Barren Island volcano blowing its roof off in a Krakatau-1883-like eruption. Shanker et al. (2001) didn’t identify the deposits left on the volcano itself by this proposed event, and some that we describe below might correspond to such an event, or to older (pre-caldera) volcanism itself. We believe that the caldera of Barren Island is bounded by a ring fault, and note that there is a small tilted block on the western end, rising to about 100 m above sea level but without a clear relationship to the caldera wall, which shows the otherwise south-dipping prehistoric pile forming the southern half of the volcano to dip northwards, towards the caldera-filling lava flows (Fig. 3.1a, b). Cole et al. (2005) provide a recent review of calderas, and the Barren Island caldera can be considered a “simple, single-event, symmetric collapse, circular basaltic caldera” following their terminology. This, as the modelling of Roche et al. (2000) suggests, may indicate a shallow-level magma chamber. This would be consistent with the observations of Luhr and Haldar (2006) that several Barren Island lavas contain disaggregated troctolitic (olivine + plagioclase) cumulates from a shallow magma chamber under the volcano. Although the timing of this caldera forming event is not known, the suggestions made by Awasthi et al. (2010) is worth mentioning the point. Correlating Nd isotopic composition of pre-caldera formations with ash layers in a

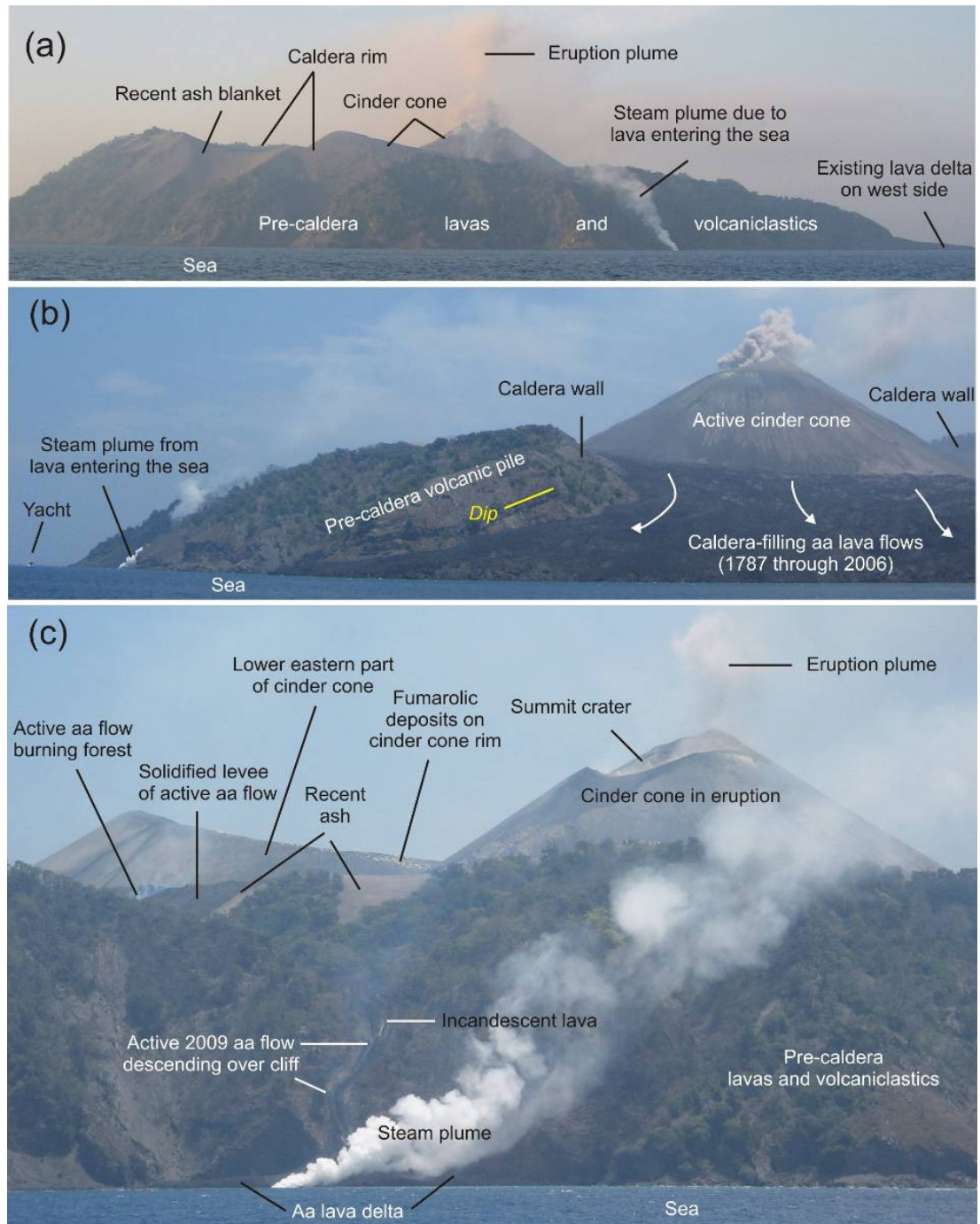


Fig. 3.2 **a-c** Most recent lava flows (of 2008-09) on Barren Island volcano have taken a route through the northern section of the caldera wall (Sheth et al 2010)

well dated sediments core near the volcano Awasthi et al., (2010) speculated that the caldera on Barren Island could have formed prior to 10 kyrs before present.

We have developed a new geological map of the Barren Island (Fig. 3.3) based on earlier information, satellite photographs and our field observations. Our map is more accurate compared all other existing ones and a major difference in this map and the previous ones is the considerably enlarged area of recently erupted lava flows at the western coast of the volcano that is represented here. In addition we have also mapped most recent (2009) lava flows that have taken a complete different route to these compared to the earlier ones (Fig. 3.3).

3.3 Prehistoric eruptions

3.3.1 Pre-caldera tuff breccias: deposits left by lahars and debris flows

The lowermost exposed prehistoric deposits on the inner caldera wall of Barren Island are polymodal deposits with sharply angular blocks of basalt as big as a metre, dispersed in a matrix of fine, ash-size, clay-like material (Fig. 3.4). These can be called as tuff breccias. The best exposures are on the western shore of the volcano just south of the 1994–95 aa flows, where several of these deposits underlie a prehistoric aa flow (Fig. 3.4a). Two distinct tuff breccia deposits are visible in Fig. 3.4, and only a few metres southwards, four distinct tuff breccia deposits are exposed, with an unconsolidated, well-sorted ash bed in the middle (Fig. 3.4c), interpreted here as a pyroclastic fall deposit. The prehistoric lava flow and the tuff breccias below have steeply dipping fractures filled by still younger coarse fragmental material almost to the base of the exposed section (Fig. 3.4a). The aa flow may correspond with the lowest of the three aa flows exposed on the northern caldera wall, below which ash and lapilli beds are seen, followed by a tuff breccia deposit (presumably corresponding to the youngest on the southern side) (Fig. 3.4d; the interpretative logs and correlations in Fig. 3.5).

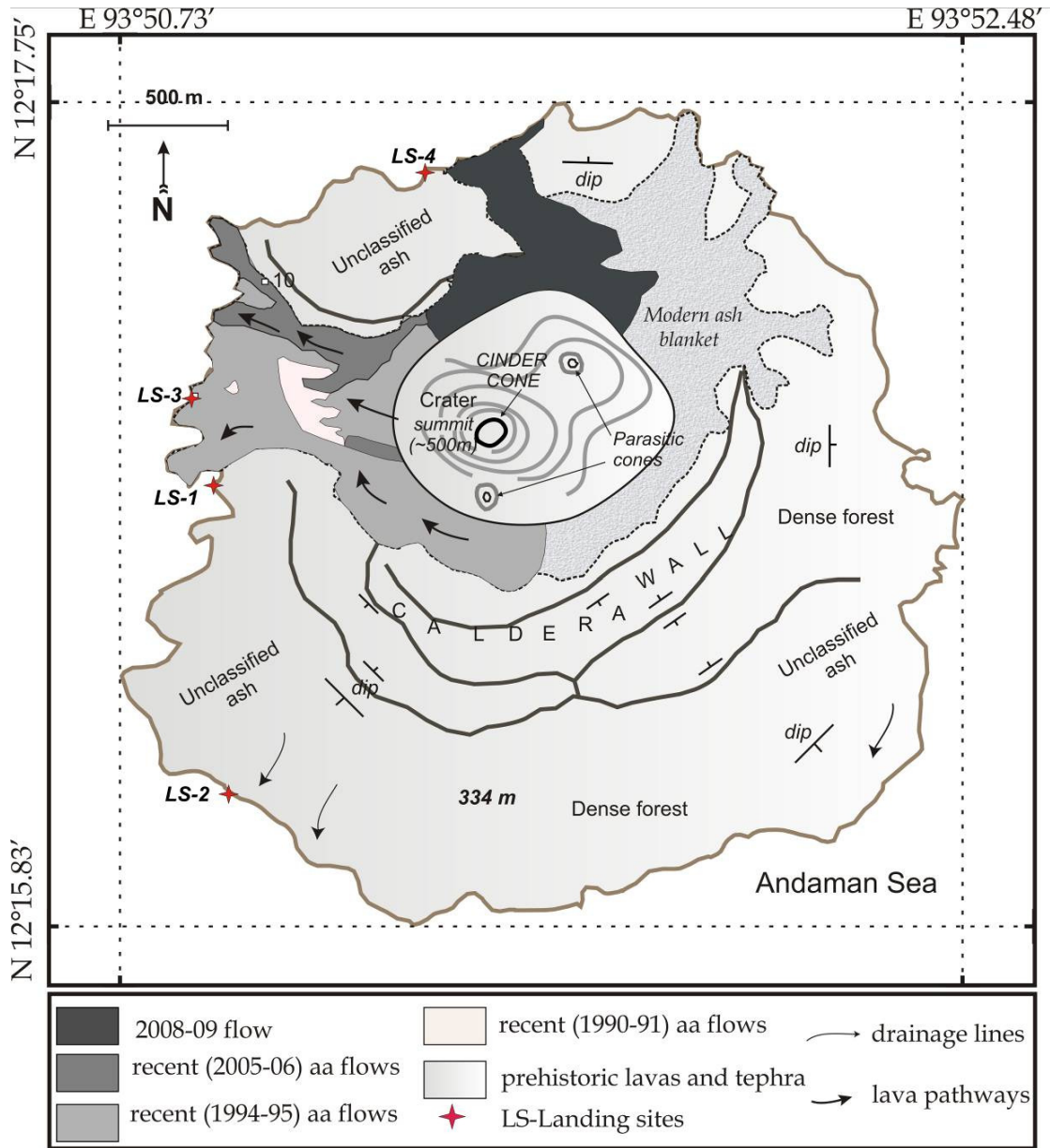


Fig. 3.3 Geological map of Barren Island Volcano based on field observations in 2008 and 2009, showing various lavas flows and structure

Shanker et al. (2001) have described these tuff breccia deposits as agglomeratic flows (e.g., their Fig. 1.9), but the total absence of bombs in them suggests that no molten rock was involved in the flows. Such tuff breccias may represent deposits of pyroclastic flows, particularly the subtype of pyroclastic flows known as block and ash flows. Alternately

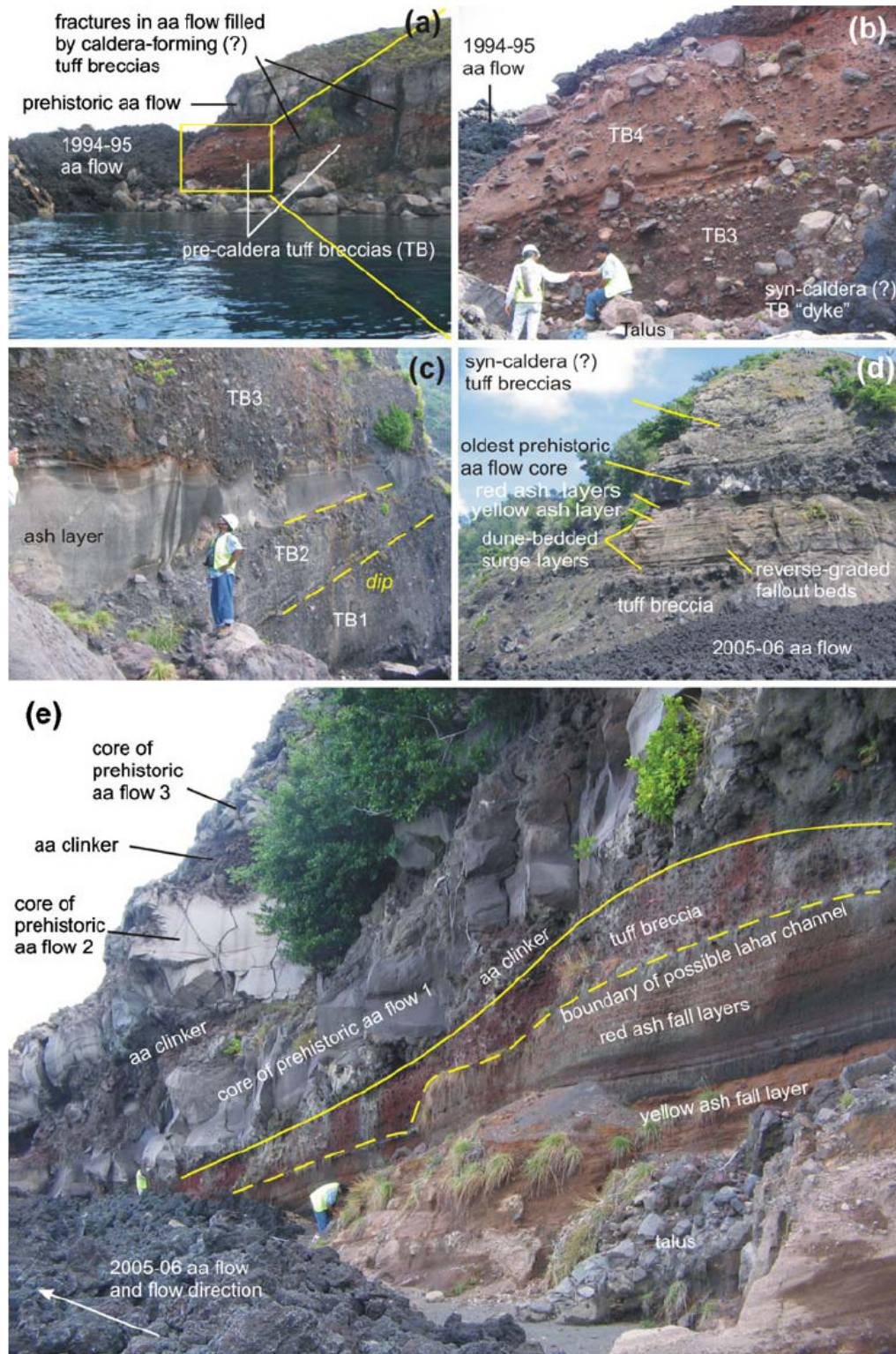


Fig. 3.4 *a-e* Prehistoric, pre-caldera tuff breccias (TB, interpreted as lahar and debris flow deposits and numbered TB1 through TB4 from oldest to youngest) and lava flows exposed on the inner caldera wall.

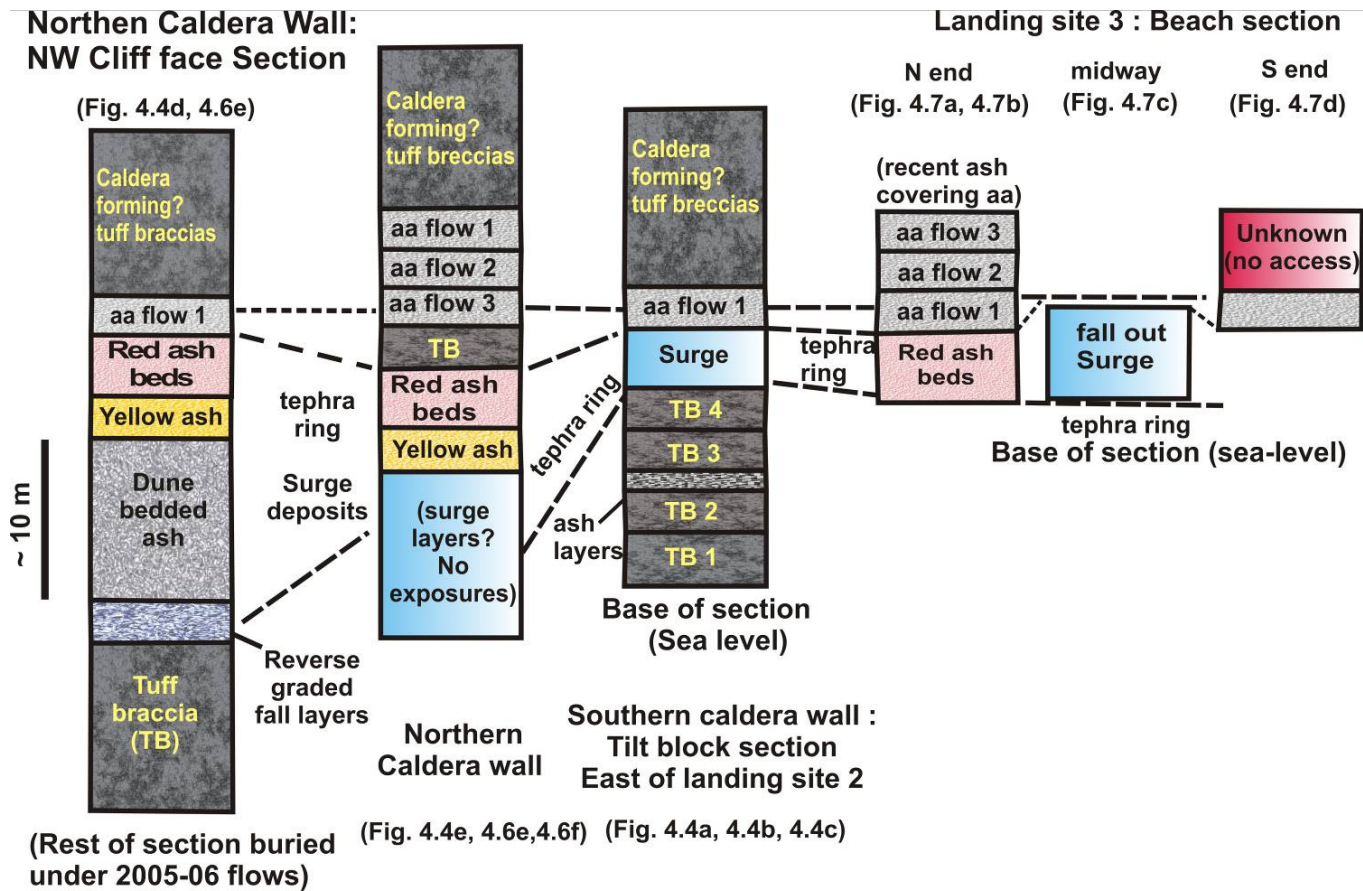


Fig 3.5 Litho logs for the six locations examined on Barren Island in the present study, with their correlations. TB 1 to TB 2 is precaldera tuff breccia deposits (Sheth et al., 2009).

tuff breccias may be the deposits left by debris avalanches or lahars, simply representing mass movements. Both are common and abundant on the large oceanic volcanoes. Whereas debris avalanche deposits are typically hummocky, lahars deposits are channelized. The prehistoric tuff breccias on Barren Island appear to be channelized (Fig. 3.4e). We did not encounter carbonized plant remains that can help distinguish the deposits of the (high-temperature) pyroclastic flows from those of lahars. On the other hand, lahars, especially highly fluid hyperconcentrated flow varieties, contain substantial water. Considering the above, the tuff breccia deposit immediately underlying the prehistoric aa flow (Fig. 3.4b) is interpreted here as a lahar deposit with rainwater as the mobilizing agent. The two similar, but block-rich, matrix-poor deposits that underlie it are interpreted here as deposits left by debris flows. Accumulations of loose, coarse (~1 m), angular rubble that can be seen on the present slopes of the volcano, only some hundred metres to the south of these outcrops, supports the interpretation that the prehistoric tuff breccias were formed essentially by mass movements.

3.3.2 Ash beds: pyroclastic surge and fall deposits

In the southern inner caldera wall section, in the tilted block described in the “Geology” section above, the lowest prehistoric aa flow and the lahar deposit beneath it are separated by ash and lapilli ash layers (Fig. 3.6a). They show mantle bedding (Fig. 3.6b) as well as dune bedding, sometimes with sags produced by angular basalt blocks (Fig. 3.6c, d). On the northern caldera wall, between the oldest prehistoric lava flow and the tuff breccia deposit are layers with reverse grading, followed upwards by ash and lapilli ash layers with dune bedding (Fig. 3.6e). They are overlain by well-bedded, well-sorted yellow and red ash layers (Fig. 3.6f). Shanker et al. (2001) report rare normal

grading in these tephra at other locations. We interpret the ash and lapilli ash beds with reverse or normal grading, or which are well sorted (e.g., Fig. 3.4c), to represent pyroclastic fall deposits, and the ash beds with dune bedding to have been deposited by the pyroclastic surges.

Surge-deposited beds overlain by fall deposits are also seen on the outermost southwestern side of the island, below the prehistoric aa flows (Fig. 3.7a-d). Therefore we believe that these prehistoric, pre-caldera pyroclastic surge and fall deposits, exposed on both the northern and the southern caldera wall sections (sandwiched between the aa flows above and the tuff breccias below), as well as on the western shore of the island, represent a complete tephra ring that existed before the eruption of the prehistoric lavas. Tephra cones, rings, and maars are characteristic products of phreatomagmatism, the explosive interaction between magma and shallow surface water or groundwater (Hamilton and Myers, 1963; Sheridan and Wohletz, 1983; Sohn and Chough, 1989; Zimanowki, 1998; Thouret, 1999; White and Houghton, 2000).

Based on Shanker et al.'s (2001) observation, that "coral beds around the western shore (of Barren Island) were badly affected (by the 1991 eruption)", it is possible that coral reefs were in existence at the time the prehistoric pyroclastic surge and fall deposits formed on Barren Island. But the fact that these deposits contain no coral reef fragments and few other accidental lithics (basalt blocks) suggests the absence, or at least non-involvement, of reefs, and certainly the dominance of juvenile magma and minimal vent quarrying. In fact there is nothing to suggest that sea water was involved in magma fragmentation. The absence of accretionary lapilli



Fig. 3.6 **a-f** Pyroclastic surge and fall deposits preserved beneath the prehistoric aa flows and above the pre-caldera tuff breccias.

throughout the outcrops examined suggests that the pyroclastic surges were more or less dry, with little external water involved (e.g., Wohletz and Sheridan 1983).

Shanker et al. (2001) have interpreted the cross-bed characteristics of the surge deposits on Barren Island as aeolian in origin. Whereas syn- or post-eruptive erosion by slumping, debris flows or wind does operate on tephra rings (Leys, 1983; Sohn and Chough, 1989; Chough and Sohn, 1990), there are no palaeosols or erosional contacts within these deposits, suggesting the rapid eruptions without breaks, and no horizons of coarse, angular rubble that might suggest reworking.

3.3.3 The prehistoric aa flows

Each of the three aa flows on the northern caldera wall exhibits a distinct clinkery base and top, and a thick, massive, unjointed or poorly jointed core between the upper and lower clinker (Fig. 3.4e). Each clinkery horizon is about a metre thick, and the cores are about 4 m thick. The upper two lava flows appear to merge into one towards the northwestern end of the cliff face.

3.3.4 Possible syn-caldera deposits

On Barren Island, it is unclear if there are deposits associated with the caldera-forming event. Shanker et al. (2001), who speculated about a giant caldera-forming prehistoric eruption, did not identify the associated deposits. Luhr and Haldar (2006) write that “Outcrop photographs in Shanker et al. (2001) show sequences of unconsolidated pyroclastic-surge deposits more than 15 m thick with prominent cross beds and bomb sags, likely from the

caldera-forming eruption.” We believe that these photographs are of the outcrops we have described as pyroclastic fall and surge deposits underlying the prehistoric lava flows, which means that they were emplaced long before the caldera-forming event. Also bombs are not observed in these deposits (only blocks, and very few of them).

The youngest deposits exposed in the caldera wall are ~50 m thick pyroclastic deposits above the prehistoric aa flows. These include mainly



Fig. 3.7 The beach section at Landing Site 2 on the western side of the island, showing (a) two prehistoric aa flows underlain by tephra deposits, (b) close-up of the lowermost aa flow and underlying red ash beds, (c) fine, dune-bedded ash representing surge deposits overlain by airfall-deposited ash with a few lithic blocks of basalt, and (d) surge deposits underlying fallout ash beds.

well-stratified ash beds with some tuff breccias (Fig. 3.8a). Following many workers (e.g., Nakamura 1964; Decker and Christiansen 1984; Robin et al., 1993) we interpret these uppermost deposits as possibly representing the caldera-forming eruption. Some of the tuff breccias have entered the fractures in the prehistoric lava flows and underlying tuff breccias (Figs. 3.4a, 3.8b, c), and these fracture filling materials sometimes have a strong superficial resemblance to dykes (Fig. 3.8c). In places the ash layers and the tuff breccias dip inward towards the centre of the caldera (Fig. 3.8d) and show mantle bedding, suggesting that they were deposited on whatever topography existed at that time (Fig. 3.8e).

3.4 Historic eruptions

Based on the accounts of Hobday and Mallet (1885), Ball (1888, 1893), Mallet (1895), Washington (1924), Raina (1987), Haldar et al. (1992a, b, 1999), Shanker et al. (2001), Haldar and Luhr (2003), Luhr and Haldar (2006), and reports from the Bulletin of the Global Volcanism Network (Smithsonian Institution, Venzke et al., 2002), Barren Island volcano had its first historically recorded eruptions in 1787, observed by passenger ships crossing the Andaman Sea. The earliest sketches of the island (sketches by Colebrooke and Captain Blair reproduced in Shanker et al., 2001) show the volcano in much its modern shape, including the breach in the caldera wall. However, the height of the central cinder cone has been shown to be a little less than that of the caldera wall and, rather unrealistically, the cinder cone has been shown to have extremely steep (50°) slopes.

The activity in 1787 is said to have started with the formation of a new cinder cone near the centre of the caldera during a Strombolian-style eruption.

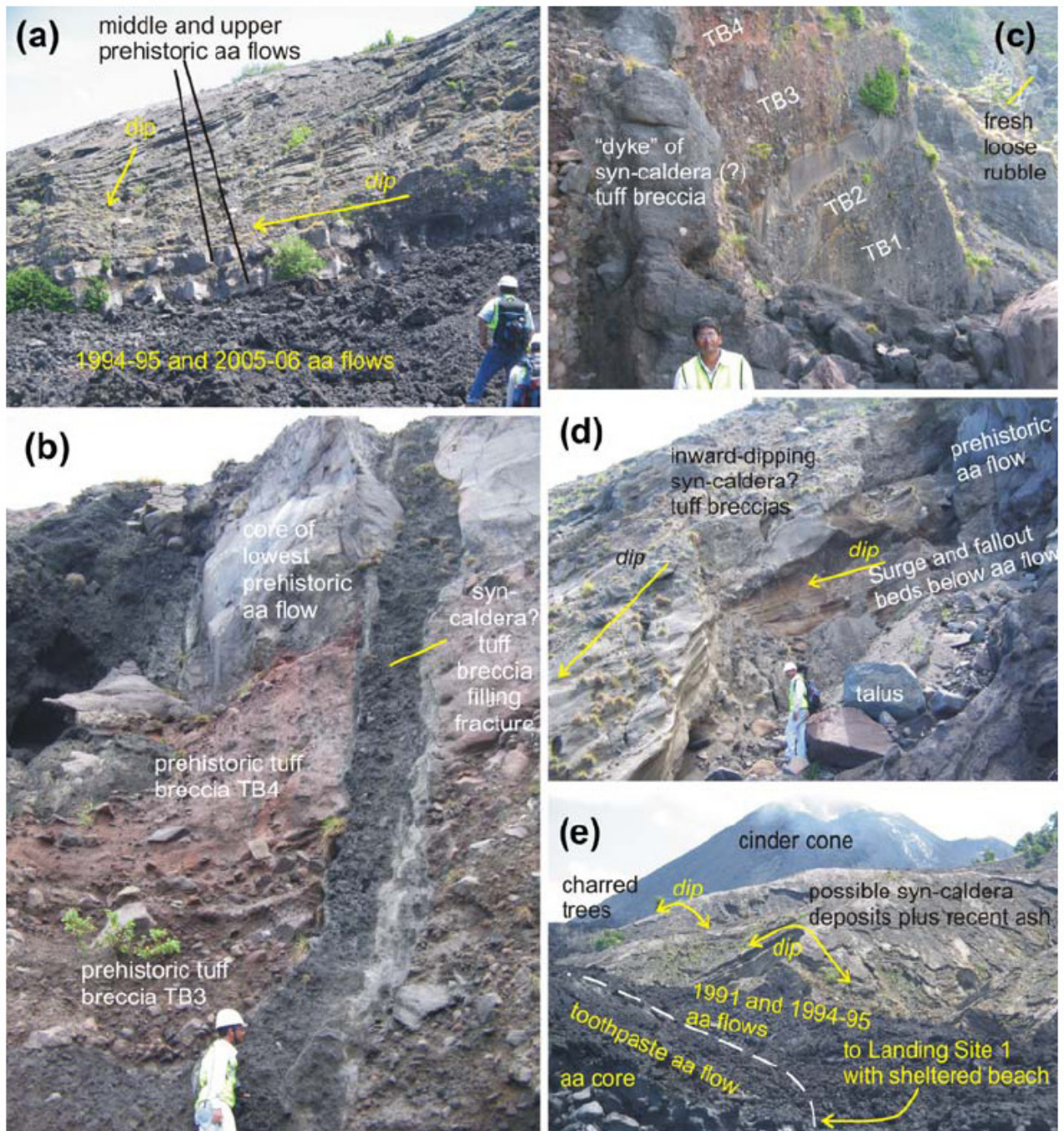


Fig. 3.8 **a-e** Uppermost prehistoric deposits that may represent the caldera-forming eruption, overlying the prehistoric lava flows and tephra layers. Frame (a) is from the northern caldera wall, and (b) through (e) are from the tilted block just south of the recent aa flow field (Landing Site 1)

Activity continued until 1832 with breaks of 2–29 years between individual eruptions. The Smithsonian Institution lists the following eruptions during this interval: 1787, 1789, 1795, 1803–1804, and 1832 (Siebert and Simkin 2002). The cinder cone grew to 305 m height and developed a summit crater ~60 m across. The eruptions occurred from three subsidiary vents about 80 m below the crater rim on the northeast, west, and south flanks of the cinder cone (Raina 1987, and references therein). Basaltic aa lavas emerged from the three subsidiary vents, flooded the annular moat between the new cinder cone and the caldera wall, and ultimately flowed westward to cascade into the sea (e.g., see Fig. 3b of Luhr and Haldar 2006). Luhr and Haldar (2006) estimate a volume of ~25 million m³ for them.

3.5 Recent eruptions

The recent (1991, 1994–95 and 2005–06, 2008–09) basalt and basaltic andesite flows have largely, apparently completely, covered and hidden the older historic (1787–1832) lava flows. Shanker et al. (2001), Haldar and Luhr (2003), and Luhr and Haldar (2006), as well as the Smithsonian Institution's Global Volcanism Program website ([http:// www.volcano.si.edu](http://www.volcano.si.edu)) offer valuable first-hand information on the recent eruptions. The 1991 flows erupted from the central cinder cone and flowed to the sea (Fig. 3.2), and the 1994–95 flows flowed along the southern margin of the 1991 lava field (Figs. 3.2, 3.9a) according to eyewitness accounts (Shanker et al., 2001), though they also appear to make up much of the lava front along the island's west coast. The 2005–06 flows travelled along the northern part of the lava field, close to the caldera wall, and reached the sea. The three eruptions have by now created a sizeable lava delta (term used by Luhr and Haldar, 2006) at the western shore of the Island (Figs. 3.1a, b, 3.2, 3.9a). We describe these

eruptions only briefly, as detailed descriptions can be found in the references cited above.

3.5.1 The 1991 eruption

This eruption began in late March 1991 from the existing cinder cone, producing thick jets of gas and red-hot lava fragments. The eruption began at the NE subsidiary vent from the 1787–1832 eruption; about 80 m below the rim of the crater of the cinder cone, and formed a new spatter cone. Lava flowed from that vent and also from the other two subsidiary vents of the historic eruption, and filled the annular moat between the central cone and the caldera by 6 April. Two new small, ~10-m-high lava dribble cones formed ~100 m and ~130 m west of the cinder cone atop these basaltic andesite lava flows, which were mostly blocky aa. These lava flows travelled westward to the sea where they buried a 12-m-high gas lighthouse on the shore and caused profuse boiling of the sea water and generation of thick steam clouds. The lava flows were individually 5–6 m thick, but by the late stages of the eruption they became ~25 m thick near the base of the cone and at the ocean entry.

Based on the mapped distribution of the 1991 lava flows, Luhr and Haldar (2006) estimate that they covered an area of ~0.26 km². Multiplying by an average lava thickness of 10 m over this area gives a total lava volume of 2.6 million m³ (not 26 million m³ as reported by them). If the ratio of tephra to lava was roughly 2:1, as estimated by eye (Haldar and Luhr, 2003), then the associated 1991 tephra volume is 5.2 million m³ (not 52 million m³ as stated by them). Therefore, while we cannot account for the lava or tephra volumes that are under the sea, we consider that a good estimate of the total 1991

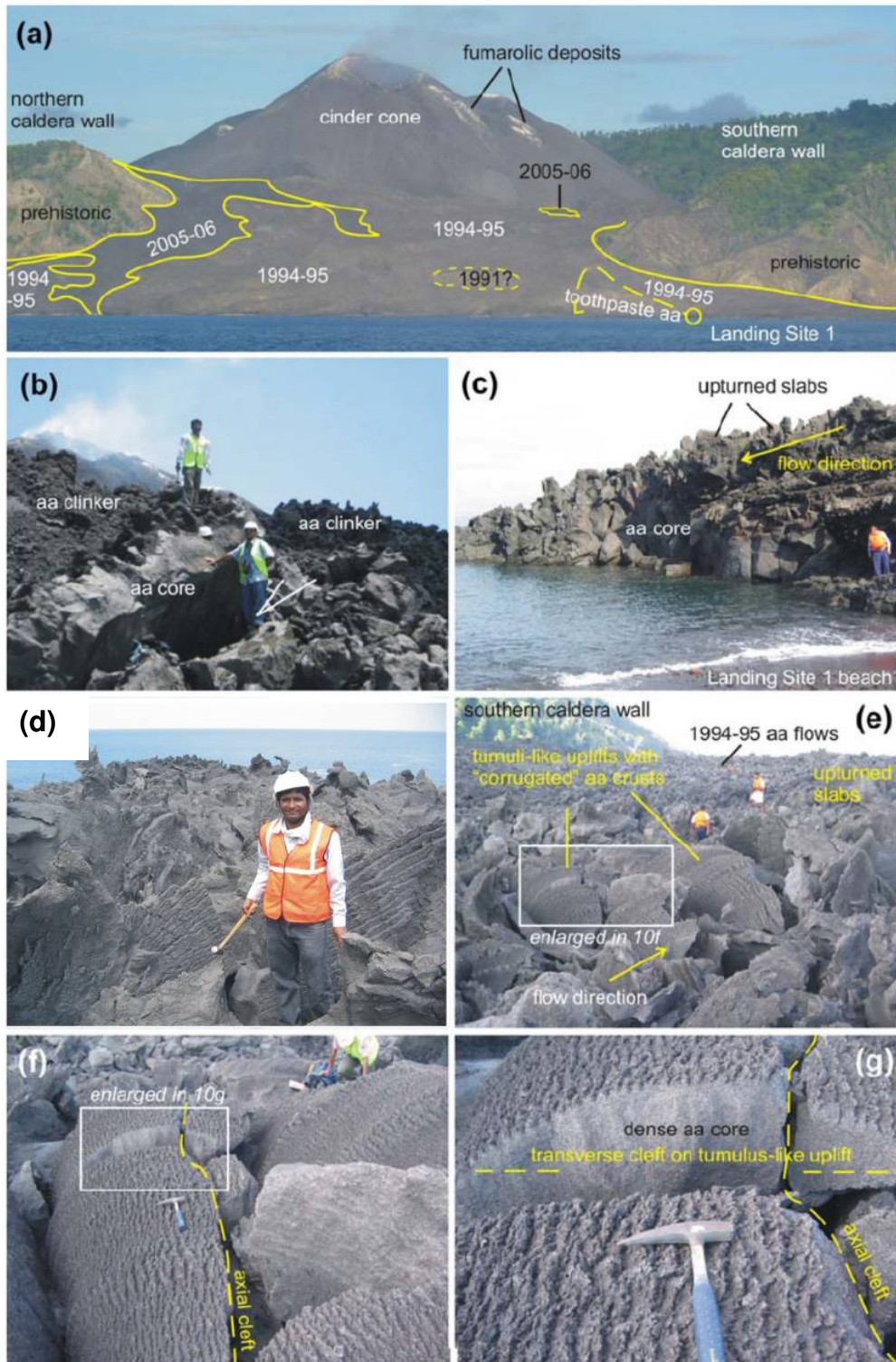


Fig. 3.9 **a-g** Recent aa flows. (a) is a panoramic view (looking east) of the recent lava flow field. Dotted boundaries are conjectural. (b) is between the L.S.3 and the northern caldera wall. (c-g) show the toothpaste aa flow at the L.S.3

magma volume (lava plus tephra) that remains on the island is ~8 million m³. Luhr and Haldar's (2006) figure of ~78 million m³ is about an order of magnitude too large.

By early May 1991 the NE flank vent was ejecting incandescent fragments in pulsing pyroclastic columns (fire fountains), and this has been described as Strombolian activity. A pulsing fountain without pauses would probably be considered Hawaiian rather than Strombolian (e.g., Valentine and Gregg 2008). By August–September this activity advanced into sub-Plinian behaviour as incandescent columns reached heights of about 1 km. Scoria and ash rained down upon the island, and a 3 m thickness of these is said to have covered the active lava flows. By late September all the three subsidiary vents on the cinder cone had broadened and merged with the central crater. The uppermost 80 m of the pre-1991 cone was removed and the summit crater, greatly broadened, was now 400 m wide, with the cone standing only 225 m high above sea level. Shanker et al., (2001) reported that the crater viewed from its rim resembled a giant funnel narrowing down to a conduit only about 25 m wide at a depth of 200 m, i.e., just 25 m above sea level. The eruption was continuing on 17 October, when the NOAA-11 satellite captured an image of a plume extending ~150 km WNW from Barren Island, but the eruption waned soon thereafter and was over by 31 October.

3.5.2 The 1994–95 eruption

This eruption started in mid-December 1994 and persisted into mid-June 1995. The event sequence for the first weeks of the 1994–1995 eruption is not known because the first GSI expedition did not arrive at Barren Island until 24 January 1995. Like the 1991 eruption, the 1994–1995 eruption has been termed mainly Strombolian in character and gained momentum over

time to each its paroxysmal stage during March 1995. It began with thick, dark smoke like jets of ash and coarser clasts from a newly created flank vent on the cinder cone, 50 m below the 225-m-high crater rim. Three flank vents subsequently developed, which along with the central vent form a N-S-trending alignment. This alignment presumably reflects the orientation of the feeder dyke underneath. The only reported dyke on the island, the dyke cutting prehistoric lavas on the southeastern caldera wall (Alam et al., 2004), has a closely similar trend (NNE-SSW), perhaps suggesting that the regional tectonic stresses have remained much the same over the exposed history of the volcano.

The 1994–1995 lavas were basalt, and the eruptive activity did not change into sub-Plinian as it did for the 1991 eruption involving basaltic andesite. By late January, a spatter cone ~100 m high formed on one of the flank vents, and stood ~50 m higher than the summit crater rim of the central cinder cone. Block-lava flows fed from this vent travelled 1.5 km to reach the sea following a route between prehistoric lavas to the south and the 1991 lavas to the north, and caused profuse steaming at the ocean entry. The lava stream from a flank vent was about 50 m wide and 6 m high. Incandescent columns ~100 m high were produced from the vents, accompanied by vigorously pulsing plumes of gas, ash, and steam at every 30 s or so and rising to 800 m before being drawn by winds into a horizontal plume. A Space Shuttle image, taken on 14 March 1995 (Luhr and Haldar, 2006; their Fig. 3d), shows the eruption plume drifting west towards the Andaman Islands. The eruption probably continued until the second week of June 1995, after which the volcano entered a strong but waning fumarolic stage.

Luhr and Haldar, (2006) mapped the 1994–95 lava flows over an area of $\sim 0.23 \text{ km}^2$. Assuming an average lava thickness of 10 m over this area gives a total lava volume of 2.3 million m^3 , not 23 million as quoted. Based on the tephra to lava ratio of roughly 1:1, as estimated by eye (Haldar and Luhr, 2003), the associated 1994–1995 tephra volume must also have a volume on the order of 2.3 million m^3 . Therefore, the total erupted magma volume during the 1994–95 eruption (excluding the lava and tephra volume that entered the sea) is ~ 4.5 million m^3 , an order of magnitude less than the ~ 46 million m^3 reported by Luhr and Haldar, (2006).

3.5.3 The 2005–06 eruption

This is an extremely brief summary written based on the Smithsonian Institution's Global Volcanism Program website, where eight individual contributors are identified (<http://www.volcano.si.edu>). This eruption began in late May 2005 with an ash plume and fresh black basalt lava flows which did not reach the sea but produced a lot of steam from heavy rainfall. In June the eruption is stated to have become Strombolian, with periodic fire fountains ~ 100 m high and a dark plume rising 1 km (again, fire fountains, especially sustained ones, are typical of "Hawaiian" eruptions, e.g., Valentine and Gregg, 2008, but there is no report of clastogenic lava flows fed by fire fountains). More lava erupted from the vent and flowed down the cinder cone. By September the lava flows reached the sea. Fire fountains from the cinder cone reached 300 m height. The eruption column's top formed a spectacular mushroom of gas and smoke, blowing to the north. Subsequent reports received from the Indian Coast Guard indicated that the eruption was continuous until at least 25 September. All active vents observed during the 2005 eruption lie in a zone trending almost N-S, an alignment also noted for active vents during the 1991 and 1994–95 eruptions. This activity continued

through January 2006. Several earthquakes of moderate magnitudes (4–5) occurred in the region around Barren Island between November 2005 and January 2006. In January 2006 geologists observed dense clusters of incandescent pyroclasts of various sizes ejected forcefully from the crater with ballistic trajectories, presumably in discrete “Strombolian” bursts. By September 2006 the activity had slowed and become sporadic. Several ash plumes and red night glows over the crater have been observed since, well into July 2007.

3.5.4 The 2008 -09 eruption

The central cinder cone was sending periodic plumes of dark ash during our first field trip in January 2007, but on our second trip in April 2008 it was in a rather quiet, fumarolic stage (Figs. 3.1a, 3.2b). Red glows over the cone at night, as well as ash plumes rising up to 2.5 km height, are reported between May and November 2008 (<http://www.volcano.si.edu>). A team of GSI’s geologists visited the Island on 7th January 2008, and landed apparently at the same site as our Landing Site 3. It reports the formation of a new cinder cone south of the existing cone, and both cones sending “Strombolian” tephra columns upward in pulsating fashion every 10–60 s. The photographs in their report (<http://www.gsi.gov.in/news.htm>) suggest instead the development of a parasitic vent southwest of the crater of the existing cinder cone.

On 30 March 2009, we landed on the lava delta on the western shore with a Gemini (inflatable rubber boat) as on previous occasions, and observed the cinder cone, one kilometre to our east, to be in vigorous eruption (Fig. 3.2c). Every few seconds a dark cloud of ash and hot gases would rise from its summit crater, expand, and rise higher and get deflected towards the south

by prevailing winds. This was reminiscent of the activity we observed in 2007. The dark clouds that were repeatedly emerging from the summit crater were accompanied by a loud, thunderous sound closely resembling the noise made by a jumbo jet flying low over one's head.

A spectacular new feature of the volcano however is a large steam plume that is rising from the sea, on the northern side of the volcano, away from the lava delta on the west (Fig. 3.2a, c). Initially, while observing this steam plume (as well as the periodic eruption plumes emerging from the cinder cone's summit crater) several kilometres from the island, on board the ship, we could not be sure whether the steam plume was rising from the sea was caused by a submarine, flank eruption (Fig. 3.2c). Getting closer to the volcano revealed that the steam plume was being caused by an active lava flow descending over the cliffs forming the outer caldera wall, on the north side (Fig. 3.2a, c). Thus we are able to confirm a fairly long (estimated to be at least half a kilometre), channelized, active lava flow on Barren Island. What is significant is that this lava flow has taken a completely different direction and route than all the historic through recent flows, which flowed westward to the sea through the caldera wall breach after erupting from the cinder cone.

What caused this major shift in the lava route (north instead of west)? It is apparent that the active lava flow is not ensuing from the summit crater of the cinder cone, as most of the historical and recent lava flows have done. The active lava flow is issuing apparently from an intermediate elevation on the cinder cone, by eroding through its loose tephra, though details were hard to distinguish given the distance of the ship from the island. The path of the active lava flow can be approximately guessed by burning vegetation as it moves through the forest on the caldera wall. It appears that the pre-existing

valley between the cinder cone and the northern caldera wall, which existed till our second visit in April 2008, has been completely filled up by deposition of voluminous new ash since then. This has therefore enabled the new, active lava flow to completely abandon the westerly route and to take a “short cut” to the sea over the northern caldera wall.

The new flow is channelized, like all Barren Island aa flows, and aa flows in general, and is currently descending at a steep angle over the outer caldera wall’s cliffs on the north side of the volcano, and into the sea. It has built a structure resembling an alluvial fan along the shore, which can be called an embryonic lava delta. Incandescent lava is seen at a few places along the steep active flow channel, particularly in the dark, and the morphology of the lava flow channel as well as the “lava fan” leaves no doubt that it is an aa flow. We were able to reach this “lava fan” by using a Gemini from the ship, carefully circumventing the steam plume and sharp rocks underneath and through seawater which was very hot (an estimated ~60–70°C). We could collect lava samples from the southern edge of this lava fan”, which are typical clinkery aa basalt in hand specimen, black in colour.

3.5.5 The 2010 - 11 eruption

Our group revisited Barren Island volcano in December 2010. They have observed the shape of the Island which is changing with time and also the nature of eruption on the volcano is changing compared with our last trips. They have observed central cinder cone was sending periodic plumes of dark ash like our first field trip in January 2007, but the intensity is more powerful than 2007. The activity of plume eruption is typical mushroom type of plumes of dark ash which pulsating in every 5 - 10 minutes (Fig. 3.10a, b),

that indicate typical strombolian nature of eruption. They have also observed that all the lava flows are covered by recent ashes which suggest that the volcano erupted huge amount of ash in between 2009-10 (3.10c, d).

3.6 The nature of the caldera-filling aa flows

Aa and pahoehoe are the two fundamental types of basaltic lava flows (e.g., Macdonald, 1953; Peterson and Tilling, 1980; Rowland and Walker, 1990). All Barren Island lava flows, prehistoric through recent, are aa, including blocky aa. There is no pahoehoe on Barren Island, arguably due to (i) somewhat lower eruption temperatures of the lavas, consistent with melt inclusion studies and water-present melting in arcs (Luhr and Haldar, 2006), and (ii) high strain rates experienced by the flowing lavas due to the steep ground slopes.

It is difficult in the field to distinguish between the aa flows issued in 1991, 1994–95 and 2005–06. The flows are distinctly channelized, as is typical of aa flows worldwide, and the whole aa flow field is made up of ridges of the aa flows sloping towards the sea but with overall surface amplitude of as much as 25 m. From a distance the aa lava streams can be distinguished by subtle colour differences (shades of grey through black, with darker shades for younger lavas), and the younger lava streams can be seen to have left some “islands” of the older lavas between them (Fig. 3.9a). All these aa flows have jagged, very sharp and highly vesicular clinker at the top (Fig. 3.9b), based on which they can be characterized as proximal aa (terminology of Rowland and Walker, 1987). They also show massive cores at several places (Fig. 3.9b, c), as do all Barren prehistoric aa flows (Fig. 3.4e), and aa flows do in general. Rowland and Walker, (1990) describe how massive cores of aa flows can climb up from below the surface clinker along ramp structures,

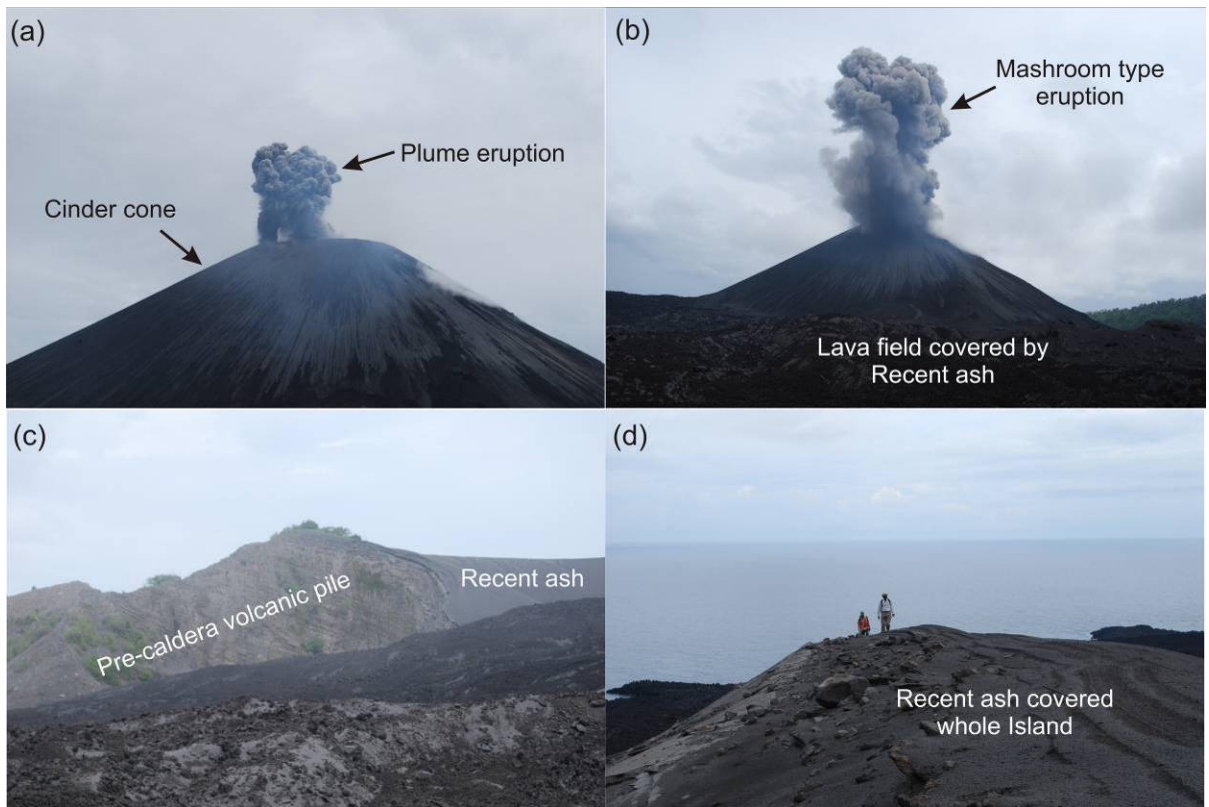


Fig. 3.10 *a-d* Most recent ash blankets (2010-2011) on Barren Island volcano covered all the lava flows of the Island

once the aa flow front has come to a halt and aa behind the front continues to flow forward. This is particularly seen in what Rowland and Walker (1990) term distal aa. One such ramp structure is shown in Fig. 3.9b.

An intriguing morphological type of aa makes up a small part of the aa flow field near Landing Site 3 on Barren Island (Figs. 3.2, 3.9c-g). Its surface crust has been extensively broken into plates or slabs throughout, whereas it shows well developed aa cores underneath (Figs. 3.8e, 3.9c). Evidently, the broken slabs of the surface crust— any of them razor sharp— were carried

along atop largely molten, mobile aa lava (which later solidified as the cores) and in the process experienced rotations, overturning, and even collisions.

An intriguing feature of this aa flow is that, locally, its surface crust is distinctly bent into convex upward shapes, resembling the tumuli common in pahoehoe flows which form by localized inflation (e.g., Anderson et al., 1999; Fig. 3.9e-g). Tumuli are most common in tube-fed pahoehoe flows (e.g., Walker, 1991; Rossi and Gudmundsson, 1996; Mattsson and Höskuldsson, 2005; Sheth, 2006), though they are also known from aa flows (e.g., Duncan et al., 2004; Lodato et al., 2007). These tumuli-like uplifts, elliptical in plan, and with long axes of 5-10 m, are approximately transverse to the overall flow direction. They also exhibit well developed, smooth, axial and axis-perpendicular clefts (Fig. 3.9e-g) usually associated with true tumuli. By analogy, these clefts should indicate periodic crack propagation from the surface downward into viscous lava, consistent with tensional cracking of bulging, uplifting crust (e.g., Anderson et al., 1999).

An interesting aspect of the convex tumuli-like features is the long, linear, closely-spaced wrinkles or “corrugations” that run across the surface, parallel to their long axes and axial clefts (Fig. 3.9f, g). Shanker et al. (2001), without giving location information, have illustrated very similar, possibly the same, outcrops, judging from their photographic figures 1.23 (showing upturned slabs) and 1.24 (showing slabs with “corrugated” surfaces). They described the latter as “pahoehoe with ropy structure”, but these lavas are neither ropy nor pahoehoe. Note that the strong visual impression of continuous grooves and ridges imparted from a distance (Fig. 3.9f) is illusory; when traced these terminate and splay laterally, and are actually arranged en echelon (Fig. 3.9g).

Guest and Stofan (2005) have described comparable examples from the 1983 eruption of Mount Etna. These Etna flows have continuous, level slabs of pahoehoe crust normally 1–2 m wide and tens of metres long, and they typically erupt from ephemeral boccas which develop at a late stage of development of an aa flow field. They call these flows “slab-cruste” flows, and note their similarities with the “toothpaste aa” flows described from Hawaii by Rowland and Walker, (1987). Toothpaste aa (also called spiny pahoehoe) typically issues from boccas within aa flows. The linear grooves and ridges of spiny pahoehoe are parallel to the local flow direction, and are believed to reflect the roughness of the boccas’ cross-sections. Tumuli are not unexpected in toothpaste aa; in fact, Walker (1991) writes that some of the best examples of tumuli are found in toothpaste aa. Rowland and Walker (1987) also illustrate imbricate stacking of surface plates or slabs on a toothpaste aa flow tongue (their Fig. 3.7), within a broader aa flow field, much as in the Barren Island flow.

We therefore consider this flow to represent a form of toothpaste lava, with which it shares many characteristics (Rowland and Walker, 1987; Guest and Stofan, 2005). This flow forms a part of the present-day western coastline as well as the edge of the lava delta. Its location is significant, as it provides indirect information about its likely age, a matter of some confusion in the literature. Shanker et al. (2001, Fig. 1.24) ascribed this toothpaste aa flow (whose corrugated surfaces they described as “ropy pahoehoe”) to the historic (1787–1832) eruptions. But if this is indeed historic, how does it form the edge of the lava delta which is overwhelmingly made up of the recent (1991, 1994–95 and 2005–06) flows? Note that this toothpaste aa flow cannot represent a long and isolated promontory of an historic aa flow, jutting out into the sea much more west than other historic flows and which the recent

lava flows might have failed to cover. No such promontory is visible in the photograph of March 1990 (Fig. 3b in Luhr and Haldar, 2006) which shows the extent of the historic flows. In fact we find no grounds for allocating this flow to the historic eruptions (~150–250 years old), and also note its freshness and lack of alteration despite the moist, tropical climate, and, most important, the absolutely total absence of vegetation on it. In comparable settings, such as Hawaii, new vegetation begins growing on lava flows only a few years after their emplacement (Macdonald et al., 1983).

The confusion is further accentuated by a January 2009 report by a GSI geologists' team, referred to earlier. This report (<http://www.gsi.gov.in/news.htm>) contains a photograph (their Fig. 4) of the lava flow on the northern side of their landing site (our Landing Site 3). This is exactly the toothpaste aa flow we have illustrated in our Fig. 3.9c, and the said report considers this flow as having erupted between July 2005 and March 2006. But this toothpaste aa flow cannot be a 2005–06 flow, because photographs of it appear in Shanker et al. (2001), and eyewitness accounts have described the 2005–06 flows as having flowed mainly along the far northern edge of the recent flow field. Therefore the most likely date for this toothpaste aa flow is either 1991 or 1994–95. Noting that the 1994–95 aa flows cover a major portion of the recent aa flow field (Fig. 3.2, 3.9a), the latter is the more probable of the two.

Recently Pal et al. (2010) attempted to explain magmatic evolution of all the eruptions on the Barren Island except 2009. They have reported that due to inaccessibility of the Island they could not able to collect 2009 eruption samples which we have collected and reported in Sheth et al., 2009. For magmatic correlation of the different eruptions of the Barren Island lavas

their approach was field and experimental based. They did petrography, major, trace and mineral chemistry of Barren lavas. Based on the petrological studies they have reported the nature of the lavas of Barren Island has changed due to magmatic differentiation during its residence in the diapers/ magma chamber. Based on mineralogical compositions they suggest that due to changing of eruption styles from Strombolian to Plinian its lava compositions have changed and argued that the recent magma chamber is shallower than older eruptions.

On the basis of major and trace element contents Pal et al. (2010) explained that the 2005 and 2006 lavas are not from same parental melt because the 2005 lava has restricted and clustering nature compared to 2006 lava and this nature imply that the earlier lava experienced more accumulation process with later one. They have also argued that the enrichment of large ion lithophile compared to high field strength elements in Barren magma is because the source mantle peridotite is already enriched with subduction zone component and mentioned low degree of partial melting on the basis of high Zr content of 2005-06 lava and other eruptions.

Further Pal et al. (2010) reported very low water content in Barren magma and produced a magma genesis model for Barren lavas. They have suggested that Barren basalt is nearly anhydrous so the melting is controlled by upwelling and pressure release process. They have used mantle diaper model which was reported by Tamura, 1994. On that model they have argued that 2005 eruption are due to thick, hot and dry rind of mantle diaper supplied substantial basaltic volcanism whereas the wet core of diapers produce lavas during 2006 eruption.

3.7 The cinder cone and recent ash cover

The central cinder cone on Barren Island has existed for the past 220 years at least, and must be described as polygenetic. In the time between the historic eruptions, which ended in 1832, and the first of the recent eruptions, in 1991, Barren Island's cinder cone managed to survive erosion, testifying to the general rule that cinder cones are well sorted and highly permeable, which means slow erosion because of little surface runoff (Segerstrom 1950; White et al., 1997). This cinder cone lost half its original height during the 1991 eruption (225 m above sea level at the end of the eruption), but grew higher and steeper again during the 1994–95 and 2005–06 eruptions, so it now rises well over 400 m above the sea. It is already active in a new eruption – so far only of tephra – that began in 2008. If activity persists, new lava flows are not unexpected.

Fine ash from the 1991 eruption, after the associated aa flows were erupted, reportedly covered the flows, and the rest of the volcano around the cinder cone was under ash up to 3 m thick. This was quickly removed by rain from over the 1991 flow as reported by Shanker et al. (2001). The possibly syn-caldera ash beds as well as the ash blanket deposited during the historic and recent eruptions are now deeply gullied (Figs. 3.8e). Fall of fine ash can also cause gullying of older, previously stable, landscapes (Segerstrom 1950, 1966). However, the recent eruptions have also deposited a large amount of dark grey ash and cinders on the southern and southeastern side that when incandescent burned part of the thick forest (Fig. 3.2c).

This page left blank intentionally

Chapter 4

Materials and Methods

In this chapter, I will discuss the various samples (rocks, sediments and water) collected for this work and the experimental techniques utilized to determine their mineralogical, textural, geochemical and isotopic characteristics. The chapter is composed of two parts: the first part describes the sampling protocols followed and the second part deals with analytical techniques.

4.1 Sampling Protocol

The samples for this thesis came from the Andaman Islands including the volcanic island called the Barren Island. These were collected during three field trips to these islands during March 2007, April 2008 and March 2009. During these trips, geological mapping and volcanological studies were carried out and sampling was done. Attempts were made to identify various types of flows, sequences of events and patterns of emissions on the volcano and a stratigraphy was built, the details of which have already been presented in the previous chapter. After proper identification of different types and sequence of volcanic materials, the samples were collected; which include scoria, lava flows, minerals and loose and consolidated ash samples. The locations of the samples are presented on geological map of the volcano (Fig. 4.1) and the other details are presented in Table 4.1. Since the geochemical characteristics of the rocks are a function of degree of alteration, attempts were made to collect very fresh samples from the interior of exposed rock outcrops to avoid alteration. Representative samples from most of the formations/flows/beds were collected for this work.

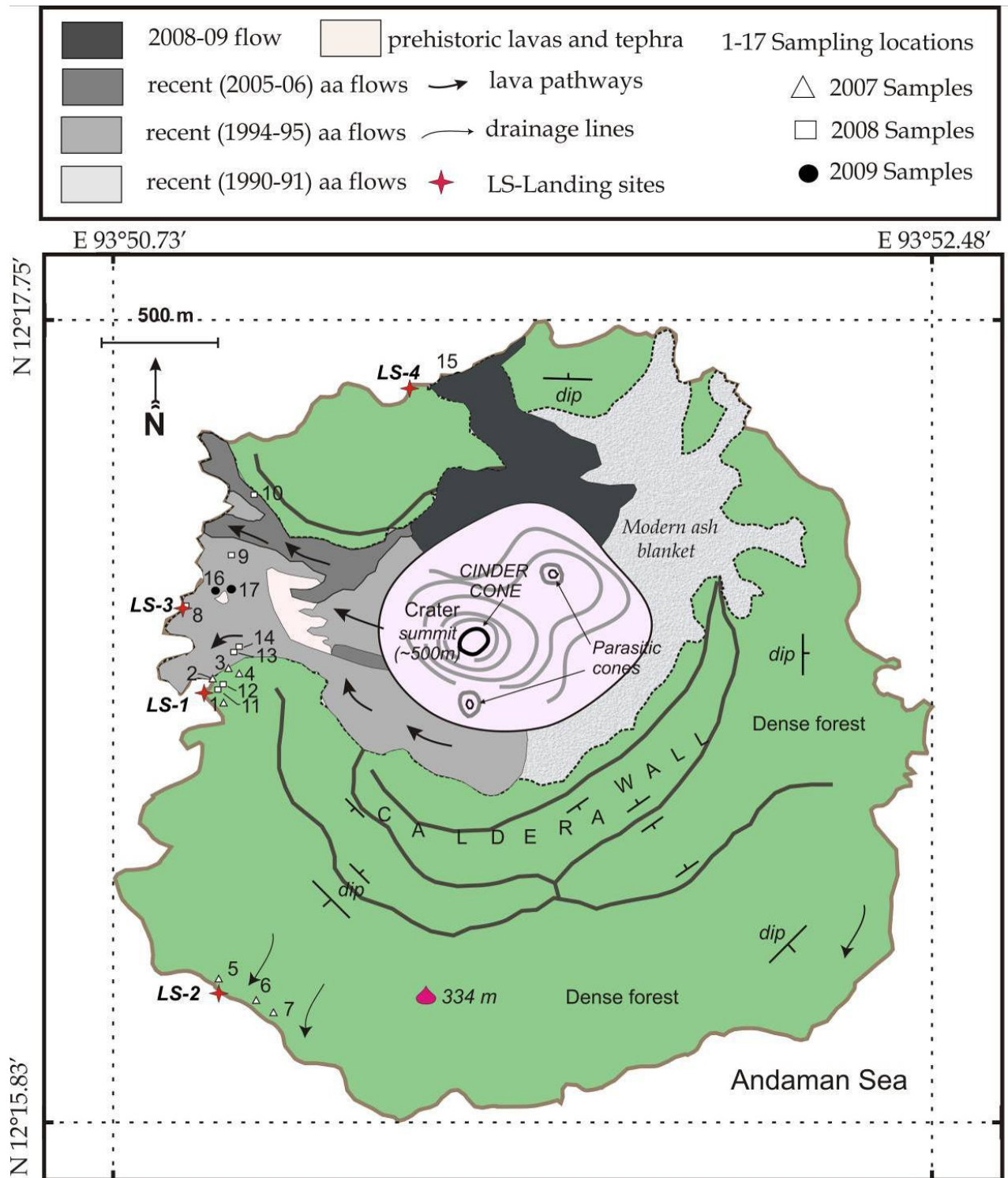


Fig. 4.1 Geological map of the Barren Island Volcano showing various lava flows and structures and sampling locations.

On the main island of the Andamans, we collected rock samples from the Ophiolite Group of rocks, particularly from those of igneous origin and samples of mud, clasts and water from the mud volcanoes. The samples from the Ophiolite Group include pillow lava, basalt, dolerite dike, gabbro, altered and fresh peridotite, andesite and plagiogranite. The sample locations are marked on Fig. 4.2 and the details of these are given in Table 4.2. Samples of mud breccia, clasts and water were collected from mud volcanoes of Baratang Island (Middle Andaman) and Hathilevel, Diglipur (North Andaman). Apart from water samples from mud volcanoes, water from springs, wells and rain were also collected. The details of these samples are given in Tables 4.3 and 4.4. All rock samples were collected in clean polythene bags, whereas water samples were collected in pre-cleaned polypropylene bottles rinsed several times with the water being sampled.

4.2 Analytical Methods

In order to achieve the scientific goals set for this thesis work, petrological, geochemical and isotopic characterization of the samples were required. Detailed and systematic approaches were adopted during this study for precise and accurate analysis of the mineralogical, major and trace elemental compositions and Sr, Nd and Pb isotopic ratios of samples. This section discusses the analytical methods utilized for the above work. Significant amount of efforts have been made during this thesis work to streamline the Sr and Nd isotope chemistry of samples in our laboratory, the details of which have been presented in next few sections.

Geochemical and isotopic characterization of samples requires well homogenization of rock and sediment samples. During this study, proper care was taken to avoid any metal contamination while powdering the

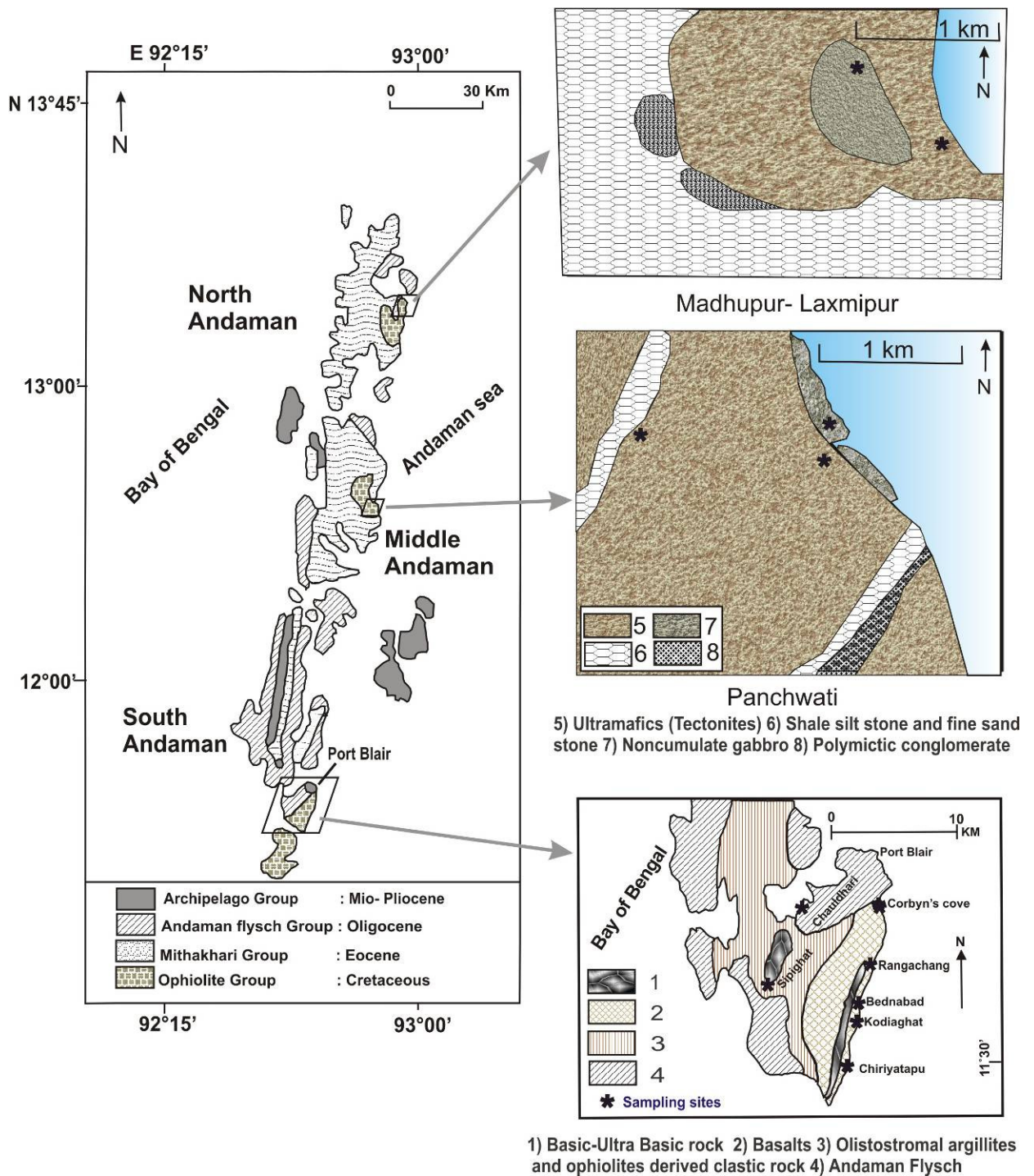


Fig. 4.2: Geological map of Andaman Islands (modified after Ray et al., 1988 and Pal and Bhattacharya 2010) with sampling locations marked on it with stars (*); a) North Andaman b) Middle Andaman c) North Andaman

Table 4.1: Descriptions of samples from lava flows and ash beds of the Barren Island Volcano (Island Arc Group), SL: Sampling Location

Sample ID	Geographical Coordinates	Short description	Sub-group
BI-07-01	N 12° 16.797', E 93° 51.008'	Massive - jointed - old lava - caldera wall, SL-1	Precaldera
BI-07-02	N 12° 16.797', E 93° 51.008'	Red - altered - lava, below from the above sample, SL-1	Precaldera
BI-07-03	N 12° 16.874', E 93° 50.939'	Plag - cpx xenoliths bearing lava - from wall, SL-2	Precaldera
BI-07-04	N 12° 16.874', E 93° 50.939'	Scoria - flow of unknown origin (1991? Or older?), SL-2	Post caldera
BI-07-05	N 12° 16.943', E 93° 51.015'	Scoria - flow of unknown origin (1991? Or older?), SL-4	Post caldera
BI-07-06	N 12° 16.89', E 93° 51.054'	Ash - from surface blanket - mixed	Post caldera
BI-07-07	N 12° 16.250', E 93° 50.932'	Core - lower most lava flow on caldera wall, SL-5	Precaldera
BI-07-08	N 12° 16.250', E 93° 50.932'	Red consolidated ash in between lava flows - caldera wall, SL-5	Precaldera
BI-07-09	N 12° 16.250', E 93° 50.932'	Core - middle lava flow on caldera wall, SL-5	Precaldera
BI-07-10	N 12° 16.250', E 93° 50.932'	Core - top lava flow on caldera wall, SL-5	Precaldera
BI-07-11	N 12° 16.09', E 93° 51.153'	Ash - from surface inside the forest, SL-6	Modern
BI-07-12	N 12° 16.969', E 93° 51.272'	Core - lava flow - flowed down over the caldera into sea, SL-7	Precaldera
BI-07-13	N 12° 16.969', E 93° 51.272'	Core - lava flow - flowed down over the caldera into sea, SL-7	Precaldera
BI-08-01	N 12° 17.078', E 93° 50.915'	Scoria - top of lava flow (94/95 flow?), SL-8	Post caldera
BI-08-02	N 12° 17.078', E 93° 50.915'	Toothpaste lava - surface - lava delta (94/95 flow?), SL-8	Post caldera
BI-08-03	N 12° 17.078', E 93° 50.915'	Core of an older flow - lava delta (94/95 flow?), SL-8	Post caldera
BI-08-04	N 12° 17.135', E 93° 51.010'	Scoria - older flow - lava delta (91 flow?), SL-9	Post caldera

Table 4.1 continued.....

BI-08-05	N 12° 17.310', E 93° 51.137'	Core - bottom most flow - caldera wall - north, SL-10	Precaldera
BI-08-06	N 12° 17.310', E 93° 51.137'	Core - top most flow - caldera wall - north, SL-10	Precaldera
BI-08-07	N 12° 17.310', E 93° 51.137'	Scoria - 2005 lava flow, SL-10	Modern
BI-08-08	N 12° 16.857', E 93° 50.950'	Plag - cpx xenoliths bearing lava - rolled boulders, SL-11	Precaldera
BI-08-09	N 12° 16.857', E 93° 50.950'	Ash layer - coarse - at LS2 (same as 07-TL-02), SL-12	
BI-08-10	N 12° 16.867', E 93° 50.952'	Plag - cpx xenoliths bearing lava - from top, SL-12	Precaldera
BI-08-11	N 12° 17.083', E 93° 50.936'	Core - lava flow 20m from LS1 (94/95 flow?), SL-13	Post caldera
BI-08-12	N 12° 17.094', E 93° 50.983'	Core - lava flow - near LS1 (near toothpaste lava) 94/95?, SL-14	Post caldera
BI-08-13	N 12° 17.094', E 93° 50.983'	Top of BI-08-12 flow - 94/95?, SL-14	Post caldera
BI-08-14	N 12° 17.078', E 93° 50.915'	Core - upturned slabs - toothpaste flow, SL-8	Post caldera
BI-08-15	N 12° 17.078', E 93° 50.915'	Top - upturned slabs - toothpaste flow, SL-8	Post caldera
BI-09-01	N 12° 17.594', E 93° 50.566'	2009 lava - hot fresh lava scoria, SL-15	Modern
BI-09-02	N 12° 17.099', E 93° 50.943'	2009 ash - falling ash collected from surface, SL-16	Modern
BI-09-03	N 12° 17.099', E 93° 50.943'	Toothpaste lava - surface, SL-17	Post caldera
BI-09-04	N 12° 17.099', E 93° 50.943'	Toothpaste lava - 30 cm, SL-17	Post caldera
BI-09-05	N 12° 17.099', E 93° 50.943'	Toothpaste lava - 5m up stream, SL-16	Post caldera
Mineral-1	N 12° 16.857', E 93° 50.950'	Inclusion in ankeramite lava - plag , SL-11	xenoliths
Mineral-2	N 12° 16.857', E 93° 50.950'	Inclusion in ankeramite lava - pyroxene, SL-11	xenoliths
BI-07-TL-01	N 12° 16.797', E 93° 51.008'	loose ash - south of 7-1, 2007 ash?, SL-1	Modern
BI-07-TL-02	N 12° 16.852', E 93° 50.939'	coarse ash - thick layer, SL-2	

Table 4.1 continued.....

BI-07-TL-03	N 12° 16.874', E 93° 50.939'	Old consolidated ash from a gully, SL-2	syncaldera
BI-07-TL-04	N 12° 16.243', E 93° 50.975'	Old - laminated ash - on beach section, SL-5	
BI-07-TL-05	N 12° 16.250', E 93° 50.932'	Ash bed in between lava flows, SL-5	
BI-07-TL-06	N 12° 17.094', E 93° 50.983'	Very old (bottom most) - laminated ash - on beach section, SL-14	
BI-08-TL-01	N 12° 17.310', E 93° 51.137'	Yellow ash - bottom most - on caldera wall - north, SL-10	Precaldera
BI-08-TL-02	N 12° 17.310', E 93° 51.137'	Red ash - below oldest flow on caldera wall - north, SL-10	Precaldera

Table: 4.2 Description of samples collected from the Ophiolite Group, Andaman Islands

Sample ID	Geographical coordinates	Location	Short description
PB-07-03	N 11° 30.34', E 92° 42.025'	Chiriyatapu	Buff coloured Basalt
PB-07-04A	N 11° 30.62', E 92° 42.41'	Chiriyatapu	Basalt
PB-07-05A	N 11° 31.85', E 92° 43.45'	Kodiyaghat	Plagiogranite
PB-07-05B	N 11° 31.85', E 92° 43.45'	Kodiyaghat	Basaltic flow/ Phlogopite also observed
PB-07-06	N 11° 33.96', E 92° 44.07'	Rangachang	Basalt (Coarse to medium grain)
PB-07-09	N 11° 38.38', E 92° 44.90'	Brooksabad	Pillow lava
PB-07-10	N 11° 38.28', E 92° 44.80'	Corbyn's Cove	Altered basalt (vein of Quartz / Zeolite)
PB-08-01	N 11° 31.847', E 92° 43.435'	Kodiyaghat	Plagiogranite
PB-08-02	N 11° 33.960', E 92° 42.071'	Rangachang	Trachyte vein in prismatic shaped with gabbro
PB-08-04	N 11° 33.960', E 92° 42.071'	Rangachang	Hydrothermal alteration product (plagio. + pyro.)

Sample ID	Geographical coordinates	Location	Short description
PB-08-06	N 11° 38.117', E 92° 44.814'	Quarry, Brooksabad	Low grade metamorphic basalt - green stone
PB-08-08	N 11° 39.700', E 92° 45.336'	Parade ground	Shale and sandstone
PB-08-11	N 11° 34.439', E 92° 40.055'	Nayasar	Green colour rock, chlorite rich
PB-08-12	N 11° 34.439', E 92° 40.055'	Nayasar	Metamorphic Basalt, quartz vein
AND-09-29	N 13°16.389', E 93°01.912'	Durgapur	Pillow lava
AND-09-31	N 13°16.224', E 92°57.748'	Madhupur	Altered Basalt
AND-09-32	N 13°16.224', E 92°53.435'	Madhupur	Serpentinite
AND-09-34	N 12°34.494', E 92°57.585'	Panchwati	Serpentinite
AND-09-46	N 12°34.494', E 92°57.585'	Sippighat	Serpentinite
AND-09-50	N 11°36.112', E 92°40.956'	Nayasar	Serpentinite
AND-09-58	N 11°29.362', E 92°42.578'	Mundapahar	Microdiorite
AND-09-60	N 11°31.271', E 92°43.043'	Chiriyatapu	Dolerite/ Gabbro

Table: 4.3 Description of mud breccia and rock clast samples collected from Mud Volcanoes of Andaman Islands

Sample ID	Geographical coordinates	Location	Short description
<i>Mud Breccia</i>			
BTMV-2	N 12°07.777', E 92°47.528'	Baratang, Middle Andaman	Fine mud collected from top of the cone
BTMV-3	N 12°07.777', E 92°47.528'	Baratang, Middle Andaman	Fine mud relatively older

Table 4.3 continued.....

BTMV-4	N 12°07.777', E 92°47.528'	Baratang, Middle Andaman	Fine mud collected from deeper part
BTMV-5	N 12°07.777', E 92°47.528'	Baratang, Middle Andaman	Fine mud collected from smaller cone
BTMV-6	N 12°07.777', E 92°47.528'	Baratang, Middle Andaman	Fine mud collected from another cone
BTMV-7	N 12°07.777', E 92°47.528'	Baratang, Middle Andaman	Fine mud collected from smaller cone
BTMV-8	N 12°07.777', E 92°47.528'	Baratang, Middle Andaman	Fine mud looking older
BTMV-9	N 12°07.777', E 92°47.528'	Baratang, Middle Andaman	Green mud (serpentine)
BTMV-10	N 12°07.777', E 92°47.528'	Baratang, Middle Andaman	Fine mud collected from top of the cone
BTMV-11	N 12°07.926', E 92°46.834'	Baratang, Middle Andaman	Fine mud collected from another site
BTMV-12	N 12°07.926', E 92°46.834'	Baratang, Middle Andaman	Green mud (serpentine)
HLMV-1	N 13°24.894', E 92°53.579'	Diglipur, North Andaman	Fine mud ,recent flow from biggest cone
HLMV-3	N 13°24.894', E 92°53.579'	Diglipur, North Andaman	Fine mud collected from 1 ft deeper level
HLMV-6	N 13°24.894', E 92°53.579'	Diglipur, North Andaman	Fine mud collected from dormant cone
HLMV-8	N 13°24.736', E 92°53.446'	Diglipur, North Andaman	Solidified mud collected from another site
HLMV-12	N 13°24.736', E 92°53.446'	Diglipur, North Andaman	Fine mud collected from cone
HLMV-15	N 13°24.660', E 92°53.442'	Diglipur, North Andaman	Fine mud collected 15 mt away from vent
HLMV-16	N 13°24.660', E 92°53.442'	Diglipur, North Andaman	Green mud (serpentine)
<i>Rock clast</i>			
BTMV-01-X2	N 12°07.777', E 92°47.528'	Baratang, Middle Andaman	Rock clast collected from first site
BTMV-01-X5	N 12°07.777', E 92°47.528'	Baratang, Middle Andaman	Rock clast collected from first site
BTMV-01-X6	N 12°07.777', E 92°47.528'	Baratang, Middle Andaman	Rock clast collected from first site

Table 4.3 continued

BTMV-02-X4	N 12°07.926', E 92°46.834'	Baratang, Middle Andaman	Rock clast collected from second site
BTMV-03-X2	N 12°07.926', E 92°46.834'	Baratang, Middle Andaman	Rock clast collected from third site
BTMV-03-X3	N 12°07.926', E 92°46.834'	Baratang, Middle Andaman	Rock clast collected from third site
BTMV-03-X4	N 12°07.926', E 92°46.834'	Baratang, Middle Andaman	Rock clast collected from third site
BTMV-03-X5	N 12°07.926', E 92°46.834'	Baratang, Middle Andaman	Rock clast collected from third site

Table: 4.4 Water samples from Mud Volcanoes and other water bodies, Andaman Islands

Sample ID	Geographical coordinates	Location	Date of collection	Short description
<i>Mud Volcanoes</i>				
BTMVW-1	N 12°07.777', E 92°47.528'	Baratang, Middle Andaman	3-Apr-09	Mud water
BTMVW-2	N 12°07.777', E 92°47.528'	Baratang, Middle Andaman	3-Apr-09	Mud water
BTMVW-3	N 12°07.777', E 92°47.528'	Baratang, Middle Andaman	3-Apr-09	Mud water
BTMVW-4	N 12°07.777', E 92°47.528'	Baratang, Middle Andaman	3-Apr-09	Mud water
BTMVW-5	N 12°07.926', E 92°46.834'	Baratang, Middle Andaman	3-Apr-09	Mud water
BTMVW-6	N 12°07.926', E 92°46.834'	Baratang, Middle Andaman	9-Dec-09	Mud water
BTMVW-7	N 12°07.926', E 92°46.834'	Baratang, Middle Andaman	12-Apr-10	Mud water
HLMVW-1	N 13°24.894', E 92°53.579'	Diglipur, North Andaman	5-Apr-09	Mud water
HLMVW-2	N 13°24.894', E 92°53.579'	Diglipur, North Andaman	5-Apr-09	Mud water

Table 4.4 continued.....

HLMVW-3	N 13°24.736', E 92°53.446'	Diglipur, North Andaman	5-Apr-09	Mud water
HLMVW-4	N 13°24.736', E 92°53.446'	Diglipur, North Andaman	5-Apr-09	Mud water
HLMVW-5	N 13°24.736', E 92°53.446'	Diglipur, North Andaman	5-Apr-09	Mud water
HLMVW-6	N 13°24.660', E 92°53.442'	Diglipur, North Andaman	5-Apr-09	Mud water
HLMVW-7	N 13°24.660', E 92°53.442'	Diglipur, North Andaman	5-Apr-09	Mud water
HLMVW-8	N 13°24.660', E 92°53.442'	Diglipur, North Andaman	9-Dec-09	Mud water
HLMVW-9	N 13°24.660', E 92°53.442'	Diglipur, North Andaman	9-Dec-09	Mud water
<i>Fresh Water Sources</i>				
NSW-1	N 13°27.185', E 94°16.527'	Narcondam Island	28-Mar-09	Narcondam Spring water
NSW-2	N 13°27.050', E 94°16.469'	Narcondam Island	28-Mar-09	Narcondam Spring water
NSW-3	N 13°27.273', E 94°16.455'	Narcondam Island	28-Mar-09	Narcondam Spring water
LBSW-1	N 13°11.625', E 93°02.181'	Diglipur, North Andaman	13-Apr-10	Lamiya bay (Mitha nala) spring water
PWSW-1	N 12°33.979', E 92°57.947'	Panchwati, Middle Andaman	14-Apr-10	Panchwati spring water
ZCWW-1	N 12°08.336', E 92°47.545'	Baratang, Middle Andaman	14-Apr-10	Well water from Baratang
PBRW	N 11°40.0', E 92°45.0'	Port Blair		Andaman rain-water, Port Blair

samples. Prior to powdering chipped sample pieces were thoroughly cleaned (repeatedly with HCl, MilliQ water and Ethyl alcohol). Powdering was done using an agate mortar and pestle. The samples were powdered to less than 75 micron size (200 mesh.), homogenized and stored in plastic bottles. These powdered samples were used for various mineralogical (powder diffraction), geochemical and isotopic studies.

4.2.1 Petrography

Petrographic studies focus on detailed descriptions of rocks in the hand specimen or under microscope or through mineralogical composition determined by techniques such as X-ray diffractometry (XRD). As the rock is an aggregate of minerals, “petrography” deals in effect with the identification of minerals and the study of their paragenesis. For the present work, we used thin section studied for the igneous rocks and XRD studies for sediment samples from the mud volcanoes.

For our work polished thin sections of rocks were prepared and analyses performed under petrological microscope Leica DM2500P microscope in IIT Bombay, Pawai and Nikon Eclipse LV100POL microscope at PRL, Ahmedabad. Based on their optical properties minerals were identified and their textural relationship were determined.

XRD was done on mud breccia samples at IIT Bombay with the help of Prof. Kanchan Pande to find out different constituent minerals in mud matrix. For this purpose a Rigaku Geigaflex, Japan, manually operated, X ray diffractometer was used. Cu-K α ($\lambda = 1.54056 \text{ \AA}$) X-ray was used as primary source. Minerals were identified from the diffractogram (Intensity vs. 2θ) using standard identification procedures (Brown and Brindley, 1980).

4.2.2 Geochemical Characterization

Major element content

The major elements are chemical elements having concentrations greater than one part per hundred (or > 1 wt %). Although concentrations of MnO, K₂O and sometimes P₂O₅ are less than 1 wt% in many basaltic rocks, they still are considered as major elements. Major elements concentrations in igneous rock help in the classification of rock types, understanding the degree of differentiation and determine trends of magma evolution. During this study, the major oxides (SiO₂, TiO₂, Al₂O₃, Fe₂O₃, MnO, MgO, CaO, Na₂O, K₂O and P₂O₅) were analyzed using X-Ray Fluorescence (XRF) spectroscopy method in an automated Phillips Axios X-ray Spectrometer (Panalytical Limited) fitted with an Rh X-ray tube, operated at 50kV and 55 mA, of 4kW power. The instrument is a national facility for Planetary Science and exploration Program (Planex) of Indian Space research Organization (ISRO) housed at Thaltej campus, Physical Research Laboratory, Ahmedabad. The instrument was set-up installed and calibrated for routine measurement of rock samples under this thesis work (Ray et al., 2008). The analyses for this work were done on pressed pellets method of the powdered samples.

Pressed pellets of our samples and rock standard were prepared; following the procedures given below. Four grams of samples igneous rock samples and two grams of mud samples were weighed accurately in a balance and transferred into an agate mortar. Each sample powder was mixed homogeneously with 1 g or 0.5 g of wax binder in a 4:1 ratio of sample: binder. The mixture was transferred to a 37 mm standard aluminum cup, filling up to two third of its volume. It was then placed under a compressor at a pressure of 150kN for 2 minutes. The pressure was removed slowly and pellet was recovered and labelled on the back.

Measurements were done with a wave-length dispersive X-ray fluorescent spectrometer which determined the intensity of X-rays diffracted from sample. Concentration of a specific element was determined by comparing the X-ray intensity with those from several standards through a calibration procedure. For calibration, appropriate set of standards were used for a given set of samples to avoid interferences and absorptions caused by matrix. For example, igneous samples were analyzed using igneous rock standards, while sedimentary rocks were analyzed with calibration using sedimentary rock standards. Some of these standards were used for determining accuracy and reproducibility of our measurements. The precision of measurements at 2σ level, based on repeated analyses of samples / standards, for major oxides was better than 2 %. The international rock standards which used for calibration of different oxides were: AGV-2, BCR-2, JA-3, JB-1a, JB-2, JB-3, JGb-1, JMS-2, MAG-1, SCO-1, SDO-1, STM-1 and W-2. Table 4.5 gives the rock type from which these standards have been prepared and their suppliers. Fig. 4.3 presents typical calibration curves, generated on the XRF using these standards, used for determination of the concentrations of various major oxides in our samples. The rock standards BHVO-2 (Basalts from Hawaiian Volcanological observatory) and BCR-2 (Basalts from Columbia River Traps) were treated as unknown to ascertain the accuracy and reproducibility of measurements. During the course of our experiment BHVO-2 (n=27) and BCR-2 (n=7) were analysed repeatedly along with the samples (Table 4.6). The measured and reported concentrations for major oxides show very good agreement within the analytical uncertainty (Fig. 4.4).

Loss on Ignition

The loss on ignition (LOI) analysis is a measure of the amount of hydrated and non-primary (i.e. not original to rock) phases. Compounds

that typically contribute to the total LOI are: volatile compounds, including H₂O, CO₂, Cl, S and other added compounds, such as O₂ or CO₂ resulting from the oxidation of FeO to Fe₂O₃ and carbonate formation. The analysis is performed for several reasons: I) to obtain an estimation of the amount of alteration of a sample, II) to prepare a sample powder for major and trace elements analysis and III) To removes phases that are not original to the rock, which could influence the major/trace element composition. Two grams each of moisture free sample powder (dried at 110°C) was transferred into a cleaned dry quartz crucible and accurately weighed.

Table 4.5: Rock standards used during the generation of major element data

Rock standards	Rock Types	Supplier
AGV-1	Andesite from Guano valley	USGS*
AGV-2	Andesite from Guano valley	USGS*
BCR-2	Columbia river basalt	USGS*
BHVO-2	Hawaiian Basalt	USGS*
JA-3	Japanese andesite	GJS**
JB-1a	Japanese basalt	GJS**
JB-2	Japanese basalt	GJS**
JB-3	Japanese basalt	GJS**
JGb-1	Japanese Gabbro	GJS**
JMS-2	Marine Mud	GJS**
MAG-1	Marine Sediments	USGS*
SCO-1	Cody Shale	USGS*
SDO-1	Shale	USGS*
STM-1	Napheline Syenite	USGS*
W-2	Diabase	USGS*

USGS*: United state geological survey and GJS**: Japanese geological Survey

The quartz crucible is placed inside a muffle furnace preheated to 1050°C for igneous rocks and 1070°C for sedimentary rocks. After igniting the sample for two hours, the furnace was switched off and allowed to cool to room temperature, the sample was weighed again and the difference in measured weight is converted into LOI by the following equation:

$$LOI = \left(\frac{(W_i - W_f)}{W_i} \right) \times 100 \quad (4.1)$$

Where W_i is initial measured weight (Sample and crucible) and W_f is the measured weight after ignition (sample and crucible). LOI is expressed in %.

Table 4.6: Measured and reported major oxide concentrations in BHVO -2 and BCR-2

Major Oxide	BHVO-2 (Reported*) wt% ± 2σ	BHVO-2 (measured) mean (n=27) wt% ± 2σ	BCR-2 (Reported*) wt% ± 2σ	BCR-2 (measured) mean (n=7) wt% ± 2σ
SiO ₂	49.90 ± 0.60	49.45 ± 0.33	54.10 ± 0.80	54.36 ± 0.04
TiO ₂	2.73 ± 0.04	2.71 ± 0.02	2.26 ± 0.05	2.37 ± 0.02
Al ₂ O ₃	13.50 ± 0.20	13.73 ± 0.06	13.50 ± 0.20	13.28 ± 0.01
Fe ₂ O ₃	12.30 ± 0.20	12.50 ± 0.32	13.80 ± 0.20	13.94 ± .034
MnO	0.17 ± 0.01	0.16 ± 0.01	0.20 ± 0.01	0.17 ± 0.01
MgO	7.23 ± 0.12	7.34 ± 0.16	3.59 ± 0.11	3.72 ± 0.01
CaO	11.40 ± 0.20	11.52 ± 0.04	7.12 ± 0.11	7.01 ± 0.01
Na ₂ O	2.22 ± 0.08	2.33 ± 0.06	3.16 ± 0.11	3.26 ± 0.01
K ₂ O	0.52 ± 0.01	0.53 ± 0.01	1.79 ± 0.05	1.85 ± 0.01
P ₂ O ₅	0.27 ± 0.20	0.23 ± 0.01	0.35 ± 0.02	0.38 ± 0.01
LOI	ND	-0.55	ND	ND
Total	100.24	99.94	0.20	100.34

* Values supplied by USGS and ND: Not determined

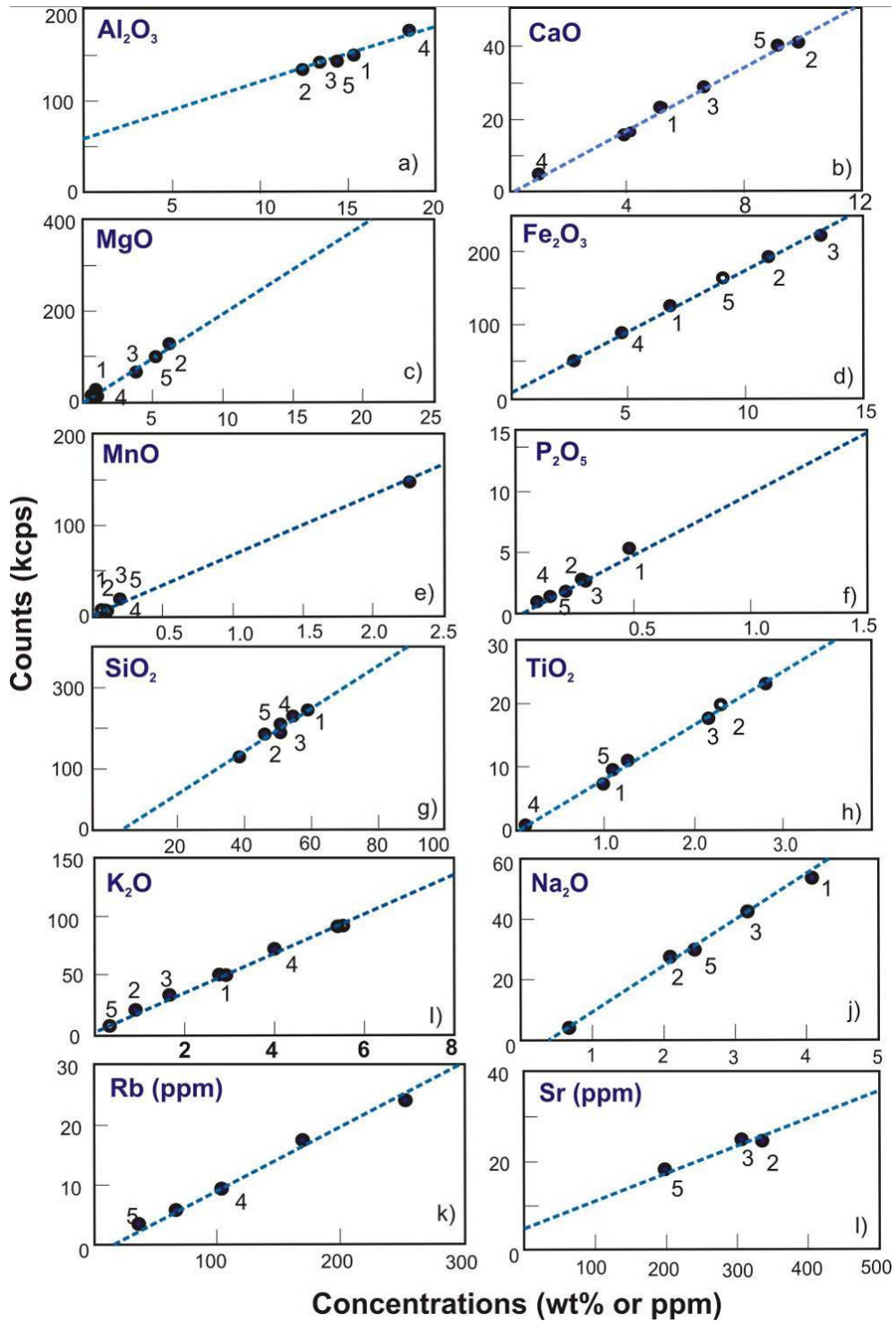


Fig. 4.3: Typical calibration curves generated using XRF for ten major element oxides (wt%) and two trace elements (in ppm) using several international rock standards. 1) AGV-2, 2) BHVO-2, 3) BCR-2, 4) STM-1 5) W-2.

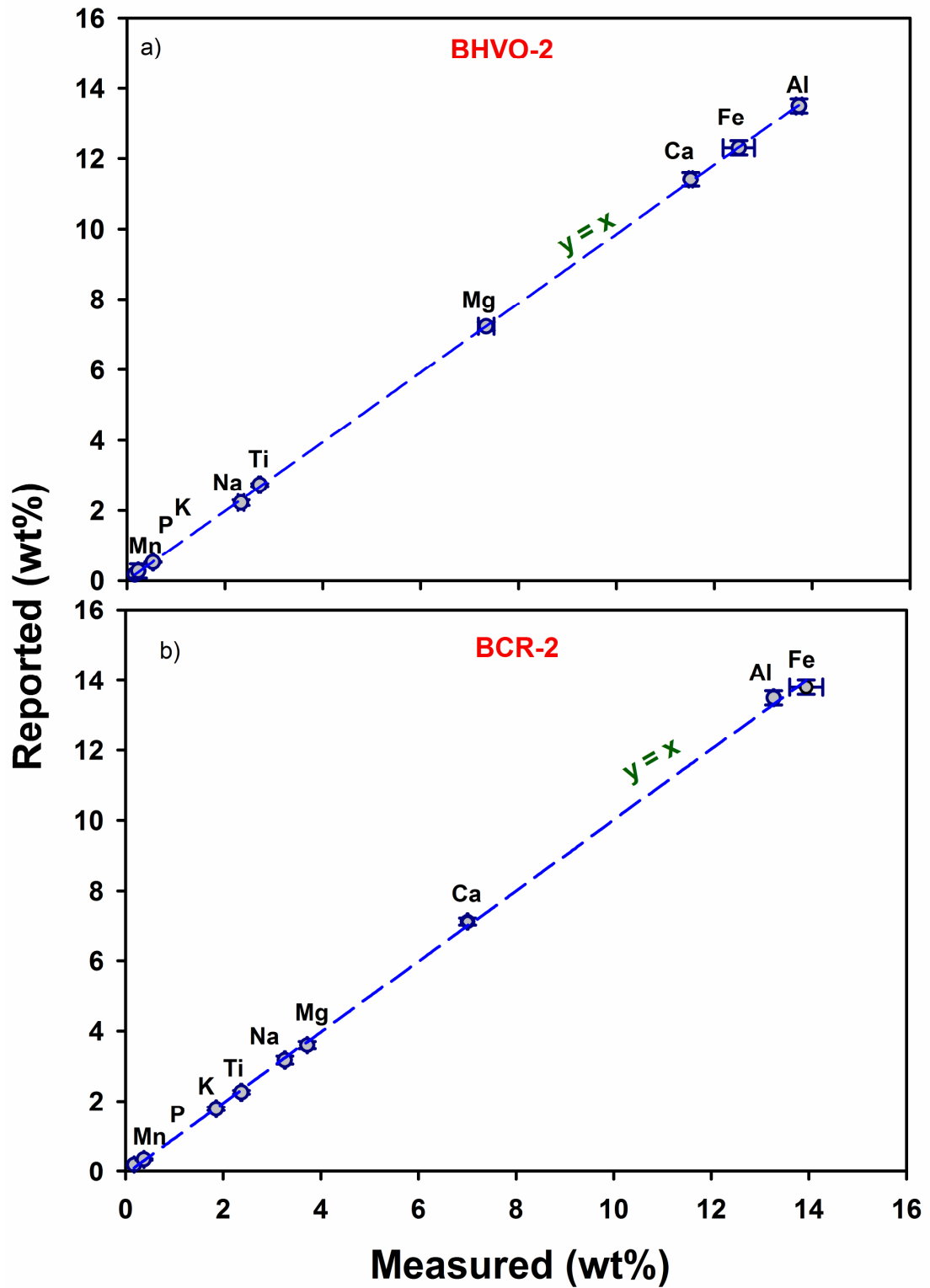


Fig.4.4: Comparison of measured and reported concentration of various major element oxides in BHVO-2 (a) and BCR-2 (b).

Trace element contents

Trace elements are chemical elements having concentrations less than 1000 ppm or 0.1 % of a rock composition. Although they do not usually form major igneous rock forming phases, they are powerful tracers of the magmatic processes. In this work, trace element contents were measured using Inductively Coupled Plasma Mass Spectrometry (ICP-MS) and Instrumental Neutron Activation Analysis (INAA) methods.

Concentrations of trace elements including 14 rare earth elements (REEs) in igneous rock samples were determined using an ICP-MS at PRL. Measurements were done on the sample solutions, in 2 % HNO₃ medium, prepared using the dissolution protocol outlined in Table 4.7

Table 4.7: Sample dissolution procedure for trace elements analysis

Step 1: ~ 50 mg of homogenized sample powder weighed into a 17ml PFA savillex teflon vial and capped with proper labelling.

Step 2: ~ 1 ml of HF + HNO₃ mixture (2:1) was added to the sample powder and thoroughly mixed.

Step 3: The vial was capped tightly and ultrasonicated for 40/60 minutes and kept overnight for complete dissolution.

Step 4: Next day, the solution vial was heated to 80°C and checked for undissolved grains. Once found completely dissolved the solution was dried down.

Step 5: Once dried, the sample was taken back into solution using 1 ml of 8 N HNO₃.

Step 6: Making sure of complete dissolution of solution was dried and taken back again in 8 N HNO₃.

Step 7: After the 2nd and 3rd dissolution in 8 N HNO₃, the sample was dried down and taken back into solution in 2% HNO₃.

Table 4.7 continued

Step 8: Capped sample solution vial was placed on the hotplate at 80°C for 30 minutes, to ensure that no white precipitate was left undissolved. The vial was uncapped and several drops of 2% HNO₃ were added to the cap. The dilute acid droplets were swirled around the cap so as to take back any liquid adhering to the cap.

Step 9: The sample solution was further diluted 1000 times in 2% HNO₃ and is kept in pre-cleaned 60 ml plastic bottle used as a Stock solution.

All acids used in the dissolution procedure were of ultra pure grade (from Sea-Star, Canada). For calibration purpose an international rock standard BHVO-2 was used sample powder of BHVO-2, BCR-2 and AGV-2 were dissolved along with the sample the same protocol as described in Table 4.7. Calibration curves were generated using blank and various dilutions of standard solutions. A few typical calibration curves are presented in Fig. 4.5. The isotopes ⁴⁵Sc, ⁵¹V, ⁵²Cr, ⁵⁹Co, ⁶⁰Ni, ⁶⁶Zn, ⁸⁵Rb, ⁸⁸Sr, ⁹⁰Zr, ⁹³Nb, ¹³⁷Ba, ¹³⁹La, ¹⁴⁰Ce, ¹⁴¹Pr, ¹⁴⁶Nd, ¹⁴⁷Sm, ¹⁵³Eu, ¹⁵⁷Gd, ¹⁵⁹Tb, ¹⁶³Dy, ¹⁶⁵Ho, ¹⁶⁶Er, ¹⁶⁹Tm, ¹⁷²Yb, ¹⁷⁵Lu, ¹⁷⁸Hf, ¹⁸¹Ta and ²³²Th, were analyzed for their respective elements. Reproducibility (external precision) of our measurements, based on the repeated analyses of sample, were better than 2% at 2σ level, for all trace elements reported here. For accuracy check, analyses of various dilutions of the international standard BHVO-2 were performed at regular intervals. As can be seen in Table 4.8, the measured and reported elemental concentrations in BHVO-2 show very good agreement within the analytical uncertainty.

Apart from analyzing them on ICP-MS some of the important trace elements in igneous rocks e.g., Ta, Rb and Th, were also analyzed using INAA for better accuracy. In addition, the samples of mud breccia that contained appreciable amounts of undissolvable organic matter were also

analyzed by INAA for their trace element contents. Carefully powdered samples for INAA were dried at 110°C and packed in Al-foils and transferred to a quartz vial together with packs of BCR-1 and BHVO-2 and sealed. Blank Al foil was also packed along with the samples and standards to determine the contribution from Al foil (if any). The sealed quartz vial was subsequently transferred into a container and sent for

Table 4.8 Comparison of measured and reported concentrations for various trace elements in BHVO-2

Trace elements	Measured concentration (ppm) $\pm 2\sigma$	Reported concentration* (ppm) $\pm 2\sigma$
Sc	31.6 \pm 3.6	31 \pm 2
V	330 \pm 36	329 \pm 18
Cr	290 \pm 31	285 \pm 28
Co	48.1 \pm 5.4	47 \pm 4
Ni	114 \pm 13.8	112 \pm 18
Rb	10.5 \pm 1.1	10.1 \pm 1.2
Cs	0.11 \pm 0.02	0.11 \pm 0.02
Sr	383 \pm 36	382 \pm 20
Y	23 \pm 2.4	23 \pm 2
Zr	159 \pm 17	160 \pm 16
Nb	16.3 \pm 1.9	16.4 \pm 0.1
Ba	129 \pm 1	128 \pm 8
La	15.1 \pm 1.5	15.6 \pm 0.1
Ce	37.3 \pm 3.6	37 \pm 2
Pr	5.35 \pm 0.86	5 \pm 0.6
Nd	24.4 \pm 3.3	24 \pm 2
Sm	6.1 \pm 0.76	5.8 \pm 1
Eu	2.06 \pm 0.23	2 \pm 0.2
Gd	6.24 \pm 0.78	5.9 \pm 0.8
Tb	0.82 \pm 0.17	0.86 \pm 0.06
Dy	5.37 \pm 0.58	4.9 \pm 0.8
Ho	0.93 \pm 0.07	0.91 \pm 0.12
Er	2.59 \pm 0.27	2.3 \pm 0.2
Tm	0.31 \pm 0.03	0.3 \pm 0.1
Yb	1.95 \pm 0.24	2.0 \pm 0.4
Lu	0.29 \pm 0.01	0.26 \pm 0.08
Hf	4.13 \pm 0.39	4.1 \pm 0.8
Ta	0.93 \pm 0.12	0.94 \pm 0.14
Pb	1.61 \pm 0.10	1.4 \pm 0.4
Th	1.12 \pm 0.19	1.18 \pm 0.18
U	0.41 \pm 0.07	0.44 \pm 0.06

*Gao et al., (2002); kent et al., (2004); Raczek et al., (2003)

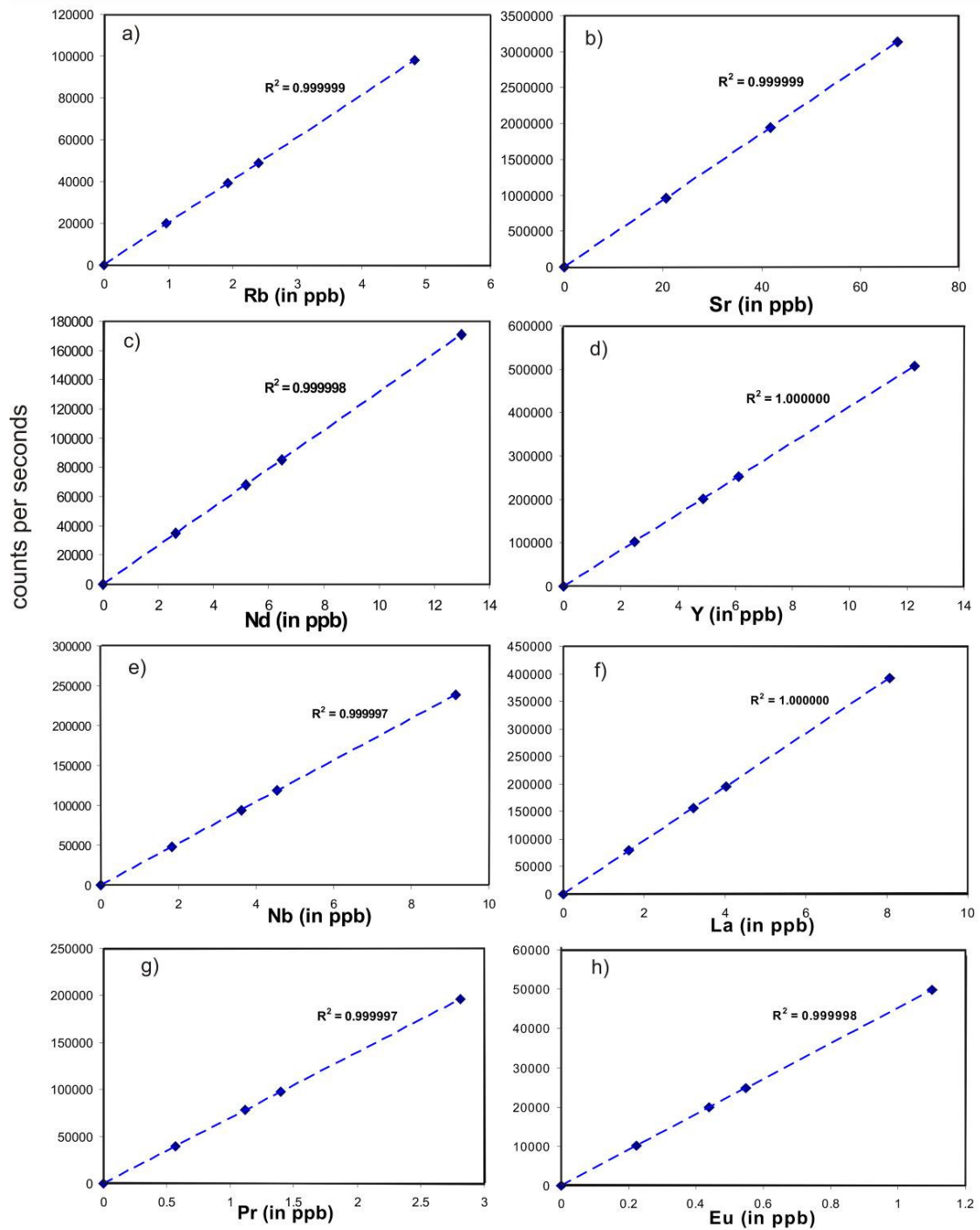


Fig. 4.5: Typical calibration curves for various trace elements generated on ICP-MS using various dilutions of a standard solution (BHVO-2).

irradiation at the CIRUS reactor of the Bhabha Atomic Research Center, Mumbai, where the samples were irradiated for 15 days. The irradiated samples were counted on a Hyper Pure Germanium (HPGE) γ -ray

detector at PRL. The 148cc, high purity Ge-detector, has a resolution of 2.2 KeV for 1333 KeV gamma ray of ^{60}Co and is housed in a 10 cm thick lead shield. The counting was repeated after appropriate cooling intervals to determine both short and long lived radioisotopes. The concentration of various elements like Ta, Rb, Th, Zr, Nb and nine rare earth elements (La, Ce, Nd, Sm, Eu, Gd, Tb, Yb and Lu) was measured by sample standard (BCR-1) comparative method as outlined by Flanagan (1976) and Laul (1979).

Table 4.9 Comparison of measured and reported concentrations for various trace elements in BCR-1 and BHVO-2 by INAA

Trace elements	BCR-1 Reported* wt%/ppm $\pm 1\sigma$	BCR-1 Measured wt% ppm $\pm 1\sigma$	BHVO-2 Reported* wt%/ppm $\pm 1\sigma$	BHVO-2 Measured wt%/ppm $\pm 1\sigma$
Fe	9.38 \pm 0.1	9.34 \pm 0.1	8.63 \pm 0.1	8.51 \pm 0.1
Co	38 \pm 0.1	37.83 \pm 0.1	45 \pm 0.1	45.2 \pm 0.1
Sc	32 \pm 0.5	31.86 \pm 0.5	32 \pm 0.5	31.63 \pm 0.2
Na	2.42 \pm 0.1	2.42 \pm 0.1	1.64 \pm 0.1	1.64 \pm 0.1
Ca	4.95 \pm 0.5	4.73 \pm 0.5	8.17 \pm 0.5	8.25 \pm 0.5
Rb	46 \pm 1	47.15 \pm 1	9.08 \pm 0.5	9.9 \pm 0.5
Sr	330 \pm 20	367 \pm 20	396 \pm 10	387 \pm 20
Ba	675 \pm 1.2	676 \pm 1	131 \pm 5	135 \pm 10
Zn	130 \pm 10	123.5 \pm 5	103 \pm 0.5	102.4 \pm 1.1
Cs	0.95 \pm 0.5	ND	0.11 \pm 0.05	0.13 \pm 0.07
Th	6 \pm 0.6	5.94 \pm 0.6	1.03 \pm 0.05	1.07 \pm 0.04
Ta	0.79 \pm 0.5	0.79 \pm 0.2	1.06 \pm 0.02	1.09 \pm 0.01
Hf	4.9 \pm 1.2	4.9 \pm 0.5	4.28 \pm 0.01	4.28 \pm 0.04
Zr	190 \pm 5	201 \pm 10	172 \pm 0.1	163 \pm 0.16
La	25.2 \pm 0.6	25.63 \pm	15.2 \pm 0.05	15.35 \pm 0.07
Ce	54 \pm 0.6	53.73 \pm	37.5 \pm 0.01	37.3 \pm 0.02
Nd	28.7 \pm 1.2	29.4 \pm	24.5 \pm 0.05	24.05 \pm 0.05
Sm	6.6 \pm 0.6	6.55 \pm	6.07 \pm 0.1	5.92 \pm 0.03
Eu	1.94 \pm 0.6	1.93 \pm	2.07 \pm 0.05	2 \pm 0.02
Gd	6.67 \pm 3	5.31 \pm 2	6.24 \pm 0.5	6.91 \pm 0.06
Tb	1.07 \pm 0.6	1.06 \pm 0.1	0.936 \pm 0.01	0.931 \pm 0.04
Yb	3.36 \pm 1.2	3.46 \pm	2 \pm 0.1	1.91 \pm 0.02
Lu	0.50 \pm 1.2	0.50 \pm	0.27 \pm 0.01	0.27 \pm 0.01

* Flanagan (1976) and Laul (1979); all are in ppm except Fe and Na in wt%

Radiogenic Isotopic ratios:

Sr and Nd isotopic ratio analyses were carried out on an Isoprobe-T Thermal Ionization Mass Spectrometer (TIMS) at the Physical Research Laboratory, Ahmedabad while the Pb isotopic ratio measurements were performed by at the Department of Earth-science, Pondicherry University, Puducherry using a Thermo-Triton TIMS. Prior to isotope ratio analyses the samples were dissolved and Sr, Nd and Pb were extracted using liquid- chromatographic techniques, the details of which are described below.

Table 4.10: Sample dissolution procedure for isotopic analyses

Step 1: ~ 50 mg of homogenized sample powder weighed into a 17ml PFA savillex teflon vial and capped with proper labelling.

Step 2: Add ~ 1.5 ml of HF + HNO₃ mixture (2:1) to the sample powder and mixed to ensure the acid accesses all the sample powder.

Step 3: The vial was capped tightly and ultrasonicated for 40/60 minutes and kept overnight for complete dissolution.

Step 4: Next day, the solution vial was heated to 80°C and checked for undissolved grains once found completely dissolved the solution was dried down.

Step 5: Once dried, the sample was taken back into solution using 1 ml of 8 N HNO₃ it.

Step 6: Making sure of complete dissolution of solution was dried and taken back again in 8 N HNO₃.

Step 7: After the 2nd and 3rd dissolution in 8 N HNO₃, the sample was dried down and taken back into solution in 2 ml of 6 N HCl.

Step 8: 2 ml of 6 N HCl sample was dried down to convert the elements to chloride.

Step 9: The final sample solution was prepared in 1 ml of 2 N HCl and capped for column chemistry

Cation-exchange chromatography was used to separate Sr and REE from other elements present in the sample. Subsequently, Nd was separated from other REE using elements specific chromatographic medium. For Sr and REE separation we used BioRad make AG 50W X8 (200 to 400 mesh size) resin, whereas the Nd separation Ln-specific resin from Eichrom (50 to 100 μm mesh) was used. The columns used were of pure quartz and of different heights depending upon the purpose, e.g., the primary columns for Sr and REE separation were 25 cm in height and had internal diameter of 0.8 cm, where as for Nd separation smaller column (height = 15 cm, ID = 0.5 cm) were used. The elution procedures, determined through calibration, are described in Table 4.11.

Table 4.11: Protocol for Sr and REE separation from sample solution

Step 1: The Dowex 50 cation exchange resin was cleaned properly using milli-Q water to remove fine floating materials from resin.

Step 2: cleaned quartz wool was fixed in the base of primary columns to hold the resin and maintained constant flow.

Step 3: The primary columns were filled with Dowex 50 cation exchange resin up to height of ~ 16 cm.

Step 4: columns were cleaned with 5 ml of 6 N HCl and subsequent conditioned with 6 ml of 2 N HCl.

Step 5: 1 ml dissolved sample solution in 2 N HCl was loaded gently onto the resin bed using pipette.

Step 6: 1 ml of 2 N HCl passed to allow complete loading

Step 7: 36 ml of 2 N HCl was passed and discarded (for removal of Fe, K, Na, Rb, Ca etc.)

Step 8: Collection for Sr: 12 ml of 2 N HCl was eluted and collected for Sr.

Table 4.11 continued

Step 9: Collection for REE: 18 ml of 6 N HCl was eluted and collected for REE cut - dried down, taken in 100 μ l of 0.18N HCl and capped for REE column chemistry.

Step 10: The collected Sr cut was dried down - ready for measurement on MS.

Step 11: Columns were cleaned 2 times with full volume of 6 N HCl and half full volume of milli-Q water for regeneration.

Table 4.12: Protocol for Nd separation from REE Cut

Step 1: The Ln-specific resin was cleaned properly using milli-Q water to remove fine floating materials from resin.

Step 2: Cleaned quartz wool was fixed in the base of columns to hold the resin and was maintained constant flow.

Step 3: The columns were filled with Ln-specific resin up to height of \sim 9 cm.

Step 4: columns were cleaned with 5 ml of 2N HCl and subsequently conditioned with 2 ml of 0.18 N HCl.

Step 5: 1 ml collected and dried REE cut (100 μ l of 0.18N HCl) was loaded gently onto the resin bed using pipette.

Step 6: Another 100 μ l of 0.18N HCl was loaded after washing the vial for each sample

Step 7: Wash- 19 ml of 0.18 N HCl was passed and discarded (for removal of La, Ce, Pr etc.)

Step 8: Collection for Nd: 7 ml of 0.3 N HCl was eluted and collected for Nd.

Step 9: Columns were cleaned with half full volume with 6 N HCl and full volume of milli-Q water for regeneration of the resin.

Step 10: The collected Nd cut was dried down and stored for Nd-analysis.

Step 11: The columns were stored in diluted acid medium for further use.

The purified Sr from a sample was loaded with 0.1 M phosphoric acid on degassed and oxidized high purity tantalum (Ta) filament whereas for purified Nd fraction was loaded on the outer degassed Ta filament of a triple filament assembly, in which outer and inner are high purity Ta filaments, while centre contains a high purity Re filament. Sr and Nd isotopic ratio measurements were done on Isoprobe-T TIMS in static mode. The ratios were corrected for instrumental mass fractionation using exponential fractionation correction (Thrilwall 1991a) and assuming $^{86}\text{Sr}/^{88}\text{Sr} = 0.1194$ and $^{146}\text{Nd}/^{144}\text{Nd} = 0.7219$. During the course of these analyses, international isotopic standard for Sr, NBS-987 and Nd isotope standard, JNdi were measured routinely. The average for $^{87}\text{Sr}/^{86}\text{Sr}$ for 131 analyses of NBS-987 was found to be 0.710227 ± 0.000028 (2σ) and for the mean $^{143}\text{Nd}/^{144}\text{Nd}$ value obtained on 53 measurements of JNdi was 0.512104 ± 0.000016 (2σ), these values are well within their recommended values 0.710248 ± 0.000023 (2σ) [Moore et al., 1982] for NBS-987 and 0.512100 ± 0.000005 (2σ) for JNdi. The above value of JNdi-1 corresponds to a value of 0.511847 for the widely used La Jolla Nd standard (Tanaka et al., 2000). The variations in $^{87}\text{Sr}/^{86}\text{Sr}$ of NBS-987 and $^{143}\text{Nd}/^{144}\text{Nd}$ of JNdi-1 standards are plotted against time for the course of this study (Fig. 4.6). The consistency and absence of any systematic offset indicate that our measurements are highly precise over a long period of time. Further, USGS rock standards BHVO-2 and BCR-2 were also analyzed for their $^{87}\text{Sr}/^{86}\text{Sr}$ and $^{143}\text{Nd}/^{144}\text{Nd}$ to establish the accuracy of our measurements. The variations of Sr and Nd isotopic ratio of BHVO-2 (N = 14) are plotted against time during course of this study. (Fig. 4.7), and these data once again, confirm the high quality (accuracy and precision) of our measurements.

Several total procedural blanks of Sr and Nd were processed along with the samples. The procedural blanks for Sr and Nd were always below

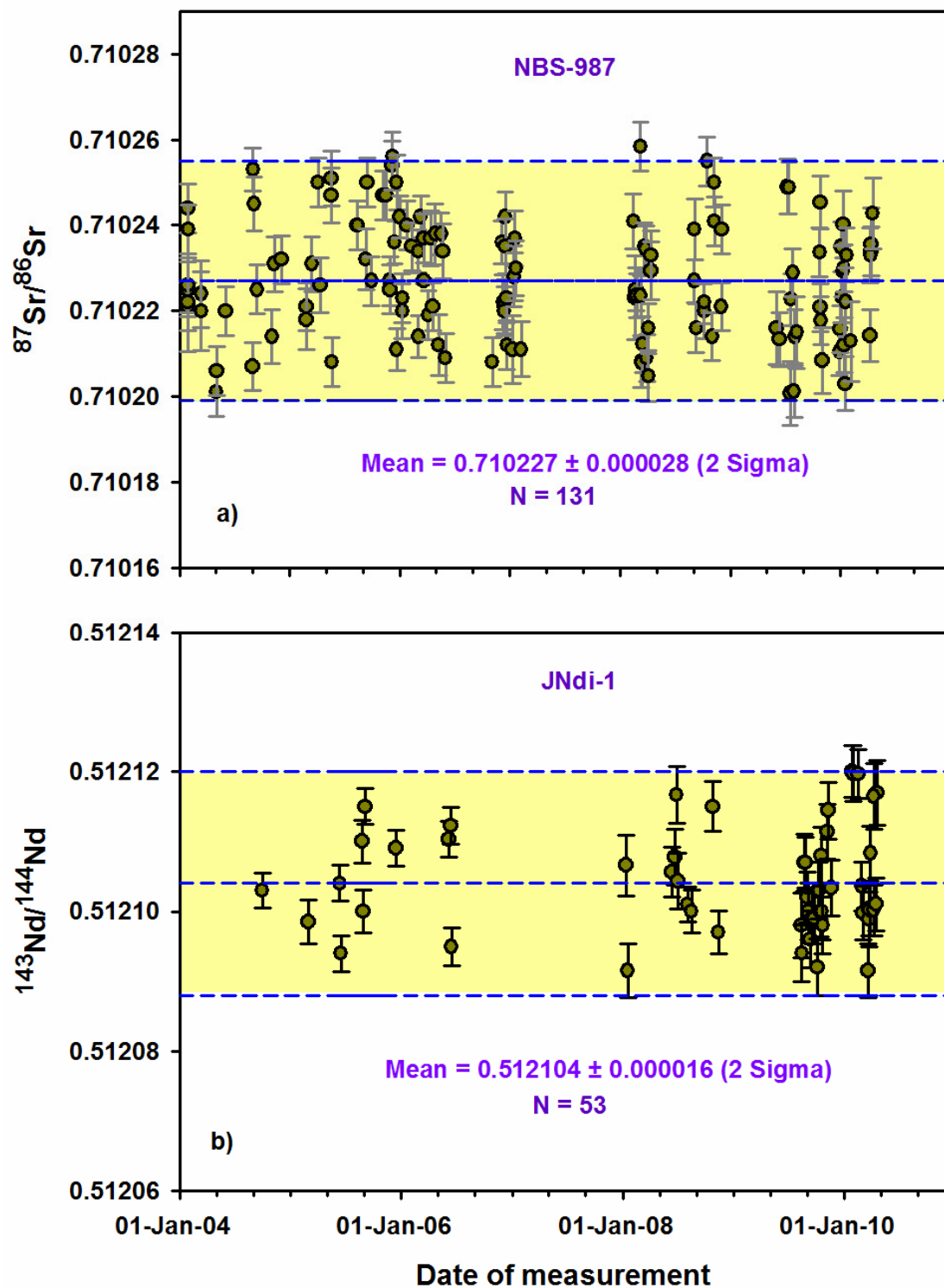


Fig. 4.6 Temporal variation of measured $^{87}\text{Sr}/^{86}\text{Sr}$ in NBS-987 (a) and $^{143}\text{Nd}/^{144}\text{Nd}$ in JNdi-1 (b). The shaded area represents mean \pm SD (2 sigma) of the data points. All the data points agree well within uncertainties with the reported value.

500pg and 400pg, respectively. These blanks are several orders of magnitude lower than typical total Sr and Nd processed during this study and hence no corrections for blanks were made.

A few samples from Barren Island were also analyzed for their Pb isotopic ratios at Pondicherry University. About 100 mg of homogenized rock powder was digested using ultra pure HF + HCl acids on 7ml savillex vial for about one hour on hot plate at 150°C. The digested fraction was carefully decanted into another savillex vial without disturbing the undigested sample. Most of the Pb was in leachable phase because Pb prefers to go into the liquid phase (solution). Leached solution was evaporated to dryness and, a small amount of clean 1 N HBr acid was added and dried it, the procedure was repeated and the final solution was prepared in 3-4 ml of 1 N HBr. Separation of Pb was then carried out using anion exchange resin following the procedure prescribed by Manhés et al. (1984). Pb was loaded on pre-cleaned high purity, degassed Re filament in chloride form with 0.1 M phosphoric acid and silica gel. Pb standard, NBS-981 was repeatedly analyzed for determining fractionation correction. The external mass fractionation correction (linear) was done taking true values from Todt et al. (1996). All reagents used were quartz distilled and total procedural blank determined was better than 200pg. During the course of these analyses, international isotopic standard for Sr, NBS-981 were measured repeatedly the average values for $^{206}\text{Pb}/^{204}\text{Pb}$, $^{207}\text{Pb}/^{204}\text{Pb}$ and $^{208}\text{Pb}/^{204}\text{Pb}$ for 18 measurements of NBS-981 were found 16.9043 ± 0.0107 (1σ), 15.4462 ± 0.0138 (1σ) and 36.5595 ± 0.0447 (1σ) respectively.

Stable oxygen and hydrogen isotopic ratios

Oxygen and hydrogen isotopic ratios of water samples from the Andamans were determined at Physical Research Laboratory using a

continuous flow Thermo Isotopic Ratio Mass Spectrometer (IRMS) Delta V Plus. The procedure details are given in Maurya et al. (2011).

The isotopic ratios are expressed in delta notation as follow:

$$\delta D = \left[\frac{\left(\frac{D}{H} \right)_{sample}}{\left(\frac{D}{H} \right)_{VSMOW}} - 1 \right] \times 10^3 \quad (4.1)$$

$$\delta^{18}O = \left[\frac{\left(\frac{{}^{18}O}{{}^{16}O} \right)_{sample}}{\left(\frac{{}^{18}O}{{}^{16}O} \right)_{VSMOW}} - 1 \right] \times 10^3 \quad (4.2)$$

The reproducibility of the measurement was better than 0.1 ‰ for $\delta^{18}O$ and 1‰ for δD based on several samples and standard measurements. The calibration experiment with international standard reference material SLAP-2 (Standard Light Antarctic Precipitation) obtained from International Atomic Energy Agency (IAEA), Vienna and Internal Laboratory standard PRL-NARM, yielded the measured values ($\delta^{18}O = -55.37$ ‰ and $\delta D = -425.1$ ‰) for SLAP-2 and ($\delta^{18}O = -4.52$ ‰ and $\delta D = -35.78$ ‰) with respect to V- SMOW (Vienna Standard Mean Ocean Water).

Total carbon(C) and nitrogen (N) contents in mud breccia

Prior to analysis of total C and N in mud breccia samples, the samples were treated with mild HCl to remove surficial precipitates. The cleaned samples were pulverized using mortar and pestle, and the powder was treated with 2 N HCl for 2 hours at 70°C to remove carbonates. To ensure complete removal of carbonates, the samples were

again treated with 2 N HCl. The residues were cleaned several times with distilled water until a neutral pH was obtained. Finally, the residue was kept for drying in an oven at 80°C.

Total C and N were measured using a Fisons NA 1500 CN elemental analyser. About 10-20 mg of dried and powdered (In agate mortar) sediment sample was packed in an aluminum cup and was introduced through an auto sampler into the combustion chamber of the analyzer, where it was combusted completely at 1080°C in presence of high purity oxygen flow. A three-point calibration was made using international standards, low organic carbon soil standard and high organic carbon sediments standards having carbon abundance $1.65 \pm 0.02\%$ and 6.72 ± 0.17 , respectively. It was cross checked by running a reference material, the Deer-river shale containing 2.53 % carbon and 0.12 % nitrogen. The total blank concentration, measured over a period of 200 days, was $1.31 \pm 0.12 \mu\text{g C}$ (Bhushan et al., 2001). The analytical precision for total carbon measurement is better than $\pm 4\%$ and for nitrogen concentration greater than 0.1 % is $\pm 8\%$.

Chapter 5

Experimental Results

This chapter deals with the results of petrological, geochemical and isotopic analyses that have been carried out in the present work. Petrographic studies consist of detailed thin section studies of lavas from the Barren Island volcano, samples from the Ophiolite Group of Andaman Islands and X-ray diffractometry of mud breccia samples. Geochemical studies include major and trace elemental characterization of lava flows and ash beds of Barren Island, samples from Ophiolite Group and samples of breccia from mud volcanoes of Andaman Islands. Strontium, neodymium and lead isotopic studies of lava and ash have been investigated in order to ascertain the geochemical processes involved in their origin and evolution, whereas those of the rock clasts and sediments from the mud volcanoes for identification of their sources. Hydrogen and oxygen isotopic studies have been done on water samples collected from the mud volcanoes and fresh water bodies of Andaman Islands to understand the chemistry of water in a subduction zone. Experimental results of all the above studies are discussed in the following paragraphs and the analytical data are presented in tabular form.

5.1 Petrographical descriptions

5.1.1 Thin section studies

The photomicrographs of thin sections are presented in Fig. 5.1 and 5.2. In these photomicrographs, Andaman ophiolites show evidences of low grade of metamorphism and evidence of hydrothermal alteration (Fig. 5.1a, b, d). They also contain spherulites, indicating the alteration of glass (Fig. 5.1f). Barren Island lavas are fresh and show large phenocryst and microphenocrysts of zoned plagioclase with fewer amounts of olivine and clinopyroxene. The groundmass is mainly glassy with small amount of

plagioclase (Fig.5.2). The detail description of this study is presented in the discussion chapter. The major features of these rocks based on petrography are listed below.

a) Andaman Ophiolites

I) Most of the rock samples in this group are highly altered and weathered, which is confirmed by presence of serpentinite, spherulites and high LOI values (Fig 5.1b, f).

II) The photomicrographs of Andaman ophiolites (Fig. 5.1a) evident that the role of the fluids in the ophiolite samples which leads to hydrothermal activity in these area. There is the indication of low grade metamorphism in these areas by the presence of green schist facies rocks.

III) Presence of flow structures in photomicrographs (Fig. 5.1f) indicates the parental magma was very viscous.

IV) Hybrid rocks are also detected in photomicrograph (Fig. 5.1d) it formed due to shearing and rugged weathering, exhibits stratification. This rock contains plagioclase, serpentinite and quartzofeldspathic minerals

V) The predominant rock types of Andaman ophiolites are Basalt, but dolerite, gabbro, pyroxenite (Fig. 5.1e) and plagiogranites (5.1c) are also observed based on thin section study. Mineralogically, phenocryst of Andaman ophiolites are dominated by plagioclase (10-30 volume %), olivine (5-10 volume %), ortho and clino pyroxenes (2-5 volume %) with intergrowth of ilmenite, magnetite. Hematite is also observed which is tabular, needle-shaped (radiating, at places) and large grains show rarely lamellar twinning. These rocks show generally porphyritic and

hypocrystalline, and exhibits textures usually of hyalo-ophitic and, at places, intergranular, sub-ophitic and variolitic.

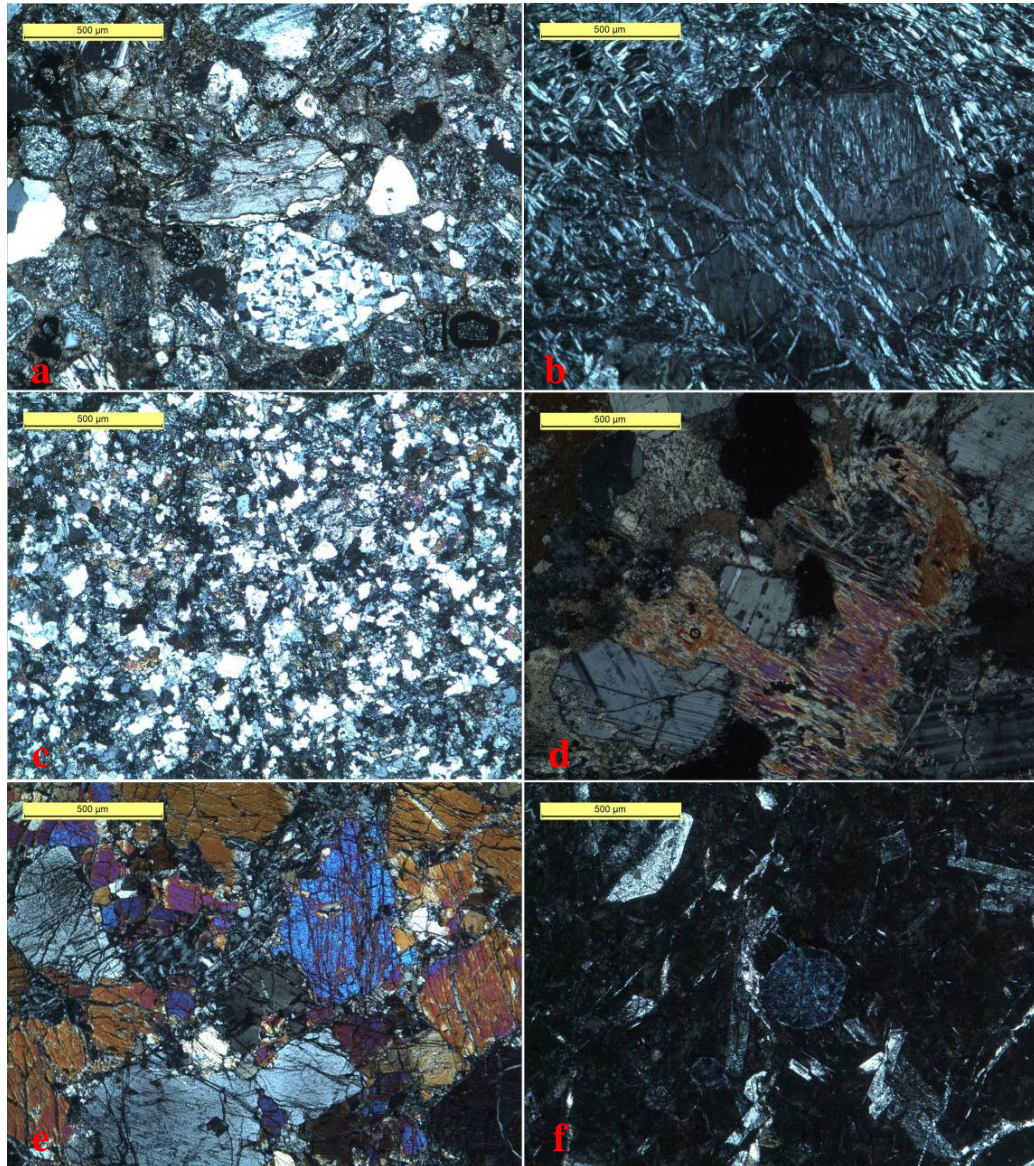


Fig.5.1 Photomicrographs of thin sections of various members of the Ophiolite Group under crossed polarized light a) Fluid activity : secondary minerals replacing earlier minerals b) Altered Basalt : basalt changes to serpentinite c) Plagiogranite : quartz and plagioclase are abundant with small fragments of green colour mineral amphibole d) Hybrid rock : formed due to shearing and weathering e) Pyroxinite: coarse grain pyroxene with altered plagioclase f) Altered Basalt : Spherulitic texture which is the product of alteration of glass, with fine lath of plagioclase.

b) Barren Island lavas

I) In Barren lavas, plagioclase is dominated megacryst and microphenocryst (~ 70%) with small amounts of phenocrysts of olivine and clinopyroxene. The groundmass of lavas is fine grained gray to dark gray, that mostly glassy (Fig. 5.2).

II) The phenocrysts of Barren lavas are well developed euhedral, tabular crystals and contain large numbers of glass inclusions (Fig. 5.2c-f).

III) Zoning and twinning are common in plagioclase and clinopyroxene phenocrysts suggest their incomplete equilibrium with surrounding liquids (Fig. 5c-e). Pyroxene are mostly fractured with greenish and associated with olivine (Fig. 5f)

IV) Corrosion of plagioclase and clinopyroxene minerals is observed in which the older minerals are corroded by newly formed melts that's shows sieve structure in photomicrographs (Fig 5.2b, d).

V) Barren lavas show porphyritic and Poikilitic (where one mineral are trapped by another mineral during crystallization). Groundmass texture of the lava flows are different form flow to flow. It varies from holocrystalline to aphenitic (Fig. 5.2).

VI) Fluidal texture is also observed, such type of feature are common in initial stage of lavas (Fig. 5.2c).

VII) Cooling cracks are observed in olivine grains (Fig. 5.2g) these grains are mostly resorbed and also showing zoning from core to rim. These types of features are common in modern and postcaldera lavas and absent in precaldera lavas

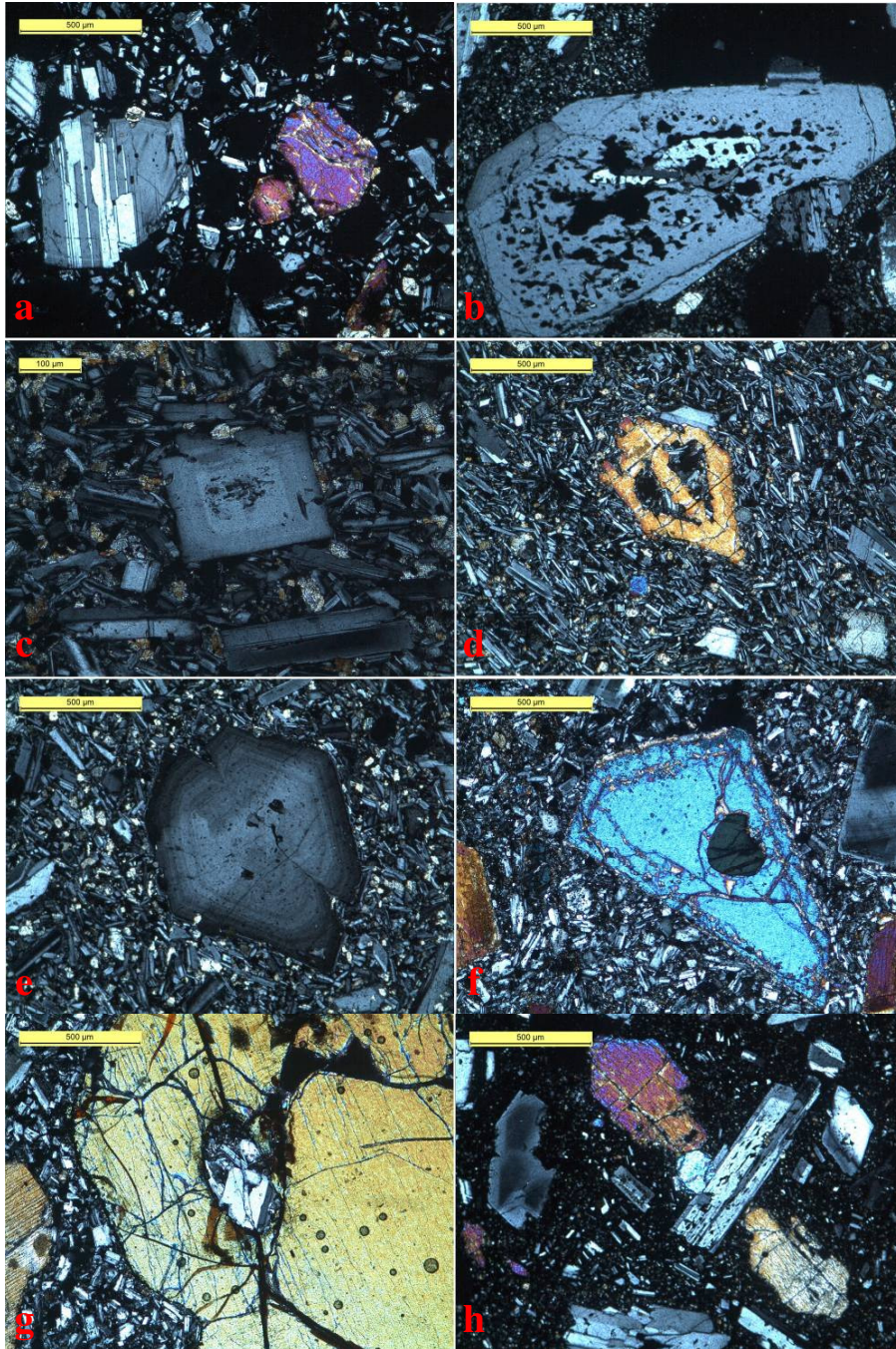


Fig. 5.2 photomicrographs of Barren island lavas in crossed polarized light: a) Clinopyroxene and plagioclase as a phenocrysts b) Corroded plagioclase megacrysts c) Euhedral phenocryst of plagioclase in a groundmass of fine grained of plagioclase and pyroxene d) Corroded pyroxene phenocrysts in a fine grained of plagioclase groundmass e) Euhedral plagioclase megacrysts with compositional zoning f) megacrysts of olivine, plagioclase and pyroxene g) Poikilitic texture: clinopyroxene crystals resorbed h) megacrysts of olivine, plagioclase and pyroxene

5.1.2 X-Ray diffractometry

As discussed chapter four for identification of the minerals in the mud breccias and serpentine clasts from mud volcanoes of Andaman, XRD technique has used. Clay minerals are identified based on their 'd' spacing and characteristic peaks. Smectite group of clay minerals (Kaolinite and mantomorillonite) are dominant in the mud breccias and serpentine clasts with lesser amounts of chlorite clay mineral are present in mud breccias which is absent in serpentine clasts (fig. 5.3). Quartz with minor amount of calcite (mainly in Baratang mud breccia) and muscovite are also observed in these clay minerals and clasts. The XRD spectrum of serpentinite clast Baratang mud breccia and Diglipur mud breccia are presented in Fig. 5.3 a, b and c respectively.

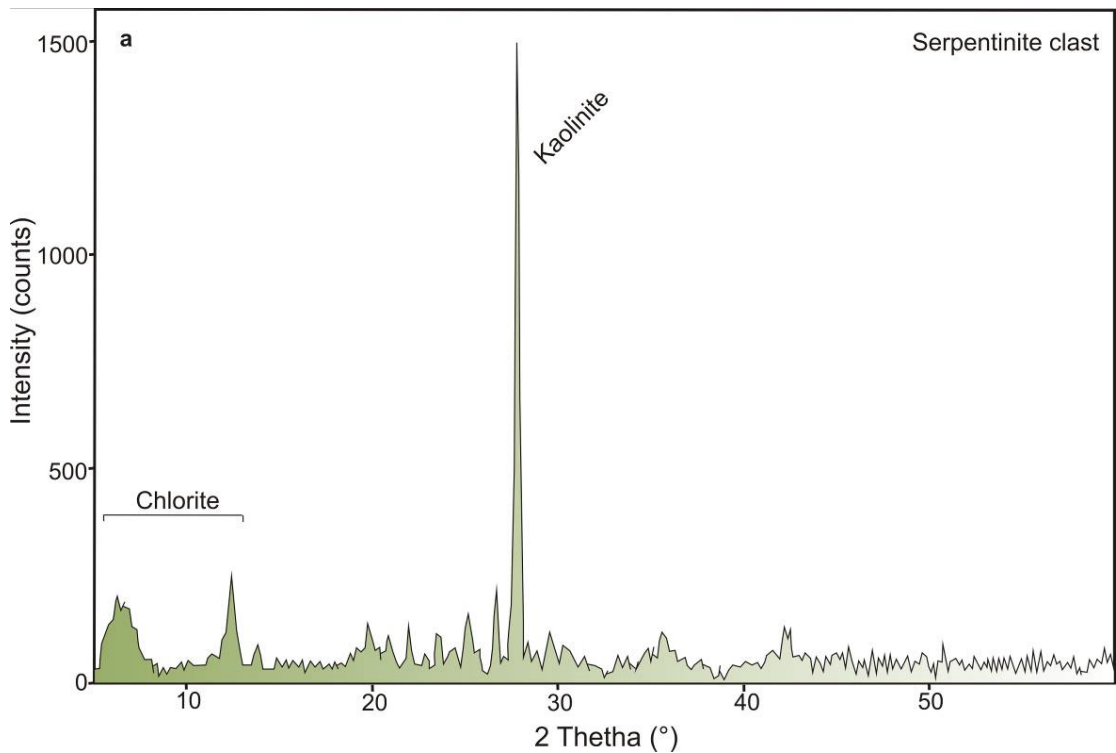


Fig. 5.3a : XRD spectrum of serpentine clast collected form Andaman mud volcanoes

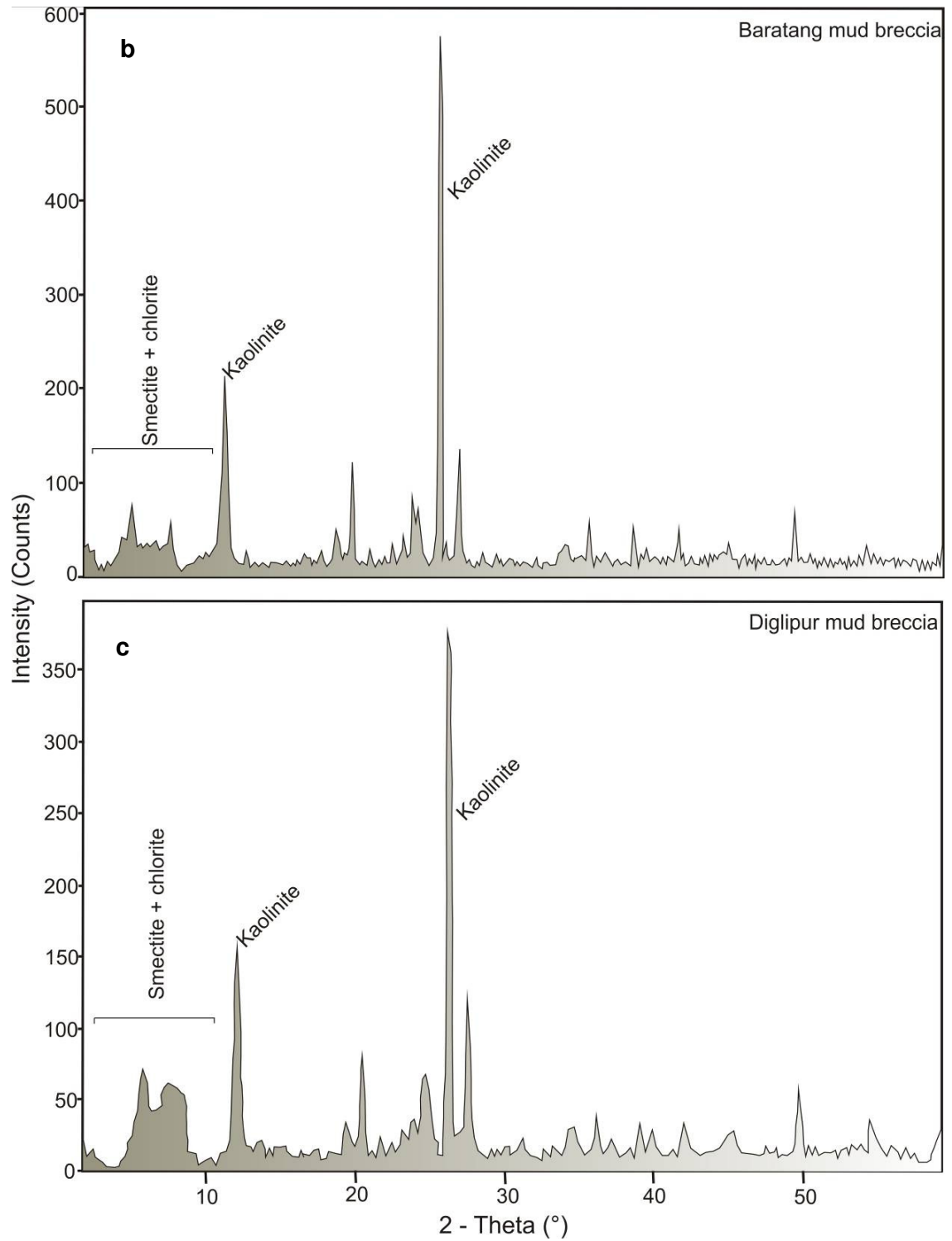


Fig. 5.3: XRD spectrum of a) Baratang mud breccia b) Diglipur mud breccia, collected form Andaman mud volcanoes

5.2 Geochemical Data

The data for major element and trace element contents, radiogenic isotopic ratios and stable isotopic ratios in rocks, sediments and fluid are presented in various tables in the subsequent pages. Concentrations of major elements are presented in 'wt%' of their oxides, whereas those of trace elements are in 'ppm'. Sr and Nd isotopic ratios measured in our samples are presented as $^{87}\text{Sr}/^{86}\text{Sr}$ and $^{143}\text{Nd}/^{144}\text{Nd}$. Since variations in $^{143}\text{Nd}/^{144}\text{Nd}$ are extremely low, we make use of the $\epsilon_{\text{Nd}}(0)$ parameter which is defined as:

$$\epsilon_{\text{Nd}}(0) = \left[\frac{\left(\frac{^{143}\text{Nd}}{^{144}\text{Nd}} \right)_S^P}{\left(\frac{^{143}\text{Nd}}{^{144}\text{Nd}} \right)_{\text{Chond}}^P} - 1 \right] \times 10^4 \quad (5.1)$$

Where subscripts 'S' and 'Chond', respectively stand for sample and Chondrites and superscript 'P' stands for present day. The present day $^{143}\text{Nd}/^{144}\text{Nd}$ ratio for chondrites is taken to be 0.512638 (Depaolo and Wasserburg, 1976). Stable 'O' and 'H' isotopic composition of waters are expressed in $\delta^{18}\text{O}$ and δD with respect to V-SMOW in '‰', as defined in chapter 4.

5.2.1 Chemistry of mud breccias and rock clasts

The results of major oxide, trace elements abundances isotopic ratios and carbon and nitrogen of mud breccias and rock clasts are presented in Table 5.1, 5.2, 5.3 and 5.4 respectively. The following are the major inferences in these data sets.

I) Major oxides data of mud breccias suggest the Diglipur samples have high percentage of silica (49-56% vs. 52-61%), alumina (12-14% vs. 13-15%), potassium and magnesium and low percentage of iron and sodium compared with Baratang samples. The rock clasts collected from these mud volcanoes shows wide variations in major oxides (33 - 92% for SiO₂, 2-32% for CaO etc.); their composition suggests their origin is sedimentary as well as igneous. The high LOI values in mud breccias suggest the secondary phase of minerals including clay minerals present in mud breccia, which contains water in their pore spaces.

II) Comparative trace elements abundances of mud breccias and clasts show high Rb, Ba, Sr, Th and Zr in Diglipur samples as compared with Baratang samples.

III) The isotopic ratios of mud breccias of Diglipur samples show high ⁸⁷Sr/⁸⁶Sr and low ¹⁴³Nd/¹⁴⁴Nd as compared with Baratang samples. The rock clasts are showing wide variations (0.70561 to 0.71574 for ⁸⁷Sr/⁸⁶Sr and 0.512136 to 0.512769 for ¹⁴³Nd/¹⁴⁴Nd their corresponding ε_{Nd} ranges - 9.8 to 2.6) in these ratios that suggesting their origin are both igneous and sedimentary, that support our earlier observation made based on major oxides.

IV) Carbon and Nitrogen in mud breccias of Baratang and Diglipur varies from 0.08 to 0.11 and 0.50 to 1.05, 0.6 to 0.13 and 0.52 to 0.88 respectively. The Baratang samples show wide variations in C/N ratio as compared with Diglipur.

Table 5.1 Major oxides compositions of mud breccias and rock clasts (X) samples collected from mud volcanoes of Andaman Islands

Sample ID	Area	SiO ₂	TiO ₂	Al ₂ O ₃	CaO	MgO	MnO	Fe ₂ O ₃	K ₂ O	Na ₂ O	P ₂ O ₅	LOI	Total
<i>BTMV-2</i>	Baratang	56.57	0.84	13.57	1.43	2.71	0.07	8.16	1.92	7.97	0.08	6.67	99.96
<i>BTMV-3</i>		55.85	0.85	13.76	1.41	2.73	0.06	8.28	1.99	3.74	0.08	6.45	95.19
<i>BTMV-4</i>		54.86	0.85	13.27	1.34	2.66	0.06	8.28	1.95	2.62	0.07	5.33	91.29
<i>BTMV-5</i>		55.16	0.84	13.38	1.31	2.66	0.06	7.99	1.93	7.78	0.07	6.48	97.66
<i>BTMV-6</i>		55.50	0.83	13.30	1.38	2.67	0.06	8.00	1.90	8.24	0.07	6.43	98.39
<i>BTMV-7</i>		55.39	0.85	13.49	1.53	2.67	0.08	8.37	1.97	2.78	0.08	9.40	96.61
<i>BTMV-8</i>		52.49	0.77	12.04	2.33	2.58	0.12	8.42	1.60	1.65	0.10	6.13	88.22
<i>BTMV-9</i>		48.10	1.25	13.66	2.37	2.73	0.10	17.43	1.54	3.79	0.13	8.16	99.26
<i>BTMV-10</i>		55.10	0.87	13.56	1.41	2.71	0.06	8.66	1.99	1.86	0.07	5.24	91.53
<i>BTMV-12</i>		49.83	1.38	14.24	5.62	3.19	0.29	6.67	1.28	2.81	0.41	7.68	93.40
<i>HLMV-3</i>	Diglipur	59.20	0.81	14.45	1.22	2.99	0.06	7.74	2.29	1.78	0.08	5.33	95.95
<i>HLMV-8</i>		57.22	0.88	13.95	1.40	2.72	0.07	7.87	2.15	2.92	0.09	6.31	95.57
<i>HLMV-12</i>		60.59	0.87	14.98	1.19	2.80	0.07	8.35	2.09	4.24	0.07	4.72	99.98
<i>HLMV-15</i>		59.41	0.87	14.57	1.27	2.79	0.07	8.24	2.06	3.98	0.08	6.58	99.92
<i>HLMV-16</i>		52.54	0.76	13.45	4.63	5.89	0.11	4.98	2.02	1.35	0.14	8.16	94.03
<i>BTMV-01-X2</i>	Baratang	61.60	0.60	8.26	0.21	1.37	0.05	4.13	1.66	1.19	0.07	2.50	81.63
<i>BTMV-01-X5</i>		48.73	0.78	13.50	4.80	2.81	0.17	10.83	1.18	1.77	0.11	5.20	89.86
<i>BTMV-01-X6</i>		48.86	0.64	10.07	5.74	2.75	0.06	6.36	0.93	3.59	0.15	7.10	86.25
<i>BTMV-02-X4</i>		91.73	0.12	2.59	0.00	0.61	0.12	1.13	0.51	0.55	0.06	1.30	98.73
<i>BTMV-03-X2</i>		50.11	0.79	10.36	3.70	2.75	0.09	6.74	0.76	3.48	0.12	5.50	84.39
<i>BTMV-03-X3</i>		50.34	0.53	14.78	10.16	2.16	0.47	13.66	1.93	1.66	2.09	4.60	102.38
<i>BTMV-03-X4</i>		63.49	0.72	12.50	2.64	0.80	0.09	2.34	0.45	4.76	0.08	9.80	97.68
<i>BTMV-03-X5</i>		33.24	0.39	7.98	31.83	2.10	0.35	12.72	0.99	0.90	0.32	11.50	102.32

Table 5.2a Trace elements abundances of rock clasts samples collected from mud volcanoes of Andaman Islands

Sample ID	Area	Co	Sc	Rb	Ba	Sr	Zn	Th	Ta	Zr	Hf
<i>BTMV-2</i>	Baratang	18.88	18.41	73	234	188	81	8.00	0.63	134	4.35
<i>BTMV-9</i>		21.25	19.12	65	211	132	100	8.46	0.63	135	4.60
<i>BTMV-10</i>		19.57	17.53	99	192	160	86	7.72	0.59	163	4.34
<i>BTMV-12</i>		18.38	28.41	39	73	113	118	2.30	0.40	156	4.97
<i>HLMV-3</i>	Diglipur	23.76	18.58	79	233	179	100	9.74	0.71	166	5.14
<i>HLMV-15</i>		19.50	18.18	73	286	214	82	7.58	0.58	145	4.19
<i>HLMV-16</i>		9.50	19.20	ND	ND	472	40	0.53	0.11	89	2.61

Table 5.2b Trace elements abundances of rock clasts samples collected from mud volcanoes of Andaman Islands

Sample ID	Area	La	Ce	Nd	Sm	Eu	Gd	Tb	Yb	Lu
<i>BTMV-2</i>	Baratang	23.39	47.26	21.71	5.11	1.21	4.51	0.74	2.76	0.41
<i>BTMV-9</i>		21.48	49.40	22.81	4.58	1.13	5.37	0.77	2.68	0.38
<i>BTMV-10</i>		21.97	45.26	20.61	4.65	1.04	4.06	0.67	2.51	0.37
<i>BTMV-12</i>		18.86	50.90	32.95	8.22	2.27	9.16	1.57	4.21	0.62
<i>HLMV-3</i>	Diglipur	24.99	54.80	23.48	4.75	1.10	4.78	0.76	2.78	0.40
<i>HLMV-15</i>		22.23	44.88	21.44	4.47	1.04	3.87	0.66	2.72	0.38
<i>HLMV-16</i>		8.34	19.80	13.36	3.87	1.80	4.60	0.88	2.80	0.40

Table 5.3 Strontium and Neodymium isotopic ratios of mud breccia and rock clasts samples (X) collected from mud volcanoes of Andaman Islands

Sample ID	Location	$^{87}\text{Sr}/^{86}\text{Sr}$	$^{143}\text{Nd}/^{144}\text{Nd}$	$\epsilon_{\text{Nd}}(0)$	
<i>BTMV-2</i>	Baratang	0.70879	0.512538	-2.0	
<i>BTMV-3</i>		0.70933	0.512494	-2.8	
<i>BTMV-4</i>		0.70917	0.512515	-2.4	
<i>BTMV-5</i>		0.70944	0.512496	-2.8	
<i>BTMV-6</i>		0.70917	0.512512	-2.5	
<i>BTMV-7</i>		0.70920	0.512525	-2.2	
<i>BTMV-8</i>		0.70895	0.512485	-3.0	
<i>BTMV-9</i>		0.70607	0.512464	-3.4	
<i>BTMV-11</i>		0.70947	0.512505	-2.6	
<i>BTMV-12</i>		0.70686	0.512910	5.3	
<i>HLMV-1</i>		Diglipur	0.70986	0.512476	-3.2
<i>HLMV-3</i>			0.70959	0.512485	-3.0
<i>HLMV-6</i>	0.70982		0.512489	-2.9	
<i>HLMV-8</i>	0.70905		0.51247	-3.3	
<i>HLMV-12</i>	0.70906		0.512525	-2.2	
<i>HLMV-15</i>	0.70854		0.512552	-1.7	
<i>HLMV-16</i>	0.70756		0.512810	3.4	

Table 5.3 continued				
<i>BTMV-01-X2</i>		<i>0.71574</i>	<i>0.512136</i>	<i>-9.8</i>
<i>BTMV-01-X5</i>		<i>0.70784</i>	<i>0.512537</i>	<i>-2.0</i>
<i>BTMV-01-X6</i>	Baratang	<i>0.70561</i>	<i>0.512769</i>	<i>2.6</i>
<i>BTMV-02-X2</i>		<i>0.71124</i>	<i>0.512291</i>	<i>-6.8</i>
<i>BTMV-02-X4</i>		<i>0.71238</i>	<i>0.512291</i>	<i>-6.8</i>
<i>BTMV-03-X1</i>		<i>0.70780</i>	<i>0.512690</i>	<i>1.0</i>
<i>BTMV-03-X3</i>		<i>0.70933</i>	<i>0.512494</i>	<i>-2.8</i>

Table 5.4 Nitrogen (N) and Carbon (%) of mud breccias and rock clasts samples collected from mud volcanoes of Andaman Islands

Sample ID	Location	Nitrogen (%)	Carbon (%)	C/N
<i>BTMV-2</i>	Baratang	<i>0.10</i>	<i>0.63</i>	<i>6.32</i>
<i>BTMV-3</i>		<i>0.09</i>	<i>0.59</i>	<i>6.89</i>
<i>BTMV-4</i>		<i>0.09</i>	<i>0.60</i>	<i>6.74</i>
<i>BTMV-5</i>		<i>0.11</i>	<i>0.61</i>	<i>5.73</i>
<i>BTMV-6</i>		<i>0.09</i>	<i>0.59</i>	<i>6.89</i>
<i>BTMV-7</i>		<i>0.10</i>	<i>0.71</i>	<i>7.26</i>
<i>BTMV-8</i>		<i>0.09</i>	<i>0.50</i>	<i>5.59</i>
<i>BTMV-9 (Serpentinite)</i>		<i>0.03</i>	<i>0.03</i>	<i>0.89</i>
<i>BTMV-10</i>		<i>0.08</i>	<i>0.65</i>	<i>8.15</i>
<i>BTMV-11</i>		<i>0.11</i>	<i>0.66</i>	<i>5.77</i>
<i>BTMV-12</i>		<i>0.10</i>	<i>1.05</i>	<i>10.43</i>
<i>BTMV-13</i>		<i>0.10</i>	<i>0.86</i>	<i>8.87</i>
<i>BTMV-14</i>		<i>0.08</i>	<i>0.61</i>	<i>7.26</i>
<i>HLMV-1</i>		Diglipur	<i>0.11</i>	<i>0.81</i>
<i>HLMV-3</i>	<i>0.12</i>		<i>0.84</i>	<i>7.28</i>
<i>HLMV-5</i>	<i>0.13</i>		<i>0.87</i>	<i>6.85</i>
<i>HLMV-6</i>	<i>0.11</i>		<i>0.81</i>	<i>7.63</i>
<i>HLMV-7</i>	<i>0.07</i>		<i>0.52</i>	<i>7.32</i>
<i>HLMV-8</i>	<i>0.06</i>		<i>0.56</i>	<i>8.68</i>
<i>HLMV-9</i>	<i>0.07</i>		<i>0.54</i>	<i>7.30</i>
<i>HLMV-11</i>	<i>0.07</i>		<i>0.54</i>	<i>7.44</i>
<i>HLMV-12</i>	<i>0.07</i>		<i>0.56</i>	<i>7.67</i>
<i>HLMV-13</i>	<i>0.08</i>		<i>0.78</i>	<i>9.75</i>
<i>HLMV-14</i>	<i>0.12</i>		<i>0.88</i>	<i>7.29</i>
<i>HLMV-15</i>	<i>0.08</i>	<i>0.52</i>	<i>6.99</i>	

5.2.2 $\delta^{18}\text{O}$ and δD of fresh water bodies, Andaman Islands

The $\delta^{18}\text{O}$ and δD of various water bodies (mud water and fresh water bodies) of Andaman Islands are presented in Table 5.5. The $\delta^{18}\text{O}$ and δD varies from -0.18 to 0.49‰ and -13.60 to -22.60‰ respectively for Baratang mud waters and 1.30 to 2.23‰ and -17.90 to -24.20‰ respectively for Diglipur mud waters. Based on $\delta^{18}\text{O}$ and δD , it is evident the Baratang mud waters are depleted in $\delta^{18}\text{O}$ and enriched in δD as compared with Diglipur mud waters. The fresh water bodies (springs and wells) and rain water of Andaman Islands show depleted pattern in $\delta^{18}\text{O}$ (-2.21 to -5.50‰) with huge variation in δD (-10.60 to -33.30‰).

Table 5.5 Oxygen and hydrogen isotopic ratios of water samples from Mud Volcanoes and other water bodies, Andaman Islands

Sample ID	Area	$\delta^{18}\text{O}$ (‰)	δD (‰)
<i>BTMVW-1</i>	Baratang	0.16	-19.30
<i>BTMVW-2</i>		0.14	-22.60
<i>BTMVW-3</i>		0.46	-20.50
<i>BTMVW-4</i>		0.40	-24.10
<i>BTMVW-5</i>		-0.23	-20.40
<i>BTMVW-6</i>		0.49	-13.60
<i>BTMVW-7</i>		-0.18	-21.70
<i>ZRWW-1</i>		-2.21	-10.60
<i>PWSW-1</i>		-3.80	-19.10
<i>HLMVW-2</i>	Diglipur	1.30	-26.30
<i>HLMVW-3</i>		2.04	-20.60
<i>HLMVW-4</i>		1.51	-21.20
<i>HLMVW-5</i>		1.93	-21.50
<i>HLMVW-6</i>		1.37	-24.20
<i>HLMVW-7</i>		2.23	-17.90
<i>HLMVW-8</i>		1.59	-23.30
<i>HLMVW-9</i>		1.66	-22.00
<i>LBSW-1</i>			-3.72
<i>PBRW</i>	Port Blair	-5.50	-33.30
<i>NSW-1</i>	Narcondam	-4.60	-25.40
<i>NSW-2</i>	Narcondam	-4.94	-27.20
<i>NSW-3</i>	Narcondam	-4.82	-26.30

5.2.3 Chemistry of rocks from Andaman Ophiolite Group

The result of major oxides (in %), trace elements abundances (ppm) and isotopic ratios are presented in Table 5.6, 5.7 and 5.8 respectively. The following are the major observations in these data sets.

I) The variations in major oxides are observed in the rock samples of Ophiolite Group of Andaman Islands. We have divided three groups based on SiO₂ and MgO compositions; the first group has low SiO₂ (39 – 45%) and high MgO (13 to 20%) contents, second group contains intermediate SiO₂ (45 to 50%) and MgO (10 to 14%) contents, this group also shows high Fe₂O₃ (10-15%) and CaO (10-16%) contents. The last group has high silica (60 to 75%) and low MgO (~5%) contents. The rock type of later group represent plagiogranites rock (Based on our megascopic and mineralogical studies), this rock type formed in last stage of ophiolite sequence, that has high silica percentage in our samples it has also high LOI (~ 7%). The alkali (Na₂O and K₂O) shows large variations in the entire group, but the other oxides (Al₂O₃, MnO, TiO₂ and P₂O₅) have very limited variations (Table 5.6).

II) Trace elements of some samples of ophiolite Group was performed by INAA techniques. The ophiolite rock samples show low concentration of Sr (~135ppm) and high concentration of Cr (2196ppm) and Co (~90ppm) indicate derived from mantle source with low degree of fractionation.

III) Sr and Nd isotopic ratios in Andaman ophiolite rocks show Indian MORB composition. Some of the samples of this group show high values of Sr and Nd isotopic ratios that indicate the rock samples suffered alteration by sea water. The Sr isotopic ratio of Andaman ophiolites varies from 0.70342 to 0.70899 and Nd isotopic ratio ranges from 0.512762 to 0.512240 corresponding $\epsilon_{Nd}(0)$ are 2.4 to 11.7.

Table 5.6 Major oxides compositions of samples collected from the Ophiolite Group, Andaman Islands

Sample ID	Group	SiO ₂	TiO ₂	Al ₂ O ₃	Fe ₂ O ₃	MnO	MgO	CaO	Na ₂ O	K ₂ O	P ₂ O ₅	LOI	Total
PB07-03	Ophiolite Group	44.68	0.98	15.75	11.88	0.41	15.85	5.78	3.28	1.08	0.08	ND	99.77
PB07-04A		48.89	1.09	13.60	10.30	0.16	9.71	11.75	3.59	0.44	0.08	ND	99.60
PB07-04B		46.27	1.03	11.91	9.67	0.14	9.00	15.38	3.19	0.32	0.09	ND	96.99
PB07-05A		61.35	0.75	12.68	7.07	0.10	5.69	8.98	1.08	0.12	0.23	ND	98.04
PB07-05B		48.34	0.82	13.86	20.44	0.12	10.32	2.97	1.67	0.20	0.11	ND	98.85
PB07-06		44.84	0.30	14.68	7.61	0.11	12.96	14.93	0.73	0.66	0.00	ND	96.83
PB07-09		44.98	0.90	10.46	8.31	0.11	8.09	19.72	3.28	0.09	0.09	ND	96.01
PB07-10A		48.94	1.31	14.68	12.51	0.23	7.37	9.36	3.35	0.86	0.15	ND	98.78
PB07-10B		48.46	0.99	18.39	9.72	0.12	2.00	16.68	0.17	0.02	0.16	ND	96.69
PB-08-01		63.66	0.64	11.32	5.86	0.09	4.92	10.13	0.39	0.04	0.21	ND	97.25
PB-08-02(A)		44.26	0.27	13.51	8.61	0.13	14.31	14.96	0.76	0.14	0.06	2.74	99.75
PB-08-02(B)		49.45	0.76	12.93	12.28	0.16	11.18	11.73	2.22	0.22	0.09	ND	101.01
PB-08-03		44.31	0.32	15.25	8.06	0.11	11.52	15.12	0.83	0.26	0.05	ND	95.82
PB-08-03(A)		44.85	0.19	17.38	6.27	0.09	12.72	15.34	0.89	0.31	0.05	3.00	101.09
PB-08-04		47.95	0.51	12.48	6.64	0.12	16.35	13.92	0.94	0.14	0.10	3.00	102.15
PB-08-05		42.92	1.36	11.03	10.97	0.17	14.65	10.11	0.90	0.07	0.09	2.60	94.86
PB-08-06		43.42	1.18	13.89	9.13	0.13	6.25	12.85	1.50	0.00	0.12	4.30	92.76
PB-08-11		75.28	0.51	9.40	3.55	0.10	1.07	3.56	2.08	1.03	0.17	7.90	104.65

Table 5.6 continued

<i>PB-08-12</i>		18.88	0.02	0.98	2.57	0.86	3.24	69.13	0.11	-0.01	0.17	4.00	99.95
<i>AND-09-17</i>	Ophiolite Group	45.90	0.87	12.67	10.55	0.21	15.76	6.05	3.09	0.03	0.08	5.40	100.61
<i>AND-09-29</i>		42.24	1.08	10.13	13.27	0.21	13.86	8.31	1.76	0.24	0.12	9.73	100.94
<i>AND-09-35</i>		45.07	0.49	10.73	6.54	0.12	9.67	19.96	0.37	0.08	0.11	3.20	96.33
<i>AND-09-46</i>		39.92	0.99	11.08	15.10	0.21	18.64	7.28	1.39	0.01	0.07	ND	94.68
<i>AND-09-58</i>		69.43	0.48	13.15	3.27	0.05	1.95	4.36	5.16	0.02	0.28	ND	98.14
<i>AND-09-62</i>		44.00	1.50	11.39	10.70	0.16	15.50	9.08	0.61	0.09	0.10	7.90	101.02

Table 5.7 Trace elements abundances of samples collected from the Ophiolite Group, Andaman Islands

Sample ID	Group	Co	Sc	Ba	Sr	Zn	Hf	La	Ce	Nd	Sm	Eu	Gd	Tb	Yb	Lu	Cr	Ca	Fe (%)	Na (%)
<i>PB-07-06</i>	Ophiolite Group	43.7	51.3	158	204	90.6	0.3	1.3	3.0	14.5	0.6	0.26	1.46	0.1	0.3	0.09	377	11.7	5.60	0.60
<i>PB-07-09</i>		36.9	30.5	ND	132	84.7	1.7	2.9	7	1.6	3.4	0.89	2.20	0.6	3.8	0.58	639	20.9	5.97	3.01
<i>PB-08-01</i>		11.3	19	101	134	62.1	6.2	10.2	25.3	8.7	4.3	1.21	7.10	0.9	3.5	0.51	71.80	3.4	4.13	2.16
<i>AND-09-32</i>		90.7	11.4	ND	ND	42.9	ND	1	ND	ND	0.1	0.02	0.34	ND	0.2	0.04	2196	ND	5.19	ND
<i>AND-09-60</i>		62.3	47.5	ND	ND	119.2	0.1	0.7	0.8	1.1	0.4	0.16	0.21	ND	0.3	0.05	2794	12.1	3.65	0.06

Table 5.8 Strontium and Neodymium isotopic ratios of samples collected from the Ophiolite Group, Andaman Islands

Sample ID	Group	$^{87}\text{Sr}/^{86}\text{Sr}$	$^{143}\text{Nd}/^{144}\text{Nd}$	$\epsilon_{\text{Nd}}(0)$
<i>PB-07-03</i>		0.70632	0.512975	6.6
<i>PB-07-04A</i>		0.70483	0.513102	9.1
<i>PB-07-05A</i>		0.70377	0.513017	7.4
<i>PB-07-05B</i>		0.70407	0.513000	7.1
<i>PB-07-06</i>		0.70382	0.513022	7.5
<i>PB-07-09</i>		0.70542	0.513131	9.6
<i>PB-07-10</i>		0.70462	0.513109	9.2
<i>PB-08-01</i>		0.70384	0.513020	7.5
<i>PB-08-02 _Host</i>	Ophiolite Group	0.70363	0.513026	7.6
<i>PB-08-02 _Tchy</i>		0.70375	0.512968	6.4
<i>PB-08-04</i>		0.70440	0.512987	6.8
<i>PB-08-06</i>		0.70478	0.513077	8.6
<i>PB-08-08</i>		0.71090	0.512235	-7.9
<i>PB-08-11</i>		0.71128	0.512276	-7.1
<i>PB-08-12</i>		0.70629	0.512220	-8.2
<i>AND-09-29</i>		0.70582	0.512762	2.4
<i>AND-09-31</i>		0.70801	ND	ND
<i>AND-09-32</i>		0.70899	0.513240	11.7
<i>AND-09-34</i>		0.71016	ND	ND
<i>AND-09-46</i>		0.70501	0.513095	8.9
<i>AND-09-50</i>	0.70584	0.513123	9.5	
<i>AND-09-58</i>	0.70402	0.513027	7.6	
<i>AND-09-60</i>	0.70342	0.513091	8.8	

5.2.3 Chemistry of lava flows and ash beds of Barren island volcano

The Major oxide, trace elements abundances and isotopic values of Barren island lavas and ash beds are presented in Table 5.9, 5.10, 5.11 respectively. The following observations are made based on data sets.

I) The Barren lavas and ash beds illustrate high alumina contents (16.19 to 23.20 %) in their lavas. The LOI is also low that indicates lavas are fresh.

II) The precaldera lavas shows high concentrations of Ba, Nd, Zr, Sm, Eu, Cr, Co and low abundance of Cs and Th compared with Postcaldera and modern lavas flows.

III) Sr and Nd isotopic ratios of lava flows range from 0.70407 to 0.70415, 0.512861 to 0.512990 and $^{206}\text{Pb}/^{204}\text{Pb}$, $^{207}\text{Pb}/^{204}\text{Pb}$ and $^{208}\text{Pb}/^{204}\text{Pb}$ vary from 17.824 to 18.405, 15.324 to 15.744, and 37.762 to 38.846 respectively.

Table 5.9 Major oxides compositions of samples from lava flows and ash beds of the Barren Island Volcano

Sample ID	Sub Group	SiO ₂	TiO ₂	Al ₂ O ₃	(FeO) _T	MnO	MgO	CaO	Na ₂ O	K ₂ O	P ₂ O ₅	LOI	Total
BI-07-01	Precaldera	56.88	0.93	19.56	6.55	0.18	2.39	8.21	4.44	0.69	0.19	-0.12	100.62
BI-07-02		52.73	0.91	16.19	6.49	0.18	7.22	7.92	5.16	0.64	0.18	1.77	100.10
BI-07-03		49.63	0.87	16.74	9.33	0.17	8.98	10.58	2.44	0.24	0.09	0.33	100.43
BI-07-07		52.35	0.99	18.71	9.07	0.18	4.01	9.17	3.91	0.49	0.15	-0.09	99.93
BI-07-08		46.70	0.68	19.45	7.66	0.14	7.44	11.88	2.47	0.26	0.08	1.19	98.80
BI-07-09		51.31	1.02	18.65	9.63	0.17	3.87	9.22	3.71	0.49	0.13	0.13	99.40
BI-07-10		52.37	1.05	18.65	9.44	0.20	3.32	9.28	3.67	0.48	0.15	-0.03	99.62
BI-07-12		53.20	0.86	18.15	7.70	0.17	5.03	9.29	3.95	0.51	0.13	0.30	100.13
BI-07-13		52.98	0.89	18.81	7.68	0.19	4.69	9.55	3.72	0.44	0.14	0.45	100.38
BI-08-05		52.05	0.86	19.02	8.26	0.16	6.43	9.73	3.41	0.46	0.11	-0.08	101.29
BI-08-06		52.25	0.90	19.02	7.72	0.17	6.34	9.79	3.38	0.44	0.16	-0.04	100.98
BI-08-08		50.22	0.73	18.43	8.41	0.17	8.87	10.60	2.96	0.31	0.14	-1.75	100.02
BI-08-10		Postcaldera	50.38	0.73	18.20	8.45	0.16	8.59	10.63	2.95	0.33	0.12	-0.04
BI-07-04	49.39		0.83	22.60	7.68	0.15	4.31	11.21	3.01	0.36	0.07	-0.19	100.27
BI-07-05	49.24		0.81	22.78	7.38	0.14	4.58	11.31	2.69	0.35	0.10	0.06	100.27
BI-07-06	49.59		0.88	20.91	8.02	0.14	5.72	10.35	2.42	0.31	0.07	1.42	100.71
BI-08-01	49.44		0.82	21.91	7.68	0.15	4.34	11.26	2.89	0.34	0.12	0.44	100.24
BI-08-02	49.00		0.81	23.45	7.11	0.14	3.79	11.39	2.69	0.36	0.10	-0.08	99.54

Table 5.9 continued

<i>BI-08-03</i>		49.51	0.77	23.23	6.76	0.14	3.71	11.10	2.93	0.38	0.10	-0.04	99.34
<i>BI-08-04</i>		50.00	0.85	22.40	7.23	0.15	3.74	11.20	3.06	0.36	0.12	-0.08	99.82
<i>BI-08-09</i>		47.48	0.83	17.17	9.45	0.18	9.28	11.21	1.99	0.30	0.11	0.30	99.35
<i>BI-08-11</i>		49.35	0.80	23.25	6.88	0.14	3.73	11.11	2.90	0.37	0.10	-0.01	99.38
<i>BI-08-12</i>		50.79	0.84	23.20	7.30	0.15	3.27	11.35	3.22	0.38	0.12	0.03	101.47
<i>BI-08-13</i>		49.09	0.80	23.82	7.10	0.14	3.86	11.41	2.63	0.35	0.10	0.16	100.25
<i>BI-08-14</i>		51.13	0.80	22.24	6.81	0.14	3.51	10.92	3.53	0.43	0.10	-0.11	100.25
<i>BI-08-15</i>		50.58	0.73	21.74	6.50	0.14	3.91	10.99	3.23	0.41	0.12	0.07	99.12
<i>BI-09-03</i>		49.45	0.86	22.63	7.23	0.15	7.76	11.26	2.92	0.39	0.08	-0.18	99.93
<i>BI-09-04</i>		50.72	0.86	22.32	7.49	0.14	7.23	11.09	3.12	0.40	0.12	-0.34	99.69
<i>BI-09-05</i>		50.43	0.87	22.03	9.43	0.14	7.49	11.06	3.09	0.40	0.12	-0.32	99.56
<i>BI-07-TL-02</i>		50.52	0.98	18.41	10.60	0.16	6.17	10.08	2.76	0.43	0.10	0.60	100.81
<i>BI-07-TL-03</i>		46.43	0.81	11.85	14.17	0.15	11.48	6.83	2.66	0.24	0.08	4.19	99.98
<i>BI-07-11</i>		48.91	0.87	19.68	7.94	0.16	6.26	10.28	2.59	0.36	0.10	1.86	99.88
<i>BI-08-07</i>		49.49	0.80	22.32	6.94	0.15	4.13	11.51	2.71	0.32	0.11	-0.03	99.23
<i>BI-09-01</i>		50.83	0.84	21.72	8.62	0.15	7.52	11.15	2.89	0.40	0.14	-0.51	100.61
<i>BI-09-02</i>		50.65	0.93	20.72	7.76	0.16	8.62	10.65	3.01	0.43	0.08	-0.49	100.93
<i>BI-07-TL-01</i>		52.97	1.17	17.48	10.48	0.18	3.85	8.87	3.31	0.58	0.11	ND	99.00

Table 5.10a Trace elements abundances of samples from lava flows and ash beds of the Barren Island Volcano

Sample ID	Sub Group	Cs	Rb	Ba	Th	Nb	Ta	La	Ce	Pr	Pb	Sr	Nd	Hf	Zr	Sm
BI-07-01	Precaldera	0.17	13.43	120.30	1.69	1.33	0.10	6.39	15.71	2.31	3.15	222.2	11.11	2.51	96.26	3.26
BI-07-02		0.15	9.71	115.80	1.71	1.15	0.09	6.02	14.91	2.18	4.89	239.0	10.48	2.27	89.00	3.04
BI-07-03		0.13	3.46	59.95	0.44	0.75	0.08	2.64	7.33	1.20	1.17	175.7	6.34	1.44	55.91	2.11
BI-07-07		0.13	7.25	86.73	0.61	0.72	0.09	3.37	9.62	1.59	1.81	209.0	8.45	2.04	78.37	2.84
BI-07-08		0.18	5.27	49.54	0.33	0.52	0.05	1.80	5.09	0.85	1.37	196.1	4.51	1.08	42.23	1.54
BI-07-09		0.24	7.73	86.44	0.67	0.80	0.06	3.52	10.01	1.66	2.34	201.1	8.78	2.15	78.71	2.95
BI-07-10		0.31	9.06	90.70	0.62	0.83	0.05	3.55	9.85	1.65	3.40	204.8	8.72	2.05	77.94	2.90
BI-07-12		0.20	9.16	87.23	0.67	0.54	0.05	3.81	10.57	1.77	3.47	201.3	9.24	2.11	82.23	2.94
BI-07-13		0.25	7.79	84.80	0.67	0.56	0.05	3.76	10.66	1.72	1.51	191.2	8.91	2.17	79.64	2.87
BI-08-05		0.20	8.87	89.09	1.11	0.61	0.08	5.22	13.28	1.99	1.20	234.3	9.61	1.76	70.56	2.68
BI-08-06		0.17	7.68	90.36	1.13	0.61	0.06	5.90	14.86	2.22	1.20	238.6	10.66	1.87	71.40	2.96
BI-08-08		0.12	4.87	55.71	0.40	0.49	0.06	2.22	6.46	1.07	1.04	180.6	5.73	1.34	52.20	1.94
BI-08-10		0.14	5.05	57.27	0.42	0.53	0.06	2.32	6.68	1.12	0.80	183.7	5.95	1.43	55.73	2.02
BI-08-TL-01		0.33	12.26	80.50	1.06	ND	0.04	2.36	10.80	ND	ND	687.0	5.72	1.67	54.18	1.92
BI-08-TL-02		0.47	12.57	79.50	1.03	ND	0.08	4.51	12.70	ND	ND	254.0	8.28	1.57	63.70	2.60
BI-07-04	Postcaldera	0.36	10.32	79.27	1.19	0.50	0.07	4.07	10.52	1.59	2.21	220.7	7.88	1.59	61.77	2.35
BI-07-05		0.38	10.73	78.77	1.13	0.59	0.06	4.21	10.79	1.63	1.55	217.5	8.00	1.60	59.25	2.38
BI-07-06		0.34	10.12	75.41	1.10	0.59	0.05	3.91	10.39	1.58	2.11	212.5	7.89	1.63	60.66	2.36

Table 5.10a continued

<i>BI-08-01</i>		0.34	10.28	78.59	1.05	0.42	0.07	3.82	9.93	1.52	1.40	225.40	7.53	1.55	61.33	2.26	
<i>BI-08-02</i>		0.37	11.33	85.10	1.22	0.43	0.08	4.31	11.15	1.70	1.49	245.60	8.41	1.70	67.57	2.50	
<i>BI-08-03</i>		0.39	11.94	89.11	1.29	0.48	0.06	4.56	11.79	1.80	3.21	256.10	8.88	1.80	71.09	2.63	
<i>BI-08-04</i>		0.35	10.50	79.76	1.09	0.41	0.06	3.95	10.25	1.57	1.35	231.00	7.75	1.60	63.08	2.31	
<i>BI-08-09</i>		0.19	6.46	59.58	0.54	0.73	0.05	2.87	7.65	1.22	1.27	196.60	6.38	1.36	51.58	2.07	
<i>BI-08-11</i>	Postcaldera	0.41	12.45	94.47	1.37	0.50	0.06	4.75	12.34	1.89	2.05	266.50	9.32	1.90	74.26	2.77	
<i>BI-08-12</i>		0.36	11.11	83.34	1.19	0.44	0.05	4.15	10.77	1.64	1.68	237.60	8.12	1.66	65.59	2.43	
<i>BI-08-13</i>		0.38	11.52	86.23	1.26	0.47	0.05	4.37	11.30	1.72	6.44	244.40	8.55	1.75	68.97	2.54	
<i>BI-08-14</i>		0.31	11.20	89.12	1.31	0.48	0.10	4.59	11.87	1.82	1.64	255.60	8.99	1.83	70.82	2.68	
<i>BI-08-15</i>		0.34	10.83	81.62	1.20	0.44	0.05	4.26	11.01	1.68	1.62	236.00	8.32	1.69	65.55	2.46	
<i>BI-09-03</i>		0.42	11.37	93.49	1.18	0.84	0.08	4.80	12.25	1.78	2.00	242.30	8.79	1.73	65.46	2.58	
<i>BI-09-04</i>		0.46	11.98	70.76	1.24	0.89	0.07	4.99	12.77	1.87	1.76	182.70	9.02	1.75	50.00	2.67	
<i>BI-09-05</i>		0.41	11.34	73.40	1.19	0.89	0.07	4.91	12.49	1.81	2.20	183.00	8.89	1.79	52.20	2.62	
<i>BI-TL-08-04</i>		0.76	9.71	65.60	0.62	ND	0.08	4.25	8.73	ND	ND	391	6.96	1.62	48.70	2.45	
<i>BI-07-11</i>		Modern	0.30	9.01	77.06	0.96	0.65	0.05	3.82	9.77	1.50	1.44	199.10	7.44	1.50	58.69	2.23
<i>BI-08-07</i>			0.33	9.84	77.94	1.03	0.37	0.08	3.69	9.61	1.48	1.26	226.90	7.32	1.52	59.48	2.21
<i>BI-09-01</i>			0.41	11.41	71.87	1.20	0.86	0.09	4.95	12.49	1.81	1.71	190.80	8.80	1.72	48.27	2.59
<i>BI-09-02</i>			0.45	12.48	82.99	1.30	1.00	0.06	5.27	13.27	1.92	1.81	184.20	9.26	1.89	56.05	2.76

Table 5.10b Trace elements abundances of samples from lava flows and ash beds of the Barren Island Volcano

Sample ID	Sub Group	Eu	Gd	Tb	Dy	Ho	Er	Tm	Yb	Lu	Sc	V	Cr	Co	Ni	Zn
BI-07-01	Precaldera	1.14	4.01	0.72	4.85	1.04	3.16	0.49	3.21	0.49	25.74	218.6	9.36	16.06	10.59	74.48
BI-07-02		1.08	3.77	0.67	4.55	0.98	2.95	0.46	2.98	0.46	24.51	179.8	18.16	15.51	18.21	74.69
BI-07-03		0.81	2.76	0.51	3.51	0.76	2.28	0.35	2.28	0.34	40.68	271.3	369.00	39.75	172.90	82.97
BI-07-07		1.09	3.75	0.70	4.78	1.04	3.10	0.48	3.14	0.48	41.85	422.9	24.20	27.60	17.50	84.85
BI-07-08		0.63	2.06	0.38	2.65	0.57	1.71	0.27	1.73	0.26	36.74	227.6	285.60	34.21	115.70	53.19
BI-07-09		1.12	3.90	0.72	4.98	1.08	3.24	0.50	3.31	0.50	40.74	397.5	28.09	26.86	16.69	84.36
BI-07-10		1.10	3.79	0.70	4.83	1.04	3.12	0.48	3.15	0.48	40.84	403.2	22.57	26.30	16.69	88.12
BI-07-12		1.02	3.81	0.69	4.70	1.02	3.07	0.48	3.10	0.47	32.11	202.1	62.01	25.57	35.92	74.04
BI-07-13		1.02	3.42	0.67	4.56	0.99	2.97	0.46	3.01	0.46	31.35	219.8	64.36	24.90	34.98	81.29
BI-08-05		0.95	3.21	0.56	3.74	0.81	2.42	0.37	2.45	0.38	31.99	265.0	278.30	32.05	122.20	82.71
BI-08-06		1.04	3.51	0.61	4.08	0.87	2.61	0.40	2.63	0.40	33.20	284.0	278.70	32.24	122.60	66.05
BI-08-08		0.76	2.57	0.48	3.29	0.71	2.14	0.33	2.17	0.33	39.36	263.2	524.00	41.44	200.60	72.83
BI-08-10		0.78	2.67	0.50	3.43	0.74	2.24	0.34	2.26	0.34	40.81	289.6	541.70	42.40	204.30	69.64
BI-08-TL-01		0.88	2.45	0.55	ND	ND	ND	ND	2.08	0.33	30.31	ND	302	28.44	ND	3124.3
BI-08-TL-02		0.88	3.09	0.54	ND	ND	ND	ND	2.01	0.35	31.94	ND	572	36.62	ND	587.7
BI-07-04	Postcaldera	0.88	2.92	0.52	3.50	0.75	2.26	0.35	2.27	0.34	29.34	274.0	88.89	24.99	60.16	61.96
BI-07-05		0.89	2.94	0.52	3.52	0.76	2.26	0.35	2.28	0.35	27.21	256.3	75.19	24.15	56.19	61.54
BI-07-06		0.89	2.91	0.52	3.53	0.75	2.26	0.35	2.29	0.35	31.37	246.0	133.5	26.12	71.67	63.48

Table 5.10b continued

<i>BI-08-01</i>		0.83	2.81	0.51	3.40	0.73	2.20	0.34	2.22	0.34	28.81	275.00	331.40	25.85	64.34	69.23	
<i>BI-08-02</i>		0.93	3.13	0.56	3.76	0.81	2.42	0.37	2.45	0.37	31.07	299.60	93.43	23.44	32.53	66.84	
<i>BI-08-03</i>		0.98	3.28	0.59	3.96	0.85	2.54	0.39	2.57	0.39	31.89	312.70	103.30	24.11	32.26	77.44	
<i>BI-08-04</i>		0.87	2.91	0.52	3.50	0.75	2.26	0.35	2.28	0.35	28.72	278.10	129.00	24.78	55.29	68.40	
<i>BI-08-09</i>		0.79	2.76	0.49	3.35	0.72	2.15	0.33	2.14	0.32	39.47	266.50	389.50	41.02	162.20	63.89	
<i>BI-08-11</i>	Postcaldera	1.03	3.46	0.62	4.17	0.89	2.68	0.41	2.71	0.41	33.45	327.70	100.40	25.07	34.30	74.75	
<i>BI-08-12</i>		0.90	3.02	0.54	3.64	0.78	2.34	0.36	2.37	0.36	29.66	289.60	91.76	22.78	32.15	67.07	
<i>BI-08-13</i>		0.94	3.17	0.57	3.82	0.82	2.46	0.38	2.49	0.38	31.04	303.50	107.90	23.90	34.00	70.24	
<i>BI-08-14</i>		0.99	3.35	0.60	4.03	0.87	2.60	0.40	2.62	0.40	32.59	312.00	101.60	25.01	35.36	72.68	
<i>BI-08-15</i>		0.91	3.08	0.55	3.71	0.79	2.39	0.37	2.40	0.37	29.60	289.20	97.88	22.78	31.78	65.75	
<i>BI-09-03</i>		0.96	3.12	0.56	3.73	0.81	2.38	0.37	2.39	0.37	32.53	303.80	38.86	22.76	29.36	70.13	
<i>BI-09-04</i>		0.98	3.21	0.57	3.82	0.82	2.45	0.38	2.44	0.37	25.04	235.20	17.23	16.68	17.88	69.19	
<i>BI-09-05</i>		0.97	3.19	0.57	3.77	0.82	2.43	0.37	2.41	0.37	25.50	237.20	22.84	17.48	22.17	72.32	
<i>BI-TL-08-04</i>		0.79	2.27	0.51	ND	ND	ND	ND	2.27	0.36	32.40	ND	469	28.02	ND	1467.9	
<i>BI-07-11</i>		Modern	0.83	2.78	0.50	3.33	0.71	2.13	0.33	2.14	0.32	33.94	250.80	193.90	34.27	116.50	66.06
<i>BI-08-07</i>			0.83	2.77	0.50	3.34	0.72	2.16	0.33	2.17	0.33	27.44	264.20	115.40	23.85	55.20	61.61
<i>BI-09-01</i>			0.95	3.11	0.56	3.69	0.79	2.37	0.36	2.34	0.36	25.20	224.60	63.54	19.43	49.52	67.40
<i>BI-09-02</i>			0.99	3.32	0.58	3.94	0.85	2.51	0.39	2.49	0.39	25.82	243.40	51.06	20.37	48.21	74.17

Table 5.11 Strontium, Neodymium and lead isotopic ratios of rock and ash samples from Barren Island Volcano

Sample ID	Sub Group	$^{87}\text{Sr}/^{86}\text{Sr}$	$^{143}\text{Nd}/^{144}\text{Nd}$	$\epsilon_{\text{Nd}}(0)$	$^{206}\text{Pb}/^{204}\text{Pb}$	$^{207}\text{Pb}/^{204}\text{Pb}$	$^{208}\text{Pb}/^{204}\text{Pb}$
BI-07-01	Precaldera	0.70407	0.512896	5.0	18.344	15.995	38.765
BI-07-02		0.70459	0.512877	4.7	18.207	15.565	38.404
BI-07-03		0.70387	0.512966	6.4	ND	ND	ND
BI-07-07		0.70391	0.512976	6.6	18.251	15.603	38.534
BI-07-08		0.70394	0.51297	6.5	18.096	15.472	38.143
BI-07-09		0.70398	0.512992	6.9	17.935	15.324	37.762
BI-07-10		0.70399	0.512976	6.6	17.990	15.441	38.063
BI-07-12		0.70400	0.51299	6.9	ND	ND	ND
BI-07-13		0.70398	0.512983	6.7	ND	ND	ND
BI-08-05		0.70387	0.512882	4.8	18.254	15.604	38.484
BI-08-06		0.70388	0.512915	5.4	ND	ND	ND
BI-08-08		0.70383	0.512964	6.4	18.254	15.654	38.595
BI-08-10		0.70379	0.512963	6.3	ND	ND	ND
Plagioclase		0.70397	ND	ND	ND	ND	ND
Pyroxene	0.70392	0.513012	7.3	ND	ND	ND	
BI-07-04	Postcaldera	0.704016	0.512907	5.2	18.405	15.744	38.846
BI-07-05		0.704047	0.512904	5.2	ND	ND	ND
BI-07-06		0.704022	0.512889	4.9	18.294	15.602	38.545
BI-08-01		0.703962	0.512892	5.0	18.120	15.584	38.295
BI-08-02		0.704001	0.512879	4.7	17.824	15.573	38.012
BI-08-03		0.703945	0.512895	5.0	18.140	15.595	38.334

Table 5.11 continued

<i>BI-08-04</i>		0.703995	0.512919	5.5	17.934	15.273	38.023	
<i>BI-08-09</i>		0.703893	0.512940	5.9	ND	ND	ND	
<i>BI-08-11</i>		0.703981	0.512892	5.0	ND	ND	ND	
<i>BI-08-12</i>	Postcaldera	0.703970	0.512889	4.9	ND	ND	ND	
<i>BI-08-13</i>		0.703995	0.512891	4.9	ND	ND	ND	
<i>BI-08-14</i>		0.703956	0.512877	4.7	ND	ND	ND	
<i>BI-08-15</i>		0.703979	0.512881	4.7	ND	ND	ND	
<i>BI-09-03</i>		0.704053	0.512872	4.6	ND	ND	ND	
<i>BI-09-04</i>		0.704154	0.512862	4.4	ND	ND	ND	
<i>BI-09-05</i>		0.704093	0.512868	4.5	ND	ND	ND	
<i>BI-07-11</i>			0.704047	0.512884	4.8	ND	ND	ND
<i>BI-08-07</i>		Modern	0.704019	0.512920	5.5	18.055	15.395	37.992
<i>BI-09-01</i>	0.704028		0.512864	4.4	ND	ND	ND	
<i>BI-09-02</i>	0.704091		0.512861	4.4	ND	ND	ND	
<i>BI-07-TL-01</i>	0.704112		0.512865	4.4	ND	ND	ND	
<i>BI-07-TL-02</i>	Not well constrained	0.70398	0.512943	5.9	ND	ND	ND	
<i>BI-07-TL-03</i>		0.70391	0.512959	6.3	ND	ND	ND	
<i>BI-07-TL-04</i>		0.70402	0.512892	5.0	ND	ND	ND	
<i>BI-07-TL-05</i>		0.70407	0.512917	5.4	ND	ND	ND	
<i>BI-07-TL-06</i>		0.70394	0.512978	6.6	ND	ND	ND	
<i>BI-08-TL-01</i>		0.70395	0.51291	5.3	ND	ND	ND	
<i>BI-08-TL-02</i>		0.70399	0.51296	6.3	ND	ND	ND	

This page left blank intentionally

Chapter 6

Discussion

In the present thesis work we have examined all the integral of the Andaman subduction zone such as obducted rocks Ophiolites Group of rocks from Andaman Islands, slab sediments (mud breccias, rock-clasts and water) which expelled from Mud volcanoes of Andaman and lava flows, ash bed samples from Barren Island volcano to understand the chemical evolution of mantle geochemistry. In present study we have used various analytical techniques (petrological, geochemical and isotopic) which have already discussed in last chapter. Apart from these techniques various models (mixing and melting) are used that is necessary to understand different processes which occur at subduction zone area. To constrain the proportion of contributions from different sources, which are affecting the pristine mantle wedge two and three components mixing models are used. Melting models are also used to ascertain degree of melting for the generation of magma beneath the arc. As we know the primary arc rock compositions control by three components; subducting slab, subducting sediments and mantle peridotite. In present study, we have considered all the above mentioned possible sources that influence the mantle geochemistry and also control the chemical composition of subduction arc lavas, these are Andaman ophiolites and serpentinite clasts as an altered oceanic crust, mud breccias as subducting sediments and I-MORB as a mantle peridotite. Water is also important constituents in subduction environment, so we have also taken a brief study of mud water that are oozing out from mud volcanoes of Andaman.

In this chapter, we have described all the models which are used in present work. The interferences of all the results that are obtained from the

geochemical (major and trace elements) and isotopic studies (Sr - Nd - Pb) with various models (mixing and melting models) are described in details.

6.1 Field observations

6.1.1 Mud volcanoes of Andaman Islands

The mud volcanoes of middle and north Andaman Islands are located along faults. Gases, water and mud breccias are continuously expelled from the mud volcanoes forming large mud mounds inside dense forest. The gases appeared to be dominated by methane emissions, confirmed by their ability to catch fire. Our field observation for the first time suggests the East Margin Thrust, which is extended all over Andaman (Malik et al., 2006) along with Jarwa Thrust are the responsible for the formation of mud volcanoes of middle and north Andaman Islands.

Field observations of Barren Island volcano has already discussed in separate chapter named volcanological studies of Barren Island Volcano.

6.2 Geochemistry of mud water

Water, methane and absorbed hydrocarbon association with mud volcanoes have been attracted scientists to work at various mud volcanoes of the globe. The source and origin of the mud water is always controversial and active field of research it is because these volcanoes are considered as window to their underlying, deep fluid source and providing insight into the origin of the fluid. At depth, fluid-sediment interactions imprint the fluid chemistry and their distinct signature is brought to the surface sediments by the ascending fluid. The analysis of shallow pore fluids (tens of cms to hundreds of mts below seafloor), therefore, provides a key to constrain the reactions occurring at depth (Dahlmann and Lange, 2003). As we discussed earlier water plays an

important role in subduction zone magmatism (Jarrad, 2003) and sediments which go along with lithospheric slab contain large fraction of total water volume that enter subduction zones. On a global average, the volume of pores and sediment grains each account for approximately 2.5% of the total slab volume, but approximately 40% and approximately 5%, respectively, of the mass of subducting water (Peacock 1990), therefore we took up geochemical investigations of water erupting out of Andaman's mud volcano, in addition to mud fluids some spring water and ground water were also examined, which can throw some light on the influence on overall fluid of Andaman subduction zone.

In order to study of the geochemistry of Andaman mud water considering the probable sources which can be affect the mud water chemistry are continuous input by ground water and water librated from clay mineral at shallow depth. After considering all possible sources we have utilized several models such as 'two components mixing model, Rayleigh model and water rock interaction model', all the models are described below.

6.2.1 Mixing model

Two components mixing model

Suppose we mix two components A and B which are in different proportions specified by a parameter 'f'. 'f' represent as a fractional contribution of source and is defined as

$$f = \frac{A}{A + B} \quad (6.1)$$

Where 'A' and 'B' are the weights of two components in a given mixture. The concentration of any elements 'X' in such mixture is:

$$X_M = X_A f + X_B (1-f) \quad (6.2)$$

Where X_A and X_B are the concentrations of element X in components A and B, respectively expressed in weight units and X_A and X_B are constant in any suite of samples. So X_M can be express in terms of linear equation:

$$X_M = f (X_A - X_B) + X_B \quad (6.3)$$

From equations (6.1) and (6.2), we can express two components mixing equation of isotopic ratio, such as:

$$R_M^x = \frac{R_A^x X_A f + R_B^x X_B (1-f)}{X_A f + X_B (1-f)} \quad (6.4)$$

Where R_M^x is an isotope ratio of X in a mixture of components A and B, X_A and X_B are concentrations of X in A and B.

6.2.2 Rayleigh Fractionation

Suppose there is a reservoir from which material is being removed with isotopic fractionation. Let 'N' is the total number of molecules in the system and 'R' is the ratio of the rare to abundant isotopic concentrations then the Rayleigh equation describing the evolution of isotopic composition of the reservoir is given by (Gonfiantini, 1981)

$$R = R_0 \left(\frac{N}{N_0} \right)^{\alpha-1} \quad (6.10)$$

Where R_0 is the initial ratio, N_0 is the initial number of molecules in the system and ' α ' is the fractionation factor. In terms of δ notation the equation can be written as:

$$\delta = \delta_0 \left(\frac{N}{N_0} \right)^{\alpha-1} + 10^3 \left(\frac{N}{N_0} \right)^{\alpha-1} - 10^3 \quad (6.11)$$

Where ' δ_0 ' is the initial isotopic composition and $\frac{N}{N_0}$ is the fraction of initial material remaining at any time. ' δ ' is defined by $\delta = \left(\frac{R_{sam}}{R_{std}} - 1 \right) \times 1000$, where R_{sam} and R_{std} are isotopic ratios in sample and standard respectively.

6.2.3 Water - rock interaction model

Suppose in the closed system condition the water-rock interaction isotopic exchange of hydrogen and oxygen can be written following two simple mass balance equations:

$$F_h \delta D_{fluid}^i + R_h \delta D_{rock}^i = F_h \delta D_{fluid}^f + R_h \delta D_{rock}^f \quad (6.12)$$

$$F_o \delta^{18}O_{fluid}^i + R_o \delta^{18}O_{rock}^i = F_o \delta^{18}O_{fluid}^f + R_o \delta^{18}O_{rock}^f \quad (6.13)$$

Where ' F_h ' and ' F_o ' are amount of hydrogen and oxygen respectively, in the water expressed in moles. ' R_h ' and ' R_o ' are those for the rock. Superscripts 'i' and 'f' stand for initial and final, respectively. From these two equations final rock compositions can be determined. The relations for the final rock compositions are:

$$\delta D_{rock}^f = \frac{\left(\frac{F_h}{R_h}\right)(\delta D_{water}^i + \Delta_{rock-water}^h) + \delta D_{rock}^f}{1 + \left(\frac{F_h}{R_h}\right)} \quad (6.14)$$

$$\delta^{18}O_{rock}^f = \frac{\left(\frac{F_o}{R_o}\right)(\delta^{18}O_{water}^i + \Delta_{rock-water}^o) + \delta^{18}O_{rock}^f}{1 + \left(\frac{F_o}{R_o}\right)} \quad (6.15)$$

Where $\Delta_{rock-water}^h$ and $\Delta_{rock-water}^o$ stand for the difference between final isotopic compositions of the rock and fluid (for hydrogen and oxygen, respectively). These are also respectively the carbon and oxygen isotopic fractionation factors between the rock and water, expressed in per mil (‰) units.

For the first time, in the present study we have tried to understand the chemistry of mud water from Andaman mud volcanoes through hydrogen and oxygen isotopes (Fig. 6.1). The analysis of the fluid geochemistry of Andaman mud volcanoes demonstrate that the origin of the fluid and over pressuring result from the clay mineral dehydration by the transformation of the smectite (S) to illite (I) in Andaman subduction zone. The transformation of smectite to illite (mineral dehydration) in Andaman area takes place at a greater depth of the accretionary prism is due to the sediment load and the geothermal gradient. In this process the minerals release their structural water and are transformed into secondary minerals, thereby freshening the ambient pore water. The main reactions are S - I transformation, opal dehydration, and deeper metamorphic reactions (e.g. Brown et al., 2001). The S - I transformation starts at about 60°C and is almost complete at about 160°C at depth 5 - 6 km (Kastner et al., 1991, Moore and Vrolijk, 1992). With increasing pressure and temperature the amounts of water released from the clay inter layers

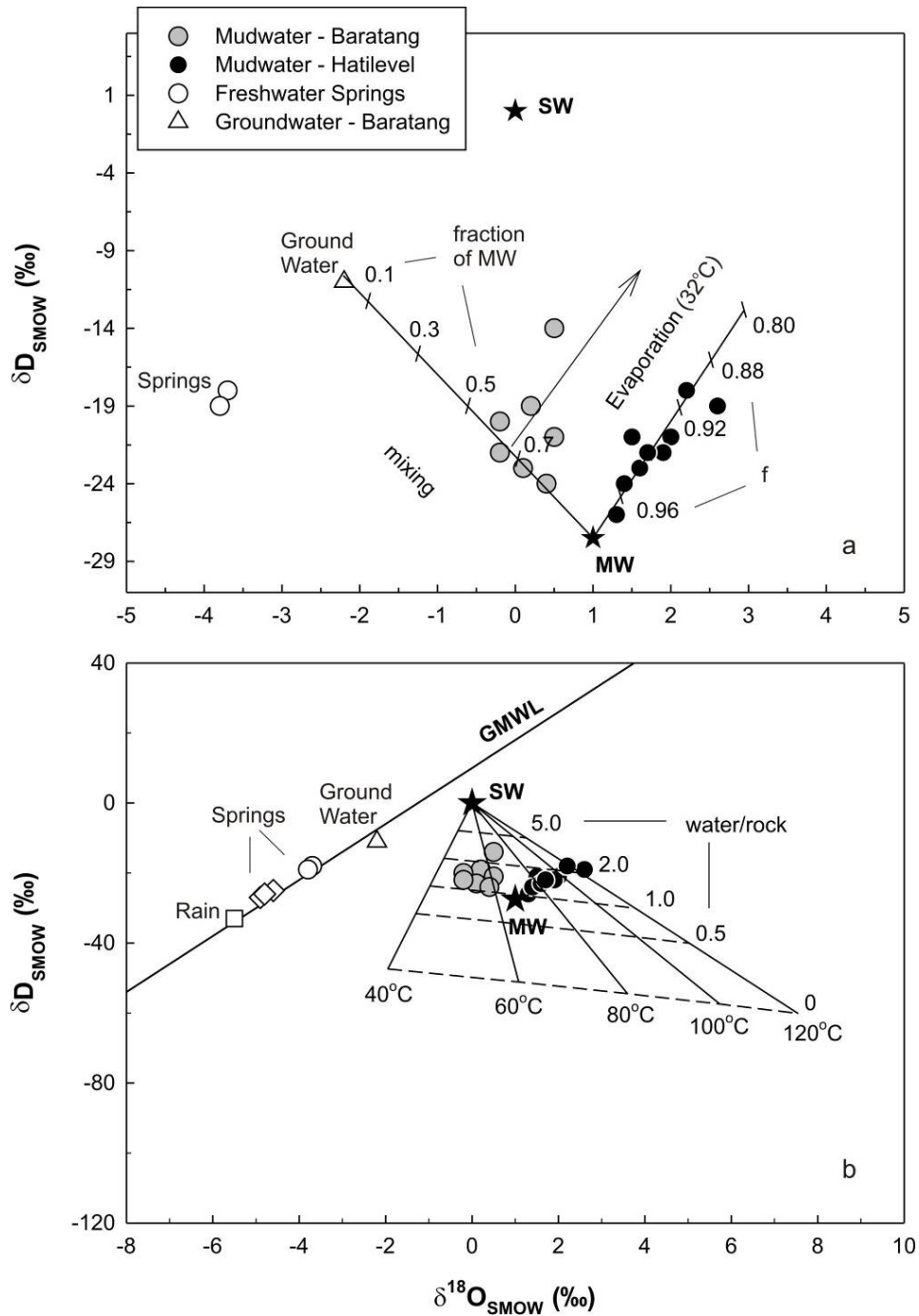


Fig.6.1 $\delta^{18}O$ and δD plots for water samples from mud volcanoes and fresh water sources of Andaman Islands (a) the data for North Andaman (Hathilevel, Diglipur) are explained by evaporation (Rayleigh fractionation) at 32°C, whereas those for middle Andaman (Baratang) are explained by binary mixing with ground water and subsequent evaporation. MW = starting compositions for mud water; f = fraction of remaining reservoir during evaporation; SW= Sea water. (b) The solid lines are evolutionary paths at different temperatures in a water-rock interaction model, where the initial water is seawater (SW) and initial rock/mineral is a smectite clay ($\delta^{18}D = -85$ ‰; $\delta^{18}O = 20$ ‰). The dashed lines join water compositions at a particular water/rock during the evolutions. GMWL = Global Mean Water Line.

increases. The interlayer water of clay minerals is generally characterized by positive $\delta^{18}\text{O}$ and negative δD values.

We have collected mud water from two different sites of Andaman Island (Middle and North). To understand the origin of Andaman mud water, we attempted a forward model and considered the initial composition of mud waters ($\delta\text{D} = -27.5\text{‰}$, $\delta^{18}\text{O} = 1\text{‰}$) to be same for waters from mud volcanoes of Baratang and Diglipur.

The plot 6.1 shows $\delta^{18}\text{O}$ and δD isotopic compositions of mud waters and fresh waters of Andaman Islands. The analysis of mud volcano from diglipur where ground water input is absent can be best explained by evaporation of primary mud water at 32°C where as isotopic trends of most of the water from Baratang are determined to be various mixture of local ground water with the deviation of few samples from mixing line showing effects of evaporation (Fig. 6.1).

Further attempt was made to understand the isotopic components of primary mud water ($\delta\text{D} = -27.5\text{‰}$, $\delta^{18}\text{O} = 1\text{‰}$). The composition of primary water is neither sea water nor fresh water or also not explained by mixing trends of these waters (Fig. 6.1) which are confirmed by high amount of smectite and low amount of illite at mud breccia that suggests deep smectite - illite transformation. In connection of this we have developed water rock interaction model. The results of our numerical model suggests the primary mud-water suggest that the water is derived from a mixture of seawater and water derived from dewatering of clay minerals within the forearc, at temperature $\sim 70^\circ\text{C}$ and depth ~ 4 km (Fig. 6.1), considering geothermal gradient of Andaman Island 15 to 20°C (Kumar et al., 2008).

6.3 Rock clasts and mud breccias from Andaman Islands

6.3.1 Petrography of rock clasts and mud breccias

A total of 25 samples of mud breccias and serpentinite clasts analyzed during this investigations. Our mineralogical data (XRD analyses) of mud breccias and clasts of mud volcanoes show Kaolinite clay mineral are dominated clay mineral with moderate amount of montmorlinite and chlorite clay minerals. Albite and small amount of muscovite are also present in these mud breccias. Calcite is also seen in XRD spectrum that is limited to Baratang mud breccias. The above mineralogical compositions suggesting mud breccias are derived from mafic rocks through alteration. The presence of calcite in mud breccias and zeolite as rock clasts from Baratang mud volcanoes suggest low grade metamorphism also play a role in this area (Orange et al., 1993).

6.3.2 Geochemistry of rock clasts and mud breccias from mud volcanoes of Andaman Islands

The geochemistry of the rock clasts and mud breccias provide important information about the sediments of subducting slab along with composition of deep seated series and can be used for revealing the evolution of the Andaman subduction zone. The geochemical analysis can also suggest the evidences of the nature of their source. In the present section, the inferences are based on major oxides and trace elements behaviours of mud volcanoes of Andaman Islands. In this study about 20 mud breccias samples and 5 serpentinite clasts (both Diglipur and Baratang areas) have been analysed.

Clues from Major oxides and trace elements

The mud breccias and serpentine clasts which are brought from mud volcanoes are plotted in the chemical classification diagram of Heron

(1988), which are extensively used for geochemical classification of mudstone and sandstone (Fig. 6.2).

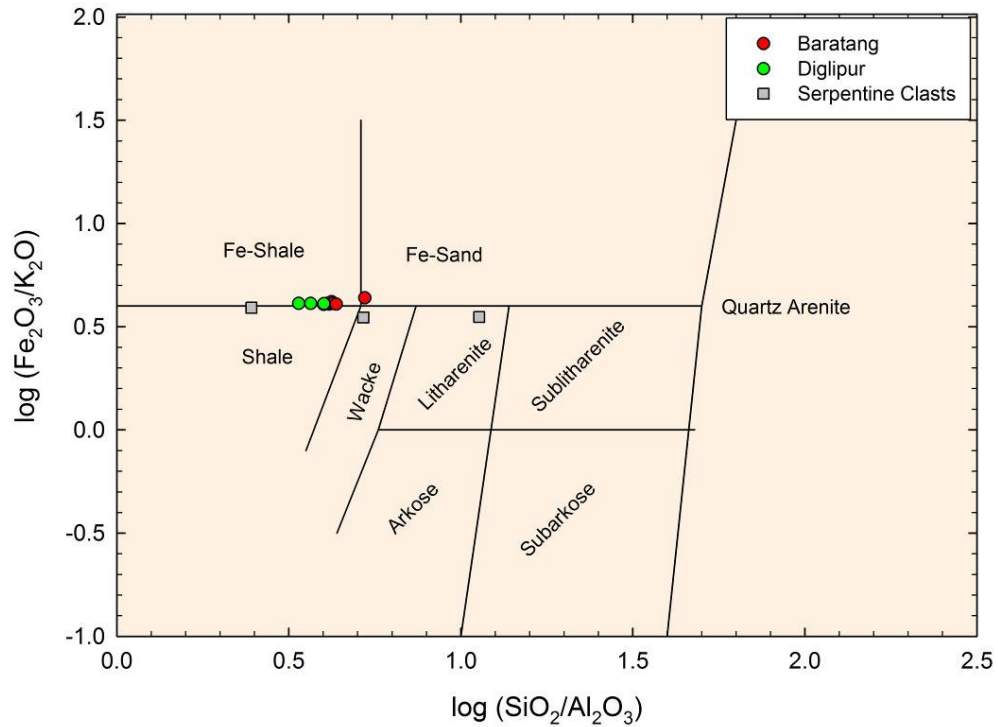


Fig. 6.2 Chemical classification of Mud breccia and serpentine clasts of mud volcanoes of Andaman using the scheme of Heron (1988)

It is observed that all the mud breccias from Baratang and Diglipur are lying on the shale and Fe shale line while serpentine clasts are scatter in the plot. The above result suggests the mud breccias are derived from deeper level in deep water regime and it has not influence by surface weathering agents.

The molecular proportions of Al_2O_3 , K_2O and Fe_2O_3 of the mud breccia and clasts are plotted in the ternary diagram (Fig. 6.3). All the data are closed to Al_2O_3 suggesting clay minerals control the composition (Wronkiewicz and Condie, 1987). The serpentine clasts show the

significant variation in iron content which indicate these are controlled by iron rich minerals.

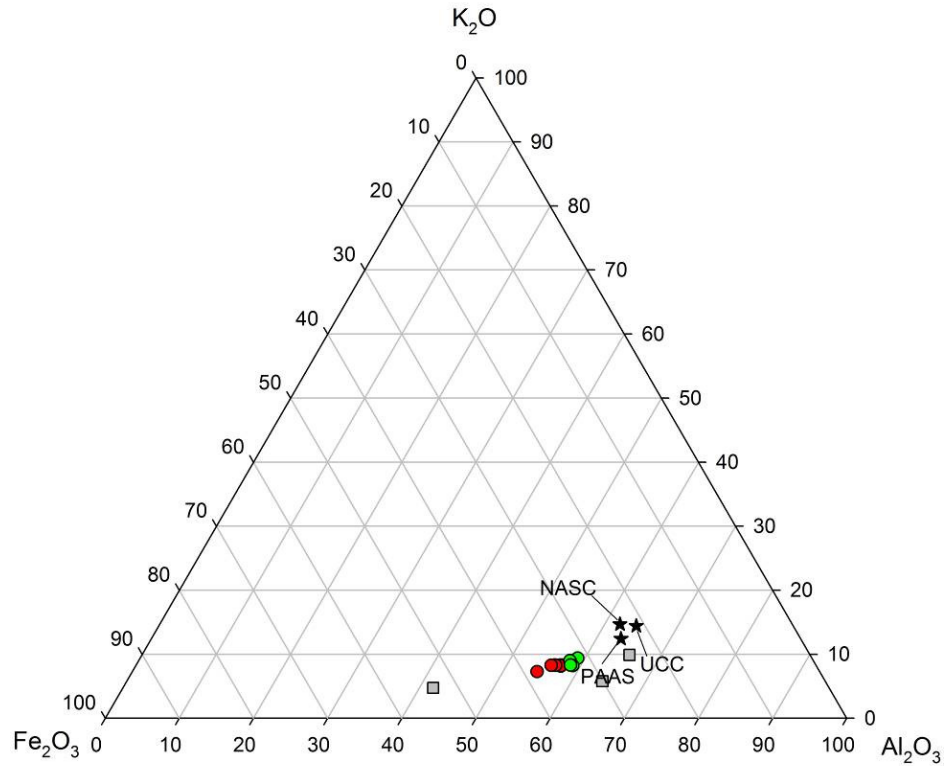


Fig. 6.3 Al₂O₃-K₂O-Fe₂O₃ diagram for the Mud breccias and serpentine clasts of mud volcanoes of Andaman using the scheme of Wronkiewicz and Condie, 1987.

'Al' and 'Ti' have been used to identify the source signature of Mud breccia and serpentine clasts because of their chemical resistance behaviour. We have used plotted bivariate plot between TiO₂ and Al₂O₃ the same scheme are used by McLennan et al., 1980 and Schieber, 1992, which has been in Fig. 6.4. In this plot the data of mud breccias fall closer to the mixing line of "3 granite + 1 basalt" line of Schieber (1992). While the serpentine clasts fall closer to "gabbro" field, so the source of the mud breccias and the serpentine clasts has different. The above inferences suggesting that mud breccias and clasts are derived from mafic rocks through alteration, which is also supported by their high Al₂O₃ contents.

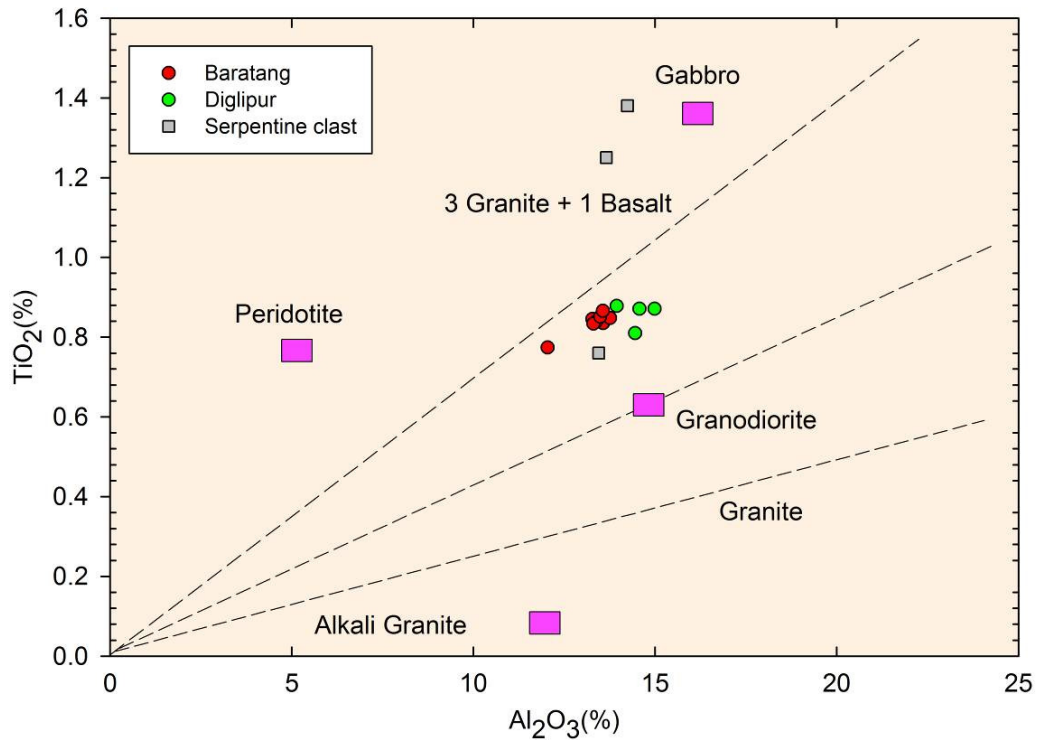


Fig. 6.4 TiO₂ vs. Al₂O₃ plot of McLennan et al. (1980) for the Mud breccias and serpentine clasts on which data from mud volcanoes of Andaman are plotted. The 'granite' and '3 granite + 1 basalt' line are from Scheber (1992.)

We have plotted variation diagram (Fig. 6.5) for all the major oxide with respect to 'Al'. 'Al' is an important component of particulate matter derived from continents (e.g., Taylor and McLennan, 1985) and is relatively immobile during transformation of sediments to rock (Stumm and Morgan, 1981). 'Al' is therefore frequently used to trace the abundance and accumulation of the terrestrial component (Murray et al., 1991, 1992). However, a small portion of 'Al' in the deep-sea sediments is also attributed to submarine weathering of ridge rocks and hydrothermal activity (McMurtry and Yeh, 1981).

Variation of Al₂O₃ versus other major oxides (Fig. 6.5) in mud breccias and clasts clear show that the Baratang and Diglipur mud

breccias are might suggest they are derived from same source. Although clasts don't show any specific trends indicate their source has different or affected by alteration. The high concentration of Na₂O with compare to K₂O may indicate the presence of sodic feldspar in the breccia (Nohara and Kato, 1985) or preferential biological removal of Na from seawater by certain calcareous organisms (Elwakeel and Riley, 1961) which are reported by Ling et al. (1995) in mud volcano ejected breccia of Andaman Islands.

Iron contents in deep sea sediments are generally associated with lithogeneous, hydrogenous and metalliferous components (Chester and Aston 1976). In the Baratang mud volcano's breccia Fe₂O₃/ Al₂O₃ ratio is more than 0.6 which is higher then pelagic clay (0.58; Taylor and McLennan, 1985) and Diglipur mud volcano's breccias are showing pelagic clay value, indicating there is excess Fe in Baratang mud breccia. The excess Fe and constant pattern of Al and Ti in Baratang mud breccia suggest that the mud breccia is not affected by detrital clays.

Ti is known as a better tracer of terregenous fraction than Al, because of the potentially large biologically affiliated Al flux (Murray et al., 1993), but a minor quantity is also derived from oceanic weathering of basalt (Bostrom et al., 1973). The TiO₂ content of the mud breccia (< 0.8%) is higher than pelagic sediments and nearly one and half times more concentrated than in CIB (Central Indian Basin) sediments (Pattan et al., 1995). The Al₂O₃/TiO₂ ratio is lower than the ratios of Post Archean Average Shale (PAAS ~ 18.9) and pelagic clay (PC ~ 20.7). This ratio is also lower in the average Pacific pelagic clay sediment (Bischoff et al., 1979), indicating an insignificant contribution of Ti from submarine weathering. Because of insignificant contribution of Ti from submarine weathering, the high Ti and Al contents of the mud breccia indicates they are derived from

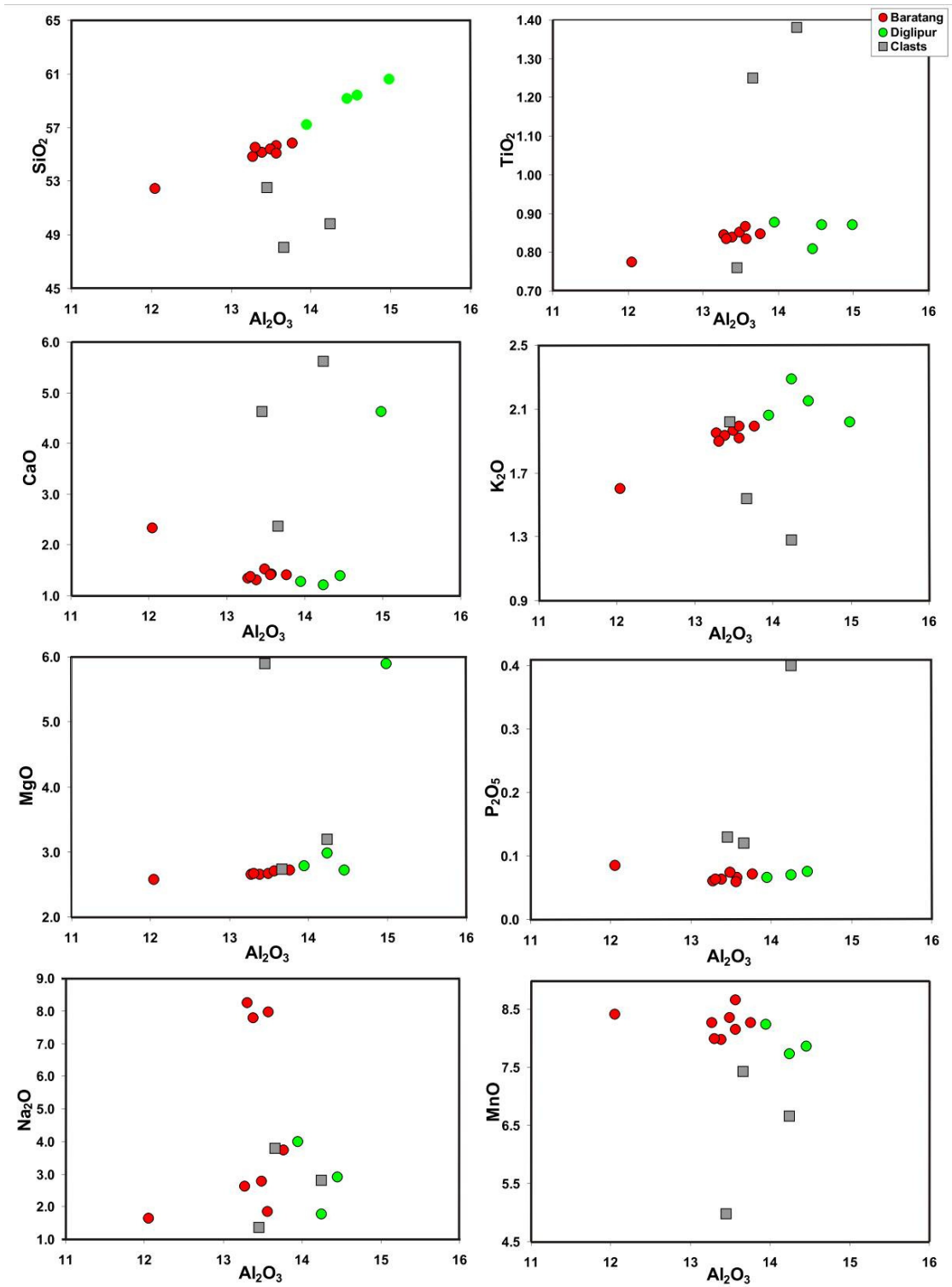


Fig. 6.5 Variation diagram of mud breccias and clasts from Mud volcanoes of Andaman Islands

'Al' rich rock or sediments. TiO_2 and Al_2O_3 show positive correlation (Fig 6.5) indicating their continental origin. This is supported by strong linear relation between potassium and alumina indicates lithogenous contribution.

Concentration variations in trace elements have been useful in understanding provenance, weathering and transportation. The Rare Earth Elements (REEs) patterns have been exclusively used in deciphering history of the sediments especially mud and mud stones (shale). The REEs, due to their group behaviour, immobile in water, and almost nonexistent inter element fractionation, faithfully preserved the source compositions (McLennan et al., 1989).

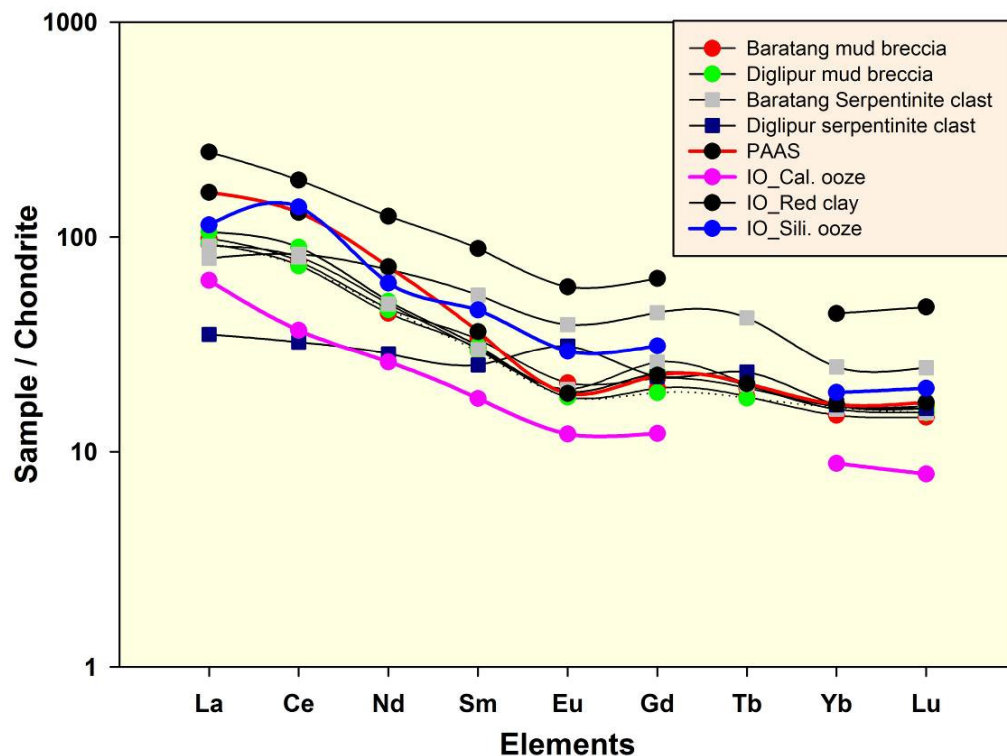


Fig.6.6 Chondrite normalized REE patterns for mud breccia, clasts compared with PAAS (McLennan et al., 1989) and Indian Ocean sediments (Pattan et al., 1995)

Chondrite normalized patterns of REE have been used for provenance studies (McLennan et al., 1989). The chondrite normalized REE patterns of mud breccia and clasts of mud volcano of Andaman along with PAAS and Indian Ocean sediments (Siliceous ooze, Calcareous ooze and red clay; Pattan et al., 1995) are plotted for comparison in Fig 6.6. The REE patterns of mud breccia are very similar to red clay of Wharton basin of Indian Ocean (Pattan et al., 1995). This suggests the source of these breccias may be red clay which is derived probably due to the supply of lateritic soil from west Australia by southeasterly winds and northeasterly aeolian transport from the adjacent Indonesian archipelago (Venkatrathnam and Biscaye, 1973), this observation are also supported by their Al_2O_3 contents.

The behaviour of serpentinite clasts of Baratang and diglipur mud volcanoes is similar except the 'Eu'. The positive 'Eu' anomaly in diglipur serpentinite clast suggests that the dominance of plagioclase in the source, as plagioclase controls the 'Eu' concentration.

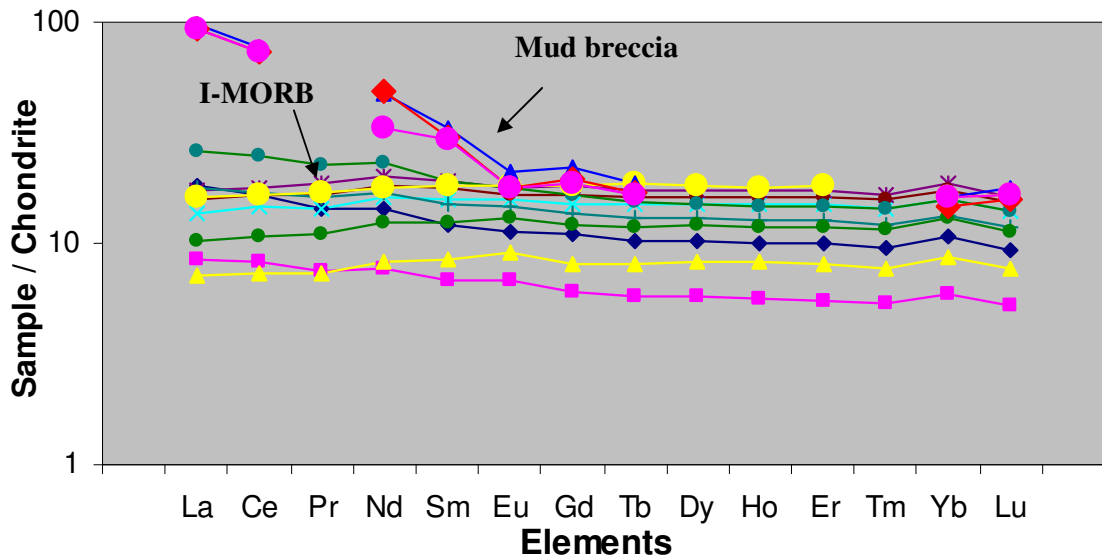


Fig.6.7 Chondrite normalized REE patterns for mud breccia, clasts compared with Indian Mid Oceanic Ridge Basalts (I-MORB) and Barren lavas

To further additional attempt was made to understand the source of mud breccias, their normalized trace elements based on a few analyses we find that the trace element patterns of mud samples are very different from average crustal materials or MORB. They are enriched in large ion lithophiles compared to MORB but depleted with respect to average crust (shale); hence the sources of mud are likely to be a mixture of both (Fig. 6.7).

6.4 Geochemistry of Andaman Ophiolite

The photomicrographs of Andaman igneous rocks are already presented in last chapter. Our petrological study on Andaman samples reveal that the most of the samples are highly altered. It took place due to sea-floor weathering and the effects of serpentinization. The predominant rock type amongst the magmatic rocks in the Andaman is Basalt. In polished thin section, it is generally porphyritic and hypocrySTALLINE and exhibits textures usually of ophitic texture and, at places, intergranular, sub-ophitic and variolitic. Their phenocrysts are dominantly of plagioclase with a little olivine and pyroxenes and opaque minerals. Spherulite structures are also identified in a highly altered sample from the contact zone between basalt and serpentinite in the quarry, nearby to Corbyn's Cove in the island of South Andaman. This sample is a hybrid one with a relict basalt portion exhibiting typical intergranular texture, being invaded by serpentinous material, and later by a quartz vein (Fig 5.1f). The Spherulites found in Andaman Island represent eutectic intergrowth of quartz and fibrous feldspar of intrusive origin (Tyrrell p. 99) and also represent the product of alteration of glass.

Plagiogranites (Fig. 2.3a) have also collected from Andaman Islands which represent the end product of sub-alkaline tholeiitic magmatism. In Andaman, Plagiogranites are associated with cumulates, which represent

its existence either by crystal-liquid fractionation process (Coleman and Peterman, 1975) or by late stage silicate liquid immiscibility process (Dixon and Rutherford, 1979). In thin section plagiogranites are medium to coarse grain, almost equigranular and subhedral in shape recognized as hypidiomorphic granular texture (Fig 5.1a). Apart from this poikilitic and granophyric textures are also seen in which lath of plagioclase feldspars are partly enclosed by big quartz crystal and shows intergrowth of quartz and plagioclase feldspar respectively.

The Andaman ophiolites are highly serpentinized, which was confirmed by field evidence, petrography of studied basalt as well as LOI %, that varies from ~ 3 -10 %. Dick and Fisher (1984) and Niu and Hekinian (1997) reported serpentinization along with sea floor weathering significantly modify the composition of ophiolites peridotite and can show the trend of depletion of elements such as large ion lithophile with Si, Mg and Ca. Recently Niu (2004) showed that sea floor weathering is more responsible for loss of MgO with compare to serpentinization. He has also argued that Cu, Zn, Ni and Cr remain unchanged during serpentinization. In present studies we have used high field strength (HFS) elements because they are relatively immobile during low grade metamorphism, alteration and sea water weathering (Niu 2004).

Based on major oxide we have observed three compositionally different units in Andaman ophiolite group. The first group has lower silica (39 -44%), high TiO₂ (1 -1.5%) and low alumina (10-14%), the second group contains low silica (45-50%), moderate TiO₂ (0.7-1%) and high alumina (15-19%) and third group has high silica (more then 60%) low TiO₂ (0.5%), moderate alumina (10-13%) and low MgO (~2%). We have plotted MnO - TiO₂ -P₂O₅ (Fig. 6.8) discrimination diagram (Mullen, 1983) to discriminate the basaltic rocks of oceanic environment. From MnO -

TiO₂ -P₂O₅ it is evident that Andaman ophiolites compositions are MORB Island Arc and also boninites composition.

In earlier studies was done by Shastry et al. (2001), Srivastava et al. (2004) suggested that the Andaman ophiolite suite from south Andaman is high Ti and Fe rich mafic rocks of MORB composition but our results shows it has varied from boninite to MORB composition. The origin of one group of Andaman ophiolites is boninitic parent magma as it does for many ophiolites suite (Dick and Bullan, 1984). Such type of magma has specific composition (moderate silica and high Mg). These types of magma are considered as the parental liquid for some Palaeozoic and Mesozoic ophiolites while it has been erupted throughout earth history (Orberger et al., 1995; Melcher et al., 1997). The boninitic magma is usually regarded as modern analogue of high magnesium and low Ti lavas occurring in ophiolites and common in supra subduction zone environment (Coish and Church, 1979; Cameron, 1985), and restricted to forearcs in modern tectonic environments; their presence in ancient assemblage is often taken to indicate a forcarc environment (Coish and Gardner 2004). The high Cr concentration, high Mg concentration and low Ti contents attest supra subduction zone (SSZ) setting of the Andaman ophiolites because above mentioned elements are used for the tectonic discrimination of ultramafic rocks. Pal , (2011) also suggested the Andaman ophiolite shows MORB - SSZ signature for mantle rocks on the basis of TiO₂ Vs Al₂O₃ relation of chromites. He has also proposed 10 -15 % of partial melting of mantle rock based on Cr # and TiO₂.

In the Andaman ophiolite suite we have collected dunite and harzburgite rock types, this rock types are also reported by Pal (2011). The origin of this type of rocks in subduction area, Pearce et al. (2000) documented that when the boninite melt interact with mantle harzburgite,

they can produce dunite, whereas when MORB melt reacting with lherzolitic mantle can produce harzburgite. The above reported statements supported our earlier observations that are based on major oxide in which we have suggested that the formation of Andaman ophiolite is the product of are polygenetic melt (boninite and MORB melts).

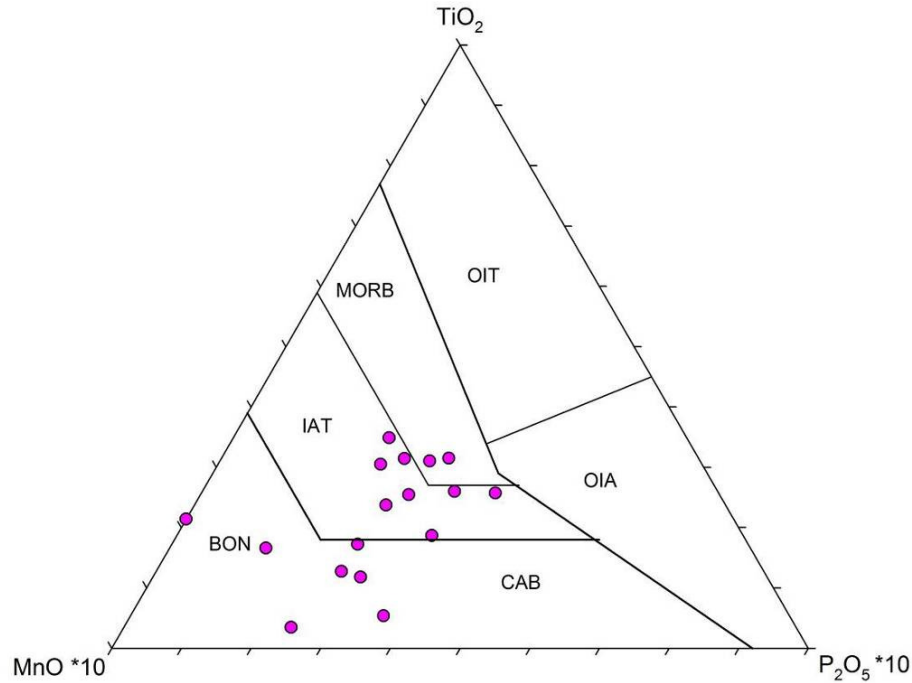


Fig 6.8 MnO-TiO₂-P₂O₅ diagram for Ophiolite group rocks of Andaman using the scheme of Mullen, 1983. IAT: Island Arc Tholeiite, CAB: Calc-Alkaline Basalt, MORB: Mid Oceanic Ridge Basalt, OIB: Ocean Island Basalt, OIA: Ocean Island Alkaline Basalt, BON: Boninite

Pal (2011) suggests the rock types harzburgite in Andaman ophiolite is not the product of MORB melt while it is influence by subduction zone fluids which leaved a harzburgitic residue in this connection he argued that the absence of any MORB extrusive rocks and presence of Island arc tholeiites (IAT) in the area, Andaman ophiolite is the product of interaction with IAT melts. Pal (2011) didn't mention about the origination of dunite rock type which has reported by Pearce et al. (2000).

Based on comparative trace elements pattern of Andaman ophiolite and Oman ophiolite rocks, Pederson et al. (2010) differ from the conclusion of Pal (2011) and they suggested that the ophiolite rock types are the product of MORB melt. They have further added that some of the parental melts of rocks of Andaman ophiolite were contaminated by slab derived fluids and also argued that it is difficult to discriminate the formation of Andaman ophiolites whether it is formed in SSZ environment or at major spreading centre. But based on similar age of the Andaman ophiolite with Oman and Troodos ophiolites, they have suggested it may be SSZ origin.

Both Pal (2011) and Pederson (2010) argued that subduction fluids have affected the Andaman ophiolite rocks but they haven't isotopic data to prove it, in present study we did isotopic analysis. The isotopic ratios with major oxide can infer about the role of the fluids along with the source of melt composition of the Andaman ophiolite rocks. In next section we will infer the role of subducted fluids and sediments in Andaman ophiolite rocks.

6.5 Radiogenic isotopic studies of mud breccias, rock clasts of mud volcanoes and ophiolite rocks of Andaman Islands

The radiogenic isotopic studies of Sr and Nd have been used in deciphering the source composition. There are a few studies of Andaman ophiolite that are based on petrological and geochemical observation. There are also very few literature on mud volcanoes of Andaman which are mainly based on micropaleontological aspects. But still there is not a single literature of these areas which deals the isotopic compositions of the Andaman ophiolite rocks and isotopic composition of mud breccia and rock clasts of mud volcanoes. So, we have undertaken isotopic studies of these rocks (Fig. 6.9 and 6.10) to ascertain its source composition.

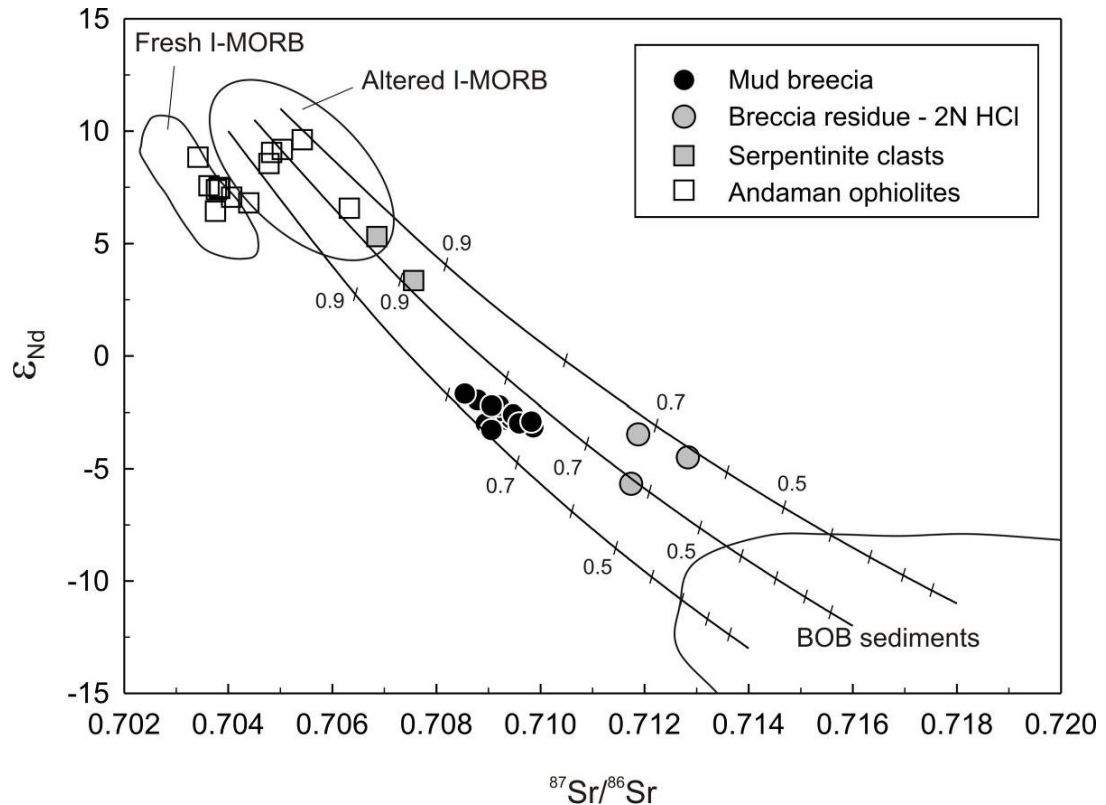


Fig.6.9: ϵ_{Nd} versus $^{87}Sr/^{86}Sr$ plot for mud matrix, HCl- residue fraction of mud matrix and serpentinite clast samples from mud volcanoes of Andaman Islands. The plot also contains data for rocks of Andaman ophiolites. The solid lines are two-component mixing curves between altered I- MORB and BOB sediments, with the numbers on them representing amount of the former in the mixture. Data sources: fresh Indian MORB (Mohaney et al 1989; Nauret et al 2006; price et al 1986), Bay of Bengal (BOB) sediments (Derry and frence-Lanord, 1996; Plank and Langmuir, 1998).

The Fig. 6.9 is in between Sr and Nd isotopic ratios for Andaman ophiolite, Mud breccia, serpentinite clasts along with the field of BOB sediments. Here we have observed most of the ophiolites data is falling in the field of I-MORB with some exception which has high Sr value with constant Nd values indicate significantly impacted by alteration with Sea water. Further we have tried to characterize the source of mud breccias. We have developed a two component mixing curves in which two end members are altered I-MORB and BOB sediments, which are the probable source for mud breccias. Furthermore two components mixing trends

show mud breccia contains ~ 70-80 % contributions from altered I-MORB and 20-30 % BOB sediments.

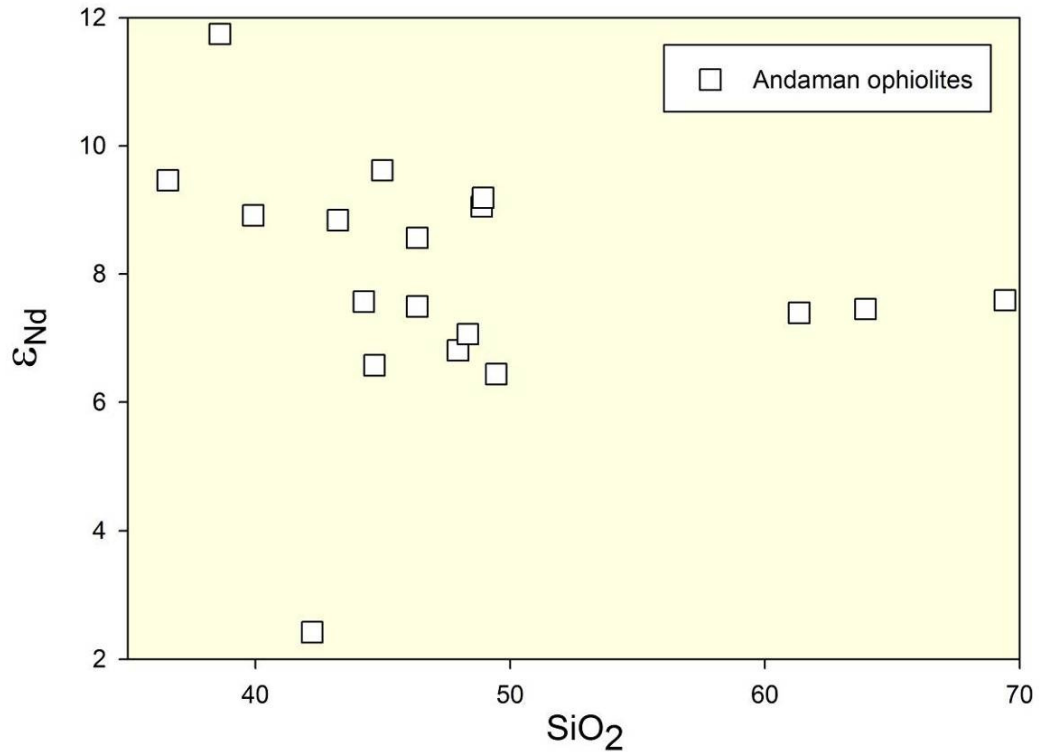


Fig. 6.10 ϵ_{Nd} versus SiO_2 plot for Andaman ophiolites of Andaman Islands. There is good negative correlation between Nd isotopes and SiO_2 compositions, which indicate origin of ophiolites through mixing of isotopically distinct magma sources.

As stated earlier there is not enough available data to draw conclusions of the role of subduction fluids and sediments in the melt of Andaman ophiolite rocks. However we have tried to find out the influence of fluids and sediments based on neodymium isotope and SiO_2 (Fig. 6.10). We have observed significant scatter in data, there is decrease in ϵ_{Nd} value with increasing SiO_2 that is consistent with isotopic variations of the ophiolite suite (Fig. 6.10) these variations in Andaman ophiolite rocks reveal an important aspect of the sediment and fluid contributions. There are further observation that show appreciable change in SiO_2 and ϵ_{Nd}

values (high SiO₂, and high ε_{Nd} value) that suggest the parental melts of these rocks had affected by subducted fluid and subducted continental sediments source. Our inferences are well supported by Pal, (2011) that has mentioned subducted fluids and sediments infected parental melt of Andaman ophiolite. This observation also confirmed that Andaman ophiolite is related with subduction processes and its origin is supra subduction origin.

6.6 Lava flows and ash beds from Barren Island (BI) Volcano

6.6.1 Petrography of lava flows

The lavas on BI are grayish black to brownish black and highly vesiculated porphyritic basaltic rocks which show porphyritic texture with glassy ground mass and contain abundant phenocrysts of plagioclase, olivine and clinopyroxene. Many of the lava flows also contain xenocrysts of plagioclase and olivine/pyroxene that are often show resorption boundaries. The plagioclase grains show well developed compositional zoning from core to rim, suggesting slow fractional crystallization of the lavas.

We have reported the toothpaste lava is part of the recent aa flow exposed at the landing Site 3 (N 23° 17.08', E 93° 50.92') on the western coast of BI (Fig. 3.9d-g), (Sheth et al., 2011). This flow issued from the cinder cone 1.5 km to the east and flowed to the coast and into the sea. Its exact eruption age is not known, since no regular monitoring of this active volcano has been in place, but Sheth et al. (2009) inferred from various evidence that it probably formed during the 1994–95 eruptions.

This flow at the coastline is notable in the entire recent aa flow field for its striking morphology. Its surface crust has been extensively broken into sheets and slabs, up to several meters across, some of which are

strongly curved (Fig. 3.9e). The sheets and slabs, which we distinguish in this paper with an arbitrary boundary of 10 cm thickness, are often razor-sharp and stand on end, with meters-deep chasms in between (Fig. 3.9d). They were carried atop along a mobile aa core, well exposed at the Landing Site 3 (Fig. 3.9c). The curved sheets and slabs, including the largest ones illustrated in Figs. 3.9e, f, g are elongate in the N-S direction, i.e., perpendicular to the flow direction (due west). They are convex upstream (Sheth et al., 2011).

All the toothpaste lava samples are crystal-rich and have a few vesicles. The rocks contain up to 46.7% crystals by volume. Plagioclase is extremely abundant as a phenocryst, commonly showing zoning or twinning, sometimes both. Many plagioclase phenocrysts are very well-developed euhedral, tabular crystals and contain large numbers of glass inclusions. Olivine and clinopyroxene phenocrysts also occur, but in small amounts, the latter showing twinning as well as zoning. The zoning common in the plagioclase crystals suggests their incomplete equilibration with surrounding liquid, and Luhr and Haldar (2006) have reported that some of the plagioclase and olivine megacrysts in BI lavas are not phenocrysts but xenocrysts, representing disaggregated troctolitic cumulate from a shallow magma chamber. The viscosity of a magma or lava is strongly dependent on its temperature and composition (silica content), among other factors (e.g., Shaw, 1972). At BI, clinopyroxene crystallization is known to follow that of plagioclase, which follows that of olivine \pm spinel (Luhr and Haldar, 2006). With a few available temperature estimates based on olivine melt-inclusion geothermometry (Luhr and Haldar 2006), and the extensive crystallization (including that of clinopyroxene) observed in our samples, we considered a temperature of 1100 °C suitable for input in the viscosity calculation we carried out using

the major oxide data following the method of Shaw (1972). (Sheth et al., 2011).

Further, based on field observation Sheth et al. (2011) suggested that the formation of BI lava with toothpaste lava squeeze-ups was considerably cooled and crystallized, and thus highly viscous, by the time it arrived at the coast based on textural and geochemical results. They believed that the high viscosity of the BI aa flow had greatly reduced its speed of advance, and the speed might have been further retarded due to its entry into the sea, or a local shallowing of basal slope near or at the coastline.

6.6.2 Clues from Major oxides, trace elements and isotopic studies

In the absence of absolute chronology, we grouped the volcanics on BI into three categories based on their relative chronology with respect to the caldera forming event in to pre-caldera, post-caldera, modern. All our interpretations below follow the above classification

We classified the lavas for BI using the standard method using total alkalis (TA), $\text{Na}_2\text{O} + \text{K}_2\text{O}$ and silica (S) contents (Le bas et al., 1986), which is one of the most useful classification schemes available for volcanic rocks. The usefulness of the TAS diagram and reason behind choosing silica and $\text{Na}_2\text{O} + \text{K}_2\text{O}$ as a basis for classification of volcanic rocks has been discussed by Cox et al., (1979). Fig 6.11 gives the results of this classification, which reveals that BI lavas have SiO_2 in the range of 45-57 wt % and are basalts or basaltic andesite.

Interestingly lavas of precaldera eruptions have wide range of compositions varying from basalt to andesite (mainly basaltic andesite), while the post caldera and modern lavas are mainly basaltic. The MgO content ranges from 3.25 to 9.28 wt % and Mg numbers [$Mg \# = (Mg^{2+} / Mg^{2+} + Fe^{2+}) * 100$] from 45 to 70. On the basis of Mg# BI lavas can be grouped into: evolved, moderately evolved and least evolved.

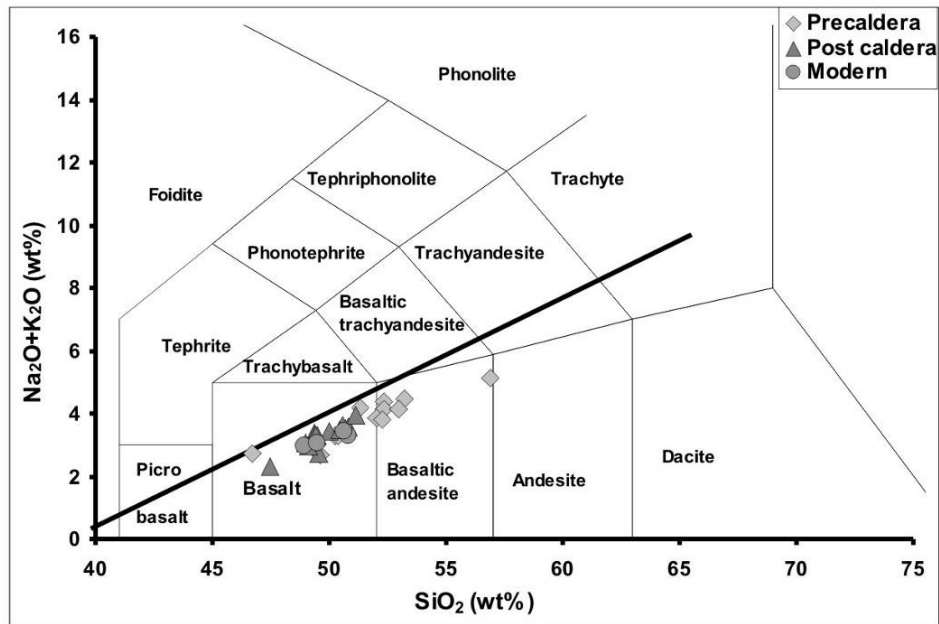


Fig. 6.11 Classification of rocks from Barren Island based on total alkali vs. Silica variation (after La Bas et al; 1986). The samples are grouped according to their chronology with respect to the caldera forming event

MnO - TiO₂ - P₂O₅ (Fig. 6.12) discrimination diagram (Mullen, 1983) to discriminate the basaltic rocks of oceanic environment. From MnO - TiO₂ - P₂O₅ ternary plot, it is evident all the BI lava flows and ash beds show Island Arc Theoliite (IAT) origin.

Variation of MgO versus other major oxides and Ni and Cr (Fig. 6.13) in BI lavas clear show that the precaldera lavas display a nice

fractional crystallization trends- depicting crystallization of olivine and plagioclase for the parental magma. This might suggest that most of the

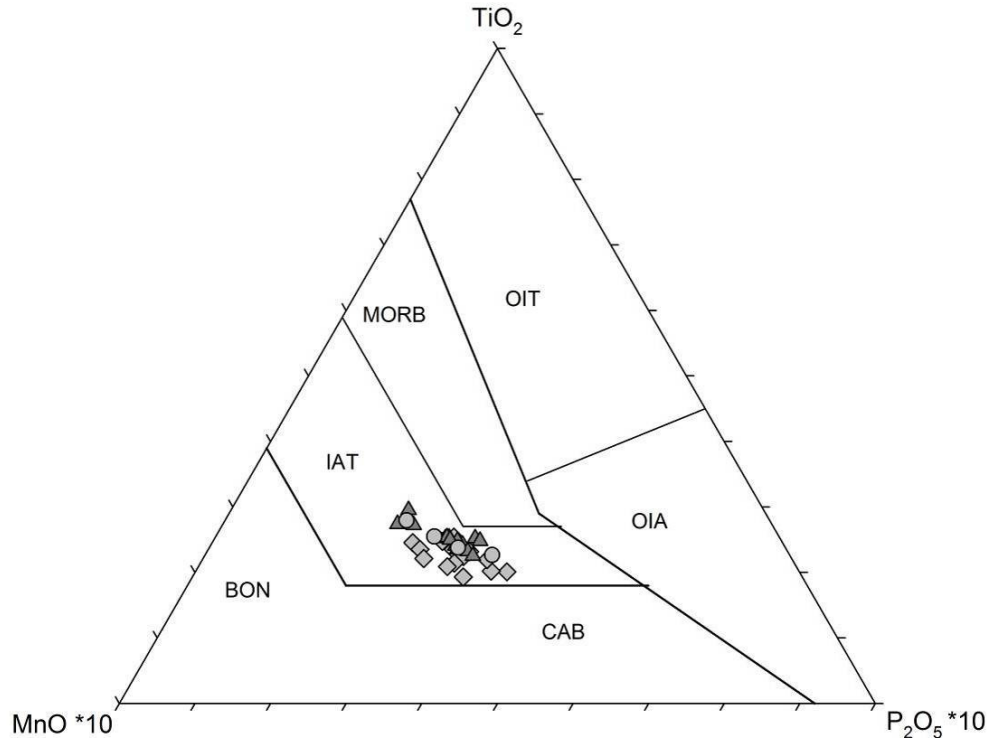


Fig 6.12 MnO-TiO₂ -P₂O₅ discrimination diagram for Barren Island lavas and ash, using the scheme of Mullen, 1983.

precaldera eruptions originated for a single magma batch. The scenario for postcaldera and modern lavas is different. Although they don't show any specific trends the constant CaO, Ni, Cr at varying MgO could possibly hint at magma mixing inside the magma chamber prior to their eruption.

Multiple trace-element patterns normalized to N-MORB are shown in Figure 6.14. During subduction, the oceanic slab devolatilizes and dehydrates to release fluids into the overlying mantle wedge. These fluids react with the mantle wedge and form a partial melt, which ultimately gives rise to lavas with arc signatures.

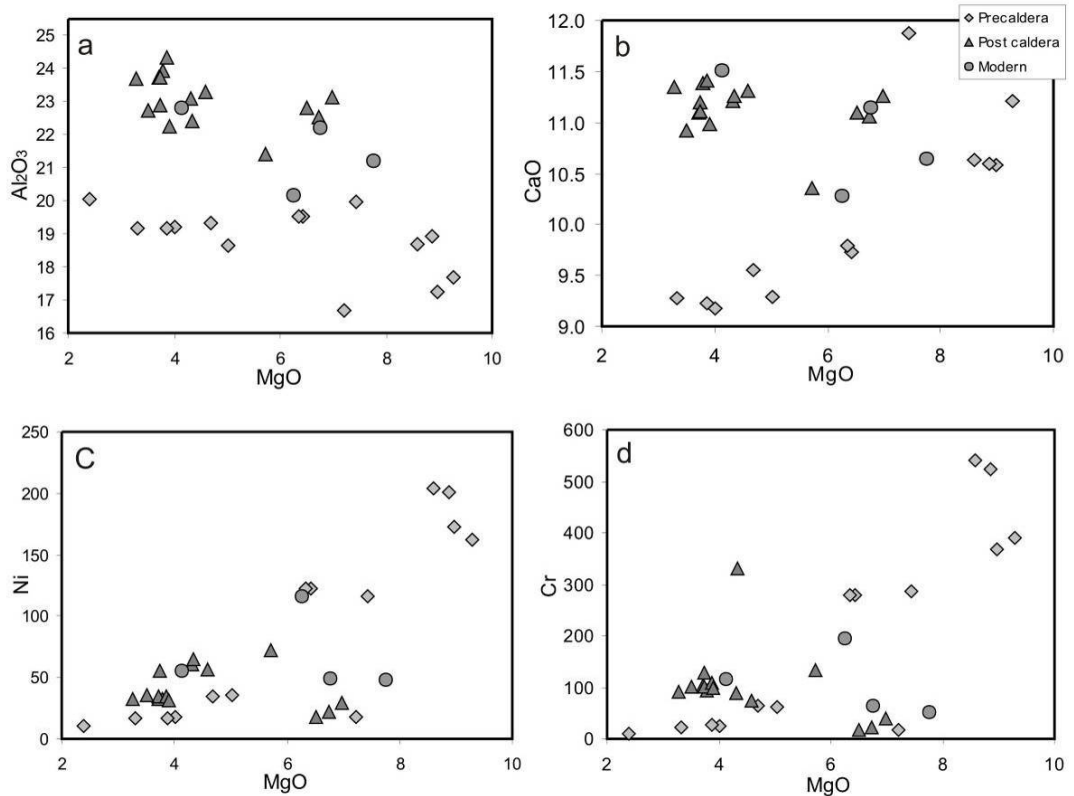


Fig. 6.13 Variation diagrams of selected major and trace elements vs. MgO in Barren Island lavas

The different fractionation stages of the samples make it difficult to directly compare with each other, but the general trend can be recognized. The modern and postcaldera lava flows and ash beds show depleted characteristics as compared to precaldera lava flows and ash beds. The N-MORB normalized trace element patterns of BI lavas show typical characteristics of arc volcanics, such as the negative Nb and Ti anomalies and positive K, Ba and Pb spikes with lesser enrichment of Sr (Fig. 6.14).

However, the magnitude of the anomalies varies between samples, and nearly all show a small depletion in Ti with respect to the REE. The relative enrichments of Ba and Rb also vary in an unsystematic way, as shown by the mafic lavas from precaldera samples. The depletion of Nb relative to large ion lithophile elements can be attributed to two processes:

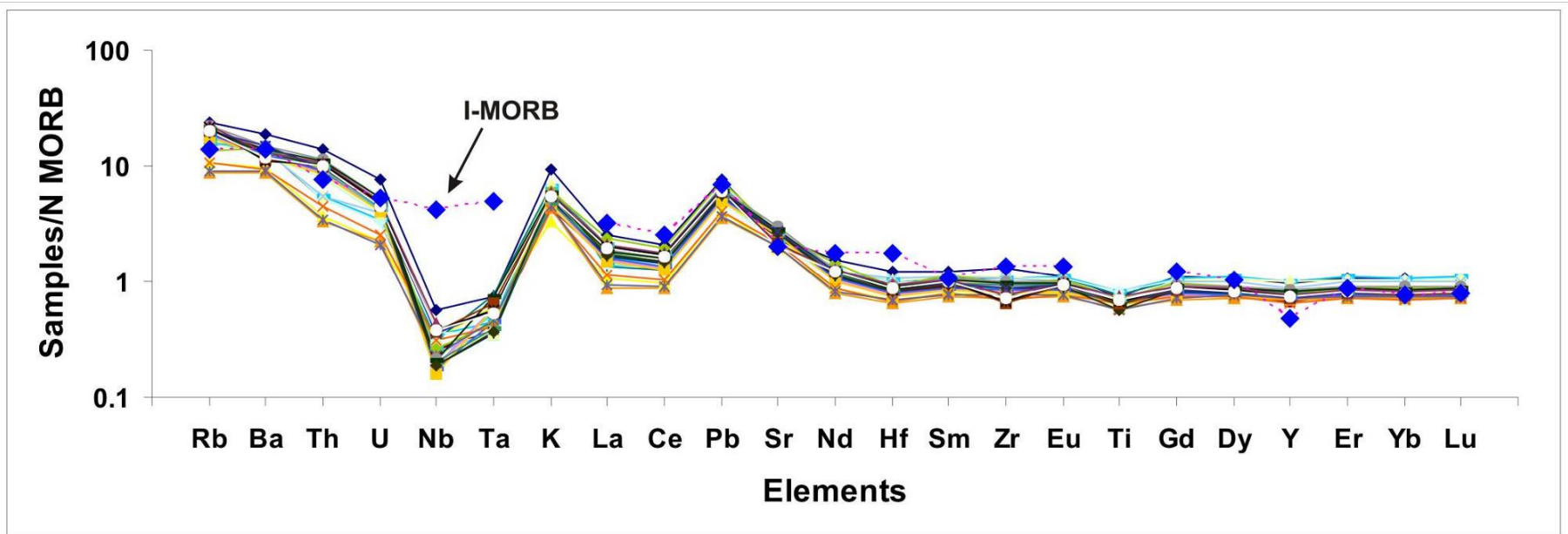


Fig. 6.15: N MORB normalized (Sun and McDonough 1989) trace element patterns for Barren Island lavas compared with the pattern of present day Indian (I) MORB

I) the addition of an LILE enrich and Nb poor fluid components to the mantle wedge or II) the preferential retention of Nb in amphibole relative to other phases in the mantle source (Howkesworth et al 1993) Similar processes can be invoked inferred for the general depletion of the high field strength elements (HFSE) Zr, Ti and Y with respect to large ion lithophile elements (LILE) in BI lavas.

The BI lava and ash samples analyzed show a variation in isotopic ratios. Although there are negative correction between Sr and Nd isotopic ratios when the full data set are considered, $^{143}\text{Nd}/^{144}\text{Nd}$ ratios varies from 0.512884 to 0.512996 while $^{87}\text{Sr}/^{86}\text{Sr}$ varies from 0.703760 to 0.704200.

The isotopic geochemistry coupled with trace elements of Island arc volcanic rocks gives an important clue to the understanding of subducting oceanic slab- wedge mantle interaction and recycling of crustal materials back into the mantle during subduction. So, in the next section, we have tried to understand how and at what level the different subducted components of such as fluids and sediments affected the adjacent mantle wedge.

6.6.3 Mantle source Characteristics

Most models of magma petrogenesis at island arcs involve three main source components: I) the mantle wedge II) the subducting slab (oceanic crust and associated sediments); III) the arc lithosphere. The majority of island arc magmas are thought to originate in the mantle wedge which has been inferred by several workers to be similar to the source of MORB (Ringwood, 1974, Ellam & Hawkesworth, 1988, Turner et al., 2003). In Andaman subduction zone, the slab is essentially the oceanic crust of Indian plate, and therefore for modelling purpose we consider

Indian-MORB (I-MORB) as the unaltered mantle wedge and sediments of Bay of Bengal (BOB) as the unaltered sediments.

In recent time the nature of the slab input to the mantle wedge is in debate because it controls the nature of the arc magma. In present studies we have tried to understand the subducted slab input for BI lavas using Nd isotopic values and some trace elements.

Experimental work (Tatsumi et al., 1986) and studies of arc lavas (McCulloch & Gamble, 1991) indicate that Nd is relatively immobile during slab dehydration, particularly with respect to the formation of aqueous fluids (Kessel et al., 2005). Ba and Ce are more mobile in fluids compared to Th, which is an indicator of sediment contribution Th is chosen over K (which gives a better discrimination between different mantle components) because it is less mobile in aqueous fluids and hence more important in the study of subducted sediments (Pearce et al., 1992). The above characteristics of trace elements were the essence of our geochemical approach and we, therefore, have used to Ba/Th, Th/Ce versus $^{143}\text{Nd}/^{144}\text{Nd}$ variations in BI lavas to assess the contribution of slab derived fluids and sediments to the mantle wedge (Fig. 6.15). From the variations in BI lavas it is evident that the mantle wedge initially was affected by the fluids derived from the slab, as reflected in high Ba/Th at constant $^{143}\text{Nd}/^{144}\text{Nd}$ in precaldera lavas. The source region was subsequently received contribution in form of particulate materials (sediments) from the slab sediments that affects both the isotopic ratios and Th content of the late precaldera, postcaldera and modern lava flows.

The high Pb/Ce and low Nb/Zr ratios in precaldera lava flows also invoked that the precaldera lavas have fluid imprints and postcaldera and modern lavas have significant sediments imprints. Comparing the ϵ_{Nd}

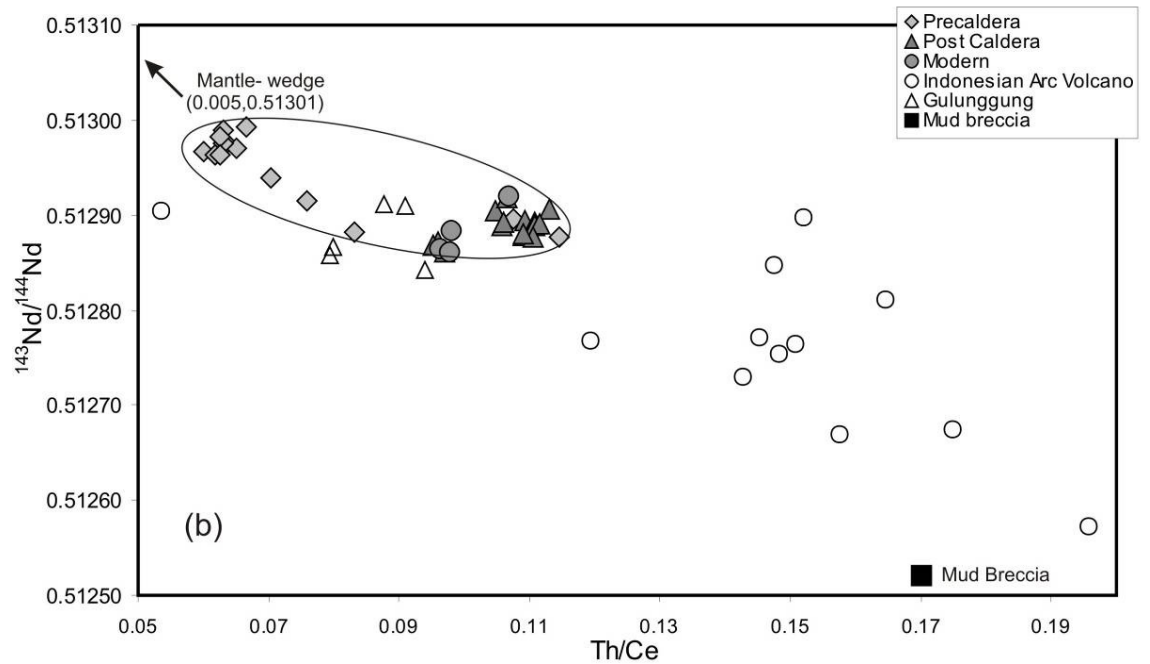
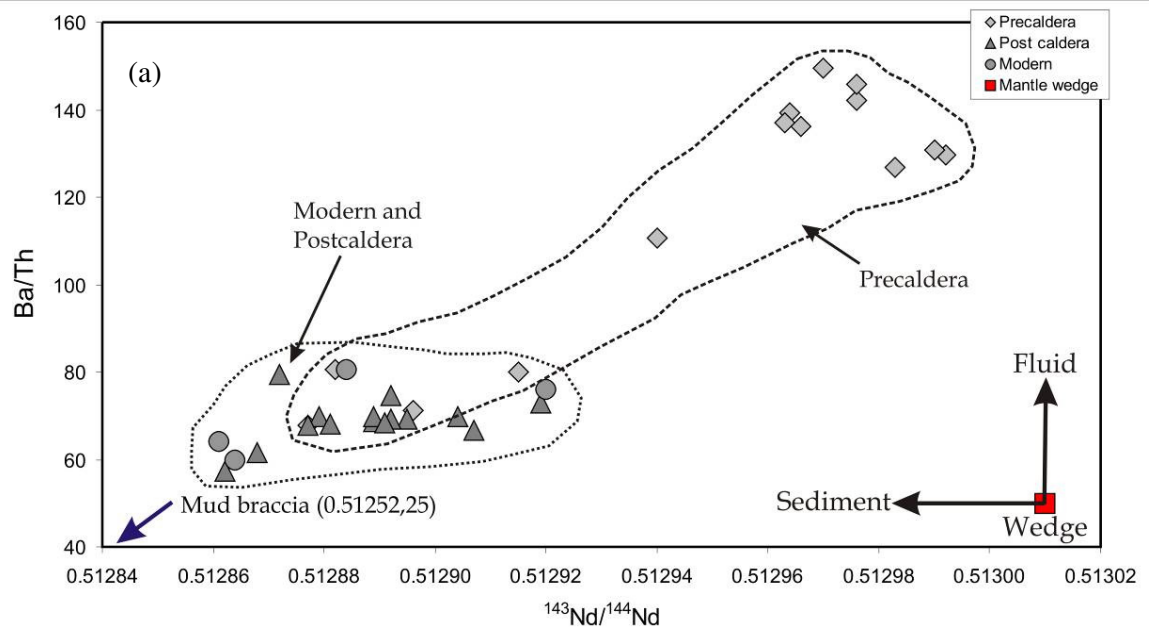


Fig. 6.15(a) $^{143}\text{Nd}/^{144}\text{Nd}$ versus Ba/Th for Barren lavas (b) Th/Ce versus $^{143}\text{Nd}/^{144}\text{Nd}$ plot for Barren lavas and Indonesian arc volcano lavas (Turner and foden 2001) has been plotted for comparison

versus of BI lavas with those of the arc lavas from Indonesia (Fig. 6.15b); we observed that the former appeared to have low contributions from slab derived materials, making them the most primitive amongst all the volcanoes in this (Fig. 6.15).

Sr and Nd isotopes are potentially more powerful indicators of the composition of the sub arc mantle and slab to mantle wedge transfer processes. Further, attempts were made to quantify the slab contributions to BI lavas using these isotopes. In this connection we developed mixing models using different end members of subduction zone components.

Fig. 6.16 shows simple binary mixing solid-solid curves between an I-MORB source and a sediment source representing Indian oceanic crust. As discussed earlier mud breccias from mud volcanoes of Andamans are deemed to represent the sediments of the subducting slab. Mixing curves are generated for different Sr/Nd ratios. Addition of 10-20 % average bulk mud sediments to I-MORB produces a curve that passes through the most isotopically primitive precaldera lavas (Fig. 6.16a). The isotopic characters of postcaldera and modern lavas, however, are inconsistent with two components mixing. Therefore we invoked a three component mixing similar to that proposed by Ellam and Hawkesworth (1988) which involved mantle wedge, subducted sediments and fluids components derived from dehydration. In stand of a fluid component we consider an altered oceanic crust (basaltic) along with I-MORB- representing the mantle wedge and mud breccia-representing slab sediments. Interaction of seawater with basalt produces significant chemical and isotopic changes (Hart et al., 1974, White & Patchett, 1984). For the altered oceanic crust end-member, we consider the serpentinite clasts found in the mud breccia since they represent material derived from the slab deep in forearc. The model curves are presented in Fig. 6.16(b) along with the data from BI

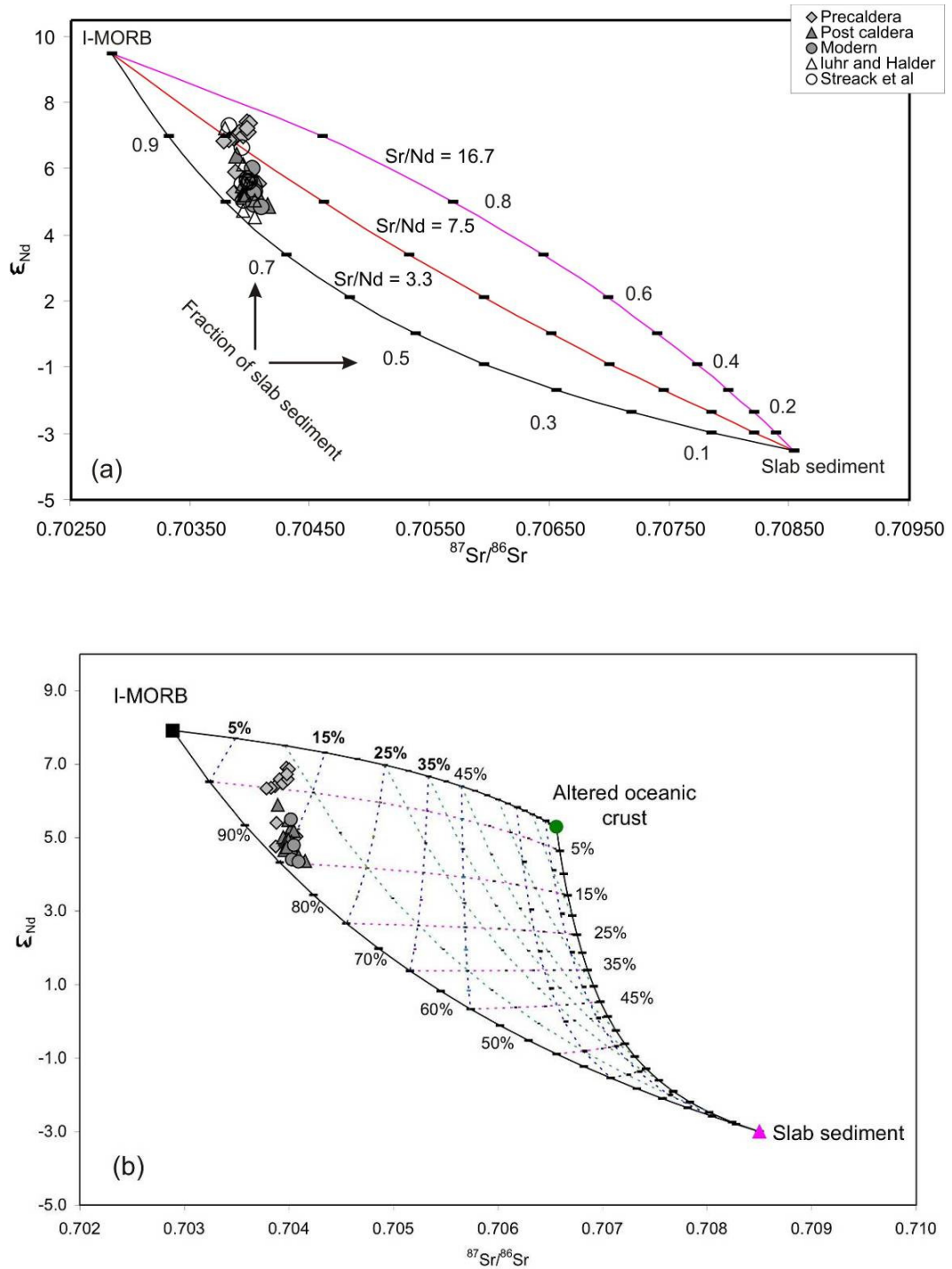


Fig.6.16 (a) ϵ_{Nd} vs. $^{87}Sr/^{86}Sr$ of BI lavas compared with two components mixing curves, where I-MORB & slab components are the two end members. Mud breccia are considered to represent the slab sediments (b) The same data, as in (a) compared with three components mixing curves involving I-MORB, slab sediments and altered oceanic crust as end members

lavas. As can be seen, the precaldera lavas contain more of I-MORB compared to others indicating their primitive nature. These lavas have higher contributions from altered oceanic crust compared to sediments, whereas the postcaldera and modern lavas have higher contribution from sediments – which support our earlier inference based on trace elements geochemistry.

The Pb isotopic data can give first impression of the identify the end members involved in the magma genesis, since, unlike in Sr and Nd isotopic plots, two components mixing lines in Pb- Pb diagrams should be straight, independent of slab to mantle transfer processes.

In the Pb isotopic variation diagram, the Pb isotopic ratios in BI lavas show linear arrays and well above the Northern Hemisphere Reference Line (NHRL) suggesting pb contribution from two distinct mantle source to these lavas (Fig. 6.17 a and b). One of the sources is a non-radiogenic source, most likely the pristine Andaman mantle wedge, and the other appears to be a source affected by radiogenic Pb derived from the slab – most likely from subducted sediments from BOB. In addition of this the scatter Pb isotopes data for BI suggests variability in the subducted components to the mantle source.

To constrain degree of melting, it is important to understand the formation and compositions of the magma, which can affect the absolute concentrations of trace elements. In order to ascertain the degree of melting, we have considered the source composition (Primary basaltic melt) has 90 % mantle peridotite, 8 % of altered oceanic crust and 2 % of subducted sediments. The trace element concentrations of these sources have been taken from Kimura et al. (2010). The above % has been taken based on our previous results of three components mixing model. In the

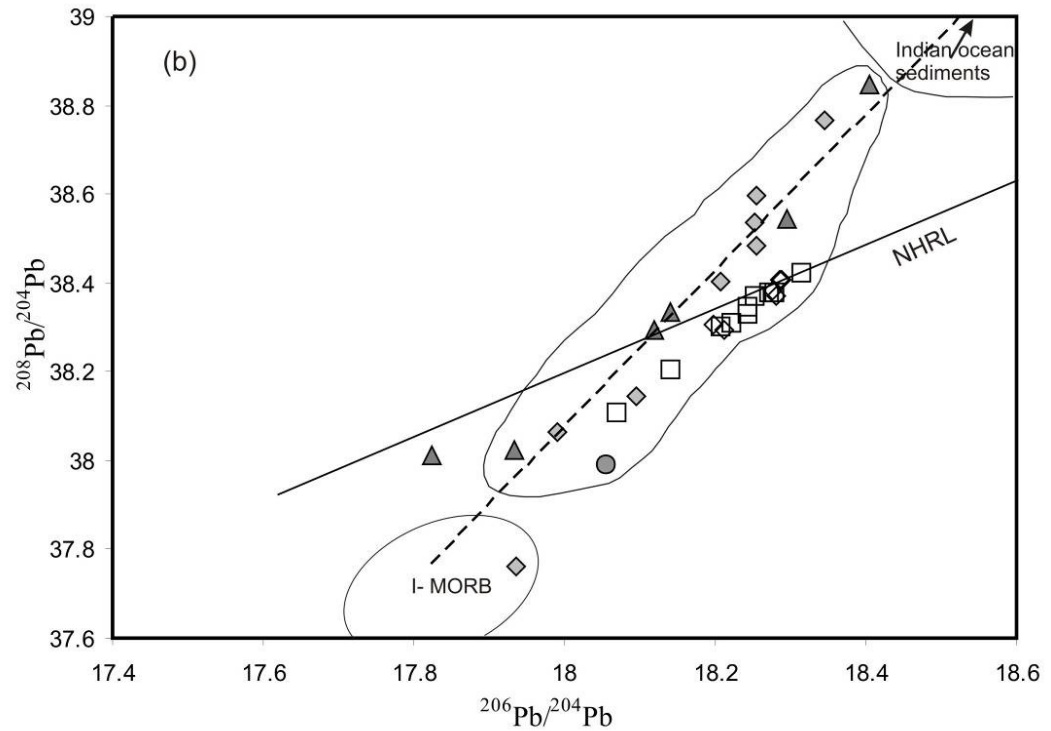
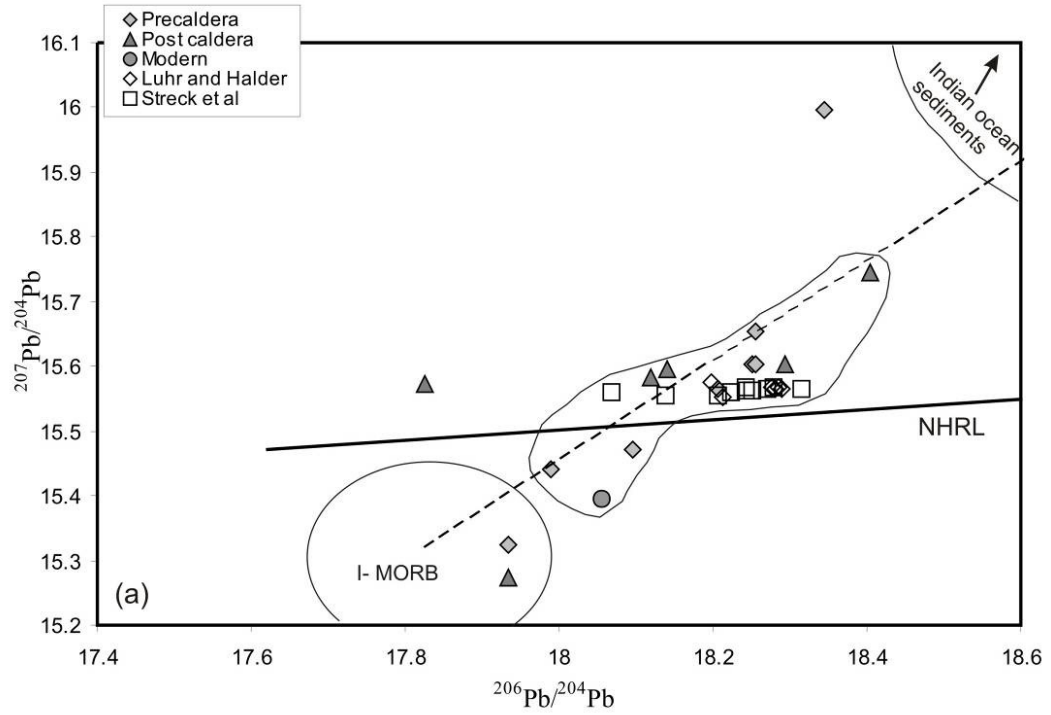


Fig. 6.17 (a) Plot of $^{208}\text{Pb}/^{204}\text{Pb}$ vs. $^{207}\text{Pb}/^{204}\text{Pb}$ (b) Plot of $^{208}\text{Pb}/^{204}\text{Pb}$ vs. $^{207}\text{Pb}/^{204}\text{Pb}$ of Barren Island lavas, NHRL (North Hemisphere Reference Line) after Hart 1984

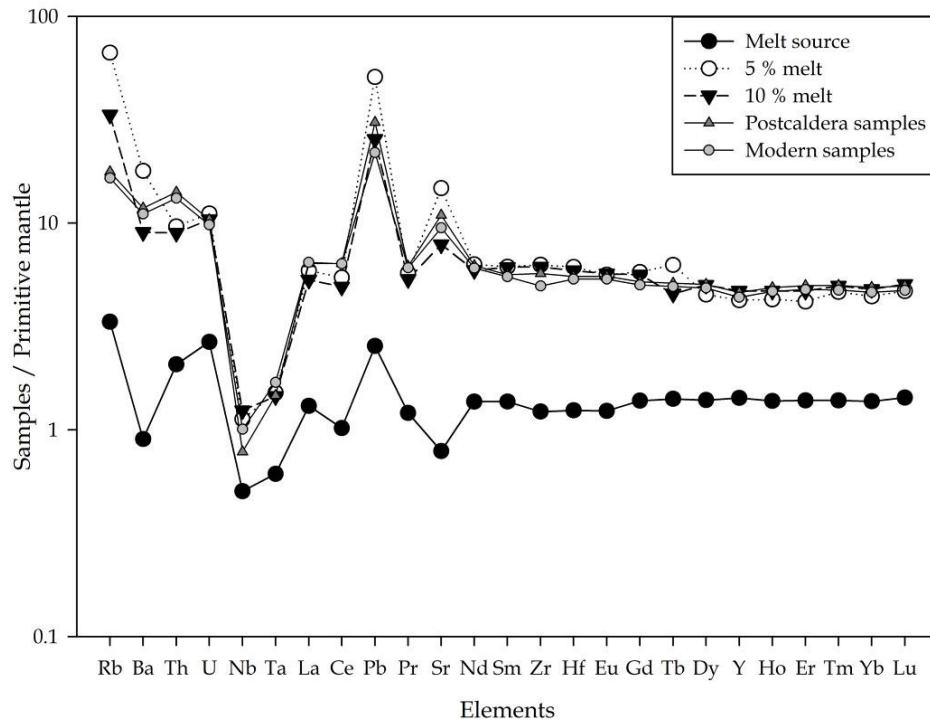
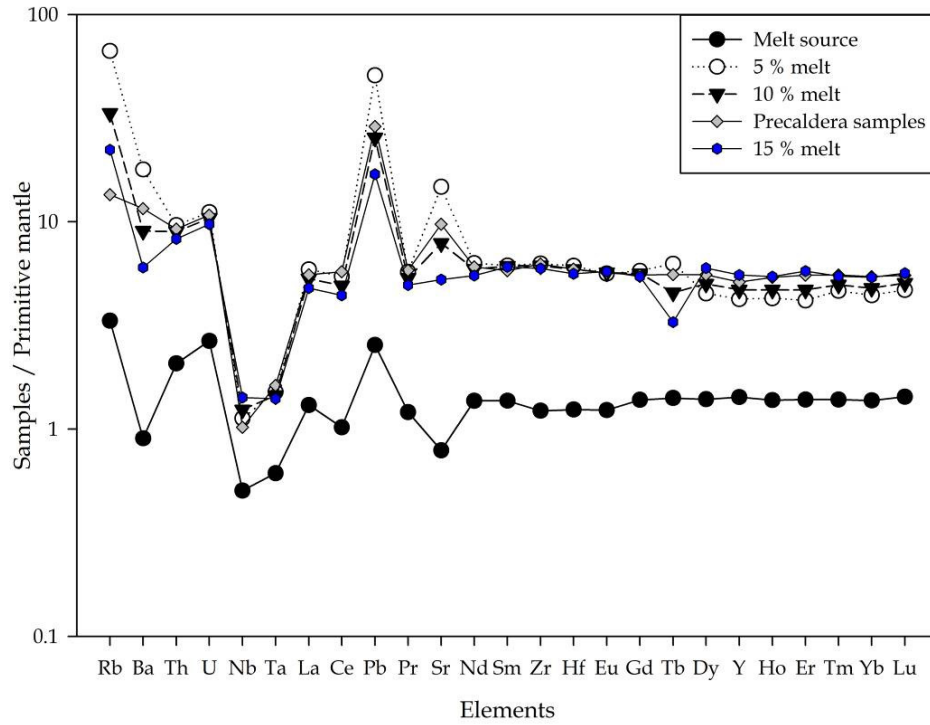


Fig. 6.18 Primitive mantle normalized trace element ratios in Barren Island lavas and its source. Based on melting model, Barren lavas show 5-15 % melting.

present melting model we have consider non batch melting in which primary melt contains 60 % olivine, 20 % orthopyroxene, 14 % clino - pyroxene, 5 % garnet and 1 % amphibole. The melt composition during melting is 10 % olivine, 10 % orthopyroxene, 33 % clinopyroxene, 39 % garnet and 8 % amphibole. The partition coefficient of all the trace elements has been taken from GERM website.

The melting model calculations for trace element abundances suggests that the precaldera lavas of Barren Island are the result of 5 -15 % of melting where as the postcaldera and modern lava produced by 5 -10 % of melting (Fig. 6.18).

Further we have tried to investigate the melting process and depth of melting through modelling of REE fractionation during partial melting. We have considered same source which we have taken for previous melting model. We have taken HREE elements (Yb, Sm, Tb) which can show both the degree/fraction of melting (F) and depth of the melt source. We estimated F using the (Yb/Sm) and (Tb/Yb) variation diagram due to its ability to resolve between F and depth of melting (Turner and Foden, 2001) because these ratios of the heavy rare earth elements (HREE) are sensitive indicator of garnet in the source and can be utilized to determine the depth of melting. Using forward modelling of mantle melting; we calculated several melting curves taking 90% mantle peridotite, 8 % Altered Oceanic Crust (AOC) and 2 % subducted sediments as a starting mantle composition (Fig. 6.19). This melting model program calculates the trace element contents of melts produced by partial melting during passive upwelling of the mantle. The path of mantle parcels through the melting zone is assumed to be governed by simple corner flow. Melting proceeds by incremental non-modal batch equilibrium melting (Shaw,

1970). The melting reaction depends on the mineral assemblage present in the parental source and also the composition in the melt.

In a plot of $(Yb/Sm)_n$ versus $(Tb/Yb)_n$ (Fig. 6.19) partial melts from mantle lherzolites occupy positions depending on the depth (and therefore, source composition - ratio of garnet to spinel in the source) and fraction of melting. The combined data from BI lavas lie close to melting path with 20-50 % of garnet in there sources. Based on garnet composition.

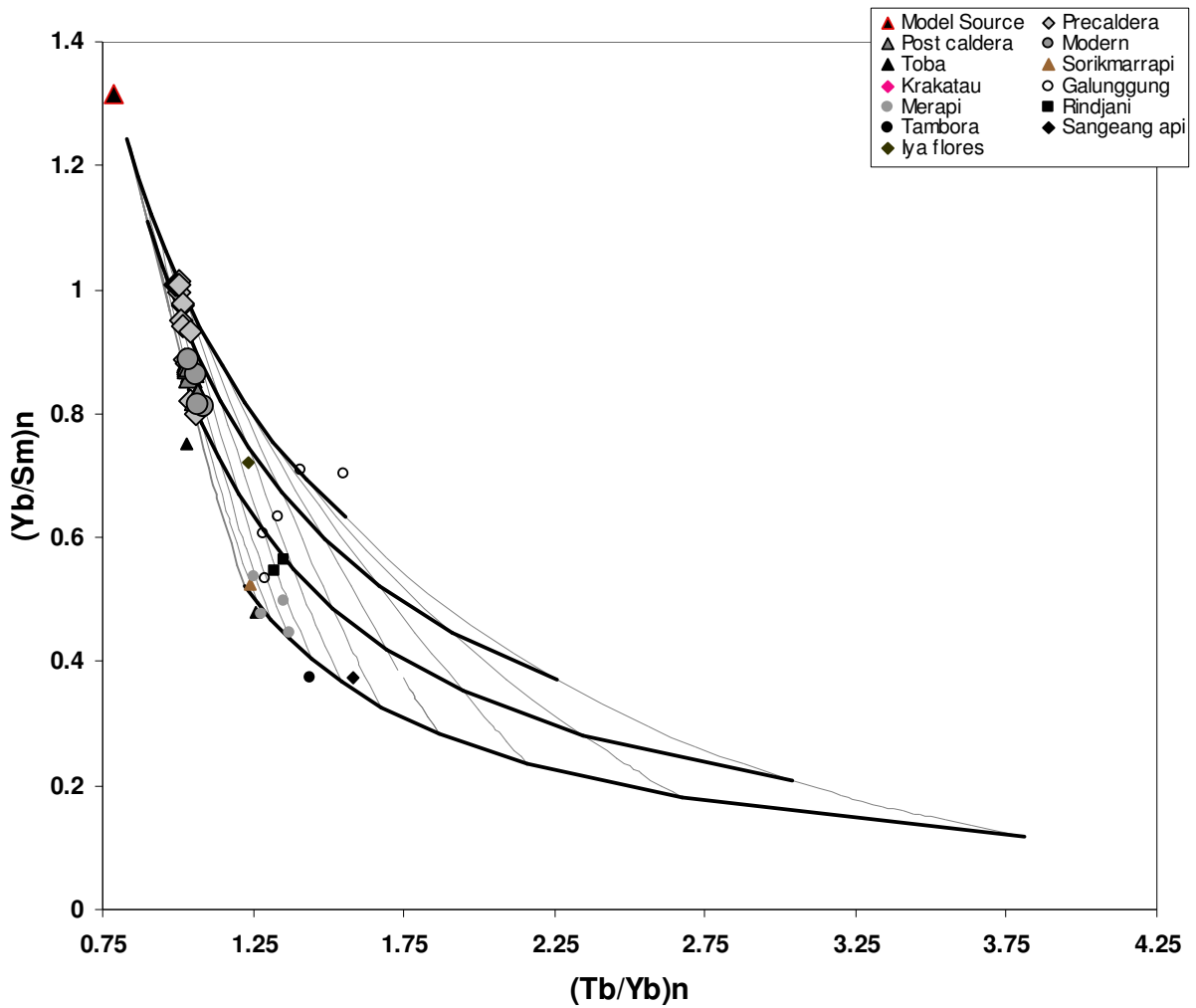


Fig 6.19 Melting model for Barren Island lavas and Indonesian arc lavas (Turner and Foden, 2001) have been plotted for comparison

in BI lavas represent 5-15 % of partial melting of a model source for precaldera lavas and 5 -10 % of postcaldera and modern lavas. These observations suggest that the BI lavas have derived from much deeper regions of the mantle wedge. Thus, a safe conclusion would be that a portion of the BI lavas may have been derived from garnet lherzolites at depths more than 100 km.

This page left blank intentionally

Chapter 7

Summary and Conclusions

Study of subduction zone is very active field of research because it is known as our planet's largest recycling system. The subducting slab deliver raw materials such as oceanic lithosphere along with oceanic sediments and Sea water to the subduction factory, where these raw materials reequilibrate with ambient mantle, triggering melting and incidentally crating continental crust on the overriding plate. In this context, the present study is an attempt to understand the processes which occurring in these zones. Towards this, we selected Andaman Subduction Zone (ASZ) for such a study that is home, being young subduction zone in the globe, which has all the morphological features which has expected in intra oceanic convergent margin recognized as good potential to understand different processes at very initial stages of chemical modifications resulting form mixing with crustal materials derived for the slab. Additional the interesting features which have attracted our attention to scientific investigations towards this zone; 1) it has one of the youngest arc volcanoes of the world called Barren Island. This has not received much attention from the international community except for the volcano watch groups. Most of the research carried out in this island is by Indian geoscientists, primarily of the Geological Survey of India, and is a very few available in the standard peer-reviewed literature, which has kept the visibility of this active volcano quite low internationally. 2) a special type of geological feature which occur in these zone known as 'Mud Volcanoes' bring materials from subducting slab can throw some light on the chemistry of subducting materials and their influence on arc volcanism which are not yet fully understood in spite of various studies on subduction zone related features.

To find answers to these above questions petrological and geochemical approach through the use of major, trace, stable and radiogenic isotopic ratios in fluid and rock samples were taken. With the help of trace element concentrations and isotopic ratios several modelling has been done in present thesis work. The major conclusions of this study are listed below. The answer to the major objectives of thesis and other inferences achieved are summarized below:

1. Mud volcanoes are excellent features which serve as a window to subducting slab and provide to understand the chemical composition of subducting slab. The erupted materials of these volcanoes also help to establish various subduction zone processes which occur at shallow depth. Through our geochemical and isotopic studies on mud volcanoes of Andamans, for the first time, we have able to characterize the chemistry of the subducting sediments at the Andaman subduction zone. The results reveal; it is the products of altered I-MORB and BOB sediments in which major contributions is from altered I-MORB. Apart from these, this work also has revealed many fascinating aspects of subduction zone processes such a dehydration of clays and decomposition of organic matter etc. at various depths in forearc.
2. Comparative studies of trace elements patterns of mud breccia with red clay suggest that one of the sources of mud breccia may be red clay which is transported from Indonesian archipelago.
3. Geochemical and isotopic studies data from Andaman Ophiolites group of rocks mimic that most of their rocks were derived from boninite parental magma. Some of the samples are also related to

Island arc magma which confirms its origin of supra subduction zone environment.

4. Volcanological studies on Barren Island reveal, it is a young and growing, mafic, island arc volcano in the Andaman Sea. Recent eruptions produced aa and blocky aa lava flows of basalt and basaltic andesite, along with tephra. We, for the first time have reported toothpaste lavas, which are very rare in arc volcanoes, on BI. In the absence of absolute chronology, we grouped the volcanics on BI into three categories based on their relative chronology with respect to the caldera forming event in to pre-caldera, post-caldera, modern.
5. Normalized trace elements patterns of BI lavas suggest that it has typical characteristics of arc volcanics, such as negative Nb and Ti and positive K, Ba and Pb spikes with lesser enrichments of Sr.
6. Major and trace elements are excellent tracers to identify the fractional crystallization. The results from trace and major elements reveal that the precaldern lavas of BI controlled by fractional crystallization of olivine and plagioclase en route to the surface while postcaldera and modern lavas show of magma mixing in the magma chamber prior to eruption.
7. Trace elements along with Nd isotopic ratios are very useful to quantify the contributions from the subducting slab in the lavas. Based on variations of fluid mobile elements (Ba, Ce) and particulate proffered trace element (Th) coupled with Nd isotopic ratios we have established the lavas of BI have contribution from fluids as well as sediments from the subducted Indian plate. Most of the precaldern

samples are affected by fluids and modern and postcaldera samples are influenced by sediments suggest during the initial phases of the volcano was least affected by slab. Comparative studies of BI lavas with all the arc lavas from Indonesia suggest that the former lavas appeared to have low contributions from slab derived materials, making them the most primitive amongst all the volcanoes in this arc.

8. The Mixing models which used in present study reveal that the parental magmas for BI lavas have had 10-20 % contributions from slab components (fluid as well as sediments). Our observations also suggest precaldera lavas are more primitive in nature that has higher contribution from oceanic altered crust with compare to sediments whereas the postcaldera and modern lavas have higher contribution from sediments
9. Our preferred model concurs with the idea of a zone of melt formation with degree of partial melting Known as melting model based on partitioning of HREE. This model suggests that magmas for BI lavas are derived from an I-MORB type of source by 5-10 % of partial melting. BI lavas lies close to melting paths with 20 - 40 % of garnet which indicate BI lavas may have derived from garnet lherzolites at depths more then 80 km.

Scope for future work

Recommendations regarding possible future work that could be undertaken in continuation of the present study are:

1. Ophiolites are considered to be important tools for understanding the tectonic and magmatic processes responsible for the formation of oceanic lithosphere. The tectonic setting of Andaman ophiolites is still in

debate so the lithological and chemical signatures (trace couple with isotopic) of Andaman ophiolites and their mantle section can provide further insights into the tectonic setting where the ophiolitic complexes formed.

2. In the absence of absolute age of BI volcano it is difficult to constrain the temporal changes in the BI lavas, so the geochronological attempts (U-Th dating, Ar-Ar dating) should be made to date volcanism on BI.
3. It has been observed that subducted sediments affected the mantle wedge beneath the Barren island volcano. In the connection Li isotopes are known as good tracer because the $\delta^7\text{Li}$ of altered oceanic crust is much higher at a given Li/Y compared to the mantle. The study along with measured Pb isotope systems which have elevated values with compare to mafic crust and mantle, will allow multiple source components to be resolved.
4. In present study, our focus was mainly on Barren Island volcano; there is one more dormant subaerially exposed arc volcano in Andaman Sea known as Narcondam. It is believed that the lavas of this volcano suffered crustal contamination. So, the details study of lavas of this volcano should give clues to understand the affect crustal interference and also its effect of fractional crystallization of the lava flows. This will give to understand chemical evolution of lava in Andaman subduction zone.

This page left blank intentionally

References

- Acharyya, S.K. (2007) Collisional emplacement history of the Naga-Andaman ophiolites and the position of the eastern Indian suture. *Journal of Asian Earth Sciences*, **29**, 239-242.
- Acharyya, S. K., Ray K. K., Roy D. K. (1989) Tectono-stratigraphy and emplacement history of the ophiolite assemblage from the Naga Hills and Andaman island arc, India. *J. Geol. Soc. India*, **33**, 4-18.
- Acharyya S. K., Ray K. K., Sengupta S. (1990) Tectonics of the ophiolite belt from Naga Hills and Andaman Islands, India. *Proc. Indian Acad.Sci. (Earth Planet. Sci.)* **99**, 187-199.
- Achyuthan, H., Eastoe, C. (1999) Mineralogy and isotopic composition of pyrites-bearing ejects from a mud volcano, Baratang, Andaman islands, *J. Geol. Soc. India*, **53**, 329-334.
- Alam M. A., Chandrasekharam D., Vaselli O., Capaccioni B., Manetti P., Santo P. B. (2004) Petrology of the prehistoric lavas and dyke of the Barren Island, Andaman Sea, Indian Ocean. In: Sheth HC, Pande K (eds) *Magmatism in India through time*. *Proc Ind Acad Sci (Earth Planet Sci)* **113**, 715-721.
- Allen S. R. (2005) Complex spatter- and pumice-rich deposits from an andesitic caldera-forming eruption: the Siwi pyroclastic sequence, Tanna, Vanuatu. *Bull volcanol* **67**, 27-41.
- Allen R., Carter A., Najman Y., Bandopadhyay P. C., Chapman H. J., Bickle M. J., Garzanti E., Vezzoli G., Andò, S., Foster G. L., Gerring C. (2007) New constraints on the sedimentation and uplift history of the Andaman-Nicobar accretionary prism, South Andaman Island. In: Draut A, Clift PD, Scholl DW (eds) *Formation and applications of the sedimentary record in arc collision zones*. *Geol Soc Am Spec Pap* **436**, 223-254A.
- Anderson S. W., Stofan E. R., Smrekar S. E., Guest J. E., Wood B. (1999) Pulsed inflation of pahoehoe lava flows: implications for flood basalt emplacement. *Earth Planet Sci Lett* **168**, 7-18.
- Awasthi N., Ray J. S., Laskar A. H. , Kumar A., Sudhakar M., Bhutani R. , Sheth H. C., Yadava M. G. (2010) Major ash eruptions of Barren Island volcano (Andaman Sea) during the past 72 kyr: clues from a sediment core record, *Bull Volcanol*, **72**: 1131-1136.

- Badve, R. M., M. A. Ghare, and C. Rajshekhkar, (1984) On the age of the ejected material from the mud volcano of Baratang Island, Andaman, *Curr. Sci.*, **53**, 814-816.
- Ball, V. (1870) Notes on the geology of the vicinity of Port Blair, Andaman Islands. *Journal Asiatic Society of Bengal* **39**, 231-239.
- Ball V., (1888) The volcanoes of Barren and Narcondam Island in the Bay of Bengal. *Geol Mag* **404**.
- Ball, V. (1893) The volcanoes of Barren and Narcondam islands in the Bay of Bengal. *Geological Magazine*, **289**.
- Banerjee, B., Subba Rao. P. B. V., Gupta, G., Joseph, E. J. and Singh, B. P. (1998) Results from a magnetic survey and geomagnetic depth sounding in the post-eruption phase of the Barren Island volcano. *Earth Planets Space* **50**, 327-338.
- Banerjee, D. (2010) Thermoluminescence and optically stimulated luminescence signals from volcanic ash: History of volcanism in Barren Island, Andaman Sea, *Quaternary Geochronology*, **1-4** doi:10.1016/j.quageo.2009.01.011.
- Bhattacharya, A., Reddy, C. S. S., Srivastav, S. K. (1993) Remote sensing for active volcano monitoring in Barren Island, India. *Photogrammetric Engineering and Remote Sensing* **59(8)**, 1293-1297.
- Bhoothalingam, S. (1972) *Techno-economic survey of Andaman and Nicobar Islands* National Council of Applied Economic Research New Delhi, 1-131.
- Bilham, R., Engdahl, R., Feldl, N. And Satyabala, S. P. (2005) Partial and Complete Rupture of the Indo-Andaman Plate Boundary 1847-2004. *Seismological Research Letters* **76(3)**, 299-311.
- Bischoff, J. L., Heath, G. R., Leinen, M., (1979) Geochemistry of deep-sea sediments from the Pacific Manganese Nodule Province. DOMES sites A, B and C. In: J.L. Bischoff and D.Z. Piper (Editors), *Marine Geology and Oceanography of the Pacific Manganese Nodule Province*, Plenum, New York, N.Y., 397-436.
- Bostrom, K., Kraemer, T. , Gartner, S., (1973) Province and accumulation rates of opaline silica, Al, Ti, Fe, Mn, Cu, Ni and Co in Pacific pelagic sediments. *Chem. Geol.*, **11**, 128-148.

- Brown, G., Brindley G. W. (1980) X-ray diffraction procedures for clay mineral identification. *In* G.W. Brindley and G. Brown (ed.) *Crystal structures of clay minerals and their X-ray identification*. Mineral. Soc. Monogr. 5. Mineralogical Society, London, 305–359.
- Brown K. M., Saler D. M., Bekins B. A., (2001) Smectite diagenesis, pore-water freshening, and fluid flow at the toe of the Nankai wedge, *Earth Planet. Sci. Lett.* **194** 97-109.
- Cameron E. N. (1975) Postcumulus and subsolidus equilibration of chromite and coexisting silicates in the eastern Bushveld Complex. *Geochim Cosmochim Acta* **39**, 1021-1033
- Cawood, P. A., Kröner, A., Collins, W.J., Kusky, T.M., Mooney, W.D., and Windley, B.F., (2009) Accretionary orogens through Earth history in : Cawood, P.A. and Kröner, A. (Eds.), *Earth Accretionary Systems in Space and Time*, Geological Society of London Special Publication **318**, 1-36.
- Chakraborty, P. P., Pal, T. (2001) Anatomy of a fore-arc submarine fan: Upper Eocene–Oligocene Andaman Flysch Group, Andaman Islands, India. *Gondwana Research*, **4**, 477–486.
- Chandrasekharam, D., Santo, A. P., Cappaccioni, B., Vaselli, O., Alam, M. A., Manetti, P., Tassi, F., (2009) Volcanological and petrological evolution of Barren Island (Andaman Sea, Indian Ocean). *J. Asian Earth Sci.* **35**, 469–487.
- Chandrasekharam D., Vaselli O., Capaccioni B., Manetti P., Alam M. A. (2003) Cold springs of the Barren Island, Andaman Sea, Indian Ocean. *Current Science* **85**, 136–137.
- Chester, R. and Aston, S. R., (1976) The geochemistry of deep sea sediments. *In*: J.P. Riley and R. Chester (Editors), *Chemical Oceanography*, **6**, Academic Press, New York, N.Y., 281-383.
- Chough S. K., Sohn Y. K. (1990) Depositional mechanics and sequences of base surges, Songaksan tuff ring, Cheju Island, Korea. *Sedimentology* **37**, 1115–1135.
- Cloos, M., (1993) Lithosphere buoyancy and collisional orogenesis: Subduction of oceanic plateaus, continental margins, island arcs, spreading ridges, and seamounts: *Geological Society of America Bulletin*, v. **105**, 715–737.

- Cochran, J. R. (2010) Morphology and tectonics of the Andaman Forearc, northeastern Indian Ocean, *Geophys. J. Int.* (2010) **182**, 631–651.
- Cole J. W., Milner D. M., Spinks K. D. (2005) Calderas and caldera structures: a review. *Earth-Sci Rev* **69**, 1–26.
- Coleman, R.G., (1977) *Ophiolites*: New York, Springer- Verlag , 220 p.
- Coleman, R. G. and Peterman, Z. E. (1975) Oceanic plagiogranites, *J. Geophys. Res.*, **80**, 1099–1108.
- Coish R. A., Church W. R. (1979) Igneous geochemistry of mafic rocks in the Betts Cove Ophiolite, Newfoundland, *Contrib Mineral Petrol* **70**, 29–39.
- Coish R. A., Gardner P. (2004) Suprasubduction-zone peridotite in the northern USA Appalachians: evidence from mineral composition *Mineral Mag* **68**, 699–708.
- Condie K. C., (1997) *Plate tectonics and crustal evolution*: Fourth edition, Butterworth-Heinemann, ISBN 0750633867, pp. 282
- Conrad C. P. , Bertelloni C. L. (2002) How Mantle Slabs Drive Plate Tectonics, *Science*, **298 (5591)**, 207-209.
- Cox, K. G., Bell, J. D., Pankhurst, R. J. (1979) *The Interpretation of Igneous Rocks*. London: Allan and Unwin 450 p.
- Curry, J. R., Moore, D.G., (1974) Sedimentary and tectonic processes in Bengal deep-sea fan and geosyncline. In: Burk, C.A., Drake, C.L. (Eds.), *The Geology of Continental Margins*. Springer, New York, 617–628.
- Curry, J. R. (2005) Tectonics and history of the Andaman Sea region. *J. Asian Earth Sci.* **25**, 187-232.
- Curry, J. R. , Emmel, F. J. , Moore, D. G., Raitt, R. W., (1982) Structure, tectonics and geological history of the northeastern Indian Ocean. In: Nairn, A.E.M., Stehli, F.G. (Eds.), *The Ocean Basins and Margins. The Indian Ocean*, **6**. Plenum Press, New York, 399–450.
- Curry, J. R., Moore, D. G., Lawver, L. A., Emmel, F. J., Raitt, R. W., Henry, M., Kieckhefer, R., (1979) Tectonics of the Andaman Sea and Burma, in *Geological and Geophysical Investigations of Continental*

Margins, eds Watkins, J.S., Montadert, L. & Dickerson, P.W., Amer. Assoc. Petrol. Geol. Memoir **29**, 189–198.

Dahlmann A., Lange G. J. de (2003) Fluid-sediment interactions at Eastern Mediterranean mud volcanoes: a stable isotope study from ODP Leg 160, Earth and Planetary Science Letters **212**, 377-391.

Dasgupta S., Mukhopadhyay M. (1993) Seismicity and plate deformation below the Andaman arc, northeastern Indian Ocean, Tectonophysics **225(4)**, 539-542.

Decker R. W., Christiansen R. L. (1984) Explosive eruption of Kilauea Volcano, Hawaii. In: National Research Council (ed) Explosive inception, evolution, and hazards (Studies in Geophysics). Nat Acad Press, Washington DC, 122-132.

DePaolo, D. J., Wasserburg, G. J. (1976) Nd isotopic variation and petrogenetic models, Geophysical Resea. Lett. **3**, 249-52.

Derry L. A., France-Lanord C. (1996) Neogene Himalayan weathering history and river $^{87}\text{Sr}/^{86}\text{Sr}$: Impact on the marine Sr record, Earth Planet. Sci. Letts. , **142**, 59-76.

Dewey, J. F., and Bird, J. M., (1971) The origin and emplacement of the ophiolite suite: Appalachian ophiolites in Newfoundland: Journal of Geophysical Research, **76**, 3179–3206, doi: 1029/JB076i014p03179.

Dick, H. J .B., Bullen, T. (1984) Chromium spinel as petrogenetic indicator in abyssal and alpine-type peridotites and spatially associated lavas. Contributions to Mineralogy and Petrology, **86**, 54–76.

Dick, H. J. B., Fisher, R. L. (1984) Mineralogical studies of the residues of mantle melting: abyssal and alpine-type peridotites. In: Kornprobst, J. (ed.) Kimberlites II: the Mantle and Crust-Mantle Relationship. Elsevier, Amsterdam, 295–303.

Dilek, Y., (2003) Ophiolite concept and its evolution, in Dilek, Y., and Newcomb, S., eds., Ophiolite Concept and the Evolution of Geological Thought: Geological Society of America Special Paper **373**, 1–16.

Dilek Y., Furnes H., (2011) Ophiolite genesis and global tectonics: Geochemical and tectonic fingerprinting of ancient oceanic lithosphere GSA Bulletin **123(3-4)**, 387–411.

- Dimitrov, L. I., (2002) Mud volcanoes – the most important pathway for degassing deeply buried sediments. *Earth Science Reviews* **59**, 49–76.
- Dixon, S., Rutherford, M. J., (1979) Plagiogranite as late-stage immiscible liquids in ophiolite and mid-ocean ridge suites; an experimental study, *Earth Planet. Sci. Lett.*, **45**, 45–60.
- Duncan A. M., Guest J. E. , Stofan E. R., Anderson S. W., Pinkerton H., Calvari S. (2004) Development of tumuli in the medial portion of the 1983 aa flow field, Mount Etna, Sicily. *J Volcanol Geotherm Res* **132**, 173–187.
- Ellam, R. M., Hawkesworth, C. J. (1988) Elemental and isotopic variations in subduction related basalts: evidence for a three component model. *Contributions to Mineralogy and Petrology* **98**, 72-80.
- ElWakeel, S. K. and Riley, I. P., (1961) Chemistry and mineralogical studies of deep sea sediments. *Geochim. Cosmochim. Acta.* **25**, 110-146.
- Flanagan F.J. (1976) Introduction to descriptions and analyses of eight new U.S.G.S. rock standards. U.S. Geological Survey Professional Paper **840**, 1-5.
- Gao S., Liu X. M., Yuan H. L., Hattendorf B., Gunther D., Chen L., Hu S. H. (2002) Determination of forty two major and trace elements in USGS and NIST SRM glasses by laser ablation-inductively coupled plasma-mass spectrometry, *Geostand. Newsl.* **26**, 181–196.
- Gass, I. G. (1990) Ophiolites and oceanic lithospheres. In: Malpas, J., Moores, E.M., Panayiotou, A. & Xenophontos, C. (eds) *Ophiolites: Oceanic Crustal Analogues. Proceedings of the Symposium, 'Troodos 1987'*. Geological Survey Department, Nicosia, 1–10.
- Gonfiantini, R., (1981) The d-notation and the mass-spectrometric measurement techniques, in *Stable Isotope Hydrology: Deuterium and Oxygen-18 in the Water Cycle*, edited by J. R. Gat and R. Gonfiantini, **35 - 84**, International Atomic Energy Agency, Vienna.
- Guest J. E., Stofan E. R. (2005) The significance of slab-crusted lava flows for understanding controls on flow emplacement at Mount Etna, Sicily. *J Volcanol Geotherm Res* **142**, 193–205.
- Hager B. H. (1984) Subducted Slabs and the Geoid: Constraints on Mantle Rheology and Flow *Jour. Of Geoph Rea.*, **89(B7)**, 6003-6015.

- Haldar D. (1989) Petrology and chemistry of recent volcanics of Barren and Narcondam islands—the only two recent volcanoes in India. *Rec Geol Surv Ind* **122(3)**, 48–49
- Haldar, D. (1991) Petrochemical studies of Barren and Narcondam islands - the only two recent volcanoes in India. *Asiatic Society Journal*, September 1991, 1-2.
- Haldar D., Chakraborty S. C., Sarkar N. K. (1994) The 1991 eruption of the Barren Island volcano in the Andaman Sea, India; an example of arc volcanism. IAVCEI Gen Assembly, Ankara Abstract
- Haldar D, Chakraborty S. C., Chakraborty P. P. (1999) The 1994–1995 eruption of the Barren Island volcano in the Andaman Sea, India: a resurgent volcanism. *Gond Geol Mag Spl* **4**, 371–384.
- Haldar D., Luhr J. F. (2003) The Barren Island volcanism during 1991 and 1994–95: eruptive style and lava petrology. *Geol Soc Ind Mem* **52**, 313–338.
- Haldar D., Lasker T., Bandyopadhyay P. C., Sarkar N. K. , Biswas J. K. (1992a) A short account of the on-going eruption of the Barren Island volcano. *Rec Geol Surv Ind* **125(3)** 87–96.
- Haldar, D., Laskar, T., Bandyopadhyay, P.C., Sarkar, N. K. and Biswas, J. K. (1992b) A note on the recent eruption of the Barren Island volcano. *India Minerals* **46**, 77-88.
- Haldar, D., Laskar, T., Bandyopadhyay, P. C., Sarkar, N. K. and Biswas, J. K. (1992c) A short account of the on-going eruption of the Barren Island Volcano. *Records of Geological Survey of India* **125**, 87-96.
- Hamilton, W. (1979) Tectonics of the Indonesian Region. U. S. Geological Survey Professional Paper **1078**, 345 pp.
- Hamilton, W.B. (1988) Plate tectonics and island arcs, *GSA Bulletin* **100 (10)**, 1503–1527.
- Hamilton, W.B., (1998) Archean magmatism and deformation were not products of plate tectonics: *Precambrian Research*, **91**, 143–179.
- Hamilton W. H., Myers W. B. (1963) Menan Buttes, cones of glassy basalt tuff in the Snake River Plain, Idaho. *Geological Survey research 1962. US Geol Surv Prof Pap* **450-E**, 114–118.

- Hansen, V. L. (2007). "Subduction origin on early Earth: A hypothesis". *Geology* **35** (12), 1059-1062.
- Helfer (1840) Notice of the Mergui Archipelago along with the new coal-field of Tenasserim, Dr. Buist, Catalogue **165**, 638.
- Herron M. M. (1988) geochemical classification of terrigenous sands and shales from core or log data, *Jour. of Sed. Pet.*, **30**, 841-883.
- Hart, S. R., Erlank, A. J., Kable, E. J. D. (1974) Sea floor basalt alteration: some chemical and Sr isotopic effects. *Contributions to Mineralogy and Petrology* **44**, 219-230.
- Hawkesworth, C. J., Gallagher K., Hergt J. M., McDermott, F., (1993) Mantle and slab contribution in arc magma *Ann. Rev. Earth Planet Sci.*, **21**, 175-204
- Hobday J. R., Mallet F. R. (1885) The volcanoes of Barren and Narcondam Islands in the Bay of Bengal. *Mem Geol Surv Ind* **21**, 251-286.
- Hochstetter, F. (1869) Geology and physical geography of Nicobar Islands. *Records Geological Survey of India* **2** (Pt 3).
- Jafar S. A. (1985) Discovery of mixed coccoliths from Mud Volcanoes of Baratang Island, Andaman. *India. Curr. Sci.* **54** (4), 170-173.
- Jafar, S. A., mainali, U. C., Singh, O. P. (1989a) Late Cretaceous Paleogene coccolith-cocktail exuded from the mud volcano of Baratang Island, Andaman and Nicobar Islands, India, *International Nanoplakton Association Newsletter*, **11**(2), 66-68.
- Jarrard, R. D. (2003) Subduction fluxes of water, carbon dioxide, chlorine, and potassium, *Geochem. Geophys. Geosyst.*, **4**(5), 8905, doi: 10.1029/ 2002GC000392.
- Johnson, M. C., J. A. T. Anderson, M. J. Rutherford, (1994) Pre-eruptive volatile contents of magmas, in *Volatiles in Magmas*, *Rev. Mineral.*, **30**, edited by M. R. Carroll and J. R. Holloway, 281-330.
- Kamesh Raju K. A., Ramprasad T., Rao P. S., Rao B. R., Varghese J. (2004) New insights into the tectonic evolution of the Andaman Basin, northeast Indian Ocean. *Earth Planet Sci Lett*, **221**, 145-162.
- Karig, D. E., Suparka, S., Moore, G. F., Hehanussa, P. E. (1979) Structure and Cenozoic evolution of the Sunda arc in the Central Sumatra Region. In *Geological and geophysical investigations of continental*

margins (eds J. S. Watkins, L. Montadert and P. W. Dickerson), **29** 223–237, American Association of Petroleum Geologists.

Karunakaran, C., Ray, K. K., Saha, S. S., (1968) Tertiary sedimentation in the Andaman– Nicobar geosyncline. *Jour Geo Soc India* **9**, 32–39.

Kessel, R., Schmidt, M. W., Ulmer, P., Pettke, T. (2005) Trace element signature of subduction-zone fluids, melts and supercritical liquids at 120–180 km depth. *Nature* **437**, 724–727.

Kastner M., Elderfield H., Martin J. B., (1991) Fluids in convergent margins: what do we know about their composition, origin, role in diagenesis and importance for oceanic chemical fluxes, *Philos. Trans. R. Soc. London* **A335** 243–259.

Kent A. J. R., Jacobsen B., Peate D. W., Waight T. E. and Baker J. A. (2004) isotope dilution MC-ICPMS–Ms Rare Earth Element analysis of Geochemical Reference Materials NIST SRM 610, NIST SRM 612, NIST SRM 614, BHVO-2G, BHVO-2, BCR-2G, JB-2, WS-E, W-2, AGV-1 and AGV-2, *Geostand. Geoanalyt. Res.* **28 (3)**, 417–429.

Khan P. K., Chakraborty P. P. (2005) Two-phase opening of the Andaman Sea: a new seismotectonic insight. *Earth Planet Sci Lett* **229**, 259–271.

Kimura, J. I., Kent A. J. R., Rowe M. C., Katakuse M., Nakano F., Hacker B. R., Keken P. E., Kawabata H., Stren R. J. (2010) Origin of cross- chin geochemical variation in quaternary lavas from the northern Izu arc: Using a quantitative mass approach to identify mantle sources and mantle wedge processes, *Geoche. Geophys. Geosys.* **11(10)**, 1–24.

Kopf, A. J. (2002) Significance of mud volcanism, *Rev. Geophys.*, **40**, B1–B49.

Kumar N. A., Ashalatha B., Sinha B., Thakur N. K. (2008) Estimates of geothermal gradients from bottom simulating reflectors, *Current Science*, **95 (10)**, 1463–67.

La Bas M. J., Le maitre R. W., Streckeisen A., Zanettin B. (1986) A chemical classification of volcanic rocks based on the total alkali silica diagram, *Journal of Petrology* **27**, 745–750.

Lagabrielle, Y., Guivel, C., Maury, R., Bourgois, J., Fourcade, S., Martin, H., (2000) Magmatic-tectonic effects of high thermal regime at the site of active ridge subduction: The Chile triple junction model: *Tectonophysics*, **326**, 255–268.

- Leys C. A. (1983) Volcanic and sedimentary processes during formation of the Sæfell tuff-ring, Iceland, *Trans Roy Soc Edinburgh: Earth Sci* **74**, 15-22.
- Ling, H. Y., V. Sharma, S. Singh, D. Mazumdar, and A. K. Mahapatra, (1995) Cretaceous and middle Eocene radiolaria from ejected sediments of mud volcanos of Baratang Island in Andaman Sea of the northeastern Indian Ocean, *J. Geol. Soc. India*, **45**, 463-469.
- Lodato L., Spampinato L., Harris A., Calvari S., Dehn J., Patrick M. (2007) The morphology and evolution of the Stromboli 2002- 2003 lava flow field: an example of a basaltic flow field emplaced on a steep slope. *Bull Volcanol* **69**, 671-679.
- Lowman, J. P. (2011) Mantle convection models featuring plate tectonic behavior: An overview of methods and progress. *Tectonophysics*, **510**, 1-16.
- Luhr J. F., Haldar D. (2006) Barren Island volcano (NE Indian Ocean): island-arc high-alumina basalts produced by troctolite contamination. *J. Volcanol Geotherm Res* **149** 177-212.
- Macdonald G. A., Abbott A. T., Peterson F. L. (1983) *Volcanoes in the sea: The geology of Hawaii*. Univ Hawaii Press, Honolulu, p 517
- Malik J. N., Murty C. V. R., EERI M., and Rai D. C., (2006) Landscape Changes in the Andaman and Nicobar Islands (India) after the December 2004 Great Sumatra Earthquake and Indian Ocean Tsunami Earthquake Spectra, **22(S3)**, S43-S66.
- Mallet, F. R. (1895) Some early allusion to the Barren Island: with a few remarks there on. *Records of Geological Survey of India* **28**, 22-34.
- Mattsson H., Höskuldsson A. (2005) Eruption reconstruction, development of flow-lobe tumuli and eruption duration in the 5900 BP Helgafell lava field (Heimaey), south Iceland. *J Volcanol Geotherm Res* **147**, 157-172.
- Maung, H., (1987) Transcurrent movements in the Burma-Andaman sea region, *Geology* **15**, 911-912.
- Mccourt, W. J., Crow, M. J., Cobbing, E. J. & Amin, T. C. (1996) Mesozoic and Cenozoic plutonic evolution of SE Asia: evidence from Sumatra,

- Indonesia. In Tectonic evolution of SE Asia (eds R. Hall and D. J. Blundell), Geol Soc of London, Spec. Pub. **106**, 321–335.
- McCulloch, M. T., Gamble, J. A. (1991) Geochemical and geodynamical constraints on subduction zone magmatism. *Earth and Planetary Science Letters* **102**, 358-374.
- McLennan, S. M., (1989) Rare earth elements in sedimentary rocks: Influence of provenance and sedimentary processes, In: B. R. Lipin and G. A. Mckay (Editors), *Geochemistry and Mineralogy*, **21**, 169-200.
- McLennan S. M., Nance W. B. and Taylor S. R. (1980) Rare earth element-thorium correlations in sedimentary rocks, and the composition of the continental crust, *Geochim. Cosmochim. Acta*, **44**, 1833-1839.
- McMurtry, G.M. and Yeh, H.W., (1981) Hydrothermal clay mineral formation of East Pacific Rise and Bauer Basin sediments. *Chem. Geol.*, **32**, 189-205.
- Melcher, F., Grum, W., Simon, G., Thathammer, V. T., Stumpfl, E. F. (1997) Petrogenesis of the ophiolitic giant chromite deposits of Kempirsai, Kazakhstan – a case study of solid and fluid inclusion in chromites, *Journal of Petrology*, **38**, 1419–1458.
- Michael G., Hall C., Lavier L. (2004) Evolving force balance during incipient subduction. *Geochemistry Geophysics Geosystems*, **5(7)**, 1-31.
- Mohaney J. J., Natland, J. H., White, W. M., Poreda, R., Bloomer, S. H., Fisher, R. L., Baxter, A. N. (1989) Isotopic and geochemical provinces of the Indian ocean spreading centers. *Jour. Of Geophy. Res.* ,**94**, 4033-4053
- Moore, D. G., Curray, J. R., Emmel, F. J. (1982) Sedimentation in the Sunda Trench and forearc region, Geological Society, London, Special Publications **10**, 245-258.
- Moore J. C., Vrolijk P., (1992) Fluids in accretionary prisms, *Rev. Geophys.* **30** 113-135.
- Mullen, E. D., (1983) MnO/TiO₂/P₂O₅: a minor element discrimination for basaltic rocks of oceanic environments and its implication for petrogenesis. *Earth and Planetary Science Letters*, **62**, 53–62.

- Murray, R. W., Brink, M. R. B., Gerlach, D. C., Russ III, G. P. and Jones, D. L., (1991) Rare earth, major and trace elements in chert from the Franciscan Complex and Monterey Group, California: Assessing REE sources to fine grained marine sediments. *Geochim. Cosmochim. Acta*, **55**, 1875-1895.
- Murray, R. W., Brink, M. R. B., Gerlach, D. C., Russ III, G. P. and Jones, D. L., (1992) Interoceanic variation in the rare earth, major, and trace element deposition chemistry of chert: Perspectives gained from the DSDP and ODP record. *Geochim. Cosmochim. Acta*, **56**, 1892-1913.
- Murray, R. W., Leinen, M., (1993) Chemical transport to the sea floor of the equatorial Pacific Ocean across a latitude transect at 135 ° W: Tracing sedimentary major, trace, and rare earth element fluxes at the Equator and the Intertropical Convergence Zone. *Geochim. Cosmochim. Acta*, **57**, 4141-4163.
- Nakamura K. (1964) Volcano-stratigraphic study of Oshima Volcano, Izu. *Bull Earthquake Res Inst Univ Tokyo* **42**, 649-728.
- Nauret F., Abouchami W., Galer S., Hofmann A.W., Hemond C., Chauvel C., Dymant J., (2006) Correlated trace element Pb isotope enrichment in Indian MORB along 18-20° S, central Indian ridge, Earth and Planetary Science Letters, **245**, 137-152.
- Neuberg J. W. , Tuffen H., Collier L. , Green D. , Powell T. , Dingwell D., (2006). The trigger mechanism of low-frequency earthquakes on Montserrat. *Jour. of Volcano. and Geotherm. Res* **153(1-2)**, 37-50.
- Nicolas, A., (1989) Structure of Ophiolites and Dynamics of Oceanic Lithosphere: Dordrecht, the Netherlands, Kluwer Academic Publishers, 367 p.
- Niu, Y. (2004) Bulk major and trace element compositions of abyssal peridotites: implications for mantle melting, melt extraction and post-melting processes beneath mid-ocean ridges. *Journal of Petrology*, **45**, 2423-2458.
- Niu, Y., Hekinian, R. (1997) Basaltic liquids and harzburgitic residues in the Garrett Transform: a case study at fast spreading ridges. *Earth and Planetary Science Letters*, **146**, 243-258.
- Niu, Y., Michael J. O'Hara, Julian A. P. (2003) Initiation of Subduction Zones as a Consequence of Lateral Compositional Buoyancy

Contrast within the Lithosphere: a Petrological Perspective. *Journal of Petrology*, **44(5)**, 851-866.

- Nohara, M. and Kato, K., (1985) Chemical compositions of pelagic deep-sea sediments its relation to the formation of authigenic mineral phase under the chemical control of sea water. In: N. Nasu et al. (Editors), *Formation of Active Ocean Ridges*. TERRAPUB, Tokyo, 893-912.
- Oldham, R. D. (1885). Notes on the geology of the Andaman island in the neighbourhood of Port Blair. *Rec. Geol. Surv. India*, **18(3)**, 133-145.
- Orange, D. L., Geddes, D. S., Moore, J. C., (1993) Structural and fluid evolution of a young accretionary complex: The Hoh rock assemblage of the western Olympic Peninsula, Washington: *Geological Society of America Bulletin*, **105**, 1053-1075.
- Orberger P., Lorand J. P., Girardeau J., Mercier J. C. C., Pitragool S. (1995) Petrogenesis of ultramafic rocks and associated chromitites in the Nan uttaradit ophiolite, northern Thailand. *Lithos* **35**, 153-182.
- Pal, T. (2011) Petrology and geochemistry of the Andaman ophiolite: melt-rock interaction in a suprasubduction-zone setting. *Jour. of the Geol. Soc., London*, **168**, 1031-1045.
- Pal T., Bandopadhyay P. C., Mitra S. K., Raghav S. (2007a) The 2005 eruption of Barren volcano: an explosive inner arc volcanism in Andaman Sea. *J Geol Soc Ind* **69**, 1195-1202.
- Pal, T., Bhattacharya A., (2010) Greenschist-facies sub-ophiolitic metamorphic rocks of Andaman Islands, Burma-Java subduction complex. *Jour. Asi. Ear. Sci.* **39**, 804-814.
- Pal, T., Chakraborty, P. P., Duttagupta, T. & Singh, C. D. (2003) Geodynamic evolution of an outer arc in convergent margin of active Burma-Java subduction complex, a document from Andaman islands, Bay of Bengal. *Geological Magazine*, **140**, 289-307.
- Pal, T., Duttagupta, T., Chakraborty, P. P. & Dasgupta, S. C. (2005) Pyroclastic deposits of Mio-Pliocene age in the Arakan Yoma-Andaman- Java subduction complex, Andaman Islands, Bay of Bengal, India. *Geochemical Journal*, **39**, 69-82.

- Pal T., Mitra S. K., Sengupta S., Katari A., Bandopadhyay P. C., Bhattacharya A. K. (2007b) Dacite-andesites of Narcondam volcano in the Andaman Sea – an imprint of magma mixing in the inner arc of the Andaman-Java subduction system. *J Volcanol Geotherm Res* **168**, 93–113.
- Pal, T., Raghav, S. R., Bhattacharya A., Bondopadhyay, P.C., Mitra, S. K., Renjit, M. L., Sankar, M. S., Ghosh, B. (2010) The 2005–06 eruption of Barren Volcano, Andaman Sea: evolution of basaltic magmatism in island arc setting of Andaman–Java subduction complex. *Journal of Asian Earth Sciences*, **39**, 12–23.
- Pattan, J. N., Rao Ch. M., Higgs N. C., Colley S., Parthiban, G. (1995) Distribution of major, trace and rare-earth elements in surface sediments of the Wharton Basin, Indian Ocean, *Chemical Geology* **121**, 201-215.
- Paul D. Lowman Jr. (1997) Global Tectonic and volcanic activity of the last one million years NASA/Goddard Space Flight Center (**Code 921**) Greenbelt, Maryland 20771.
- Peacock S. M. (1990) Fluids Processes in Subduction Zones, *Science*, **248**, 329-337.
- Pearce, J. A., Barker, P. E., Edwards, S. J., Parkinson, I. J. & Leat, P. T. (2000) Geochemistry and tectonic significance from the South Sandwich arc-basin system, South Atlantic Contributions to Mineralogy and Petrology, **139**, 36– 53.
- Pearce, J. A., Laan, S. R. V. D., Arculus, R. J., Murton, B. J., Ishii, T., Piaate, D. W., Parkinson, J. J. (1992) Boninite and hartzburgite from leg 125 (Bonin-Mariana forearc): A case study of magma genesis during the initial stages of subduction. *Proc. ODP Sci. Res.* **125**, 623–659.
- Pearce J. A., Lippard S. J., Roberts S. (1984) Characteristics and tectonic significance of supra-subduction zone ophiolites, Geological Society, London, Special Publications, **16**, 77-94
- Peacock S. M. (1990) Fluid processes in subduction zones, *Science* **248**, 329–37.
- Pedersen R. B., Searle M. P., Carter A., Bandopadhyay P.C. (2010) U-Pb zircon age of the Andaman ophiolite: implications for the beginning of subduction beneath the Andaman–Sumatra arc *Jour. of the Geol Soc, London*, **167**, 1105–1112.

- Plank, T., Langmuir, C. H. (1998) The chemical composition of subducting sediments and its consequences for the crust and mantle, *Chemical Geology*, **145**, 325–394.
- Pluijm B. A. V., Marshak S. (2004) *Earth Structure: An Introduction to Structural Geology and Tectonics*, W. W. Norton and company pp.656, ISBN 0-393-92467-X
- Poddar, M. C., (1954) Mud volcanoes of south Baratang Island, *Indian Miner.*, **8(4)**, 251–256.
- Prince R. C., Kennedy, A. K., Riggs-sneeringer, M., frey, F. A. (1986) Geochemistry of basalts from Indian ocean triple junction: implication for the generation & evolution of Indian ocean ridge basalts, *Earth and Planetary Science Letters*, **78**, 397-396.
- Raczek I., Jochum K. P. and Hofmann A. W. (2003) Neodymium and Strontium Isotope Data for USGS Reference Materials BCR-1, BCR-2, BHVO-1, BHVO-2, AGV-1, AGV-2, GSP-1, GSP-2 and Eight MPI-DING Reference Glasses, *Geostand. Newsl.* **27(2)**, 173–179.
- Rajshekhar, C. (1985) Foraminifera from the ejected material of mud volcano, Baratang Island, Andaman, India, *Bull. Geol. Min. Met. Soc. India*, **52**, 147-158.
- Rajshekhar, C. (1989) Foraminiferal evidences for sediments of Santorian age occurring on Baratang Island, Andaman, India, *Journal of the Geological Society of India*, **33**, 19-31.
- Rajshekhar, C. (1992) The genus *Hantkenina* from Baratang island, Andaman, India, *Journal of the Geological Society of India*, **39(6)**, 495-501.
- Reddy, C. S. S., Bhattacharya, A. (1997) Post-Eruption monitoring of Barren Island volcano, Andaman Sea, Bay of Bengal, India, *Geocarto International*, **12:3**, 71-76.
- Raina V. K. (1987) A note on sulphur occurrence in the volcanoes of the Bay of Bengal. *Ind Mineral* **41**, 79–86.
- Rao D. R., Rai H., Kumar J. S. (2004) Origin of oceanic plagiogranite in the Nidar ophiolitic sequence of eastern Ladakh, India, *Current Science* **87(7)**, 999 – 1005.
- Ray, D., Rajan S., Ravindra R., Jana A. (2011) Microtextural and mineral chemical analyses of andesite–dacite from Barren and Narcondam

islands: Evidences for magma mixing and petrological implications, *J. Earth Syst. Sci.* 120(1), 145–155.

Ray, K. K. (1982) A review of the geology of Andaman-Nicobar islands. *Geol. Surv. India, Misc. Pub.*, **41(2)**, 110-125.

Ray, K. K., Sengupta, S., Van Den Hui, H. J. (1988) Chemical characteristics of volcanic rocks of Andaman Ophiolite, India. *Jour. of the Geol. Soc., London*, **145**, 393–400.

Ray, K. K., Sengupta, S., Van Den Hui, H. J. (1987). Unusual composition from the cumulate section of Andaman ophiolite. *J. Geol. Soc. India*, **30**, 249-254.

Ray R., Shukla A. D., Sheth H. C., Ray J. S., Duraiswami R. A., Vanderkluysen L., Rautela C. S., Mallik J. (2008) Highly heterogeneous Precambrian basement under the central Deccan Traps, India: Direct evidence from xenoliths in dykes, *Gond. Res.* **13**, 375-385.

Ringwood, A. E. (1974) The petrological evolution of island arc systems *Journal of the Geological Society, London* **130**, 183-204.

Rink, P. H. (1847) *Die Nikobar Inseln. Eine Geographische Skizze, mitspecieller Beru'ksichtigung der Geognosie, Kopenhagen.* Translated Selections, Records Government India LXXVII, 540.

Robin C., Eissen J. P., Monzier M. (1993) Giant tuff cone and 12-km wide associated caldera at Ambrym volcano (Vanuatu, New Hebrides arc). *J Volcanol Geotherm Res* **55**, 225–238.

Roche O., Druitt T. H., Merle O. (2000) Experimental study of caldera formation. *J Geophys Res* **105B**, 395–416.

Rossi M. J., Gudmundsson A. (1996) The morphology and formation of flow-lobe tumuli on Icelandic shield volcanoes. *J Volcanol Geotherm Res* **72**, 291–308.

Rowland S. K., Walker G. P. L. (1987) Toothpaste lava: characteristics and origin of a lava structural type transitional between pahoehoe and aa. *Bull Volcanol* **49**, 631–641.

Rowland S. K., Walker G. P. L. (1990) Pahoehoe and aa in Hawaii: volumetric flow rate controls the lava structure. *Bull Volcanol* **52**, 615–628.

- Roy, D.K., Acharyya, S.K., Ray, K.K., Lahiri, T.C., Sen, M.K. (1988) Nature of occurrence and depositional environment of the oceanic pelagic sediments associated with the ophiolite assemblage, South Andaman Island. *Indian Minerals*, **42**, 31-56.
- Roy, T. K. (1983) Geology and hydrocarbon prospects of Andaman-Nicobar basin: In: *Petroliferous Basins of India*. Petroleum Asia Jour. KDM, IPE, ONGC, Dehra Dun, India, 37-50.
- Schieber (1992) A Combined petrological - geochemical provenance study of the Newland formation, Mid Proterozoic of Montana, *Geol. Mag.*, **129**, 223-237.
- Segerstrom K. (1950) Erosion studies at Paricutin volcano, State of Michoacan, Mexico. *US Geol Surv Bull* **956-A**, 1-164.
- Segerstrom K. (1966) Paricutin, 1965 – aftermath of eruption. *US Geol Surv Prof Pap* **550-C**, 93-101.
- Sengupta S., Ray K. K., Acharyya S. K., de Smeth J. B. (1990) Nature of ophiolite occurrences along the eastern margin of the Indian plate and their tectonic significance. *Geology*, **8(5)**, 439-442.
- Sewell R. B. S., (1925). A Study of the Nature of the Sea Bed and of the Deep-Sea Deposits of the Andaman Sea and Bay of Bengal , " *Memoirs Asiatic Soc. Bengal*, **9(2)**, 27-50.
- Shanker R., Haldar D., Absar A., Chakraborty S. C. (2001) Pictorial monograph of the Barren Island volcano: the lone active volcano in the Indian subcontinent. *Geol Surv Ind Spec Publ* **67**, 87.
- Shastry A., Srivastava R. K., Chandra R. and Jenner G. A. (2001) Fe-Ti enriched mafic rocks from south Andaman ophiolite suite: implication of late stage liquid immiscibility; *Curr. Sci.* **80** 453-454.
- Shaw, D.M., (1970) Trace element fractionation during anatexis. *Geochim. Cosmochim. Acta*, **34**, 237-243.
- Shaw, H. R., (1972) Viscosities of magmatic silicate liquids: an empirical method of prediction. *Am. J. Sci.* **272**, 870-893.
- Sheridan M. F., Wohletz K. H. (1983) Hydro volcanism: basic considerations and review. In: Sheridan MF, Barberi F (eds) *Explosive volcanism*. *J Volcanol Geotherm Res* **17**, 1-29.

- Shervais, J. W., Kimbrough D. L., Renne P., Hanan B., Murchey B., Snow C. A., Schuman M. M. Z., Beaman J. (2004) Multi-Stage Origin of the Coast Range Ophiolite, California: Implications for the Life Cycle of Supra-Subduction Zone Ophiolites, *International Geology Review*, **46**, 289-315.
- Sheth H. C. (2006) The emplacement of pahoehoe lavas on Kilauea and in the Deccan Traps. *J Earth Syst Sci* **115**, 615-629.
- Sheth H. C., Ray J. S., Bhutani R., Kumar A., Smitha R. S. (2009) Volcanology and eruptive history of the Barren Island volcano, Andaman Sea, *Bulletin of Volcanology*, **71**, 1021-1039.
- Sheth H. C., Ray J. S., Bhutani R., Kumar A., Awasthi N. (2010) The latest (2008-09) eruption of Barren Island volcano, and some thoughts on its hazards, logistics, and geotourism aspects, *Current Science*, **98(5)**, 620-626.
- Sheth H. C., Ray J. S., Kumar A., Bhutani R., Awasthi N. (2011) Toothpaste lava from Barren Island Volcano (Andaman Sea), *Journal of Volcanological and Geothermal Research*, **202**, 73-82.
- Siebert L., Simkin T. (2002) *Volcanoes of the world: an illustrated catalogue of Holocene volcanoes and their eruptions*, Smithsonian Institution, Global Volcanism Program Digit Information Series, GVP-3. <http://www.volcano.si.edu/gvp/world>.
- Silver, P. G., Behn M. D. (2008). Intermittent Plate Tectonics? *Science*, **319**, 85-88.
- Simkin T., Siebert L. (1994) *Volcanoes of the world*. Geosci, Tucson, p 249.
- Singh, O. P., Subramanya, S. M., Sharma, V., (2000) Early Neogene multiple microfossil biostratigraphy, John Lawrence Island: Andaman Sea: *Micropalaeontology*, **46**, 343-352.
- Spohn, T. and Schubert, G., (1982) Modes of Mantle Convection and the Removal of Heat From the Earth's Interior *J. Geophys. Res.*, **87**, 4682-4696.
- Srinivasa sarma D. Jafri S.H., Flecher I.R., Mcnaughton N. J. (2010) Constraints on the Tectonic Setting of the Andaman Ophiolites, Bay of Bengal, India, from SHRIMP U-Pb Zircon Geochronology of Plagiogranite. *Jour of Geology*, **118(6)**, 691-697.

- Srivastava R. K., Chandra R., Shastry A. (2004) High-Ti type N-MORB parentage of basalts from the south Andaman ophiolite suite, India. *Jour. of Earth Sys. Sci.*, **113(4)**, 605-618.
- Stern, R. J., (2002) Subduction zones, *Rev. Geophys.*, **40(4)**, 1012, doi:10.1029/2001RG000108.
- Streck M.J., Ramos F., Haldar D., Duncan R.A., (2011) The Intra-oceanic Barren Island and Narcondam Arc volcanoes, Andaman Sea: Implications for subduction input and crustal overprint of a depleted mantle source, *Topics of igneous petrology* J.S. Ray et al. (edition) Springer, 258-273.
- Stumm W., Morgan J. J. (1981) *Aquatic Chemistry: An Prologue Emphasizing Chemical Equilibria in Natural Waters*. John Wiley & Sons, New York, **780** p.
- Subba Rao P. B. V. (2008) Regional conductance map of Andaman and Nicobar region. *Gondwana Res* **13**, 386-395
- Sun, S. S. and McDonough, W. F. (1989) Chemical and isotopic systematics of oceanic basalts: implication for mantle composition and processes. In: Saunders, A. D. and Norry, M. J. (eds) *Magmatism in the Ocean Basin*, Geological Society, London, Special Publication **42**, 313-345.
- Tamura, Y., (1994) Genesis of island arc magmas by mantle-derived bimodal magmatism: evidence from the Shirahama Group, Japan. *Journal of Petrology* **35**, 619-645.
- Tarbuck E.J., Lutgens F.J. (2006) *Earth Science*, eleventh edition, Pearson, Prentice hall Publications, pp 726
- Tatsumi, Y. (2005) The subduction factory: How it operates in the evolving Earth, *GSA Today*, **15(7)**, 4-10.
- Tatsumi, Y., Eggins, S., (1995) *Subduction zone magmatism*: Boston, Blackwell Science, 211 p.
- Tatsumi, Y., Hamilton, D. L. & Nesbitt, R. W. (1986) Chemical characteristics of fluid phase released from a subducted lithosphere and origin of arc magmas: evidence from high-pressure experiments and natural rocks. *Journal of Volcanology and Geothermal Research* **29**, 293-309.

- Taylor S. R., McLennan S. M. (1985) *The Continental Crust: its Composition and Evolution*. Blackwell scientific publications, **312** pp.
- Turner, S., Foden, J. (2001) U, Th and Ra disequilibria, Sr, Nd and Pb isotope and trace element variations in Sunda arc lavas: predominance of a subducted sediment component. *Contributions to Mineralogy and Petrology* **142**, 43-57.
- Tyrrell G. W. (1926) *Principles of Petrology*, B. I. Publications Pvt. Ltd., pp 349.
- Venkatrathnam, K., Biscaye, P. E., (1973) Clay mineralogy and sedimentation on the eastern Indian Ocean. *Deep- Sea Res.*, **20**, 727-738.
- Vohra, C.P., Halder, D. & Ghosh Roy, A.K. (1989) The Andaman–Nicobar ophiolite complex and associated mineral resources—current appraisal. In: Ghosh, N.C. (ed.) *Phanerozoic Ophiolites of India*. Sumna, Patna, 281–315.
- Wakabayashi, J., Ghatak, A., and Basu, A.R., (2010) Tectonic setting of supra subduction zone ophiolite generation and subduction initiation as revealed through geochemistry and regional field relationships: *Geological Society of America Bulletin*, **122**, 1548-1568 doi: 10.1130/B30017.1.
- Walker G. P. L. (1991) Structure, and origin by injection of lava under surface crust, of tumuli, “lava rises”, “lava-rise pits”, and “lavainflation clefts” in Hawaii. *Bull Volcanol* **53**, 546–558.
- Washington H. S. (1924) The lavas of Barren and Narcondam Islands. *Am J. Sci.* **7(5)**, 22.
- White J. D. L, Houghton B. (2000) Surtseyan and related phreatomagmatic eruptions. In: Sigurdsson H, Houghton BF, McNutt SR, Rymer H, Stix J (eds) *Encyclopedia of volcanoes*. Academic, New York, 495–511.
- White J. D. L., Houghton B. F., Hodgson K. A., Wilson C. J. N. (1997) Delayed sedimentary response to the A.D. 1886 eruption of Tarawera, New Zealand. *Geology* **25**, 459–462.
- White, W. M., Patchett, J. (1984) Hf-Nd-Sr isotopes and incompatible element abundances in island arcs: implications for magma origins

and crustal-mantle evolution. *Earth and Planetary Science Letters* **67**, 167-185.

Wilson, M., (1989), *Igneous Petrogenesis: A Global Tectonic Approach*, ISBN13:978-0-4125-3310-5 pp. 466.

Wohletz K. H., Sheridan M. F. (1983) Hydrovolcanic explosions II. Evolution of basaltic tuff rings and tuff cones. *Am J Sci* **283**, 384-413.

Wronkiewicz D.J. and Condie K. C. (1987) Geochemistry of archean shales from the Witwatersand supergroup, South Africa: source-area weathering and provenance, *Geochim. Cosmochim. Acta*, **51**, 2401-2416.

Zaw K., Acharyya S. K., Maung H. (1989) Comments and Reply on "Transcurrent movements in the Burma-Andaman Sea region" *Geology* **17**, 93-98.

Zimanowki B. (1998) Phreatomagmatic explosions. In: Freundt A, Rosi M (eds) *From magma to tephra*. Elsevier, Amsterdam, 25-53.

This page left blank intentionally

List of Publications

I. In Refereed Journals:

1. H. C. Sheth, J. S. Ray, R. Ray, L. Vanderklusen, J. J. Mohany, **A. kumar**, A. D. Shukla and others: *Geology and geochemistry of Panchmarhi dykes and sills Satpura Gondwana Basin, central India* problems of dyke-sill-flow correlations of deccan Traps, *Contributions to Mineralogy and Petrology*, **158**, 357-380, 2009
2. H. C. Sheth, J. S. Ray, R. Bhutani, **A. Kumar**, R. S. Smitha : *Volcanology and eruptive history of the Barren Island volcano, Andaman Sea*, *Bulletin of Volcanology* , **71**, 1021-1039, 2009
3. H. C. Sheth, J. S. Ray, R. Bhutani, **A. Kumar**, N. Awasthi : *The latest (2008-09) eruption of Barren Island volcano, and some thoughts on its hazards, logistics, and geotourism aspects*, *Current Science*, vol. **98** no 5 , 620-626, 2010
4. N. Awasthi, J. S. Ray, A. H. Laskar , **A. Kumar** , M. Sudhakar, R. Bhutani H. C. Sheth & M. G. Yadava : *Major ash eruptions of Barren Island volcano (Andaman Sea) during the past 72 kyr: clues from a sediment core record*, *Bull Volcanol*, **72**: 1131-1136, 2010
5. H. C. Sheth, J. S. Ray, **A. Kumar**, R. Bhutani, N. Awasthi : *Toothpaste lava from Barren Island Volcano (Andaman Sea)*, *Journal of Volcanological and Geothermal Research*, **202**, 73-82, 2011
6. **A. Kumar**, J. S. Ray and others: *Fluid and sediment contributions to Barren Island lavas: constraints form geochemistry*, *Journal of Petrology* (In preparation)

7. **A. Kumar**, J. S. Ray and others: *Geochemistry of Mud Breccia and Water from Mud Volcanoes of Andaman Island, Applied Geochemistry* (In preparation)

II. In Proceedings/Abstracts of Symposium/Conference:

1. **A. Kumar**, J. S. Ray and R. Bhutani: *Fluid and sediment contributions to Barren Island lavas: constraints from geochemistry 14th ISMAS symposium cum workshop on mass spectrometry*, November 7-11, 2011, Munnar, 245-248, ISBN 978-81-904442-4-8.

2. **A. Kumar** and J. S. Ray: *Geochemistry of lavas from Barren Island Volcano, Andaman Sea, Goldschmidt conference abstract 2010, Geochem Cosmochem. Acta, A 554*, 2010

3. **A. Kumar** and J. S. Ray: *Geochemistry of Mud Breccia and Water from Mud Volcanoes of Andaman island SE05-A023 AOGS 2010*

4. **A. Kumar**, J. S. Ray and A. D. Shukla: *Geochemical studies of mud samples from mud volcanoes of Andaman Islands, India. International Conference on "Terrestrial Planets: Evolution through Time" January 22-25, 2008 PRL Ahmedabad*

5. **A. Kumar**, D. K. Rao and S. K. Bhattacharya: *Oxygen and Hydrogen isotopic compositions of water from few selected Himalayan rivers, India 12th ISMAS symposium cum workshop on mass spectrometry*, March 25-30, 2007, Goa, ISBN 81-7525-056-9.